Stimuli-Responsive Lactonization-Based Persulfide Generators

विद्या वाचस्पति की
उपाधि की अपेक्षाओं की आंशिक पूर्ति में प्रस्तुत शोध प्रबंधक

A thesis submitted in partial fulfillment of
the requirements of the degree of
Doctor of Philosophy

द्वारा / By

भरत एस. चौधरी / BHARAT S. CHOUDHARY

पंजीकरण सं. / Registration No.: **20193655**

शोध प्रबंधक पर्यवेक्षक / Thesis Supervisor

प्रो. हरिनाथ चक्रपाणि / Prof. Harinath Chakrapani

IISER PUNE

भारतीय विज्ञान शिक्षा एवं अनुसंधान संस्थान पुणे

INDIAN INSTITUTE OF SCIENCE EDUCATION AND RESEARCH, PUNE- 411008

2025

Dedicated to.....

My family

CERTIFICATE

Certified that the work incorporated in this thesis entitled **"*Stimuli-Responsive Lactonization-Based Persulfide Generators*"** submitted by **Choudhary Bharat Swaroopram Gangadevi** was carried out by the candidate under my supervision. The work presented here or any part of it has not been included in any other thesis submitted previously for the award of any degree or diploma from any other university or institution.

C. Harinath

Date: 18/02/2025

Supervisor
Prof. Harinath Chakrapani
Professor
IISER, Pune

DECLARATION

Name of Student: **Choudhary Bharat Swaroopram Gangadevi**

Reg. No.: **20193655**

Thesis Supervisor: **Prof. Harinath Chakrapani**

Department: **Chemistry**

Date of joining program: **1st August 2019**

Date of Pre-Synopsis Seminar: **27th November 2024**

Title of Thesis: **Stimuli-Responsive Lactonization-Based Persulfide Generators**

I declare that this written submission represents my idea in my own words and where others' ideas have been included; I have adequately cited and referenced the original sources. I declare that I have acknowledged collaborative work and discussions wherever such work has been included. I also declare that I have adhered to all principles of academic honesty and integrity and have not misrepresented or fabricated or falsified any idea/data/fact/source in my submission. I understand that violation of the above will be cause for disciplinary action by the Institute and can also evoke penal action from the sources which have thus not been properly cited or from whom proper permission has not been taken when needed.

The work reported in this thesis is the original work done by me under the guidance of **Prof. Harinath Chakrapani**.

Date: 18/02/2025

Signature of the student

Table of contents

Chapter 2. Real-Time Monitoring of Persulfide Generation

Chapter 3. Development of Esterase-Triggered Persulfide Generator *via* 3-MST Pathway

General remarks

- Thin-layer chromatography (TLC) was performed using silica gel 60 GF254 precoated aluminium-backed plates (0.25 mm thickness), and visualization was accomplished by irradiation with short and long UV light at 254 and 365 nm, respectively, or by staining with bromocresol green or phosphomolybdic acid (PMA) for the identification of carboxylic acid or alcohols respectively.
- All reactions were carried out under nitrogen or argon atmosphere with freshly dried solvents under anhydrous conditions, and yields refer to chromatographically homogenous materials unless otherwise stated.
- All evaporations were carried out under reduced pressure on Büchi and Heildoph rotary evaporator below 45 °C unless specified otherwise.
- ^{19}F spectra were recorded on a JEOL (376 MHz) using an external reference (α, α, α-trifluorotoluene, δF = -63.72 ppm).
- ^{1}H and ^{13}C spectra were recorded on JEOL or Bruker 400 MHz (or 100 MHz for ^{13}C) spectrometers using tetramethylsilane (TMS) as an internal standard.
- Chemical shifts (δ) are reported in ppm downfield from CDCl3 (δ = 7.26 and 77.2 ppm) or DMSO-*d6* (δ = 2.50 and 39.5 ppm) or CD3OD (δ = 3.31 and 49.0 ppm) for ^{1}H and ^{13}C-NMR respectively as an internal reference. The coupling constants (*J*) are given in Hz. Multiplicities are indicated using the following abbreviations: br (broad), m (multiplet), s (singlet), d (doublet), t (triplet), q (quartet), dd (doublet of doublet), dt (doublet of triplet).
- Column chromatography was performed using Ranked silica gel (60-120 mesh) and (100-200 mesh) eluting with petroleum ether and ethyl acetate (EtOAc).
- Preparative High-Performance Liquid Chromatography (Prep HPLC) was carried out on a Combiflash EZ Prep UV equipped with a Kromasil®C-18 preparative column (21.5 mm x 250 mm, 10 μm) at a flow rate of 12 mL/min.
- High-resolution mass spectra were obtained from HRMS-ESI-QTOF (quadrupole time-of-flight).
- FT-IR spectra were recorded using Bruker ALPHA FT-IR spectrometer and reported in cm^{-1}.
- HPLC analysis data was obtained using Agilent Technologies 1260 Infinity, C18 reversed-phase column (4.6 mm × 250 mm, 5 μm).

- LC/MS experiments were performed either on a Sciex X500R QTOF mass spectrometer fitted with an Exion UHPLC system or on a Bruker Daltonics ESI-QTOF (Maxis Impact) mass spectrometer connected to a Thermo Dionex (Ultimate 3000) micro-LC system in a positive ion mode using high-resolution multiple reaction monitoring (MRM-HR) and information-dependent acquisition (IDA) methods or Agilent 6545 Quadrupole Time-Of-Flight (QTOF) LC-MS/MS with a Phenomenex®C-18 reverse phase column (250 mm × 4.6 mm, 5 μm).
- Absorbance measurements were carried out using SHIMADZU, UV-2600 UV-Vis spectrophotometer.
- Fluorescence measurements were carried out using a Horiba Jobin Yvon Fluorolog Fluorescence Spectrophotometer or an EnSight Multimode Plate Reader (PerkinElmer) in a 96-well plate format.
- All statistical analysis was carried out using GraphPad Prism 8.0.1 software unless specified.

Abbreviations

ACN – Acetonitrile

AcOH – Acetic acid

AD – Alzheimer's disease

ALP – Alkaline phosphatase

APAP – Acetaminophen

ARE – Antioxidant responsive element

ATP – Adenosine triphosphate

Arab – Arabinose

au – Arbitrary unit

boc –*tert*-butyloxycarbonyl

bs – Broad singlet

BSA – Bovine serum albumin

BTA – Biotin thiol assay

^{t}BuOH – Tertiary-butanol

B_2pin_2 – Bis(pinacolato)diboron

CARS – Cysteinyl-^{t}RNA synthetase

CAT – Cysteine aminotransferase

Calcd - Calculated

CBS – Cystathionine-β-Synthase

CBr_4 – Carbon tetrabromide

Cbz-Cl – Benzyl chloroformate

$CDCl_3$ – Chloroform-D

$CHCl_3$ – Chloroform

CH_2Cl_2 – Dichloromethane

CN^- – Cyanide ion

CPCA – Cyclopropane carboxylic acid

CPCSEA – Committee for the purpose of control and supervision of experiments on animals

Ctrl – Control

CSE – Cystathionine-γ-Lyase

CTAB – Cetyltrimethylammonium bromide

Cys – Cysteine

Cys-SSH – Cysteine persulfide

C28/I2 – Human chondrocyte cells

DAS - Diallyl sulfide

DADS - Diallyl disulphide

DATS - Diallyl trisulfide

DBU - 1,8-Diazabicyclo[5.4.0]undec-7-ene

dd – Doublet of doublet

DCC – *N*, *N'*-Dicyclohexylcarbodiimide

DCM – Dichloromethane

DEA/NO – sodium 2-(*N*, *N*-diethylamino)-diazenolate-2-oxide

DIPEA – Diisopropyl ethyl amine

DMAP – *N*, *N'*-Dimethylaminopyridine

DMEM – Dulbecco's Modified Eagle's Medium

DMF – *N*, *N'*-Dimethyl formamide

DMPPDA – *N*, *N'*–dimethyl-*p*-phenylenediamine sulfate

DMSO – Dimethyl sulfoxide

DNA – Deoxyribonucleic acid

D_2O – Deuterium Oxide

DPBS – Dulbecco's Phosphate-Buffered Saline

dt – Doublet of triplet

DTT – Dithiothreitol

DTPA – Diethylenetriaminepentaacetic acid

δ - Delta (in ppm)

equiv. **–** Equivalents

ELISA **–** Enzyme-linked immunosorbent assay

ER **–** Endoplasmic reticulum

Es **–** Esterase

ESI – Electron spray ionization

ESIPT – Excited state intramolecular proton transfer

Et_3N – Triethylamine

EtOH – Ethanol

EtOAc – Ethyl acetate

Et_2O – Diethyl ether

FBS – Fetal bovine serum

FDNB – Fluorodinitrobenzene

FeCl3 – Ferric Chloride

FRET – Förster resonance energy transfer

FT-IR – Fourier-transform infrared spectroscopy

5-FU – 5-Fluoro uracil

g – Gram

GAPDH – Glyceraldehyde-3-phosphate dehydrogenase

GFP – Green fluorescent protein

GSK3β – Glycogen synthase kinase-3 beta

GSH – Glutathione

GS-SH – Glutathione persulfide

GST – Glutathione *S*-Transferase

Gal – Galactose

Glu – Glucose

h – Hours

HBr – Hydrobromic acid

HCl – Hydrochloric acid

HeLa – Cervical cancer cell line

His – Histidine

HO-1 – Heme oxygenase-1

H_2O – Water

H_2O_2 – Hydrogen peroxide

H_2S – Hydrogen sulfide

H_2S_2 – Hydrogen persulfide

H_2S_n – hydrogen polysulfide

H_2-DCF-DA – 2',7'-dichlorodihydrofluorescein diacetate

HNO_3 – Nitric acid

HepG2 –hepatocellular carcinoma cells

HPE-IAM – *N*-(4-hydroxyphenethyl)-2-iodoacetamide

HPLC – High-performance liquid chromatography

HRMS – High-resolution mass spectrometry

Hz – Hertz

H9c2 – Cardiomyocyte cells

IAA – Iodoacetic acid

IAB – Iodoacetyl-PEG_2-biotin

IAM – Iodoacetamide

IAP – Iodoacetamide-linked biotin

IKK – IκB kinase

IL-6 – Interleukin 6

IL-12 – Interleukin 12

IκB – inhibitor of κB

Im – Imidazole

IR – Infrared

J – Coupling constant

KEAP 1– Kelch-like ECH- associated protein 1

KCl – Potassium chloride

KOAc – Potassium acetate

K_2CO_3 – Potassium carbonate

KH_2PO_4 – Monopotassium phosphate

λ_{max} – Absorbance maximum

λ_{ex} – Excitation wavelength

λ_{em} – Emission wavelength

LAH – Lithium aluminium hydride

LC/MS – Liquid chromatography-mass spectrometry

LDA – Lithium diisopropylamide

LPS – Lipopolysaccharide

Lys – Lysine

m – Multiplet

M – Molar

MALDI – Matrix-Assisted Laser Desorption Ionization

MEF – Mouse embryonic fibroblasts

Me – Methyl

MeOH – Methanol

mg – Milligram

Min. – Minutes

MHz – Megahertz

mL – Millilitre

mM – Millimolar

mmol – Millimoles

mg/mL – Milligram per litre

mBBr – Monobromobimane

MMTS – *S*-methylmethanethiosulfonate

MI/R – myocardial ischemia/reperfusion

MRM-HR – High-resolution multiple reaction monitoring

MS – Mass spectrum

MSBT - Methyl sulfonyl benzothiazole

3-MP – 3-mercapto pyruvate

3-MST – 3-Mercaptopyruvate sulfur transferase

MTT – 3-(4,5-Dimethylthiazol-2-yl)-2,5-diphenyltetrazolium bromide

MW – Molecular weight

m/z – Mass to Charge ratio

μM – Micromolar

NAC – *N*-acetyl cysteine

NACMe – *N*-acetylcysteine methyl ester

NAC-SS-Py – *N*-acetylcysteine pyridyl disulfide

NAD^+ – nicotinamide adenine dinucleotide

NADH – Reduced nicotinamide-adenine-dinucleotide phosphate

$NaNO_3$ – Sodium nitrate

$NaClO_2$ – Sodium chlorite

NaCl – Sodium chloride

NaOH – Sodium hydroxide

NaOMe – Sodium methoxide

NBF-Cl – 4-chloro-7-nitrobenzofurazan

NEM – *N*-ethylmaleimide

NFGFHD – National Facility for Gene Function in Health and Disease

NFκB – Nuclear factor kappa-light-chain-enhancer of activated B cells

$NaHCO_3$ – Sodium bicarbonate

NaSH - Sodium hydrosulfide

Na_2S – Sodium sulfide

Na_2SO_4 – Sodium sulphate

NMR – Nuclear magnetic resonance

NQO1 – NAD(P)H quinone oxidoreductase 1

nM – Nanomolar

nm – Nanometer

Nrf2 - Nuclear factor erythroid 2-related factor 2

NTR – Nitroreductase

N2a – Neuroblastoma cell line

N_2 – Nitrogen gas

ns – nonsignificant

$^{\bullet}OH$ – Hydroxyl radical

$O_2^{\bullet-}$ – Superoxide radical

$ONOO^-$ – Peroxynitrite

OA – Osteoarthritis

PBS – Phosphate buffer saline

$Pb(OAc)_2$ – Lead Acetate

PbS – Lead sulfide

PCC – Pyridinium chlorochromate

PCDL – Personal compound database library

$Pd(dppf)Cl_2$ – [1,1'-Bis (diphenylphosphino)ferrocene]palladium (II) dichloride

PD - Parkinson's disease

pH – Potential of hydrogen

Ph – Phenyl

PLE – Porcine liver esterase

PMSF – Phenylmethanesulfonyl fluoride

PPh3 – Triphenylphosphine

ppm – Parts per million

Pro – Proline

ProPerDP – Protein persulfide detection protocol

PTP1B – Protein-tyrosine phosphatase 1

Py – Pyridine

% – Percent

qPerS-SID – Quantitative persulfide site identification

QTOF – Quadrupole time-of-flight

ROS – Reactive oxygen species

RSS – Reactive sulfur species

RSSH – Persulfide

RT – Retention time

rt – Room temperature

s – Singlet

S_8 – elemental sulfur

SDS PAGE – Sodium dodecyl sulfate-polyacrylamide gel electrophoresis

Ser – Serine

SNU 398 – Hepatocellular carcinoma cells

SQR – sulfide: quinone reductase

t – Triplet

TBDMS-Cl – *Tert*-butyldimethylsilyl chloride

TCEP – Tris(2-carboxyethyl)phosphine

TEA – Triethylamine

TFA – Trifluoroacetic acid

THF – Tetrahydrofuran

Threo – Threonine

TLC – Thin layer chromatography

TLR4 – Toll-like receptor-4

TMS – Tetramethylsilane

TNF-α – Tumor necrosis factor-α

TST – Thiosulfate sulfurtransferase

Trx – Thioredoxin

Tyr – Tyrosine

$t_{1/2}$ – Half-life

UV – Ultraviolet

Vit C – Vitamin C

μg – Microgram

μM- Micromolar

μL – Microliter

μm – Micrometer

v/v – Volume/volume

w/v – Weight/volume

wt – Wild type

w/o – without

WST-8 – 2- (2-methoxy-4-nitrophenyl)-3- (4-nitrophenyl)-5- (2,4-disulfophenyl)-2H tetrazolium, monosodium salt

$Zn(OAc)_2$ – Zinc Acetate

Acknowledgements

I embarked on my PhD journey just before the COVID-19 pandemic began, a time filled with challenges and uncertainty. Despite these hurdles, I successfully reached the finish line! I am deeply grateful to the incredible individuals who supported and guided me throughout this transformative journey, helping me navigate unexpected obstacles and achieve my doctorate degree.

To start with, I would like to express my deepest gratitude to my thesis supervisor, Prof. Harinath Chakrapani, for his invaluable guidance and constant support he provided me throughout my Ph.D. journey. He constantly kept me motivated and encouraged in my ups and downs in the Ph.D. especially during COVID-19 and amid the fire incident at IISER Pune. He has always believed in my true potential, which has motivated me to push myself and conduct higher-quality research. Without his support and guidance, it would have been impossible for me to reach this milestone. I am extremely grateful to have worked under his mentorship.

I am extremely grateful to our collaborators, Dr. Rachit Agarwal (IISc, Bangalore) and his group members, Dr. Akshi Vashistha and Ankan Ghosh, for their continued support that helped me to make significant progress in projects and complete my Ph.D. dissertation. I would like to thank Dr. Amrita Hazra (IISER Pune) and her group members for their help and cooperation. I am also grateful to Dr. Siddhesh Kamat (IISER Pune) and his group members, Arnab and Aakash, for their help in LC/MS experiments.

I would like to sincerely thank my RAC members, Prof. Srinivas Hotha (IISER Pune) and Prof. Sridhar Rajaram (JNCASR, Bangalore), for their important suggestions, ideas, and valuable feedback during RAC meetings. I would like to thank the former director of IISER Pune, Prof. Jayant B. Udgaonkar, and the current director, Prof. Sunil S. Bhagwat, for providing excellent infrastructure and facilities at IISER Pune. I would like to thank Prof. H.N. Gopi (Former chair of the chemistry department) and Prof. Nirmalya Ballav (Current chair of the chemistry department) for providing world-class facilities. I gratefully acknowledge the funding agency UGC for the fellowship.

I have had the privilege of working alongside an amazing group of individuals whose unwavering support, guidance, and encouragement made my six-year journey seamless. A special thanks to my former lab members: - Dr. Anand, Dr. Laxman, Dr. Suman, Dr. Prerona, Dr. Pooja Kumari, Dr. Amol, Dr. Minhaj, Dr. Preeti, Dr. Ajay, Dr. Amogh, Harshit, Gaurav,

Farhan, Hariprasad, Mahima, Shayandeep, Manjima, Jishnu, Amal for all the lovely moments, encouragement and support. A sincere and special thanks to Dr. Anand (Andy) for being a friend and mentor and helping me learn the biochemical assays. Thanks to Simran for her helping hand in the animal experiment. I sincerely thank my current labmates, Dr. Kavita, Dr. Ravi, Utsav, Simran, Pooja T, Abhishek, Arnab, Vartika, Harshal, Rutuja, Malavika, Mufeeda, Pratiksha, Sam, Sanjay, Anisha, Dr. Akshaya, Divyanshu, Mathew, Panchami, and Dipti, for their unwavering support and constant help and for maintaining a healthy lab environment. I have been fortunate enough to make close friends at IISER, and I am thankful to Onkar, Sandip, and Akshay.

I also thank instrument operators (NMR, Microscopy, and HRMS), non-teaching staff, and administrative staff for their timely help.

Sports has been an important of my IISER life, especially cricket. A special thanks to Team Alchemist for allowing me to play under their banner.

Finally, I would like to acknowledge the most important people in my life "my family"- my father, Swaroopram Choudhary; my mother- Gangadevi Choudhary (maa); my brothers - Mukesh Choudhary and Rajesh Choudhary, for all their sacrifices; for all the love and their continuous support in everything.

Bharat Choudhary

Abstract

Reactive sulfur species (RSS), including thiols, hydrogen sulfide (H_2S), persulfides, and polysulfides, play crucial roles in physiological and pathological processes. These species contribute to redox signaling, cellular defence, and metabolic regulation. The generation of RSS within cells occurs through various enzymatic pathways, and enhancement of such species has beneficial effects. Hence, reliable generation of these species upon activation by particular stimuli is necessary. Although several methodologies are known, several generate electrophilic by-products, which are cytotoxic in nature. Hence, to overcome these limitations, we considered the formation of a lactone as a key step in the generation of persulfide, and this strategy is expected to generate persulfide along with a non-electrophilic by-product. Firstly, using a biphenyl-based scaffold, an esterase-sensitive persulfide donor was developed. Upon activation by esterase, this compound produces a persulfide and non-electrophilic lactone as a by-product. Along with the generation, the analytical detection of these species remains challenging due to their reactive and transient nature. Secondary assays are needed to detect persulfide generated by these chemical tools. Since the lactone is fluorescent, this strategy produced a reporter for persulfide as well, eliminating the need for secondary assays for persulfide detection. Symptomatic with persulfide generation, the donor was able to protect cells from oxidative stress. Using a similar biphenyl scaffold, we next prepared a compound that generates persulfide upon entry into cells through 3-mercaptopyruvate sulfurtransferase (3-MST), an enzyme involved in the biosynthesis of persulfide. The compound was found to efficiently generate H_2S/persulfide in biochemical assays and permeated cells to enhance persulfides, and the compound was found to promote antioxidant response. Next, to enhance the selectivity from a therapeutic benefit standpoint, the reactive oxygen species (ROS)-activated persulfide generators were synthesized and validated as persulfide generators through 3-MST pathway. We found a good anti-inflammatory response in an animal model for oxidative stress. This strategy was next extended to a known thiol-based radioprotectant WR-1065. This new prodrug undergoes activation by H_2O_2 and generates WR-1065 and a benign lactone.

Together, we have developed distinct approaches for the generation of persulfide, along with non-electrophilic lactone byproducts, and some have an in-built fluorescence reporter. The approaches developed herein will help address important questions regarding the generation and detection of persulfides and understand their therapeutic utility.

Chapter 1. Introduction

1.1. H_2S and persulfides in Biology

Ever since life first appeared on Earth, sulfur has been a necessary component of all living organisms and is involved in the synthesis of the amino acids cysteine and methionine, fundamental building blocks of life.[1] Cysteine, which is often located in the active site of enzymes, contributes to enzymatic catalysis,[2] while methionine plays a role in regulating metabolic processes, the innate immune system, and digestive functions in mammals.[3] Similarly, sulfur-containing proteins and peptides, such as glutathione (GSH), are integral to the cell's antioxidant machinery, protecting biomolecules from oxidative damage under stress conditions.[4,5] Furthermore, sulfur atoms are key components of Fe-S clusters, coenzymes, and metabolic mediators, underscoring their multifaceted biological significance.[6–9]

In addition to sulfur-containing amino acids, hydrogen sulfide (H_2S), a small gaseous molecule, has emerged as a critical player in intracellular signaling and cellular pathophysiology.[10–12] H_2S influences various physiological systems, including the gastrointestinal, neuronal, cardiovascular, respiratory, renal, and hepatic systems, and is associated with processes such as vasorelaxation, angiogenesis, apoptosis, aging, and metabolism.[13] Its role as an antioxidant is particularly significant in maintaining cellular redox homeostasis.[14] However, an imbalance in H_2S levels can disrupt this homeostasis, leading to diseased states.[15] Similarly, while sulfur-derived entities termed reactive sulfur species (RSS) can be beneficial, they may also damage biomolecules at elevated concentrations.[16,17] This duality in sulfur's functions is attributed to its versatile and interconvertible oxidation states (Figure 1.1).[18,19]

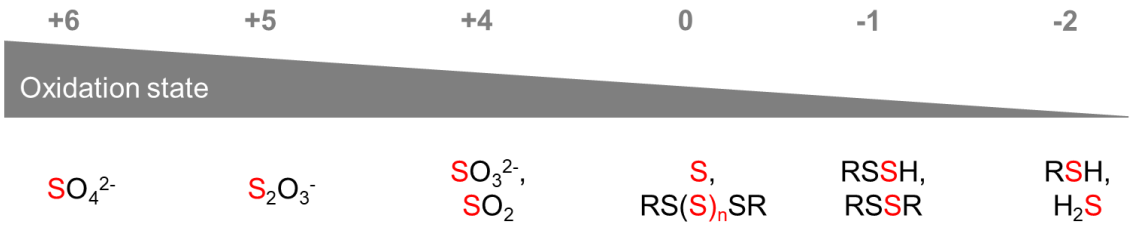

Figure 1.1. Biologically relevant reactive sulfur species with variable oxidation states of sulfur.

Persulfides (RSSH) have recently gained recognition as significant contributors to H_2S biology.[20] They are highly reactive and unstable species formed within cells, and participate in various biological processes.[21,22] Studies have shown that persulfides are more effective

antioxidants than H_2S, making them highly capable of mitigating oxidative stress and inflammation.[23] Additionally, like H_2S, cellular persulfides play a critical role in signaling pathways and are associated with several cardiovascular and neurological disorders.[23] Therefore, maintaining proper levels of persulfides within cells is essential for cellular health and function. Some of the examples of the biologically prevalent persulfides are shown in Figure 1.2.[21,22]

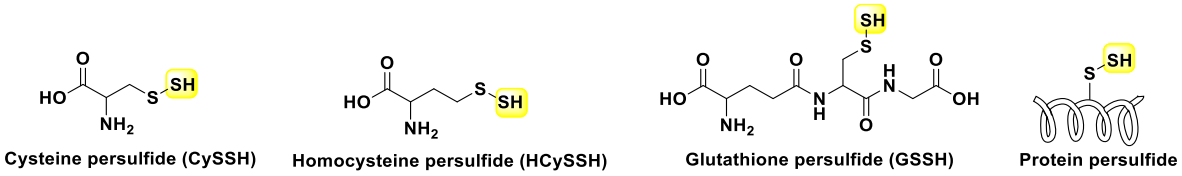

Figure 1.2. Structures of biologically relevant persulfides.

1.2. Physiological relevance of persulfidation

In addition to small-molecule persulfides, the importance of protein persulfides has been reported.[24] Protein persulfidation, also known as *S*-sulfhydration, is an oxidative post-translational modification on the cysteine residue of a protein where an additional sulfhydryl (-SH/S^-) group is added to a cysteine residue.[24] Several studies on protein persulfidation have shown it to be a key biological process involved, directly or indirectly, in various pathophysiological conditions,[25] including protection against oxidative stress,[26–28] antioxidant response *via* the KEAP1-Nrf2 pathway,[14,29] anti-inflammatory response,[30–32] neurodegenerative disorders,[33–35] DNA repair,[36] and smooth muscle relaxation.[37] Some examples of the role of persulfidation are discussed below.

1.2.1. Antioxidant response through KEAP1-Nrf2

One mechanism by which persulfidation exerts its antioxidant effects in cells is through the KEAP1-Nrf2 signaling pathway.[37] KEAP1, an oxidative stress sensor protein, typically forms a complex with Nrf2 under normal conditions (Figure 1.3). As part of the ubiquitin ligase system, KEAP1 facilitates the ubiquitination of the Nrf2 complex, leading to its proteasomal degradation.[38] However, under oxidative stress, a free cysteine residue on KEAP1 has been reported to undergo persulfidation through H_2S or persulfides. This modification leads to a conformational change and dissociation of the KEAP1-Nrf2 complex, allowing free Nrf2 to translocate to the nucleus. Once in the nucleus, Nrf2 binds to antioxidant-responsive elements (ARE), activating them. The activation of ARE triggers the release of antioxidant-responsive proteins, such as GST, NQO1, and HO-1.[29]

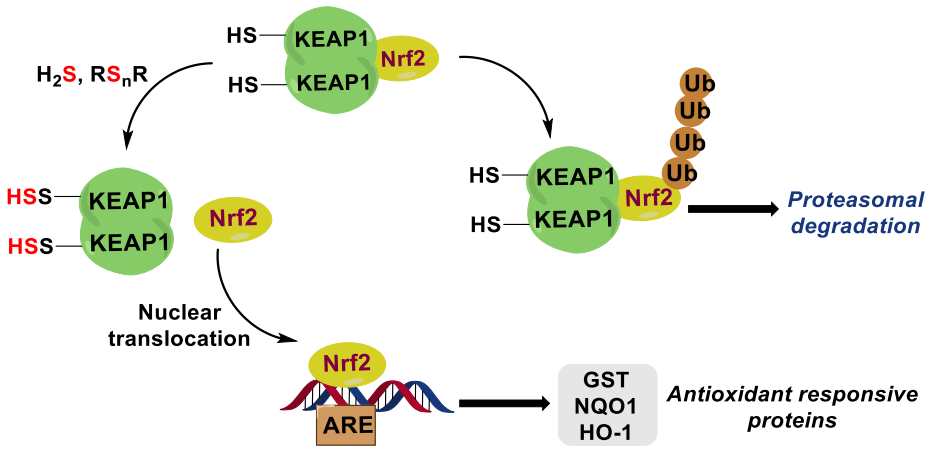

Figure 1.3. Antioxidant response mechanism *via* KEAP1-Nrf2 persulfidation.

1.2.2. Protection from oxidative stress

Protein persulfidation can directly protect protein thiols.[39,40] Protein thiols may be oxidized by ROS to sulfenic acids (R−SOH); further oxidation to sulfinic ($R-SO_2H$) and sulfonic acids ($R-SO_3H$) is considered an irreversible modification (Figure 1.4).[26] As a free thiol on the cysteine residue of protein is essential for catalytic reactions carried out by several proteins, irreversible oxidation can deactivate the protein function. In such cases, H_2S or a persulfide intervenes in the oxidation process at the sulfenic acid stage; the sulfenic acid converts to a persulfide.[27,28] The newly formed persulfide would then be oxidized by ROS to form an *S*-sulfocysteine, from which the free thiol can be brought back *via* reduction by thioredoxin (Trx), a bioreductive enzyme (Figure 1.4).[41]

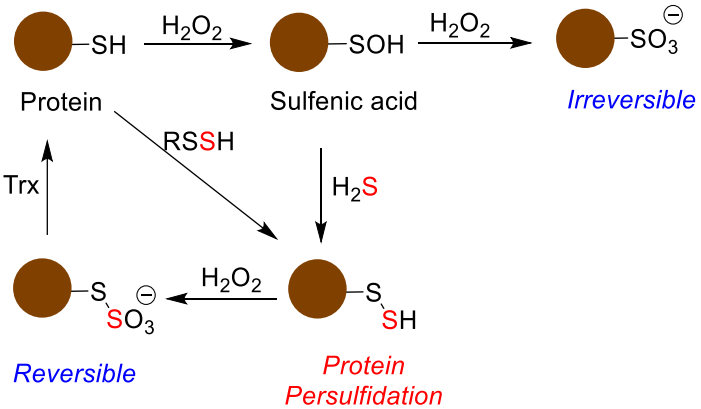

Figure 1.4. Protection of protein from oxidative stress through persulfidation.

1.2.3. Persulfidation in inflammation

The innate immune response involves nuclear factor kappa B (NF-κB), a transcription factor consisting of two subunits, p65 and p50. In unstimulated cells, NF-κB is retained in the

cytoplasm by the inhibitor of κB (IκB), which forms a complex with it.[37] Upon activation, IκB kinase (IKK) phosphorylates IκB, leading to its ubiquitination and subsequent release of NF-κB. This allows NF-κB to undergo phosphorylation and translocate to the nucleus, where it promotes the expression of pro-inflammatory cytokines such as TNF-α, IL-6, IL-12, etc.[30] Studies have shown that H_2S can exert anti-inflammatory effects by persulfidating the Cys38 residue of the p65 subunit of NF-κB. This modification reduces its phosphorylation, nuclear translocation, and DNA-binding activity (Figure 1.5).[31,32] Additionally, persulfides and polysulfides have been found to negatively regulate toll-like receptor 4 (TLR4)-mediated inflammatory responses. They effectively suppress inflammation induced by lipopolysaccharides (LPS) in macrophages and *in vivo* in a mouse endotoxin shock model, likely through inhibition of the IKK/NF-κB signaling pathway.[32]

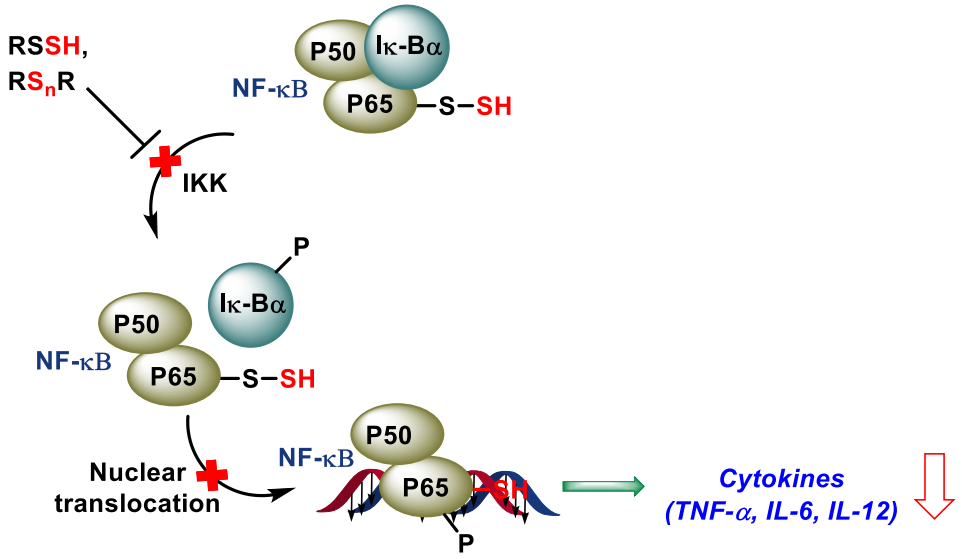

Figure 1.5. Persulfidation of NF-κB triggers an anti-inflammatory effect.

1.2.4. Persulfidation in neurodegenerative diseases

Parkin, an E3 ubiquitin ligase, is essential for degrading damaged neurons or molecules through proteasomal ubiquitination. Mutations in the parkin protein are implicated in the development of Parkinson's disease, causing the accumulation of toxic soluble proteins in the proteasome.[37] Persulfidation of parkin has been shown to enhance its activity. However, in Parkinson's disease patients, persulfidation levels are significantly reduced, leading to the buildup of toxic proteins and ultimately resulting in cell death (Figure 1.6).[35]

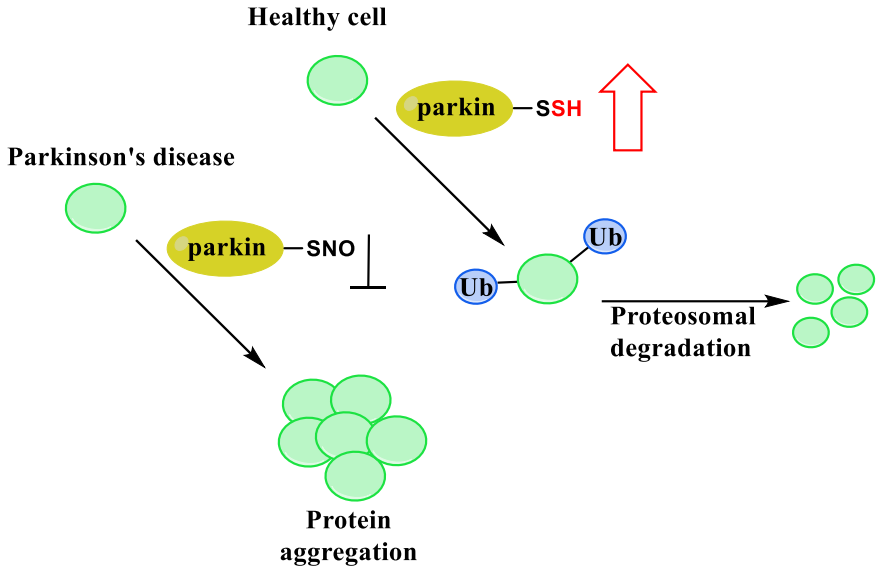

Figure 1.6. Regulation of parkin activity *via* persulfidation.

Alzheimer's disease is characterized by the accumulation of microtubule-associated proteins, including Tau and β-amyloid peptides. The hyperphosphorylation of Tau, mediated by glycogen synthase kinase 3β (GSK3β), disrupts its structural conformation and diminishes its ability to bind to microtubules. This results in Tau aggregation and neurotoxic effects. H_2S donors have demonstrated neuroprotective properties by persulfidating GSK3β, thereby suppressing its activity and preventing Tau hyperphosphorylation.[33]

1.3. Biosynthesis of persulfides

Persulfides are produced in cells *via* enzymatic biosynthetic pathways. For example, cysteine persulfide (Cys-SSH), a well-known persulfide, is synthesized from cystine with the involvement of the enzymes cystathionine-β-synthase (CBS) and cystathionine γ-lyase (CSE).[21,42] Additionally, recent studies have shown that cysteinyl-tRNA synthetases (CARS) can generate Cys-SSH from L-cysteine (Figure 1.7).[43]

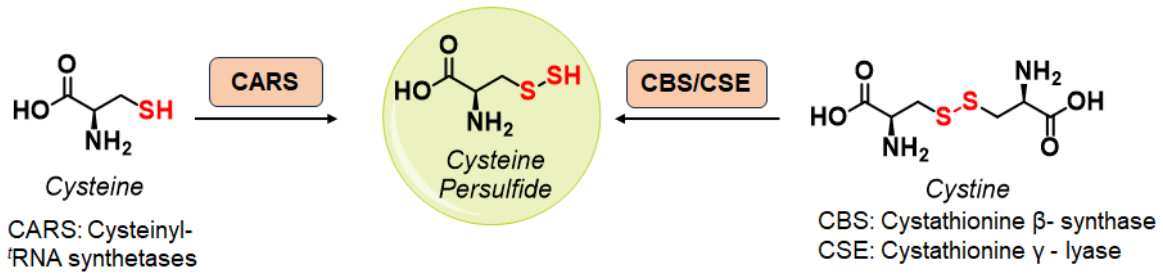

Figure 1.7. Cysteine persulfide formation from CBS, CSE, and CARS.

Another broad class of enzymes, known as sulfurtransferases, is present across various organisms and is responsible for the persulfide biosynthesis and sulfur trafficking in the

cells.[44–46] These enzymes are widely distributed and perform various functions, including sulfur metabolism, iron-sulfur cluster formation,[47] cyanide detoxification,[48,49] and selenium metabolism.[47] The catalytic cycle of this enzyme follows a two-step mechanism. First, the active site cysteine forms a transient persulfide intermediate (RS-SH) by accepting sulfur from a donor compound. Subsequently, the sulfur is transferred to a thiophilic acceptor, regenerating the enzyme's native state. Thiophilic acceptors can include proteins like thioredoxin or small molecule thiol such as glutathione, which generates the GS-SH persulfide and can further mediate protein trans-persulfidation (Figure 1.8).[44,45,50,51]

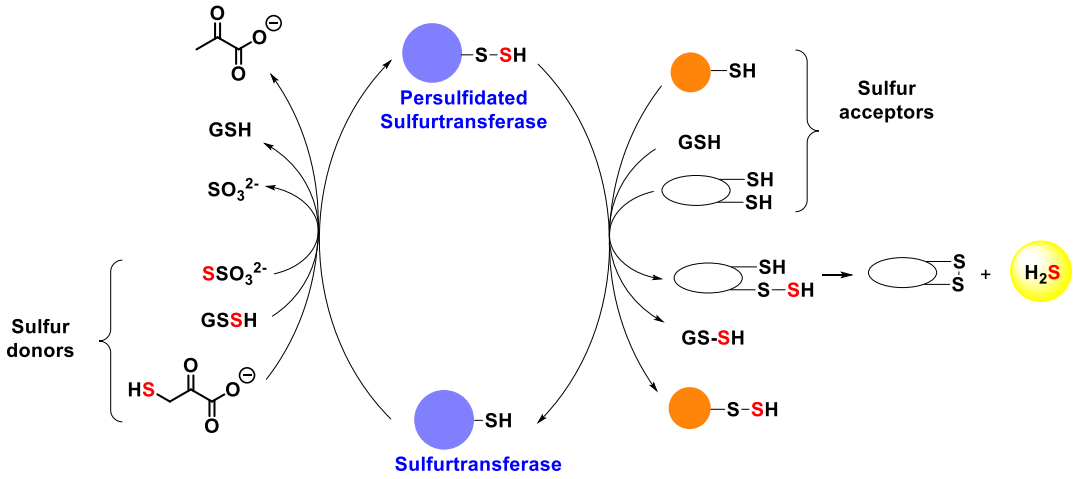

Figure 1.8. Substrate scope of sulfurtransferases and products.

3-Mercaptopyruvate sulfurtransferase (3-MST),[45,50] thiosulfate sulfurtransferase (TST),[52] and sulfide quinone reductase (SQR)[44] are the key sulfurtransferase enzymes that play a critical role in the formation of persulfides and sulfur transfer.

Among all the sulfurtransferases discussed, 3-MST has gained significant attention over the years due to its role in the biosynthesis of H_2S, persulfides, and polysulfides, as well as its involvement in sulfur trafficking.[52–54] 3-mercaptopyruvate (3-MP), the natural substrate of 3-MST, is physiologically produced from L-cysteine through the action of cysteine aminotransferase (CAT) in the presence of α-ketoglutarate.[50,55] 3-MST utilizes 3-MP as the sulfur acceptor to form a transient persulfide intermediate in its active site cysteine and an enolate of pyruvate as the byproduct (Figure 1.9.A).[50,55] The crystal structure analysis of human 3-MST bound to 3-MP revealed that Arg188 and Arg197 stabilize the incoming 3-MP through electrostatic interactions with its carboxyl and carbonyl groups. The catalytic triad consisting of His74, Ser250, and Asp63 plays a crucial role in activating the catalytic site residue, Cys248.[50,55]

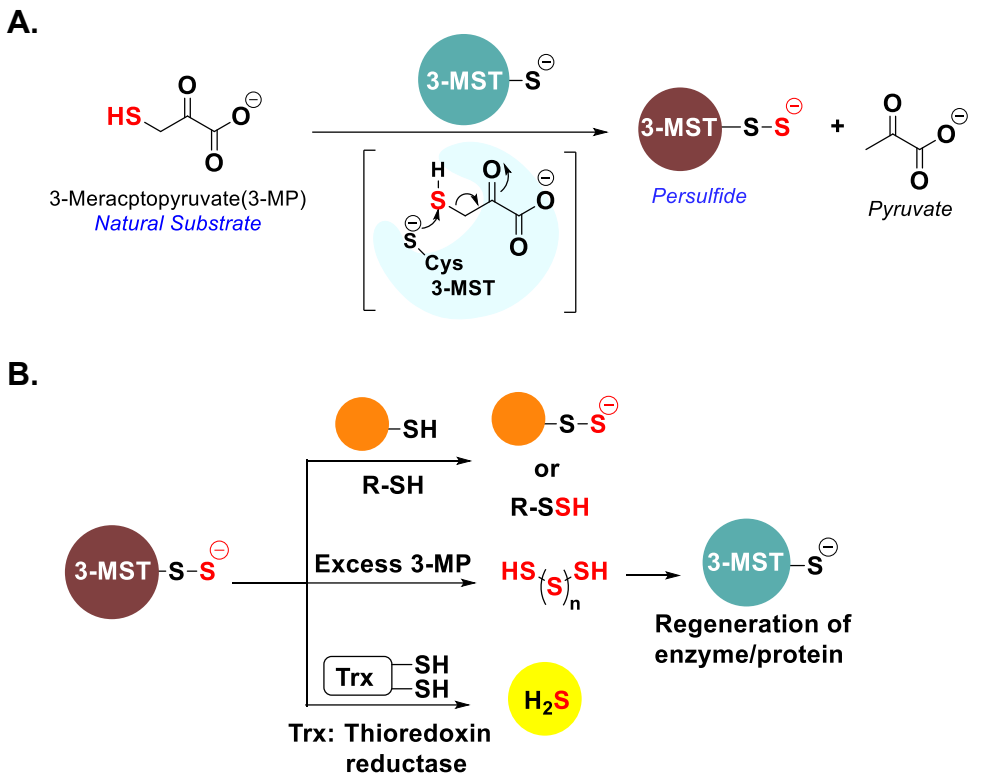

Figure 1.9. (A) Reaction mechanism for turnover of 3-mercaptopyruvate (3-MP) by 3-mercaptopyruvate sulfurtransferase (3-MST) to form a transient 3-MST persulfide intermediate and pyruvate as the byproduct. (B) The 3-MST persulfide can undergo reduction to generate H_2S or transfer the sulfur to other acceptor proteins or small-molecule thiol.

The sulfur from the persulfide intermediate can be transferred to target proteins or reduced by thioredoxin to produce H_2S.[45,54,55] Additionally, further turnover of 3-MP by the 3-MST persulfide has been shown to generate polysulfides (Figure 1.9.B).[45,54,55]

The H_2S, persulfide, and polysulfides generated from 3-MST play a key role in the signaling pathways.[56] The activity of 3-MST is correlated with changes in its expression levels.[56] For instance, 3-MST levels are elevated in obese patients[57,58] and schizophrenia patients[59] but decline with aging.[60–62] In diabetes, its expression varies by tissue, decreasing in cardiac and smooth muscle but increasing in skeletal muscle.[63,64] Dysregulation of 3-MST is linked to pathophysiological conditions, such as mental retardation and anxiety-like behaviour in 3-MST knockout mice[65] and exacerbated joint calcification and osteoarthritis.[66]

1.4. Persulfide Generators

Protein persulfidation is a critical signaling mechanism facilitated by persulfides, enabling a wide range of physiological functions. However, the inherent instability of persulfides, which rapidly undergo disproportionation in aqueous environments, presents a significant challenge for their controlled in situ generation.[67] The primary report of the synthesis of low molecular weight persulfides was first reported in 1954 by Horst and Gerwalt.[68] However, their potency for protein persulfidation and the biological relevance of these persulfides were not explored. The attempts to isolate persulfides have largely been unsuccessful, except for a few sterically hindered variants in organic media, limiting their utility in exploring their biological functions.[20,23,69–71]

To better understand the intricate biochemistry of persulfides and their role in sulfur signaling, it is essential to develop persulfide generators or prodrugs. These generators should ideally be shelf-stable, cell-permeable, and capable of releasing active sulfur species in response to specific stimuli (Figure 1.10).

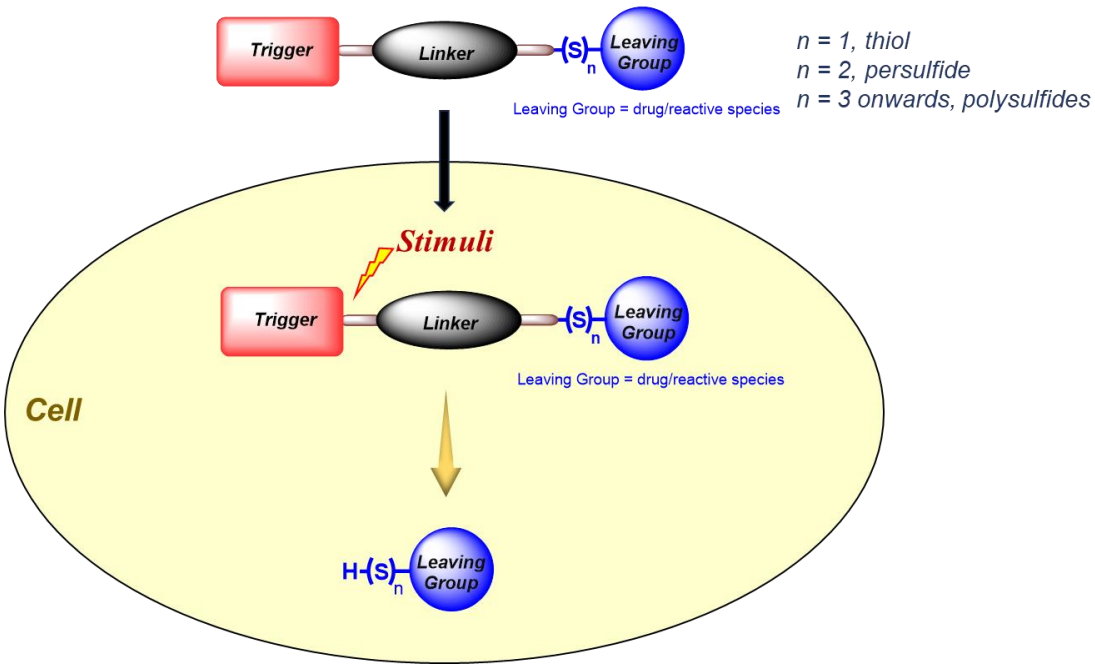

Figure 1.10. Prodrug strategy for intracellular generation of reactive sulfur species.

The prodrug typically consists of three parts: a) **Trigger**: The functional group or chemical moiety that initiates the release of the active drug. The trigger responds to specific physiological conditions or stimuli, such as enzymatic triggers (e.g., esters cleaved by carboxylesterases), chemical triggers (e.g., pH, H_2O_2, i.e., ROS), and external triggers (e.g., light). b) **Leaving group**: The leaving group is the portion of the prodrug that detaches from

the drug molecule during activation. Its role is to facilitate the drug or reactive species release without interfering with the efficacy of the active drug or reactive sulfur species. In the case of reactive sulfur species generators, if n = 1 (thiol generator), n = 2 (persulfide generator), and n = 3 onwards (polysulfide generator). c) **Linker**: The linker connects the active drug or reactive species to the trigger. It modulates the stability and release rate and determines the time and location of drug activation. In recent years, a plethora of reactive sulfur species generators have been developed, and mostly, the significant advancement in designing stimuli-responsive persulfide generators is discussed below.

1.4.1. Persulfide generators based on linker

As discussed above, the linker connects the active drug or reactive sulfur species to the trigger, and the ideal linker should be stable, cleavable, and biocompatible. Based on the linker, the persulfide generators can be further classified as follows:

1.4.1.1. Without linker

One example of a prodrug without a linker is amifostine (**WR-2721**), which is a clinically used radioprotectant in chemotherapy or radiotherapy in order to protect normal tissues. It is converted into its active form, **WR-1065**, by alkaline phosphatase (ALP), an enzyme present in normal tissues (Figure 1.11).[72,73] The active form acts as a scavenger of free radicals, reducing damage to normal cells without significantly protecting tumor cells.[74,75] This selectivity arises because normal tissues can metabolize the drug more effectively than tumor tissues.

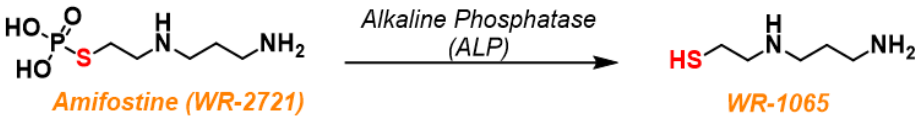

Figure 1.11. Activation of amifostine by ALP produces active **WR-1065**.

Another example is the phenacyl thiol, the 3-MST artificial substrate developed in our lab that enhances the intracellular H_2S and sulfane sulfur pool, as explained earlier in the persulfide biosynthesis *via* 3-MST (Figure 1.12).[76] A library of artificial substrates was developed and evaluated for the H_2S and persulfide generation, antioxidant, and anti-inflammatory properties in both cellular and animal models. However, the artificial substrate gets cleaved by thiols, which limits its selectivity towards esterase.

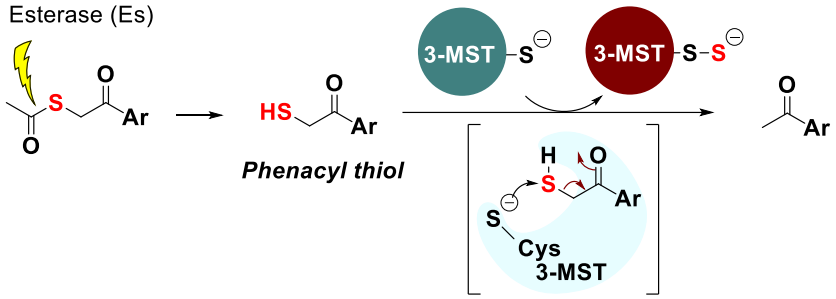

Figure 1.12. Artificial 3-MST substrate developed in our lab.

Prodrugs without linkers can be advantageous due to their simplicity and ease of synthesis. However, they are often less effective for achieving controlled, targeted, or stimuli-responsive drug or reactive species release, leading to off-target effects. So, incorporating a linker adds complexity but greatly enhances the versatility and efficacy of prodrug systems.

1.4.1.2. Self-immolative linker

To enhance the controlled and targeted release, persulfide generators with prodrugs with self-immolation linkers have been developed. Upon activation by a trigger (e.g., enzymatic cleavage or environmental stimulus), these linkers undergo a cascade of intramolecular rearrangement reactions to release the active persulfide. This design is highly versatile and can be tailored to specific applications. Further, these linkers based on the intramolecular rearrangement can be classified as discussed below.

1.4.1.2.A. 1,2-Self-immolative linker

In the 1,2-self-immolation linker, the term "1,2" refers to the spatial rearrangement of functional groups within the linker, positioned in close proximity to facilitate the self-elimination process in order to generate the persulfide (Figure 1.13). A few examples of persulfide generators based on the 1,2-elimination strategy are discussed below.

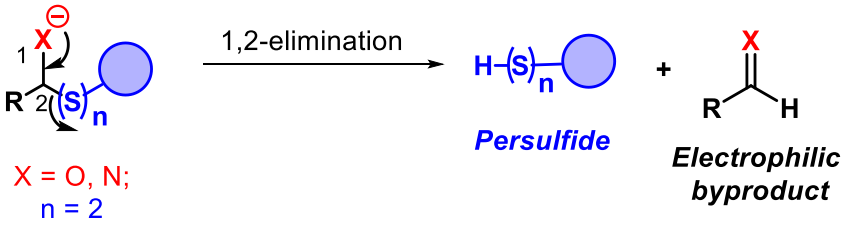

Figure 1.13. Schematic representation of 1,2-self-immolation-based persulfide generator.

One of the earliest reports of a persulfide generator was reported from Ming Xian and co-workers, a biomimetic persulfidation precursor comprising 9-fluorenylmethyl disulfide

(**FmSSPy-A**) was developed. This disulfide undergoes thiol exchange with small-molecule or protein thiols to form a base-sensitive disulfide (RSS-Fm). Upon reaction with a base, such as 1,8-diazabicyclo[5.4.0]undec-7-ene (DBU), the adduct generates a persulfide through a 1,2-elimination mechanism. Using BSA as a model protein, the researchers demonstrated the method's potential for persulfidating proteins (Figure 1.14).[77] However, the use of DBU as a base may influence reactivity studies in certain cases.

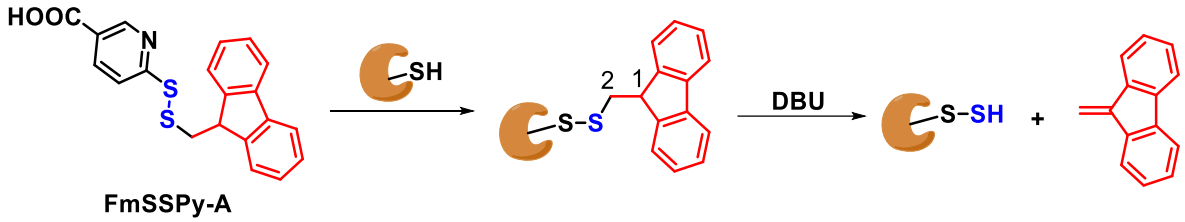

Figure 1.14. Mechanism for persulfide generation from **FmSSpy-A**.

Wang and co-workers have developed a series of esterase-sensitive persulfide generators using the 1,2-elimination strategy (Figure 1.15).[78] The authors demonstrated the tunable release of persulfides by varying the esters and showcased their therapeutic potential in a murine model of myocardial infarction/reperfusion (MI/R) injury.

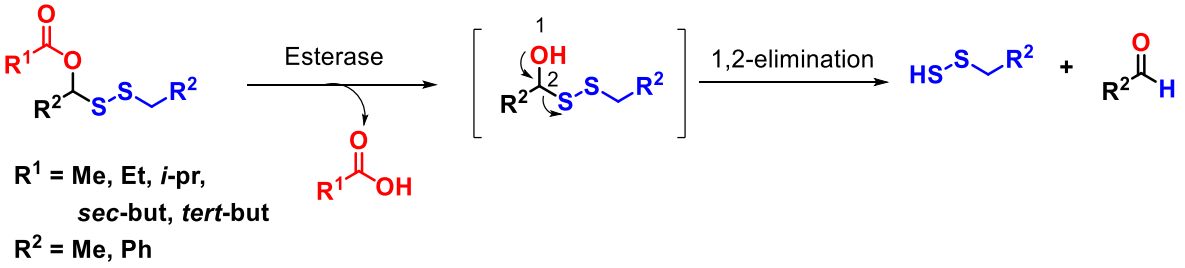

Figure 1.15. Esterase-sensitive persulfide generators.

Along the same line, a class of persulfide generators based on a 1,2-elimination strategy and sensitive to fluoride was reported from the same group (Figure 1.16).[79] The rate of persulfide release was reported to vary based on the substituents attached to the silicon atom. Additionally, the compounds were found to undergo hydrolysis in acidic conditions to produce persulfides, although the hydrolysis process was exceptionally slow.

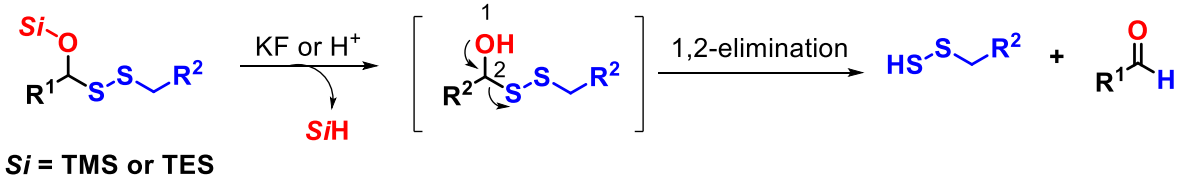

Figure 1.16. Fluoride-sensitive persulfide generators.

Toscano and co-workers reported a pH-sensitive persulfide prodrug. In an aqueous buffer at pH 7.4, the amine group in the *S*-substituted thioisothiourea scaffold is neutralized, triggering a 1,2-elimination reaction that produces a persulfide along with arylcyanamide as a byproduct (Figure 1.17).[80] The rate of persulfide release was tuned by varying the substituents on the aryl ring.

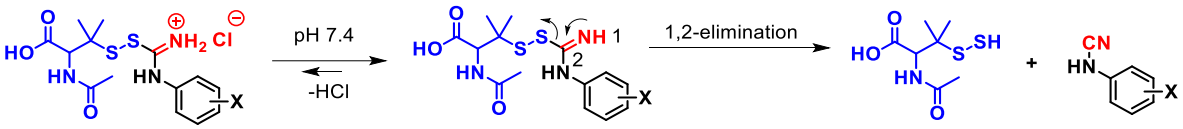

Figure 1.17. pH-sensitive thioisothiourea-based persulfide precursors.

1.4.1.2.B. 1,4-Self-immolative linker

In the 1,4-self-immolation linker, the "1,4" designation refers to the spatial rearrangement of functional groups within the linker, where the trigger group and the self-immolating moiety are separated by four atoms (Figure 1.18).

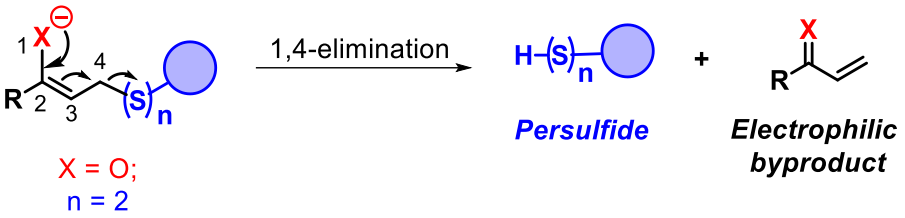

Figure 1.18. Schematic representation of persulfide generator based on 1,4-self-immolation.

Based on the retro Michael reaction 1,4-O,S relay mechanism, our lab developed a persulfide donor, which gets selectively activated by hydrogen peroxide (H_2O_2), a reactive oxygen species (ROS), and produces cinnamaldehyde as a byproduct (Figure 1.19).[81] The persulfide donor exhibited cytoprotective effects in the cells against oxidative stress. One concern with the strategy mentioned above is the potential formation of cinnamaldehyde, which is considered a mild electrophile despite being commonly used in the food industry.

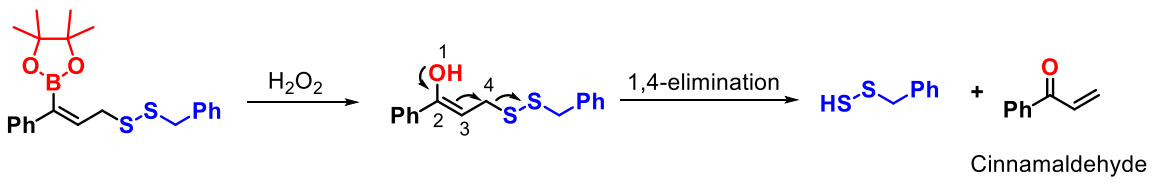

Figure 1.19. ROS-activated persulfide generator based on 1,4-elimination strategy.

1.4.1.2.C. 1,6-Self-immolative linker

The term "1,6" in the 1,6-self-immolation strategy indicates that the functional groups involved in the self-immolation process are separated by six atoms within the linker structure**,** and it is mainly considered to be across the phenyl or aromatic ring (Figure 1.20).

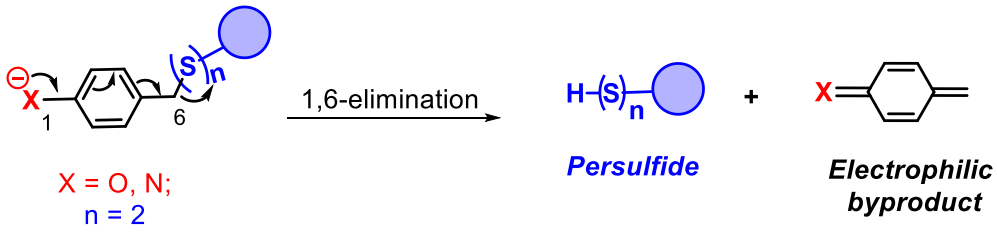

Figure 1.20. Schematic representation of 1,6-self-immolation-based persulfide generators.

Matson and co-workers developed a discrete NAC persulfide precursor (**BDP-NAC**), which is inert under normal physiological conditions, but under oxidative conditions, like in the presence of H_2O_2, it undergoes 1,6- self-immolation to release a persulfide species (Figure 1.21).[82] Even though the molecule exhibited cytoprotective properties, the release of toxic quinone methide as a byproduct was a major disadvantage of this strategy.

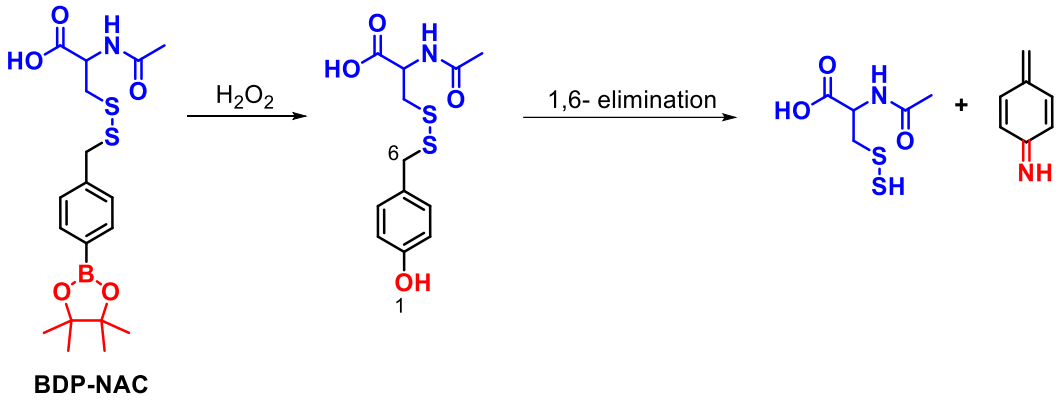

Figure 1.21. Boronate ester-based persulfide donor **BDP-NAC**, sensitive to H_2O_2.

Using a similar 1,6-elimination strategy, the same group has reported a persulfide prodrug (**NDP-NAC**) responsive to nitroreductase (NTR) and NADH (Figure 1.22).[83] **NDP-NAC** was found to have a significant impact on the gut microbiome composition in mice, more so than H_2S or a non-persulfide-containing negative control. The compound promoted the growth of bacteria from the *Turicibacter* genus, especially *Turicibacter sanguinis*, which supports metabolism and gastrointestinal health. On the other hand, the compound inhibited the growth of opportunistic and pathogenic gut bacteria. This study suggests that the controlled delivery

of RSSH to the gut could be beneficial for modulating the gastrointestinal microbiome during disease conditions.

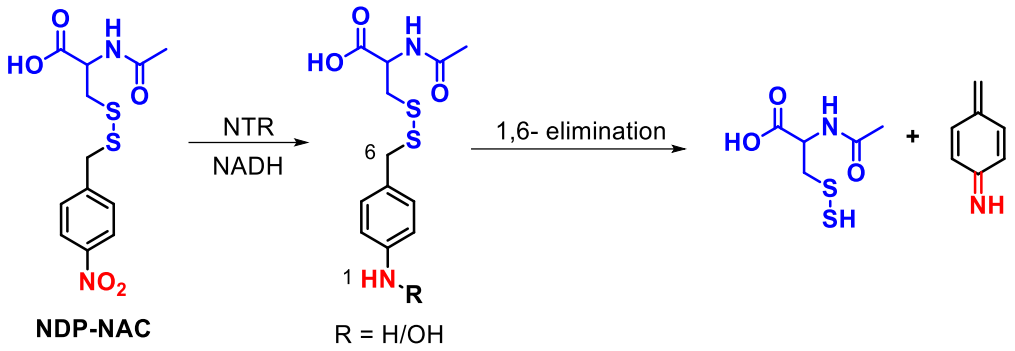

Figure 1.22. Nitroreductase (NTR) activated persulfide generator (**NDP-NAC**).

The same group also developed a polymeric persulfide prodrug, **poly(EDP-NAC)** and **EDP-NAC**, which can be triggered by esterase (Es), utilizing a 1,6-elimination strategy (Figure 1.23).[84] While **poly(EDP-NAC)** was significantly slower than the monomeric **EDP-NAC**, it was found to be more effective in protecting cardiomyocytes from cytotoxicity induced by 5-fluorouracil (5-FU).

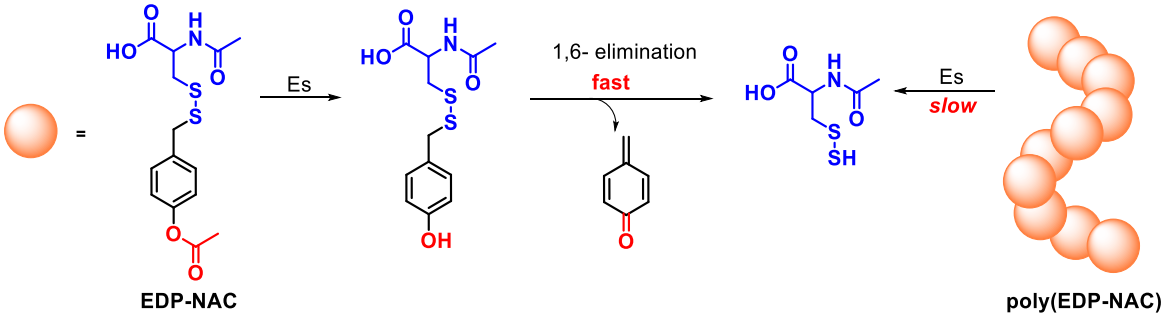

Figure 1.23. Esterase-sensitive **EDP-NAC** & **poly(EDP-NAC)** based persulfide precursors.

Using a similar framework to BDP-NAC, Matson, and colleagues also reported superoxide-activated persulfide generators, **SOPD-NAC** and **SOPD-Pep** (Figure 1.24).[85] Both these compounds scavenge superoxide and then decompose to release persulfides (RSSH). They were able to protect the cardiomyocytes by alleviating the oxidative stress. Additionally, **SOPD-Pep** showed better anti-inflammatory activity in macrophages, greater than **SOPD-NAC** and several H_2S-releasing control compounds.

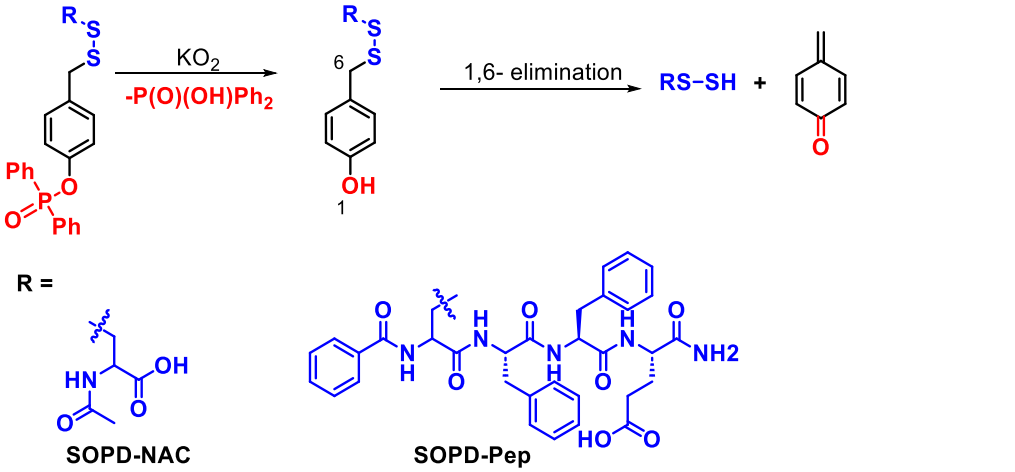

Figure 1.24. Superoxide-activated persulfide generators.

Recently, Zhen and co-workers, using a 1,6-*N*,*S*-relay, developed a peroxynitrite-activated NAC persulfide donor. The 2-oxo-2-phenylacetamide trigger initially reacts with peroxynitrite, subsequently leading to the release of persulfide, which serves as a secondary quencher of peroxynitrite (Figure 1.25).[86] This compound significantly lowered the intracellular levels of peroxynitrite induced by acetaminophen (APAP) in HepG2 cells and mitigated oxidative stress in H9c2 cardiac cells.

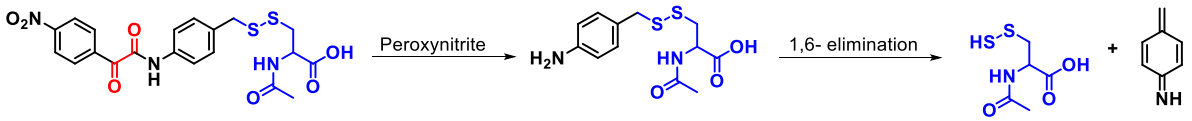

Figure 1.25. Peroxynitrite-activated persulfide donor.

1.4.1.3. Cyclization-based persulfide generators

To overcome the limitations of the electrophilic byproducts, researchers have utilized intramolecular cyclization for the generation of persulfide (Figure 1.26.A). The persulfide generator, upon activation by particular stimuli, forms an intermediate that undergoes rapid cyclization (lactonization) to generate persulfide and a benign lactone as a byproduct. Trimethyl-lock systems are rapid and efficient in undergoing rapid lactonization due to the phenomenon known as the Thorpe-Ingold effect (Figure 1.26.B).[87] It states that the increasing steric favors the ring closure and intramolecular reactions. Using the cyclization strategy, persulfide generators have been reported, which are discussed below.

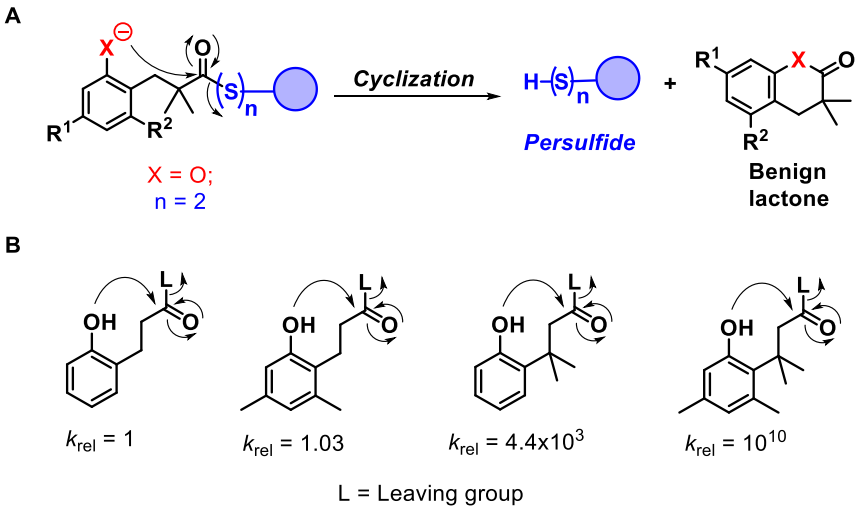

Figure 1.26. (A) Schematic representation for cyclization-based persulfide generators and (B) k_{rel} shows steric-assisted faster cyclization due to the Thorpe-Ingold effect.

Binghe Wang and coworkers developed an esterase-sensitive glutathione persulfide (GS-SH) generator **BW-GP-401** using the trimethyl lock system, which gets activated by esterase and cyclizes to form a lactone, releasing GS-SH in the process (Figure 1.27.A).[88] The donor exhibited inhibitory effects towards glyceraldehyde 3-phosphate dehydrogenase (GAPDH) and cytoprotective effects under highly oxidative conditions in the cellular environment. Using a similar strategy, hydrogen persulfide (H_2S_2) generators were developed (Figure 1.27.B).[89]

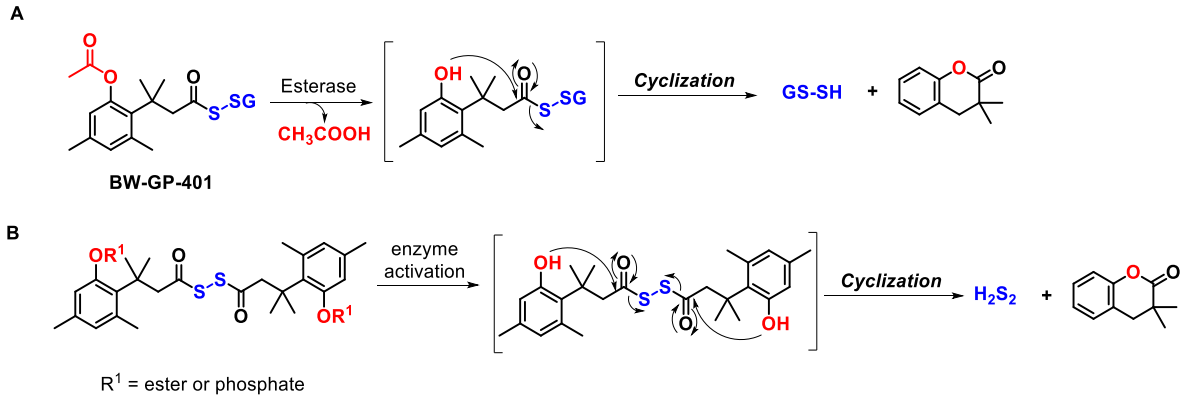

Figure 1.27. (A) Esterase-sensitive glutathione persulfide prodrug. (B) Trimethyl lock-based H_2S_2 donor activated by esterase and phosphatase.

Lukesh and co-workers further leveraged the boronate ester scaffold to develop an H_2O_2-responsive persulfide generator, **RAH393**. Upon activation by H_2O_2, the phenolate undergoes intramolecular cyclization to release *N*-acetyl cysteamine persulfide and an innocuous lactone by-product (Figure 1.28).[90] **RAH393** was able to protect the HeLa cells

from H_2O_2-induced oxidative stress, underlining the utility of **RAH393** as a potential therapeutic against oxidative stress.

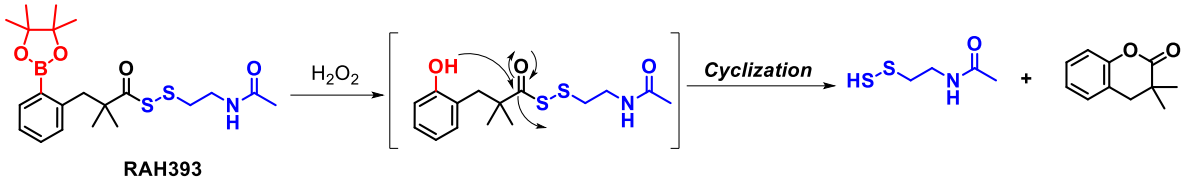

Figure 1.28. Boronate ester-based persulfide donor **RAH393** responsive to H_2O_2.

Recently, by exploiting the cyclization strategy, our lab has developed a *β*-glucosidase responsive persulfide donor. Upon cleavage by *β*-glucosidase, the phenolate undergoes an intramolecular cyclization to generate persulfide along with a benign heterocyclic byproduct (Figure 1.29).[91] The compound also exhibited a cytoprotective effect against oxidative stress.

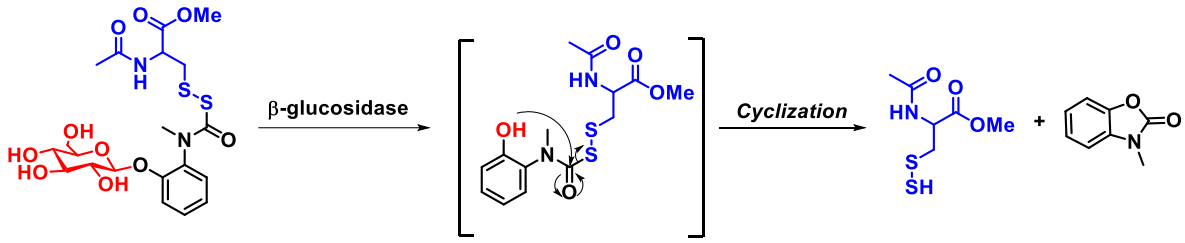

Figure 1.29. *β*-Glucosidase-responsive persulfide generator.

Using a similar framework of **BW-GP-401**, Bowen and co-workers have recently reported a cyclopropyl ester-based *N*-acetylcysteine persulfide donor **CPS-3** (Figure 1.30).[92]

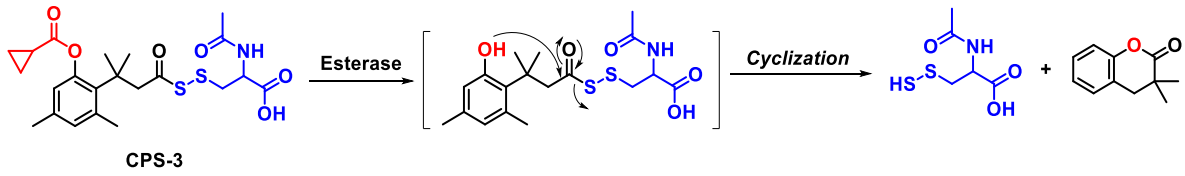

Figure 1.30. Trimethyl lock-based esterase-sensitive persulfide generator.

1.4.2. Other persulfide generators

Apart from the persulfide generators discussed above, there are some other persulfide donors, such as pH, hydrolysis, and thiol-activated persulfide precursors. Also, there are reports of the use of light as a stimulus for the generation of persulfide.

1.4.2.1. pH and hydrolysis-based persulfide generators

Galardon and colleagues were among the first to develop a persulfide precursor, **P***. In an aqueous buffer with a pH > 6, the precursor (P*) undergoes spontaneous rearrangement *via* an acyl transfer, generating a persulfide *in situ* (Figure 1.31.A).[93] This prodrug has since been widely used in various biochemical studies to investigate persulfide biochemistry. Yang and co-workers designed a similar approach to generate cysteine persulfides using a persulfidated cysteine precursor (**PSCP**) (Figure 1.31.B).[94] **PSCP** was demonstrated to generate persulfides and polysulfides in liver cancer cell lines and showed specific anti-cancer activity in the liver cancer cell line SNU 398.

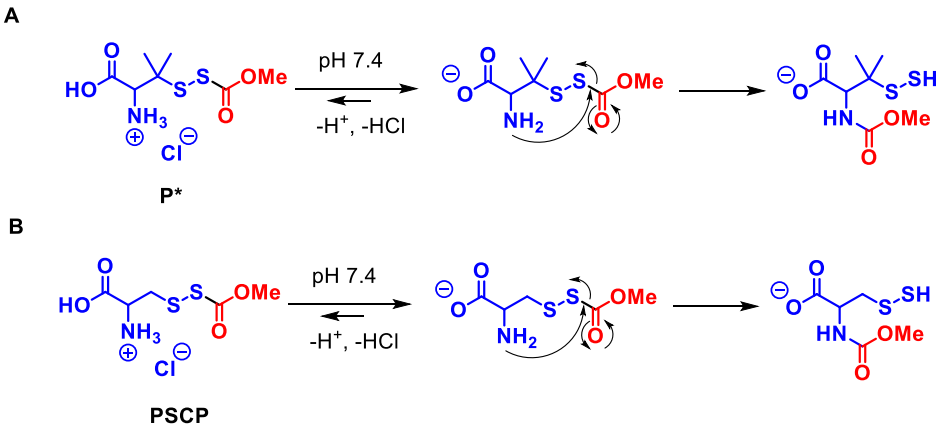

Figure 1.31. pH-sensitive persulfide precursors (A) **P*** and (B) **PSCP** based on -S to -N methoxycarbonyl transfer.

Toscano and the group have developed a class of pH-sensitive hydrolysis-based persulfide generators. The terminal quaternary ammonium salts, upon neutralization in pH 7.4 buffer, form an active amine nucleophile that subsequently undergoes an intramolecular cyclization and cyclic urea as a byproduct from the alkylamine-substituted perthiocarbamate scaffold (Figure 1.32).[95] These precursors exhibited cytoprotective effects against hydrogen peroxide-induced toxicity in H9c2 cells and cardioprotective effects against myocardial ischemic/reperfusion injury.

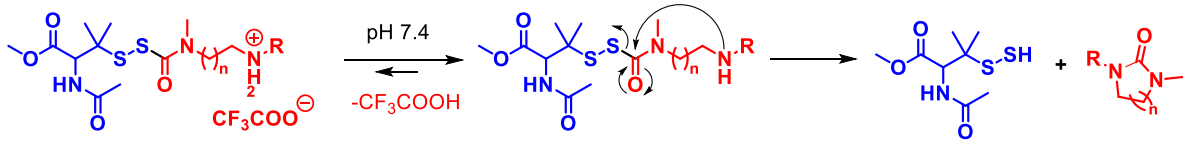

Figure 1.32. Perthiocarbamates, pH-sensitive persulfide precursors.

Ming Xian and co-workers have reported diacyl disulfides as precursors for hydrogen persulfide (H_2S_2). These precursors undergo hydrolysis by following two pathways, one that generates H_2S_2 and the other that generates H_2S and elemental sulfur (S_8) (Figure 1.33).[96] The generation of sulfane sulfur from these precursors can be attributed to a combination of both pathways.

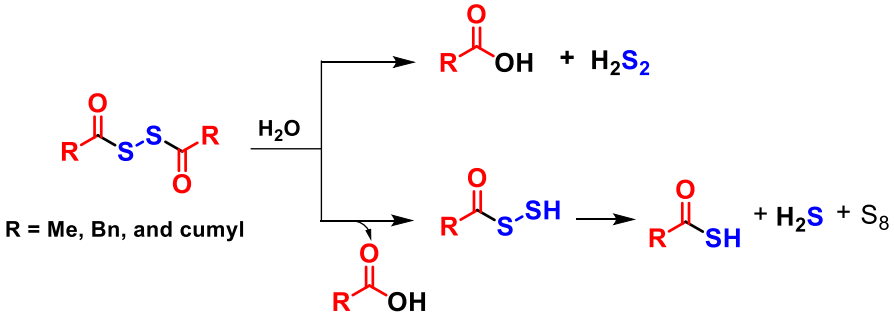

Figure 1.33. Diacyl disulfide hydrolysis-based persulfide precursors.

1.4.2.2. Thiol-activated persulfide generators

Diallyl disulfide (**DADS**) and diallyl trisulfide (**DATS**) are organosulfur compounds derived from garlic, formed as decomposition products of allicin, and are well-known H_2S donors.[97–99] Both compounds have demonstrated promising biological effects, such as inducing relaxation in rat aorta rings, attributed to their H_2S-releasing capability.[100] However, Huang and coworkers have shown that **DADS** releases only a small amount of H_2S through a slow

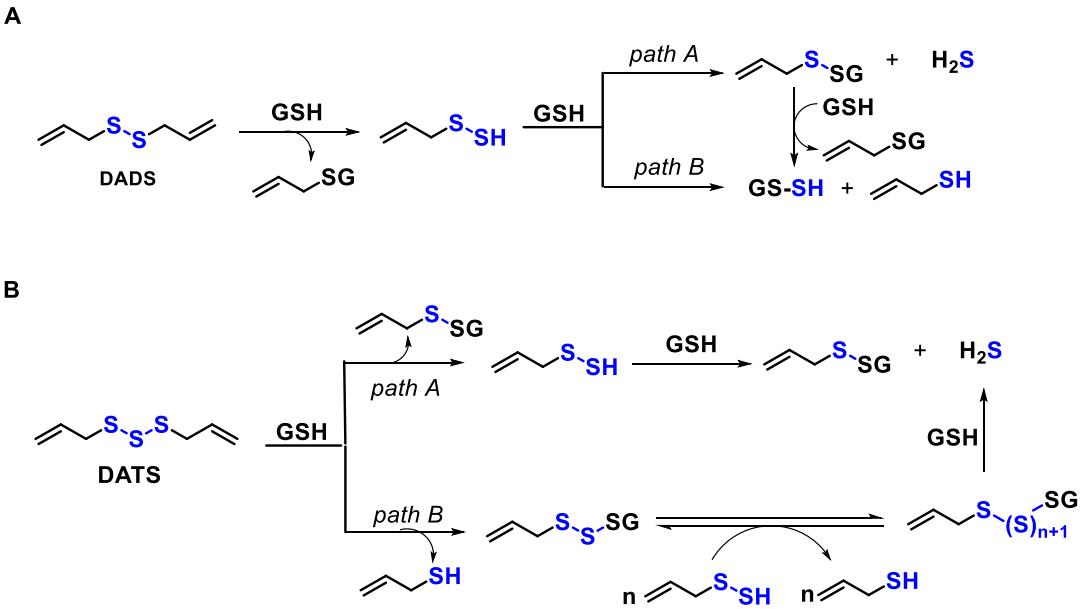

Figure 1.34. Reaction of GSH with (A) diallyl disulfide (**DADS**) and (B) diallyl trisulfide (**DATS**) to produce persulfide and H_2S.

reaction with GSH via an α-carbon nucleophilic substitution pathway (Figure 1.34.A). In contrast, **DATS** reacts quickly with GSH, producing H_2S in high yield (Figure 1.34.B).[101] While the pharmacological effects of garlic-derived polysulfides have traditionally been attributed to H_2S generation, recent studies suggest that reactive sulfur species (RSSH), such as allyl-SSH and GSSH, may play a role in their biological activity.

Ming Xian and group have reported a simple method for generating persulfides and polysulfides from cyclic acyl disulfides.[102] They developed two series of compounds, dithiolane, and benzodithiolane, which were tested with physiologically relevant nucleophiles like thiols and amines. When dithiolanes reacted with *n*-$BuNH_2$, they generated polysulfide species, likely through the formation of a persulfide intermediate. In contrast, reactions with thiols *n*-BuSH appeared to produce multiple intermediates, as thiols can attack both the carbonyl and disulfide functional groups (Figure 1.35.A). On the other hand, benzodithiolane demonstrated greater stability, exhibiting slow reactivity with amines and no reactivity with thiols (Figure 1.35.B).[102]

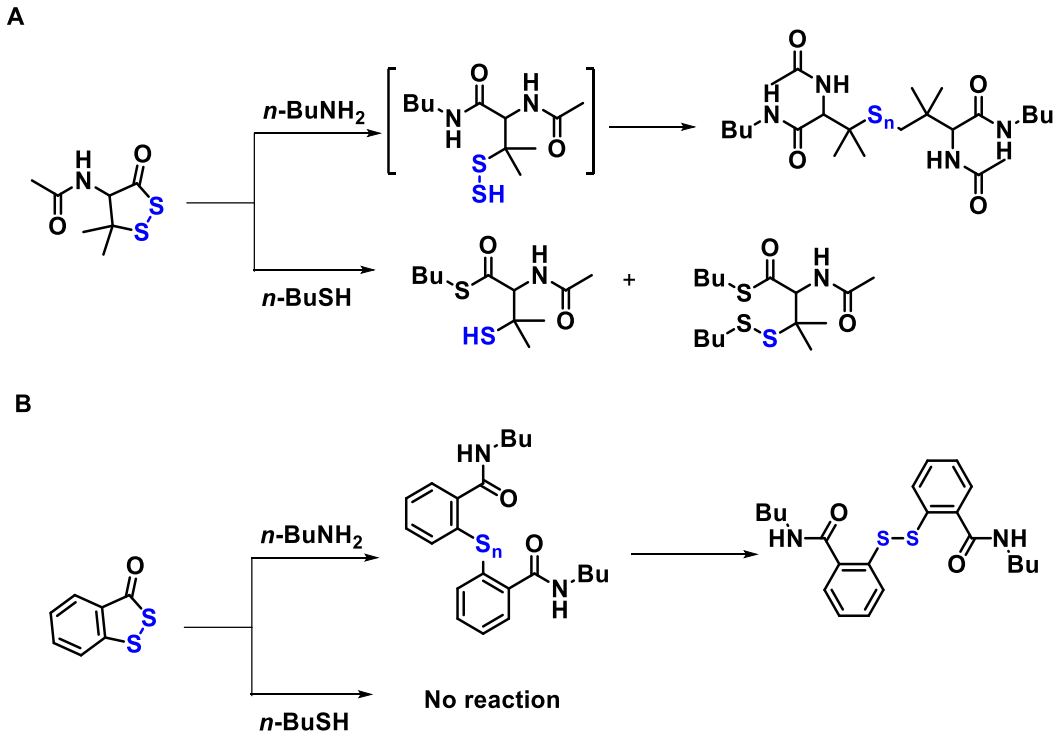

Figure 1.35. Cyclic acyl disulfides (A) dithiolane and (B) Benzodithiolane as persulfide generators.

1.4.2.3. Light-activated persulfide generators

The photochemical release of biomolecules from light-sensitive precursors has been a widely used strategy in biological research, providing precise spatial and temporal control over the

delivery of an effector species. Pradeep Singh and coworkers have reported a one- and two-photon-activated persulfide generator. The *o*-nitro benzyl moiety, upon cleavage by UV light, generates *N*-acetyl cysteine (NAC) persulfide (Figure 1.36).[103] These photo precursors protected the HeLa cells from H_2O_2-induced oxidative stress upon UV irradiation, underlining the cytoprotective property of the RSSH.

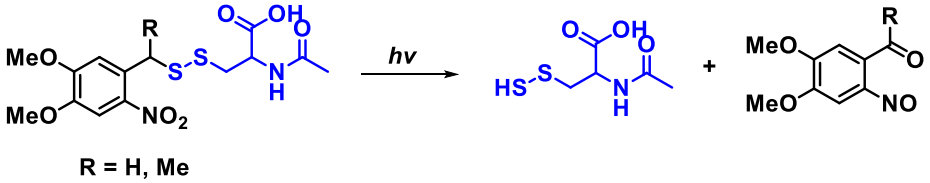

Figure 1.36. UV light-activated persulfide generation from *O*-nitrobenzyl-protected photo precursors.

The same group has reported a light-activated H_2S_2 donor based on an excited-state intramolecular proton transfer (ESIPT) phenomenon. The donor, upon irradiation with light, produces H_2S_2 along with a fluorescence reporter (Figure 1.37).[104]

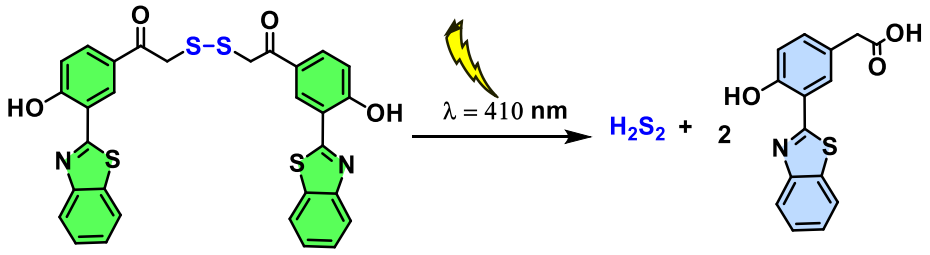

Figure 1.37. Light-activated H_2S_2 generator using ESIPT mechanism.

1.4.3. Limitations with existing persulfide generators

A plethora of persulfide generators have been developed in order to understand the role of persulfide in cellular signaling pathways, but they are associated with certain limitations. Many persulfide donors are chemically unstable and are prone to decomposition or disproportionation, particularly in aqueous or physiological conditions.[23,105,106] The release of the persulfide from some generators is uncontrolled, leading to the reduced efficacy of persulfide and increased side effects. Due to the lack of trigger specificity, site-directed or targeted delivery of persulfide is challenging, limiting its therapeutic potential. Also, most of the persulfide generators are associated with the generation of electrophilic byproducts such as aldehyde and quinone methide, which are cytotoxic in nature.[107,108] To overcome the limitation of electrophilic byproducts, cyclization-based persulfide donors have been developed, which generate innocuous byproducts. The use of light as a stimulus for the

persulfide generation limits its applicability to the cellular system. However, to detect the persulfide generated from the donors, secondary assays are needed, which are associated with some caveats which will be discussed in section 1.5. There are very few persulfide donors developed that produce persulfide along with a fluorescence reporter. The synthetic complexity of the persulfide donors limits their scalability. Hence, to overcome these limitations of existing prodrug strategies, the development of versatile persulfide generators is in urgent need.

1.5. Persulfide detection

Detection of persulfide has been a major challenge due to its short half-life and interference from other reactive sulfur species like thiols, sulfenic acids, and disulfides.[23] Enormous efforts have been made towards developing chemical tools or techniques for the detection and quantification of persulfides.[20,23,25,105,106,109–111]

1.5.1. Direct measurement and electrophilic trapping agents

The initial methods relied on the direct detection of persulfides using NMR and spectrophotometric analysis of RSSH; however, this method is of limited utility as the RSSH UV-visible signature lies between 335 and 340 nm with a weak extinction coefficient (300 M^{-1} cm^{-1}).[112,113] The IR spectra of thiols and persulfides are similar, which limits the applicability in complex mixtures (Figure 1.38.A).[71]

The first reported method for protein persulfide detection was cyanolysis. The cold cyanolysis method involves the cyanide ion (CN^-) attack on the outer sulfur atom of persulfide to produce a thiocyanate ion (SCN^-), which then reacts with a ferric ion (Fe^{3+}) to form a ferric thiocyanate complex $Fe(SCN)_6^{3-}$ (λ_{max} = 460 nm). This allows for the spectroscopic determination of protein persulfide (Figure 1.38.A).[112,114–116] However, due to CN^- ion reactivity with other sulfane sulfur-containing species, this method is only suitable for purified proteins and is not compatible with detecting RSSH in biological samples.

Another spectroscopic method for indirectly detecting protein persulfides involves their reaction with 1-fluoro-2,4-dinitrobenzene, resulting in the formation of mixed disulfides.[116] Subsequent treatment with 1,4-dithiothreitol (DTT) releases 2,4-dinitrobenzenethiol, which exhibits a characteristic absorbance at 408 nm under alkaline conditions (1 M NaOH). Using an extinction coefficient of 13,800 M^{-1} cm^{-1} for 2,4-dinitrobenzenethiol, the concentration of protein persulfides can be determined (Figure 1.38.A).[116]

Researchers have leveraged the nucleophilicity of persulfides to aid in their quantification/identification *via* the addition of electrophilic trapping reagents (Figure 1.38.A).[117,118] Several trapping reagents have been utilized for these purposes, including dinitrofluorobenzene (**FDNB**),[116,119] *N*-ethylmaleimide (**NEM**),[80,120] iodoacetamide (**IAM**) derivatives,[120–123] S-methylmethanethiosulfonate (**MMTS**),[35,78] and monobromobimane (**mBBr**)[21,77] (Figure 1.38.B). The derivatized or trapped persulfide can be detected by LC/MS analysis.

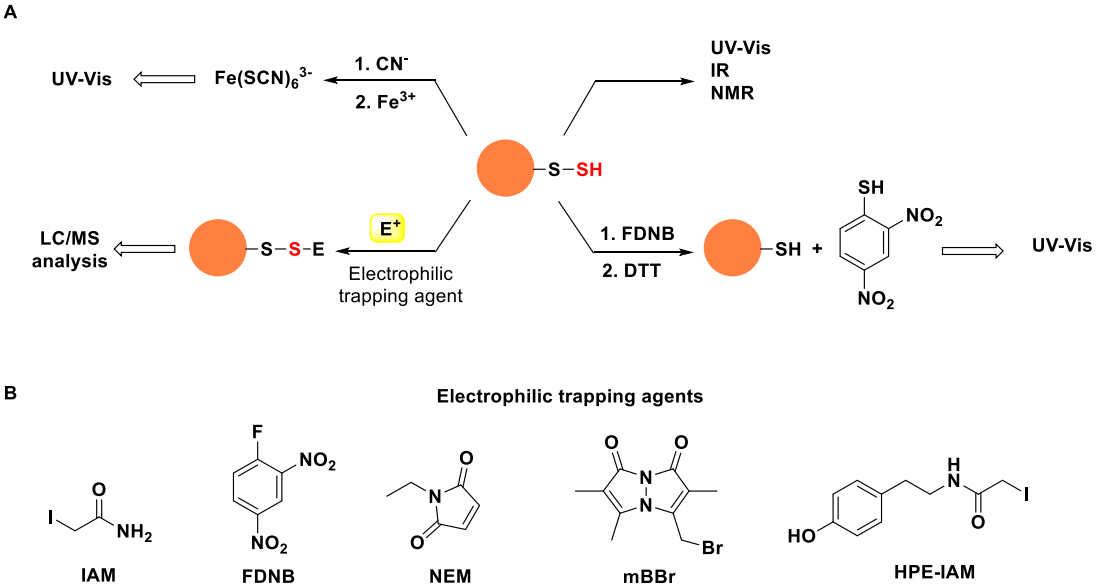

Figure 1.38. (A) Methodological approaches for the detection of persulfides and (B) Structures of the electrophilic (E^+) trapping agents. **IAM**: iodoacetamide, **FDNB**: 1-Fluoro-2,4-dinitrobenzene, **NEM**: *N*-ethyl maleimide, **mBBr**: monobromobimane, **HPE-IAM**: hydroxyphenyl ethyl iodoacetamide.

1.5.2. Persulfide labeling methods

Protein-SSH derivatization has also been used in proteomic studies of protein persulfidation (protein-SSH). Considering that persulfides (-SSH) and thiols (-SH) are nucleophilic species, they both should react with common thiol-blocking or electrophilic reagents (E^+), such as MMTS, IAA, MSBT, etc., in **step 1** to form mixed disulfides. Then, in **step 2**, the electrophilic-tagged persulfides are reduced by DTT or TCEP or attacked by nucleophiles (Nu) labeled with a fluorophore, an affinity tag, etc. Finally, in **step 3**, various techniques such as Western blotting, LC/MS, and fluorescence can be employed to detect the reduced persulfide or the labeled persulfide (Figure 1.39).[23,106,109] Thus, detection of protein-SSH mainly relies on multi-step reactions that first block the –SSH/-SH residues and then manipulate the disulfide adducts generated from –SSH to differentiate –SSH from –SH.[110]

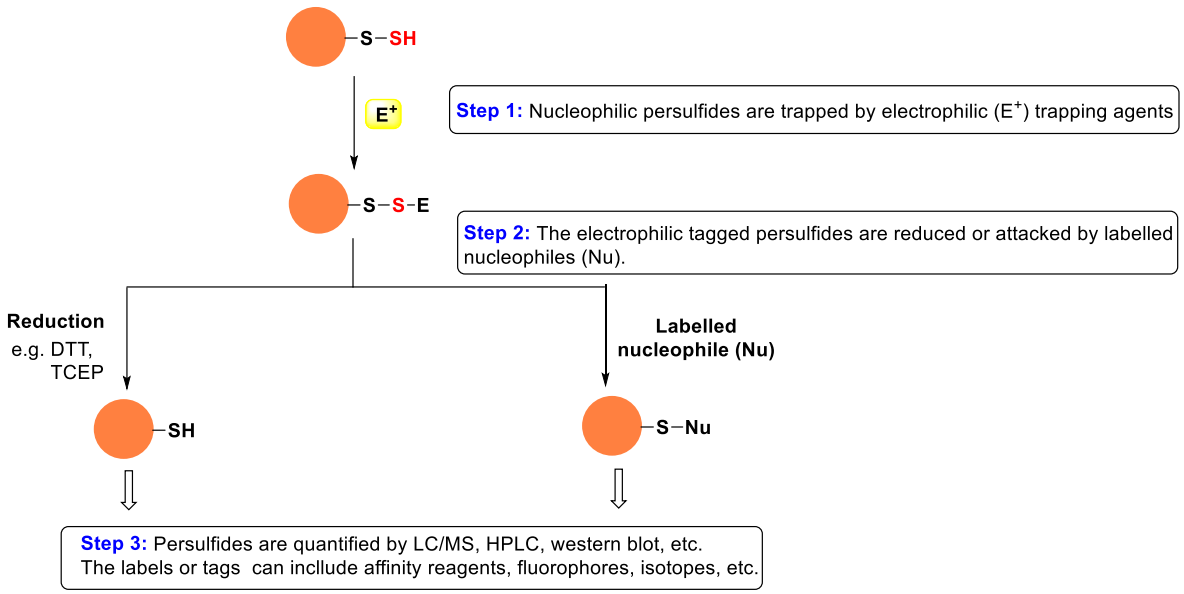

Figure 1.39. Schematic depicting the protocol for the labeling methods used for the detection and quantification of persulfides.

Using the aforementioned protocol, several labeling methods or assays have been developed for the detection and quantification of the protein persulfides. The methods developed so far are summarized in Table 1.1. The first method for labeling protein persulfide was a modified-biotin switch assay reported by Snyder and co-workers using *S*-methylmethanethiosulfonate (**MMTS**) as a blocking agent, biotin-HPDP as a nucleophile and followed by detection of protein persulfide using western blotting.[24,117] Similarly, Tonks and co-workers developed a three-step method to label protein persulfides using iodoacetic acid (**IAA**), dithiothreitol (DTT), and iodoacetamide-linked biotin (**IAP**).[124] This approach was used to study H_2S-mediated inactivation of PTP1B during ER stress, though DTT may cause false positives by reducing native disulfide bonds. Similarly, the protein persulfide derivatized using NEM-fluorophore was detected *via* loss of fluorescent signal.[125]

Ming Xian and co-workers have reported a tag-switch assay by using methylsulfonyl benzothiazole (**MSBT-A**) to block both protein thiols and RSSH.[41,126] Unlike thiols, RSSH forms reactive disulfides with MSBT-A, which can subsequently react with cyanoacetate derivatives containing reporter molecules (e.g., **CN-Cy3**, **CN-Bot**, or **CN-Biotin**). This enables efficient detection of RSSH *via* fluorescence or Western blotting.[41,126] The tag-switch assay strategy can also be found in the dimedone-switch method, where 4-chloro-7-nitrobenzofurazan (**NBF–Cl**) was used as a tag, and then the tagged persulfides were labeled with dimedone-based probes and further detected using Western blotting or LC/MS-MS analysis.[62]

In 2016, Nagy and colleagues developed the Protein Persulfide Detection Protocol (**ProPerDP**), a specific and easy method for detecting protein persulfides in cells and tissues.[127] The protocol involves alkylating protein-SH and –SSH groups with iodoacetyl-PEG_2-biotin (**IAB**), isolating biotin-linked proteins using streptavidin beads, and selectively releasing persulfide-derived proteins with DTT. These proteins can then be quantified or visualized *via* SDS-PAGE.[127]

Around the same time as ProPerDP, Hatzoglou and co-workers developed a biotin-thiol assay (**BTA**) for identifying protein persulfides using a similar mechanism. Maleimide-linked biotin labels protein –SH and –SSH groups, and after trypsin digestion, biotin-labeled peptides are isolated with streptavidin beads.[128] Disulfide-linked peptides are reduced with DTT, eluted, and analyzed *via* LC/MS-MS to identify and quantify persulfides. Another method, **qPerS-SID**, combined with stable isotope labeling, enabled quantitative persulfide proteomics analysis.[129,130]

Our lab has recently developed a "clickable tag-switch" method,[131] where the tag-switch method was modified by using an alkyne-based nucleophile that displaces the protein persulfide tagged with **MSBT-A**, and then the protein-alkyne adduct can be reacted with a commercially available fluorophore azide or biotin azide *via* copper-catalyzed click reaction. Finally, the labeled persulfidated protein can be visualized using SDS-Page or fluorescence.[131] So, using the multistep process, several labeling methods have been developed and utilized for the detection and quantification of the protein persulfides.

Table 1.1. Different protein persulfide labeling methods.

Labelling method	Electrophile or tag	Reducing agent	Nucleophile	Detection technique
Modified-biotin switch assay	1) MMTS 2) IAA 3) NEM-fluorophore	2) DTT 3) DTT	1) Biotin-HPDP 2) IAP-biotin	Western blotting, LC/MS-MS, Fluorescence
Tag-switch assay	MSBT-A		CN-Biotin, CN-Bot, CN-Cy3	Fluorescence, Western blotting, LC/MS-MS
Dimedone-switch assay	NBF-Cl		Dimedone-based probe	Western blotting, LC/MS-MS
Protein Persulfide Detection Protocol (ProPerDP)	IAB	DTT		SDS-PAGE
Biotin Thiol Assay (BTA)	Biotin-maleimide	DTT		LC/MS-MS
Clickable tag-switch assay	MSBT-A		CN-alkyne then fluorophore or biotin azide	SDS-PAGE

1.5.3. Fluorescent probes

Apart from the electrophilic trapping agents and labeling methods, several fluorescent probes have been developed for the analysis of the total sulfane sulfur pool. The first such probes were developed by Ming Xian and co-workers, **SSP1** and **SSP2**.[132] Sulfane sulfur reacts with a nucleophilic thiol in the nonfluorescent **SSP1** or **SSP2** probe to form a persulfide intermediate, which in turn reacts with an electrophilic ester group, leading to spontaneous cyclization and release of the fluorophore (Figure. 1.40.A).[132] Also, additionally, in these series, **SSP4**,[133] **SSP5**,[134] and **SSNIP**[135] has been developed.

The same group has developed a probe, **DSP-3,** for the detection of hydrogen persulfide/polysulfides (H_2S_n).[136] The authors employed 2-fluoro-5-nitrobenzoic ester as the recognition group. The **DSP** probes sense H_2S_n based on a two-step mechanism: an SNAr reaction with the recognition unit and a subsequent intramolecular cyclization by the persulfide intermediate to release the fluorophore (Figure. 1.40.B).[110,136,137] Several other probes have been developed for the detection of H_2S_n.[110,137,138]

Apart from the turn-on fluorescent probes, a few Förster resonance energy transfer (FRET) based fluorophores have been developed for persulfide detection.[139–144] Ojida and co-workers developed the FRET-based dual-emission fluorescent probes that exploit the higher reactivity of persulfides compared to thiols.[144] These probes emit red fluorescence initially, which shifts to blue upon reacting with persulfides, enabling clear differentiation between reacted and unreacted states. A pyronine derivative demonstrated strong selectivity for Na_2S_2 over thiols (Figure 1.40.C).[144]

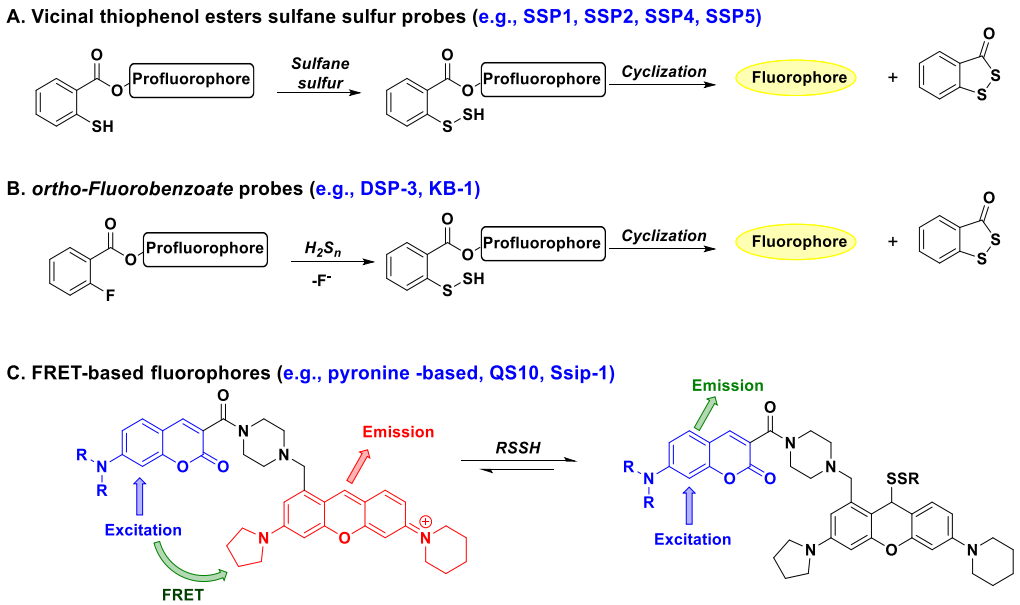

Figure 1.40. Reactions of persulfides with selected sulfane sulfur fluorescent probes.

1.5.4. Limitations with existing methods for persulfide detection

Although several chemical tools or techniques have been developed for the detection and quantification of persulfides, they are associated with certain limitations,[23,105,106,110] such as

1) Selectivity issues: many methods are not able to differentiate the persulfide, thiol, and polysulfides.

2) Stability and reactivity of probes: instability of certain probes in cellular conditions, and they are not highly selective towards persulfide.

3) Quantification challenges: Many methods are qualitative or semi-quantitative, limiting their ability to accurately measure persulfide concentrations. Also, collateral consumption of the persulfide during its detection leads to a lower yield of persulfide.

Several limitations are associated with reported persulfide generators and their detection tools. Therefore, the development of versatile persulfide generators along with the non-electrophilic byproduct and/or fluorescent reporter is in urgent need**.**

1.6. Motivation and outline of the thesis

With the development of reliable tools for the generation and detection of persulfides, their role in cellular signaling and functional significance is becoming clearer. In recent years, small-molecule persulfide generators have gained significant attention as effective persulfidating agents and as a crucial approach to mitigating oxidative and electrophilic stress. Due to the tendency of persulfides to undergo disproportionation in aqueous solutions, researchers have focused on designing in situ persulfide generators and developed an array of persulfide detection tools. The chemical tools for the persulfide generation and detection reported thus far have certain limitations, including:

a) Lack of trigger specificity.

b) Formation of potentially electrophilic byproducts.

c) Need of secondary assays for the detection of persulfides.

To address these gaps, our aim was to design, synthesize, and evaluate persulfide generators with the following characteristics.

a) Cell-permeable and triggerable persulfide generator, and the trigger should be selective.

b) Generation of non-electrophilic byproducts.

c) Fluorescence reporter for the real-time monitoring of persulfide generation to eliminate the need for secondary assays for persulfide detection.

We considered the formation of a lactone as a key step in the generation of persulfide, and this strategy will generate persulfide along with a non-electrophilic lactone as a by-product upon activation by particular stimuli (Figure 1.41). Lactonization in such systems is reported to be quite rapid,[87,145] hence, persulfide generation will likely occur during lactonization, leading to a release of the persulfide as well as the by-product in a single molecular step.

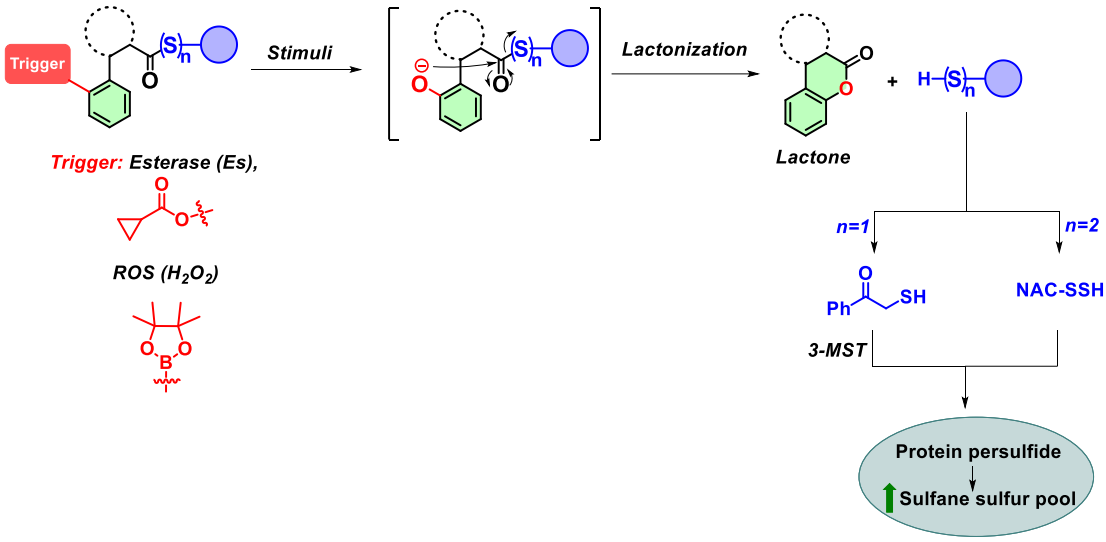

Figure 1.41. Design of persulfide generator using lactonization reaction with non-electrophilic lactone byproduct formation.

Based on the above design, in **Chapter 2,** using a biphenyl-based scaffold, an esterase-sensitive persulfide donor was developed. Upon activation by esterase, this compound produces a persulfide along with a non-electrophilic lactone as a byproduct. Since the lactone is fluorescent, this strategy also produced a reporter for persulfide, enabling the real-time monitoring of persulfide generation. The persulfide generator was able to protect the cells from oxidative stress. Although this persulfide generator eliminates the need for secondary assays for the persulfide detection, it suffered certain drawbacks, such as challenging synthesis and disulfide bonds being susceptible to reaction with the thiols, leading to non-specific reactions.

In **Chapter 3,** using the similar biphenyl scaffold, we next prepared a compound that generates persulfide upon entry into cells. We utilized the persulfide biosynthetic machinery to develop an esterase-sensitive artificial substrate for the enzyme 3-mercaptopyruvate sulfurtransferase (3-MST). The compound was found to efficiently generate H_2S/persulfide in biochemical assays, permeated cells to enhance persulfides, and the compound was found

to promote antioxidant response in chondrocytes. The esterase-activated persulfide generators limit the selectivity due to the ubiquitous nature of esterase.

Next, to enhance the selectivity from a therapeutic benefit standpoint, the reactive oxygen species (ROS)-activated persulfide generators were synthesized. In **Chapter 4.1**, by exploiting the 3-MST persulfide biogenesis, ROS-activated 3-MST artificial substrate was developed. Similar biochemical assays were conducted to validate the H_2S/persulfide generation from the compound in the presence of H_2O_2. The compound exhibited good *in vivo* anti-inflammatory response in animal model.

In **Chapter 4.2,** we extended the same ROS system to another pharmacological thiol, and a WR-1065 prodrug, a known thiol-based radioprotectant, was developed. This prodrug was found to be activated by H_2O_2 to generate the lactone and the pharmacologically active thiol WR-1065.

Together, we have developed two distinct approaches for the generation of persulfide, along with non-electrophilic lactone byproducts, and some have an in-built fluorescence reporter. The approaches developed herein will help address important questions regarding the generation and detection of persulfides and understand their therapeutic utility.

1.7. References

(1) Brosnan, J. T.; Brosnan, M. E. The Sulfur-Containing Amino Acids: An Overview. *J. Nutr.* **2006**, *136* (6), 1636S-1640S.

(2) Nagahara, N. Catalytic Site Cysteines of Thiol Enzyme: Sulfurtransferases. *J. Amino Acids* **2011**, *2011*, 1–7.

(3) Martínez, Y.; Li, X.; Liu, G.; Bin, P.; Yan, W.; Más, D.; Valdivié, M.; Hu, C.-A. A.; Ren, W.; Yin, Y. The Role of Methionine on Metabolism, Oxidative Stress, and Diseases. *Amino Acids* **2017**, *49* (12), 2091–2098.

(4) Mishanina, T. V; Libiad, M.; Banerjee, R. Biogenesis of Reactive Sulfur Species for Signaling by Hydrogen Sulfide Oxidation Pathways. *Nat. Chem. Biol.* **2015**, *11* (7), 457–464.

(5) Kabil, O.; Vitvitsky, V.; Banerjee, R. Sulfur as a Signaling Nutrient Through Hydrogen Sulfide. *Annu. Rev. Nutr.* **2014**, *34* (1), 171–205.

(6) Rouault, T. A.; Tong, W. H. Iron–Sulfur Cluster Biogenesis and Human Disease. *Trends Genet.* **2008**, *24* (8), 398–407.

(7) Meriläinen, G.; Schmitz, W.; Wierenga, R. K.; Kursula, P. The Sulfur Atoms of the Substrate CoA and the Catalytic Cysteine Are Required for a Productive Mode of Substrate Binding in Bacterial Biosynthetic Thiolase, a Thioester-dependent Enzyme. *FEBS J.* **2008**, *275* (24), 6136–6148.

(8) Kessler, D. Enzymatic Activation of Sulfur for Incorporation into Biomolecules in Prokaryotes. *FEMS Microbiol. Rev.* **2006**, *30* (6), 825–840.

(9) Leustek, T. Sulfate Metabolism. *Arab. B.* **2002**, *1*, e0017.

(10) Gallyas, F. Involvement of Redox-signalling in Endogenous Hydrogen Sulfide Production. *Br. J. Pharmacol.* **2012**, *166* (8), 2228–2230.

(11) Stein, A.; Bailey, S. M. Redox Biology of Hydrogen Sulfide: Implications for Physiology, Pathophysiology, and Pharmacology. *Redox Biol.* **2013**, *1* (1), 32–39.

(12) KIMURA, H. Hydrogen Sulfide and Polysulfides as Signaling Molecules. *Proc. Japan Acad. Ser. B* **2015**, *91* (4), 131–159.

(13) Singh, S.; Lin, H. Hydrogen Sulfide in Physiology and Diseases of the Digestive Tract.

Microorganisms **2015**, *3* (4), 866–889.

(14) Xie, Z.-Z.; Liu, Y.; Bian, J.-S. Hydrogen Sulfide and Cellular Redox Homeostasis. *Oxid. Med. Cell. Longev.* **2016**, *2016* (1).

(15) Han, Y.; Shang, Q.; Yao, J.; Ji, Y. Hydrogen Sulfide: A Gaseous Signaling Molecule Modulates Tissue Homeostasis: Implications in Ophthalmic Diseases. *Cell Death Dis.* **2019**, *10* (4), 293.

(16) Baskar, R.; Li, L.; Moore, P. K. Hydrogen Sulfide-induces DNA Damage and Changes in Apoptotic Gene Expression in Human Lung Fibroblast Cells. *FASEB J.* **2007**, *21* (1), 247–255.

(17) Truong, D. H.; Eghbal, M. A.; Hindmarsh, W.; Roth, S. H.; O'Brien, P. J. Molecular Mechanisms of Hydrogen Sulfide Toxicity. *Drug Metab. Rev.* **2006**, *38* (4), 733–744.

(18) Bouroushian, M. *Electrochemistry of Metal Chalcogenides*; Monographs in Electrochemistry; Springer Berlin Heidelberg: Berlin, Heidelberg, 2010.

(19) Bora, P.; Chauhan, P.; Pardeshi, K. A.; Chakrapani, H. Small Molecule Generators of Biologically Reactive Sulfur Species. *RSC Adv.* **2018**, *8* (48), 27359–27374.

(20) Park, C. M.; Weerasinghe, L.; Day, J. J.; Fukuto, J. M.; Xian, M. Persulfides: Current Knowledge and Challenges in Chemistry and Chemical Biology. *Mol. Biosyst.* **2015**, *11* (7), 1775–1785.

(21) Ida, T.; Sawa, T.; Ihara, H.; Tsuchiya, Y.; Watanabe, Y.; Kumagai, Y.; Suematsu, M.; Motohashi, H.; Fujii, S.; Matsunaga, T.; Yamamoto, M.; Ono, K.; Devarie-Baez, N. O.; Xian, M.; Fukuto, J. M.; Akaike, T. Reactive Cysteine Persulfides and S-Polythiolation Regulate Oxidative Stress and Redox Signaling. *Proc. Natl. Acad. Sci.* **2014**, *111* (21), 7606–7611.

(22) Sawa, T.; Motohashi, H.; Ihara, H.; Akaike, T. Enzymatic Regulation and Biological Functions of Reactive Cysteine Persulfides and Polysulfides. *Biomolecules* **2020**, *10* (9), 1245.

(23) Filipovic, M. R.; Zivanovic, J.; Alvarez, B.; Banerjee, R. Chemical Biology of H 2 S Signaling through Persulfidation. *Chem. Rev.* **2018**, *118* (3), 1253–1337.

(24) Mustafa, A. K.; Gadalla, M. M.; Sen, N.; Kim, S.; Mu, W.; Gazi, S. K.; Barrow, R. K.;

Yang, G.; Wang, R.; Snyder, S. H. H 2 S Signals Through Protein S-Sulfhydration. *Sci. Signal.* **2009**, *2* (96).

(25) Yang, C.; Devarie-Baez, N. O.; Hamsath, A.; Fu, X.; Xian, M. S-Persulfidation: Chemistry, Chemical Biology, and Significance in Health and Disease. *Antioxid. Redox Signal.* **2020**, *33* (15), 1092–1114.

(26) Paulsen, C. E.; Carroll, K. S. Cysteine-Mediated Redox Signaling: Chemistry, Biology, and Tools for Discovery. *Chem. Rev.* **2013**, *113* (7), 4633–4679.

(27) Filipovic, M. R. *Persulfidation (S-Sulfhydration) and H 2 S*; 2015.

(28) Dóka, É.; Ida, T.; Dagnell, M.; Abiko, Y.; Luong, N. C.; Balog, N.; Takata, T.; Espinosa, B.; Nishimura, A.; Cheng, Q.; Funato, Y.; Miki, H.; Fukuto, J. M.; Prigge, J. R.; Schmidt, E. E.; Arnér, E. S. J.; Kumagai, Y.; Akaike, T.; Nagy, P. Control of Protein Function through Oxidation and Reduction of Persulfidated States. *Sci. Adv.* **2020**, *6* (1).

(29) Yang, G.; Zhao, K.; Ju, Y.; Mani, S.; Cao, Q.; Puukila, S.; Khaper, N.; Wu, L.; Wang, R. Hydrogen Sulfide Protects Against Cellular Senescence via S -Sulfhydration of Keap1 and Activation of Nrf2. *Antioxid. Redox Signal.* **2013**, *18* (15), 1906–1919.

(30) Aggarwal, B. B.; Gupta, S. C.; Kim, J. H. Historical Perspectives on Tumor Necrosis Factor and Its Superfamily: 25 Years Later, a Golden Journey. *Blood* **2012**, *119* (3), 651–665.

(31) Du, J.; Huang, Y.; Yan, H.; Zhang, Q.; Zhao, M.; Zhu, M.; Liu, J.; Chen, S. X.; Bu, D.; Tang, C.; Jin, H. Hydrogen Sulfide Suppresses Oxidized Low-Density Lipoprotein (Ox-LDL)-Stimulated Monocyte Chemoattractant Protein 1 Generation from Macrophages via the Nuclear Factor KB (NF-KB) Pathway. *J. Biol. Chem.* **2014**, *289* (14), 9741–9753.

(32) Zhang, T.; Ono, K.; Tsutsuki, H.; Ihara, H.; Islam, W.; Akaike, T.; Sawa, T. Enhanced Cellular Polysulfides Negatively Regulate TLR4 Signaling and Mitigate Lethal Endotoxin Shock. *Cell Chem. Biol.* **2019**, *26* (5), 686-698.e4.

(33) Giovinazzo, D.; Bursac, B.; Sbodio, J. I.; Nalluru, S.; Vignane, T.; Snowman, A. M.; Albacarys, L. M.; Sedlak, T. W.; Torregrossa, R.; Whiteman, M.; Filipovic, M. R.; Snyder, S. H.; Paul, B. D. Hydrogen Sulfide Is Neuroprotective in Alzheimer's Disease

by Sulfhydrating GSK3β and Inhibiting Tau Hyperphosphorylation. *Proc. Natl. Acad. Sci.* **2021**, *118* (4).

(34) Hannula, M. J.; Myöhänen, T. T.; Tenorio-Laranga, J.; Männistö, P. T.; Garcia-Horsman, J. A. Prolyl Oligopeptidase Colocalizes with α-Synuclein, β-Amyloid, Tau Protein and Astroglia in the Post-Mortem Brain Samples with Parkinson's and Alzheimer's Diseases. *Neuroscience* **2013**, *242*, 140–150.

(35) Vandiver, M. S.; Paul, B. D.; Xu, R.; Karuppagounder, S.; Rao, F.; Snowman, A. M.; Seok Ko, H.; Il Lee, Y.; Dawson, V. L.; Dawson, T. M.; Sen, N.; Snyder, S. H. Sulfhydration Mediates Neuroprotective Actions of Parkin. *Nat. Commun.* **2013**, *4* (1), 1626.

(36) Zhao, K.; Ju, Y.; Li, S.; Altaany, Z.; Wang, R.; Yang, G. S-sulfhydration of <scp>MEK</Scp> 1 Leads to <scp>PARP</Scp> -1 Activation and <scp>DNA</Scp> Damage Repair. *EMBO Rep.* **2014**, *15* (7), 792–800.

(37) Kang, M.; Hashimoto, A.; Gade, A.; Akbarali, H. I. Interaction between Hydrogen Sulfide-Induced Sulfhydration and Tyrosine Nitration in the K ATP Channel Complex. *Am. J. Physiol. Liver Physiol.* **2015**, *308* (6), G532–G539.

(38) Kaspar, J. W.; Niture, S. K.; Jaiswal, A. K. Nrf2:INrf2 (Keap1) Signaling in Oxidative Stress. *Free Radic. Biol. Med.* **2009**, *47* (9), 1304–1309.

(39) Woo, H. A.; Chae, H. Z.; Hwang, S. C.; Yang, K.-S.; Kang, S. W.; Kim, K.; Rhee, S. G. Reversing the Inactivation of Peroxiredoxins Caused by Cysteine Sulfinic Acid Formation. *Science (80-.).* **2003**, *300* (5619), 653–656.

(40) Wood, Z. A.; Poole, L. B.; Karplus, P. A. Peroxiredoxin Evolution and the Regulation of Hydrogen Peroxide Signaling. *Science (80-.).* **2003**, *300* (5619), 650–653.

(41) Wedmann, R.; Onderka, C.; Wei, S.; Szijártó, I. A.; Miljkovic, J. L.; Mitrovic, A.; Lange, M.; Savitsky, S.; Yadav, P. K.; Torregrossa, R.; Harrer, E. G.; Harrer, T.; Ishii, I.; Gollasch, M.; Wood, M. E.; Galardon, E.; Xian, M.; Whiteman, M.; Banerjee, R.; Filipovic, M. R. Improved Tag-Switch Method Reveals That Thioredoxin Acts as Depersulfidase and Controls the Intracellular Levels of Protein Persulfidation. *Chem. Sci.* **2016**, *7* (5), 3414–3426.

(42) YAMANISHI, T.; TUBOI, S. The Mechanism of the L-Cystine Cleavage Reaction

Catalyzed by Rat Liver γ-Cystathionase1. *J. Biochem.* **1981**, *89* (6), 1913–1921.

(43) Akaike, T.; Ida, T.; Wei, F.-Y.; Nishida, M.; Kumagai, Y.; Alam, M. M.; Ihara, H.; Sawa, T.; Matsunaga, T.; Kasamatsu, S.; Nishimura, A.; Morita, M.; Tomizawa, K.; Nishimura, A.; Watanabe, S.; Inaba, K.; Shima, H.; Tanuma, N.; Jung, M.; Fujii, S.; Watanabe, Y.; Ohmuraya, M.; Nagy, P.; Feelisch, M.; Fukuto, J. M.; Motohashi, H. Cysteinyl-TRNA Synthetase Governs Cysteine Polysulfidation and Mitochondrial Bioenergetics. *Nat. Commun.* **2017**, *8* (1), 1177.

(44) Melideo, S. L.; Jackson, M. R.; Jorns, M. S. Biosynthesis of a Central Intermediate in Hydrogen Sulfide Metabolism by a Novel Human Sulfurtransferase and Its Yeast Ortholog. *Biochemistry* **2014**, *53* (28), 4739–4753.

(45) Nagahara, N.; Yoshii, T.; Abe, Y.; Matsumura, T. Thioredoxin-Dependent Enzymatic Activation of Mercaptopyruvate Sulfurtransferase. *J. Biol. Chem.* **2007**, *282* (3), 1561–1569.

(46) Bordo, D.; Bork, P. The Rhodanese/Cdc25 Phosphatase Superfamily. *EMBO Rep.* **2002**, *3* (8), 741–746.

(47) Mueller, E. G. Trafficking in Persulfides: Delivering Sulfur in Biosynthetic Pathways. *Nat. Chem. Biol.* **2006**, *2* (4), 185–194.

(48) Nagasawa, H. T.; Goon, D. J. W.; Crankshaw, D. L.; Vince, R.; Patterson, S. E. Novel, Orally Effective Cyanide Antidotes. *J. Med. Chem.* **2007**, *50* (26), 6462–6464.

(49) Huang, J.; Niknahad, H.; Khan, S.; O'Brien, P. J. Hepatocyte-Catalysed Detoxification of Cyanide by l- and d-Cysteine. *Biochem. Pharmacol.* **1998**, *55* (12), 1983–1990.

(50) Yadav, P. K.; Yamada, K.; Chiku, T.; Koutmos, M.; Banerjee, R. Structure and Kinetic Analysis of H2S Production by Human Mercaptopyruvate Sulfurtransferase. *J. Biol. Chem.* **2013**, *288* (27), 20002–20013.

(51) Libiad, M.; Yadav, P. K.; Vitvitsky, V.; Martinov, M.; Banerjee, R. Organization of the Human Mitochondrial Hydrogen Sulfide Oxidation Pathway. *J. Biol. Chem.* **2014**, *289* (45), 30901–30910.

(52) Nagahara, N.; Katayama, A. Post-Translational Regulation of Mercaptopyruvate Sulfurtransferase via a Low Redox Potential Cysteine-Sulfenate in the Maintenance of Redox Homeostasis. *J. Biol. Chem.* **2005**, *280* (41), 34569–34576.

(53) Nagahara, N.; Nishino, T. Role of Amino Acid Residues in the Active Site of Rat Liver Mercaptopyruvate Sulfurtransferase. *J. Biol. Chem.* **1996**, *271* (44), 27395–27401.

(54) Shibuya, N.; Tanaka, M.; Yoshida, M.; Ogasawara, Y.; Togawa, T.; Ishii, K.; Kimura, H. 3-Mercaptopyruvate Sulfurtransferase Produces Hydrogen Sulfide and Bound Sulfane Sulfur in the Brain. *Antioxid. Redox Signal.* **2009**, *11* (4), 703–714.

(55) Huang, G.-T.; Yu, J.-S. K. Enzyme Catalysis That Paves the Way for S-Sulfhydration via Sulfur Atom Transfer. *J. Phys. Chem. B* **2016**, *120* (20), 4608–4615.

(56) Rao, S. P.; Dobariya, P.; Bellamkonda, H.; More, S. S. Role of 3-Mercaptopyruvate Sulfurtransferase (3-MST) in Physiology and Disease. *Antioxidants* **2023**, *12* (3), 603.

(57) Caira, S.; Iannelli, A.; Sciarrillo, R.; Picariello, G.; Renzone, G.; Scaloni, A.; Addeo, P. Differential Representation of Liver Proteins in Obese Human Subjects Suggests Novel Biomarkers and Promising Targets for Drug Development in Obesity. *J. Enzyme Inhib. Med. Chem.* **2017**, *32* (1), 672–682.

(58) Li, M.; Xu, C.; Shi, J.; Ding, J.; Wan, X.; Chen, D.; Gao, J.; Li, C.; Zhang, J.; Lin, Y.; Tu, Z.; Kong, X.; Li, Y.; Yu, C. Fatty Acids Promote Fatty Liver Disease via the Dysregulation of 3-Mercaptopyruvate Sulfurtransferase/Hydrogen Sulfide Pathway. *Gut* **2018**, *67* (12), 2169–2180.

(59) Ide, M.; Ohnishi, T.; Toyoshima, M.; Balan, S.; Maekawa, M.; Shimamoto-Mitsuyama, C.; Iwayama, Y.; Ohba, H.; Watanabe, A.; Ishii, T.; Shibuya, N.; Kimura, Y.; Hisano, Y.; Murata, Y.; Hara, T.; Morikawa, M.; Hashimoto, K.; Nozaki, Y.; Toyota, T.; Wada, Y.; Tanaka, Y.; Kato, T.; Nishi, A.; Fujisawa, S.; Okano, H.; Itokawa, M.; Hirokawa, N.; Kunii, Y.; Kakita, A.; Yabe, H.; Iwamoto, K.; Meno, K.; Katagiri, T.; Dean, B.; Uchida, K.; Kimura, H.; Yoshikawa, T. Excess Hydrogen Sulfide and Polysulfides Production Underlies a Schizophrenia Pathophysiology. *EMBO Mol. Med.* **2019**, *11* (12).

(60) Nagahara, N.; Nagano, M.; Ito, T.; Suzuki, H. Redox Regulation of Mammalian 3-Mercaptopyruvate Sulfurtransferase; 2015; pp 229–254.

(61) Tomita, M.; Nagahara, N.; Ito, T. Expression of 3-Mercaptopyruvate Sulfurtransferase in the Mouse. *Molecules* **2016**, *21* (12), 1707.

(62) Zivanovic, J.; Kouroussis, E.; Kohl, J. B.; Adhikari, B.; Bursac, B.; Schott-Roux, S.;

Petrovic, D.; Miljkovic, J. L.; Thomas-Lopez, D.; Jung, Y.; Miler, M.; Mitchell, S.; Milosevic, V.; Gomes, J. E.; Benhar, M.; Gonzalez-Zorn, B.; Ivanovic-Burmazovic, I.; Torregrossa, R.; Mitchell, J. R.; Whiteman, M.; Schwarz, G.; Snyder, S. H.; Paul, B. D.; Carroll, K. S.; Filipovic, M. R. Selective Persulfide Detection Reveals Evolutionarily Conserved Antiaging Effects of S-Sulfhydration. *Cell Metab.* **2019**, *30* (6), 1152-1170.e13.

(63) Zhang, Y.; Yang, J.; Wang, T.; Wang, S.-G.; Liu, J.-H.; Yin, C.-P.; Ye, Z.-Q. Decreased Endogenous Hydrogen Sulfide Generation in Penile Tissues of Diabetic Rats with Erectile Dysfunction. *J. Sex. Med.* **2016**, *13* (3), 350–360.

(64) Jin, S.; Pu, S.-X.; Hou, C.-L.; Ma, F.-F.; Li, N.; Li, X.-H.; Tan, B.; Tao, B.-B.; Wang, M.-J.; Zhu, Y.-C. Cardiac H 2 S Generation Is Reduced in Ageing Diabetic Mice. *Oxid. Med. Cell. Longev.* **2015**, *2015*, 1–14.

(65) Suwanai, Y. Functional Analysis of 3-Mercaptopyruvate Sulfurtransferase Using Knockout Mice. *Adv. Tech. Biol. Med.* **2015**, *04* (01).

(66) Nasi, S.; Ehirchiou, D.; Chatzianastasiou, A.; Nagahara, N.; Papapetropoulos, A.; Bertrand, J.; Cirino, G.; So, A.; Busso, N. The Protective Role of the 3-Mercaptopyruvate Sulfurtransferase (3-MST)-Hydrogen Sulfide (H2S) Pathway against Experimental Osteoarthritis. *Arthritis Res. Ther.* **2020**, *22* (1), 49.

(67) Kawamura, S.; Kitao, T.; Nakabayashi, T.; Horii, T.; Tsurugi, J. Aralkyl Hydrodisulfides. VIII. Alkaline Decomposition and Its Competition with Nucleophiles. *J. Org. Chem.* **1968**, *33* (3), 1179–1181.

(68) Von Horst Bohme und Gerwalt Zinner. Uber Darstellung Und Eigenschaften Von. *Justus Liebigs Ann. der Chemie*, **1954**, *585* (1952), 142–149.

(69) Heimer, N. E.; Field, L.; Waites, J. A. Organic Disulfides and Related Substances. 44. Preparation and Characterization of 1-Adamantyl Hydrodisulfide as a Stable Prototype of the Series. *J. Org. Chem.* **1985**, *50* (21), 4164–4166.

(70) Bailey, T. S.; Zakharov, L. N.; Pluth, M. D. Understanding Hydrogen Sulfide Storage: Probing Conditions for Sulfide Release from Hydrodisulfides. *J. Am. Chem. Soc.* **2014**, *136* (30), 10573–10576.

(71) Bailey, T. S.; Pluth, M. D. Reactions of Isolated Persulfides Provide Insights into the

Interplay between H2S and Persulfide Reactivity. *Free Radic. Biol. Med.* **2015**, *89*, 662–667.

(72) Santini, V.; Giles, F. J. The Potential of Amifostine: From Cytoprotectant to Therapeutic Agent. *Haematologica* **1999**, *84* (11), 1035–1042.

(73) Koukourakis, M. I. Review Paper Amifostine in Clinical Oncology : Current Use and Future Applications. **2002**, *13*, 181–209.

(74) Dziegielewski, J.; Baulch, J. E.; Goetz, W.; Coleman, M. C.; Spitz, D. R.; Murley, J. S.; Grdina, D. J.; Morgan, W. F. WR-1065, the Active Metabolite of Amifostine, Mitigates Radiation-Induced Delayed Genomic Instability. *Free Radic. Biol. Med.* **2008**, *45* (12), 1674–1681.

(75) Singh, V. K.; Seed, T. M. The Efficacy and Safety of Amifostine for the Acute Radiation Syndrome. *Expert Opin. Drug Saf.* **2019**, *18* (11), 1077–1090.

(76) Bora, P.; Manna, S.; Nair, M. A.; Sathe, R. R. M.; Singh, S.; Sreyas Adury, V. S.; Gupta, K.; Mukherjee, A.; Saini, D. K.; Kamat, S. S.; Hazra, A. B.; Chakrapani, H. Leveraging an Enzyme/Artificial Substrate System to Enhance Cellular Persulfides and Mitigate Neuroinflammation. *Chem. Sci.* **2021**, *12* (39), 12939–12949.

(77) Park, C. M.; Johnson, B. A.; Duan, J.; Park, J. J.; Day, J. J.; Gang, D.; Qian, W. J.; Xian, M. 9-Fluorenylmethyl (Fm) Disulfides: Biomimetic Precursors for Persulfides. *Org. Lett.* **2016**, *18* (5), 904–907.

(78) Zheng, Y.; Yu, B.; Li, Z.; Yuan, Z.; Organ, C. L.; Trivedi, R. K.; Wang, S.; Lefer, D. J.; Wang, B. An Esterase-Sensitive Prodrug Approach for Controllable Delivery of Persulfide Species. *Angew. Chemie Int. Ed.* **2017**, *56* (39), 11749–11753.

(79) Kang, J.; Xu, S.; Radford, M. N.; Zhang, W.; Kelly, S. S.; Day, J. J.; Xian, M. O→S Relay Deprotection: A General Approach to Controllable Donors of Reactive Sulfur Species. *Angew. Chemie Int. Ed.* **2018**, *57* (20), 5893–5897.

(80) Khodade, V. S.; Toscano, J. P. Development of S -Substituted Thioisothioureas as Efficient Hydropersulfide Precursors. *J. Am. Chem. Soc.* **2018**, *140* (50), 17333–17337.

(81) Bora, P.; Chauhan, P.; Manna, S.; Chakrapani, H. A Vinyl-Boronate Ester-Based Persulfide Donor Controllable by Hydrogen Peroxide, a Reactive Oxygen Species (ROS). *Org. Lett.* **2018**, *20* (24), 7916–7920.

(82) Powell, C. R.; Dillon, K. M.; Wang, Y.; Carrazzone, R. J.; Matson, J. B. A Persulfide Donor Responsive to Reactive Oxygen Species: Insights into Reactivity and Therapeutic Potential. *Angew. Chemie Int. Ed.* **2018**, *57* (21), 6324–6328.

(83) Dillon, K. M.; Morrison, H. A.; Powell, C. R.; Carrazzone, R. J.; Ringel-Scaia, V. M.; Winckler, E. W.; Council-Troche, R. M.; Allen, I. C.; Matson, J. B. Targeted Delivery of Persulfides to the Gut: Effects on the Microbiome. *Angew. Chemie Int. Ed.* **2021**, *60* (11), 6061–6067.

(84) Dillon, K. M.; Carrazzone, R. J.; Wang, Y.; Powell, C. R.; Matson, J. B. Polymeric Persulfide Prodrugs: Mitigating Oxidative Stress through Controlled Delivery of Reactive Sulfur Species. *ACS Macro Lett.* **2020**, *9* (4), 606–612.

(85) Wang, Y.; Dillon, K. M.; Li, Z.; Winckler, E. W.; Matson, J. B. Alleviating Cellular Oxidative Stress through Treatment with Superoxide-Triggered Persulfide Prodrugs. *Angew. Chemie Int. Ed.* **2020**, *59* (38), 16698–16704.

(86) Xu, Y.; Xu, B.; Wang, J.; Jin, H.; Xu, S.; Wang, G.; Zhen, L. Peroxynitrite-Promoted Persulfide Prodrugs with Protective Potential against Paracetamol Poisoning. *Chem. – A Eur. J.* **2022**, No. Figure 1.

(87) Levine, M. N.; Raines, R. T. Trimethyl Lock: A Trigger for Molecular Release in Chemistry, Biology, and Pharmacology. *Chem. Sci.* **2012**, *3* (8), 2412.

(88) Yuan, Z.; Zheng, Y.; Yu, B.; Wang, S.; Yang, X.; Wang, B. Esterase-Sensitive Glutathione Persulfide Donor. *Org. Lett.* **2018**, *20* (20), 6364–6367.

(89) Yu, B.; Zheng, Y.; Yuan, Z.; Li, S.; Zhu, H.; De La Cruz, L. K.; Zhang, J.; Ji, K.; Wang, S.; Wang, B. Toward Direct Protein S-Persulfidation: A Prodrug Approach That Directly Delivers Hydrogen Persulfide. *J. Am. Chem. Soc.* **2018**, *140* (1), 30–33.

(90) Hankins, R. A.; Suarez, S. I.; Kalk, M. A.; Green, N. M.; Harty, M. N.; Lukesh, J. C. An Innovative Hydrogen Peroxide-Sensing Scaffold and Insight Towards Its Potential as an ROS-Activated Persulfide Donor. *Angew. Chemie - Int. Ed.* **2020**, *59* (49), 22238–22245.

(91) Bora, P.; Sathian, M. B.; Chakrapani, H. Enhancing Cellular Sulfane Sulfur through β-Glycosidase-Activated Persulfide Donors: Mechanistic Insights and Oxidative Stress Mitigation. *Chem. Commun.* **2022**, *58* (18), 2987–2990.

(92) Yu, B.; Kang, T.; Xu, Y.; Liu, Y.; Ma, Y.; Ke, B. Prodrugs of Persulfide and Sulfide: Is There a Pharmacological Difference between the Two in the Context of Rapid Exchanges among Various Sulfur Species In Vivo ? *Angew. Chemie Int. Ed.* **2022**, *61* (20).

(93) Artaud, I.; Galardon, E. A Persulfide Analogue of the Nitrosothiol SNAP: Formation, Characterization and Reactivity. *ChemBioChem* **2014**, *15* (16), 2361–2364.

(94) Zhang, X.; Chen, M.; Ni, X.; Wang, Y.; Zheng, X.; Zhang, H.; Xu, S.; Yang, C. Metabolic Reprogramming of Sulfur in Hepatocellular Carcinoma and Sulfane Sulfur-Triggered Anti-Cancer Strategy. *Front. Pharmacol.* **2020**, *11*.

(95) Khodade, V. S.; Pharoah, B. M.; Paolocci, N.; Toscano, J. P. Alkylamine-Substituted Perthiocarbamates: Dual Precursors to Hydropersulfide and Carbonyl Sulfide with Cardioprotective Actions. *J. Am. Chem. Soc.* **2020**, *142* (9), 4309–4316.

(96) Xu, S.; Wang, Y.; Parent, Z.; Xian, M. Diacyl Disulfides as the Precursors for Hydrogen Persulfide (H2S2). *Bioorg. Med. Chem. Lett.* **2020**, *30* (4), 126903.

(97) Munday, R.; Munday, J. S.; Munday, C. M. Comparative Effects of Mono-, Di-, Tri-, and Tetrasulfides Derived from Plants of the Allium Family: Redox Cycling in Vitro and Hemolytic Activity and Phase 2 Enzyme Induction in Vivo. *Free Radic. Biol. Med.* **2003**, *34* (9), 1200–1211.

(98) Yagdi, E.; Cerella, C.; Dicato, M.; Diederich, M. Garlic-Derived Natural Polysulfanes as Hydrogen Sulfide Donors: Friend or Foe? *Food Chem. Toxicol.* **2016**, *95*, 219–233.

(99) Pluth, M.; Bailey, T.; Hammers, M.; Hartle, M.; Henthorn, H.; Steiger, A. Natural Products Containing Hydrogen Sulfide Releasing Moieties. *Synlett* **2015**, *26* (19), 2633–2643.

(100) Benavides, G. A.; Squadrito, G. L.; Mills, R. W.; Patel, H. D.; Isbell, T. S.; Patel, R. P.; Darley-Usmar, V. M.; Doeller, J. E.; Kraus, D. W. Hydrogen Sulfide Mediates the Vasoactivity of Garlic. *Proc. Natl. Acad. Sci.* **2007**, *104* (46), 17977–17982.

(101) Liang, D.; Wu, H.; Wong, M. W.; Huang, D. Diallyl Trisulfide Is a Fast H 2 S Donor, but Diallyl Disulfide Is a Slow One: The Reaction Pathways and Intermediates of Glutathione with Polysulfides. *Org. Lett.* **2015**, *17* (17), 4196–4199.

(102) Kang, J.; Ferrell, A. J.; Chen, W.; Wang, D.; Xian, M. Cyclic Acyl Disulfides and Acyl

Selenylsulfides as the Precursors for Persulfides (RSSH), Selenylsulfides (RSeSH), and Hydrogen Sulfide (H 2 S). *Org. Lett.* **2018**, *20* (3), 852–855.

(103) Chaudhuri, A.; Venkatesh, Y.; Das, J.; Gangopadhyay, M.; Maiti, T. K.; Singh, N. D. P. One- and Two-Photon-Activated Cysteine Persulfide Donors for Biological Targeting. *J. Org. Chem.* **2019**, *84* (18), 11441–11449.

(104) Chaudhuri, A.; Venkatesh, Y.; Jena, B. C.; Behara, K. K.; Mandal, M.; Singh, N. D. P. Real-Time Monitoring of a Photoactivated Hydrogen Persulfide Donor for Biological Entities. *Org. Biomol. Chem.* **2019**, *17* (39), 8800–8805.

(105) Dillon, K. M.; Matson, J. B. A Review of Chemical Tools for Studying Small Molecule Persulfides: Detection and Delivery. *ACS Chem. Biol.* **2021**, *16* (7), 1128–1141.

(106) Khodade, V. S.; Aggarwal, S. C.; Eremiev, A.; Bao, E.; Porche, S.; Toscano, J. P. Development of Hydropersulfide Donors to Study Their Chemical Biology. *Antioxid. Redox Signal.* **2022**, *36* (4–6), 309–326.

(107) Thompson, D. C.; Thompson, J. A.; Sugumaran, M.; Moldéus, P. Biological and Toxicological Consequences of Quinone Methide Formation. *Chem. Biol. Interact.* **1993**, *86* (2), 129–162.

(108) Ali, K.; Mishra, P.; Kumar, A.; Reddy, D. N.; Chowdhury, S.; Panda, G. Reactivity vs. Selectivity of Quinone Methides: Synthesis of Pharmaceutically Important Molecules, Toxicity and Biological Applications. *Chem. Commun.* **2022**, *58* (42), 6160–6175.

(109) Lau, N.; Pluth, M. D. Reactive Sulfur Species (RSS): Persulfides, Polysulfides, Potential, and Problems. *Curr. Opin. Chem. Biol.* **2019**, *49*, 1–8.

(110) Shieh, M.; Xu, S.; Lederberg, O. L.; Xian, M. Detection of Sulfane Sulfur Species in Biological Systems. *Redox Biol.* **2022**, *57*, 102502.

(111) Vignane, T.; Filipovic, M. R. Emerging Chemical Biology of Protein Persulfidation. *Antioxid. Redox Signal.* **2023**, *39* (1–3), 19–39.

(112) Wood, J. L. Sulfane Sulfur; 1987; pp 25–29.

(113) Cuevasanta, E.; Möller, M. N.; Alvarez, B. Biological Chemistry of Hydrogen Sulfide and Persulfides. *Arch. Biochem. Biophys.* **2017**, *617*, 9–25.

(114) Massey, V.; Edmondson, D. On the Mechanism of Inactivation of Xanthine Oxidase

by Cyanide. *J. Biol. Chem.* **1970**, *245* (24), 6595–6598.

(115) Toohey, J. I. Sulphane Sulphur in Biological Systems: A Possible Regulatory Role. *Biochem. J.* **1989**, *264* (3), 625–632.

(116) Branzoli, U.; Massey, V. Evidence for an Active Site Persulfide Residue in Rabbit Liver Aldehyde Oxidase. *J. Biol. Chem.* **1974**, *249* (14), 4346–4349.

(117) Pan, J.; Carroll, K. S. Persulfide Reactivity in the Detection of Protein S -Sulfhydration. *ACS Chem. Biol.* **2013**, *8* (6), 1110–1116.

(118) Cuevasanta, E.; Lange, M.; Bonanata, J.; Coitiño, E. L.; Ferrer-Sueta, G.; Filipovic, M. R.; Alvarez, B. Reaction of Hydrogen Sulfide with Disulfide and Sulfenic Acid to Form the Strongly Nucleophilic Persulfide. *J. Biol. Chem.* **2015**, *290* (45), 26866–26880.

(119) Venkatesh, Y.; Kiran, K. S.; Shah, S. S.; Chaudhuri, A.; Dey, S.; Singh, N. D. P. One- and Two-Photon Responsive Sulfur Dioxide (SO2) Donors: A Combinatorial Drug Delivery for Improved Antibiotic Therapy. *Org. Biomol. Chem.* **2019**, *17* (10), 2640–2645.

(120) Francoleon, N. E.; Carrington, S. J.; Fukuto, J. M. The Reaction of H2S with Oxidized Thiols: Generation of Persulfides and Implications to H2S Biology. *Arch. Biochem. Biophys.* **2011**, *516* (2), 146–153.

(121) Numakura, T.; Sugiura, H.; Akaike, T.; Ida, T.; Fujii, S.; Koarai, A.; Yamada, M.; Onodera, K.; Hashimoto, Y.; Tanaka, R.; Sato, K.; Shishikura, Y.; Hirano, T.; Yanagisawa, S.; Fujino, N.; Okazaki, T.; Tamada, T.; Hoshikawa, Y.; Okada, Y.; Ichinose, M. Production of Reactive Persulfide Species in Chronic Obstructive Pulmonary Disease. *Thorax* **2017**, *72* (12), 1074–1083.

(122) Kasamatsu, S.; Ida, T.; Koga, T.; Asada, K.; Motohashi, H.; Ihara, H.; Akaike, T. High-Precision Sulfur Metabolomics Innovated by a New Specific Probe for Trapping Reactive Sulfur Species. *Antioxid. Redox Signal.* **2021**, *34* (18), 1407–1419.

(123) Yadav, P. K.; Martinov, M.; Vitvitsky, V.; Seravalli, J.; Wedmann, R.; Filipovic, M. R.; Banerjee, R. Biosynthesis and Reactivity of Cysteine Persulfides in Signaling. *J. Am. Chem. Soc.* **2016**, *138* (1), 289–299.

(124) Krishnan, N.; Fu, C.; Pappin, D. J.; Tonks, N. K. H 2 S-Induced Sulfhydration of the Phosphatase PTP1B and Its Role in the Endoplasmic Reticulum Stress Response. *Sci.*

Signal. **2011**, *4* (203).

(125) Sen, N.; Paul, B. D.; Gadalla, M. M.; Mustafa, A. K.; Sen, T.; Xu, R.; Kim, S.; Snyder, S. H. Hydrogen Sulfide-Linked Sulfhydration of NF-KB Mediates Its Antiapoptotic Actions. *Mol. Cell* **2012**, *45* (1), 13–24.

(126) Zhang, D.; Macinkovic, I.; Devarie-Baez, N. O.; Pan, J.; Park, C.; Carroll, K. S.; Filipovic, M. R.; Xian, M. Detection of Protein S-Sulfhydration by a Tag-Switch Technique. *Angew. Chemie Int. Ed.* **2014**, *53* (2), 575–581.

(127) Dóka, É.; Pader, I.; Bíró, A.; Johansson, K.; Cheng, Q.; Ballagó, K.; Prigge, J. R.; Pastor-Flores, D.; Dick, T. P.; Schmidt, E. E.; Arnér, E. S. J.; Nagy, P. A Novel Persulfide Detection Method Reveals Protein Persulfide- and Polysulfide-Reducing Functions of Thioredoxin and Glutathione Systems. *Sci. Adv.* **2016**, *2* (1).

(128) Gao, X.-H.; Krokowski, D.; Guan, B.-J.; Bederman, I.; Majumder, M.; Parisien, M.; Diatchenko, L.; Kabil, O.; Willard, B.; Banerjee, R.; Wang, B.; Bebek, G.; Evans, C. R.; Fox, P. L.; Gerson, S. L.; Hoppel, C. L.; Liu, M.; Arvan, P.; Hatzoglou, M. Quantitative H2S-Mediated Protein Sulfhydration Reveals Metabolic Reprogramming during the Integrated Stress Response. *Elife* **2015**, *4*.

(129) Longen, S.; Richter, F.; Köhler, Y.; Wittig, I.; Beck, K.-F.; Pfeilschifter, J. Quantitative Persulfide Site Identification (QPerS-SID) Reveals Protein Targets of H2S Releasing Donors in Mammalian Cells. *Sci. Rep.* **2016**, *6* (1), 29808.

(130) Orsenigo, F.; Conze, L. L.; Jauhiainen, S.; Corada, M.; Lazzaroni, F.; Malinverno, M.; Sundell, V.; Cunha, S. I.; Brännström, J.; Globisch, M. A.; Maderna, C.; Lampugnani, M. G.; Magnusson, P. U.; Dejana, E. Mapping Endothelial-Cell Diversity in Cerebral Cavernous Malformations at Single-Cell Resolution. *Elife* **2020**, *9*.

(131) Manna, S.; Agrawal, R.; Yadav, T.; Kumar, T. A.; Kumari, P.; Dalai, A.; Kanade, S.; Balasubramanian, N.; Singh, A.; Chakrapani, H. Orthogonal Persulfide Generation through Precision Tools Provides Insights into Mitochondrial Sulfane Sulfur. *Angew. Chemie Int. Ed.* **2024**, *63* (46).

(132) Chen, W.; Liu, C.; Peng, B.; Zhao, Y.; Pacheco, A.; Xian, M. New Fluorescent Probes for Sulfane Sulfurs and the Application in Bioimaging. *Chem. Sci.* **2013**, *4* (7), 2892–2896.

(133) Shieh, M.; Ni, X.; Xu, S.; Lindahl, S. P.; Yang, M.; Matsunaga, T.; Flaumenhaft, R.; Akaike, T.; Xian, M. Shining a Light on SSP4: A Comprehensive Analysis and Biological Applications for the Detection of Sulfane Sulfurs. *Redox Biol.* **2022**, *56*, 102433.

(134) Neill, D. L.; Chang, Y.-C.; Chen, W.; Li, L.; Xian, M. A Smartphone Based Device for the Detection of Sulfane Sulfurs in Biological Systems. *Sensors Actuators B Chem.* **2019**, *292*, 263–269.

(135) Jiang, G.; Li, M.; Wen, Y.; Zeng, W.; Zhao, Q.; Chen, C.; Yuan, H.; Liu, C.; Liu, C. Visualization of Sulfane Sulfur in Plants with a Near-Infrared Fluorescent Probe. *ACS Sensors* **2019**, *4* (2), 434–440.

(136) Liu, C.; Chen, W.; Shi, W.; Peng, B.; Zhao, Y.; Ma, H.; Xian, M. Rational Design and Bioimaging Applications of Highly Selective Fluorescence Probes for Hydrogen Polysulfides. *J. Am. Chem. Soc.* **2014**, *136* (20), 7257–7260.

(137) Liu, H.; Radford, M. N.; Yang, C.; Chen, W.; Xian, M. Inorganic Hydrogen Polysulfides: Chemistry, Chemical Biology and Detection. *Br. J. Pharmacol.* **2019**, *176* (4), 616–627.

(138) Gupta, N.; Reja, S. I.; Bhalla, V.; Kumar, M. Fluorescent Probes for Hydrogen Polysulfides (H 2 S n , n > 1): From Design Rationale to Applications. *Org. Biomol. Chem.* **2017**, *15* (32), 6692–6701.

(139) Takano, Y.; Hanaoka, K.; Shimamoto, K.; Miyamoto, R.; Komatsu, T.; Ueno, T.; Terai, T.; Kimura, H.; Nagano, T.; Urano, Y. Development of a Reversible Fluorescent Probe for Reactive Sulfur Species, Sulfane Sulfur, and Its Biological Application. *Chem. Commun.* **2017**, *53* (6), 1064–1067.

(140) Umezawa, K.; Kamiya, M.; Urano, Y. A Reversible Fluorescent Probe for Real-Time Live-Cell Imaging and Quantification of Endogenous Hydropolysulfides. *Angew. Chemie Int. Ed.* **2018**, *57* (30), 9346–9350.

(141) Liu, T.; Peng, Q.; Wang, J.; Yu, C.; Huang, X.; Luo, Q.; Zeng, Y.; Hou, Y.; Zhang, Y.; Luo, A.; Zou, Z.; Chen, M.; Peng, Y. A FRET-Based Ratiometric Fluorescent Probe for Hydrogen Polysulfide Detection in Living Cells and Zebrafish. *Spectrochim. Acta Part A Mol. Biomol. Spectrosc.* **2022**, *267*, 120524.

(142) Zhang, J.; Zhu, X.-Y.; Hu, X.-X.; Liu, H.-W.; Li, J.; Feng, L.; Yin, X.; Zhang, X.-B.; Tan, W. Ratiometric Two-Photon Fluorescent Probe for in Vivo Hydrogen Polysulfides Detection and Imaging during Lipopolysaccharide-Induced Acute Organs Injury. *Anal. Chem.* **2016**, *88* (23), 11892–11899.

(143) Han, Q.; Mou, Z.; Wang, H.; Tang, X.; Dong, Z.; Wang, L.; Dong, X.; Liu, W. Highly Selective and Sensitive One- and Two-Photon Ratiometric Fluorescent Probe for Intracellular Hydrogen Polysulfide Sensing. *Anal. Chem.* **2016**, *88* (14), 7206–7212.

(144) Kawagoe, R.; Takashima, I.; Uchinomiya, S.; Ojida, A. Reversible Ratiometric Detection of Highly Reactive Hydropersulfides Using a FRET-Based Dual Emission Fluorescent Probe. *Chem. Sci.* **2017**, *8* (2), 1134–1140.

(145) Caswell, M.; Schmir, G. L. Formation and Hydrolysis of Lactones of Phenolic Acids. *J. Am. Chem. Soc.* **1980**, *102* (14), 4815–4821.

Chapter 2. Real-Time Monitoring of Persulfide Generation

2.1. Introduction

Persulfides have been reported to be reactive, acidic and have lower reduction potentials compared to their corresponding thiols.[1,2] Persulfides are known to mitigate oxidative stress by preventing the overoxidation of proteins, or by upregulation of antioxidant genes mediated by persulfidation of the KEAP1-Nrf2 axis.[3–5] Persulfidation of the proteins have possible therapeutic applications in the treatment of various disorders such as Parkinson's, Alzheimer's, and osteoarthritis.[2,6,7] Therefore, enhancing the persulfides has emerged as an important therapeutic strategy to attenuate oxidative stress. Due to the unstable nature of persulfides, generating the persulfides in the biological milieu in a controlled manner is quite challenging. To overcome these challenges, a prodrug strategy has been adopted. Persulfide prodrugs activated by an enzyme,[8–12] light,[13,14] reactive oxygen species (ROS),[15–18] pH,[19,20] fluoride[19] and peroxynitrite[21] have been reported. However, these tools are associated with some limitations, such as the generation of electrophilic byproducts such as a quinone methide[10,11,15,18,21] or an aldehyde[8,13,14,17] which may contribute to electrophilic stress.[22,23] Another challenge associated with persulfides is their detection; their inherent instability makes their detection quite challenging. There is a need for secondary assays for the detection of persulfides[24]: i) the nucleophilic persulfide can be trapped by an electrophilic trapping agent (e.g., iodoacetamide) or ii) using persulfide-specific turn-on fluorescent probes (e.g., SSP2) as shown in Figure 2.1. Also, both these detection methods involve the consumption of persulfide unit in order to detect it.

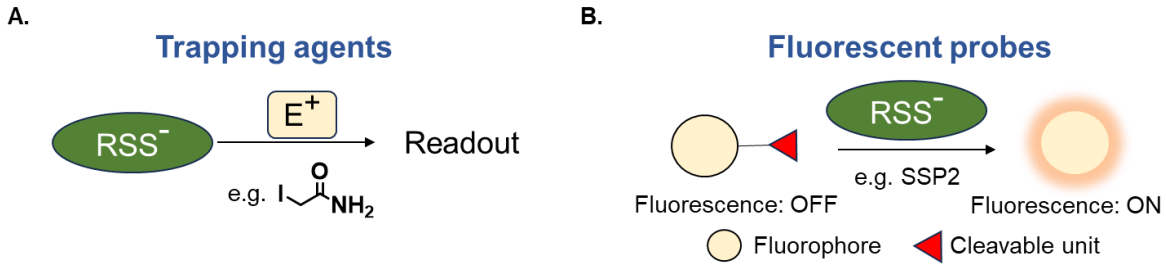

Figure 2.1. Detection of persulfides using (A) electrophilic trapping agents and (B) persulfide-sensitive turn-on fluorescent probes.

To overcome the need for secondary assays for the detection of the persulfides, the latent fluorophore strategy can be employed, which enables the real-time monitoring of the persulfide, i.e., a chemical tool that generates persulfide along with a fluorescence reporter.

Upon activation by particular stimuli, the protective group gets cleaved (Step 1), leading to the formation of an intermediate, which subsequently dissociates (Step 2) to release persulfide along with a fluorescence reporter (Figure 2.2).

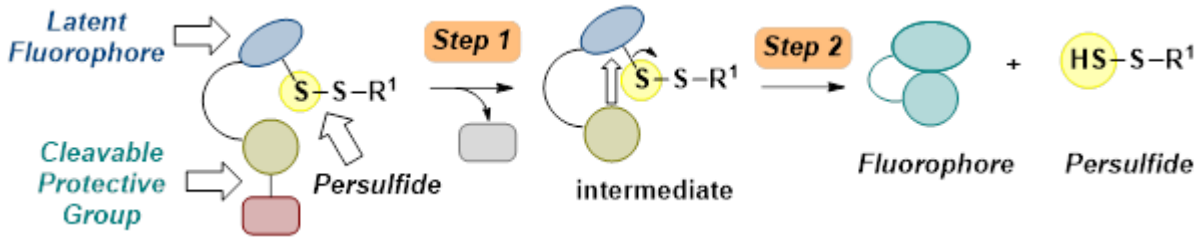

Figure 2.2. General design for a cleavable persulfide donor with a fluorescence reporter

Recently, a donor that generates persulfide (H_2S_2) as well as a fluorescence reporter upon activation by light was reported (Scheme 2.1)[14] However, the applicability of this tool may be limited by the generation of electrophilic byproducts. The use of light in cellular experiments also has limitations.

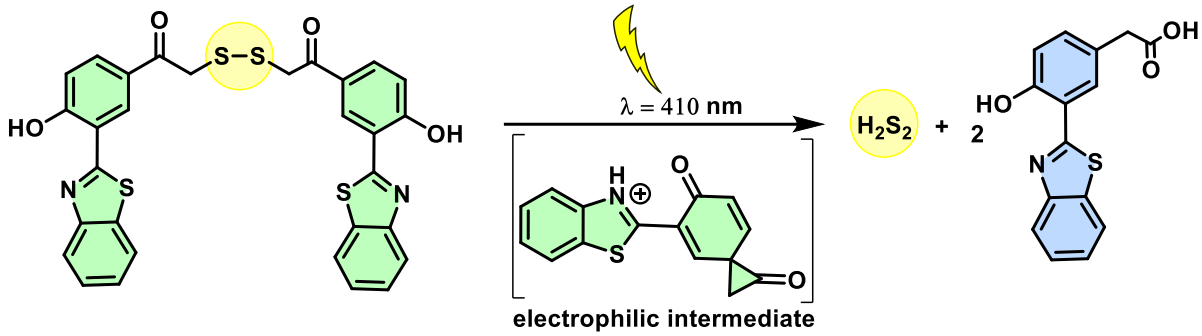

Scheme 2.1. Light-activated H_2S_2 donor with a fluorescence reporter.

The possibility of developing a strategy where the generation of a persulfide and a fluorophore would occur in the same molecular step was considered. To achieve this goal, we considered lactonization as the key step in persulfide generation (Scheme 2.2.A). Hence, a biphenyl-based system was chosen here, cleavage of the ester by esterase (Es) should lead to lactonization, which generates a lactone that belongs to a class of known fluorophores.[25,26] Lactonization in such systems is reported to be quite rapid,[27] hence, the persulfide generation will likely occur during lactonization, leading to a nearly concomitant release of the persulfide and the production of a fluorescence signal. The initial development of the biphenyl system has been included in my colleague's thesis, Sushma Tejasri (NTR-activated H_2S donor),[28] Amal SK (Esterase-activated benzyl persulfide donor),[29] and was further developed with the help of Dr. Anand in our lab. Wang and coworkers have reported a similar strategy for the development

of hypoxia-activated anti-cancer drug (FDU) release, which also strengthens our hypothesis (Scheme 2.2.B).[26]

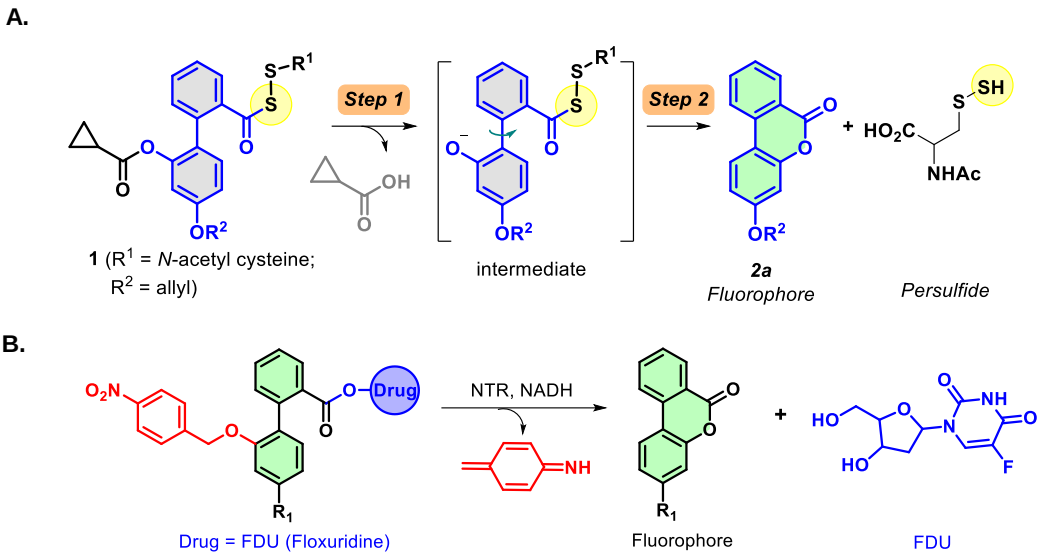

Scheme 2.2. (A) Design of a biphenyl-based esterase-activated NAC persulfide generator and (B) Hypoxia-activated anticancer drug release based on the biphenyl system.

2.2. Result and discussion

2.2.1. Synthesis

To test our hypothesis, the persulfide donor was synthesized in 8 steps. Compounds **2a** and **2b** were synthesized following a reported protocol.[30,31] The lactone **2a** was subjected to LAH reduction to give compound **3,** followed by silyl protection of the resulting alcohol to yield compound **4**. Compound **4** was then esterified with cyclopropyl carboxylic acid using classical DCC/DMAP conditions to give compound **5**, followed by silyl group deprotection under acidic conditions afforded compound **6**. Oxidation of the primary alcohol of compound **6** in two steps gave carboxylic acid **8**. The carboxylic acid compound **8** was converted to its corresponding thiocarboxylic acid **10** using Lawesson's reagent, and finally coupled with NAC-pyridyl disulfide (**NAC-SS-Py**) **9**[15] to provide the persulfide donor **1** in 18% yield (Scheme 2.3).

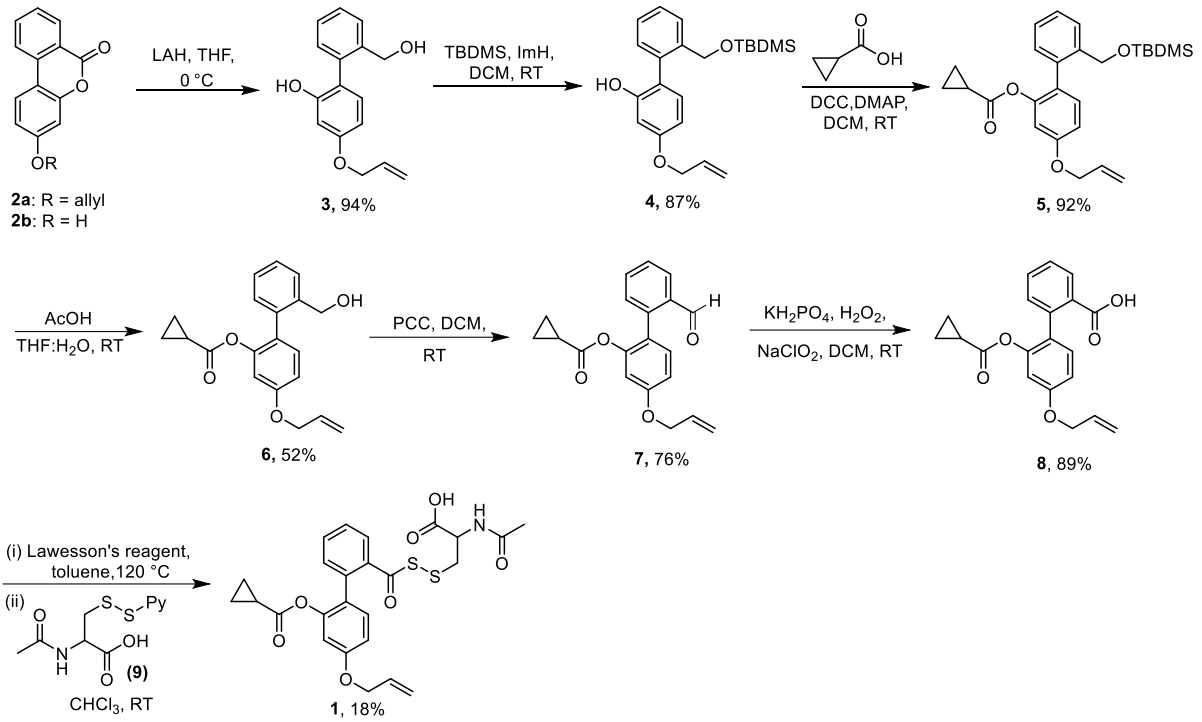

Scheme 2.3. Synthesis of NAC-SSH persulfide donor **1**.

2.2.2. Methods for the detection of 2a and persulfide

The compound **1**, upon activation by esterase (Es), generates the fluorophore lactone **2a** and NAC persulfide in a concomitant manner. The fluorophore lactone **2a** formation can be monitored by fluorescence-based experiment (λ_{ex} = 330 nm; λ_{em} = 432 nm) and cellular imaging

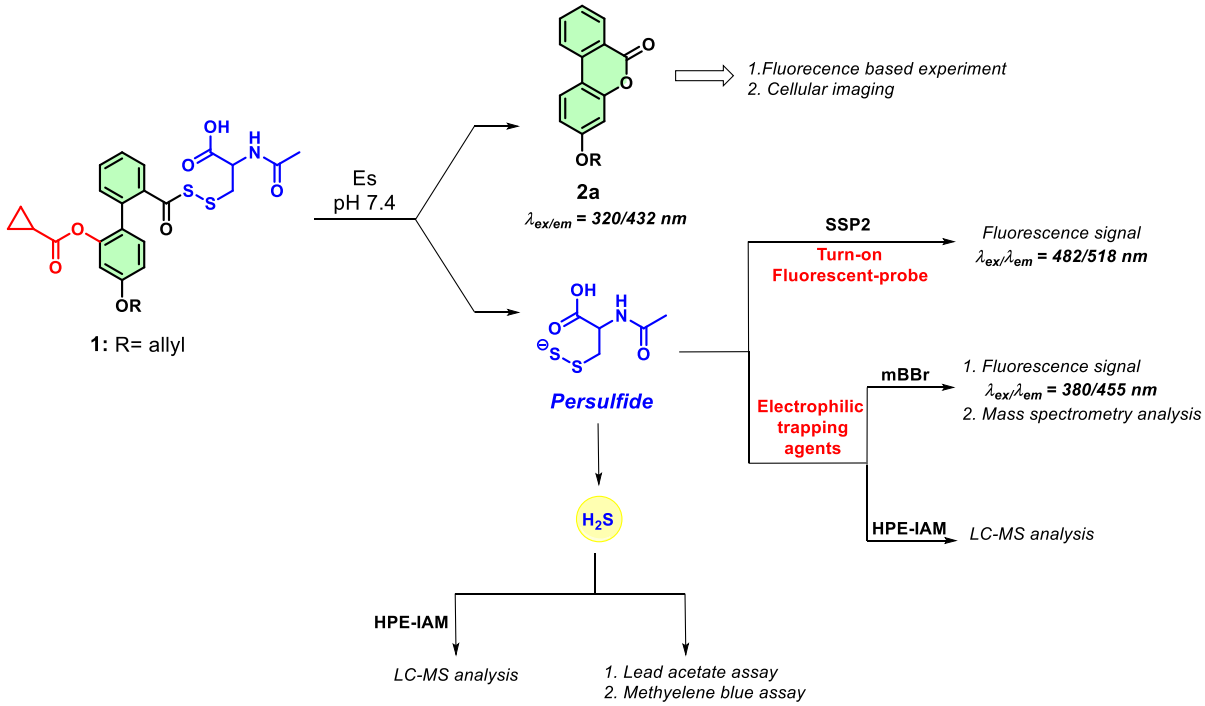

Scheme 2.4. Tools for detection of lactone **2a** and NAC persulfide generated from **1** in the presence of Es.

using confocal microscopy. The NAC persulfide can be detected by trapping it with electrophilic agents (**mBBr** or **HPE-IAM**) or by a persulfide-sensitive turn-on fluorescent probe (**SSP2**) (Scheme 2.4).

2.2.3. Photophysical properties of 2a and 2b

Firstly, the photophysical properties of **2a** and **2b**, such as absorbance and fluorescence profiles were studied in PBS (pH 7.4).

2.2.3.1. Measurement of UV absorbance of 2a and 2b

The UV absorbance spectrum of **2a** and **2b** was recorded in PBS buffer (pH 7.4) at room temperature. The absorbance maximum (λ_{max}) of **2a** and **2b** was observed at 320 nm (Figure 2.3).

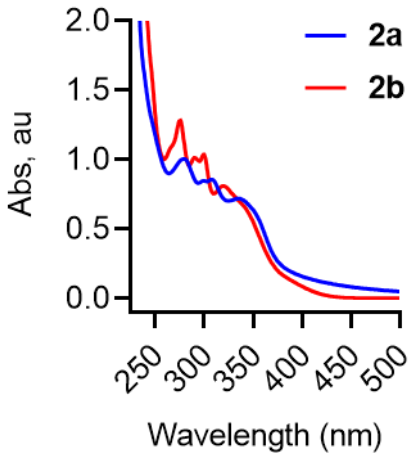

Figure 2.3. The UV absorption spectrum for compounds **2a** and **2b** (100 µM) were measured in PBS (pH 7.4).

2.2.3.2. Measurement of fluorescence of 2a and 2b

The fluorescence spectra for **2a and 2b** were recorded in PBS (pH 7.4). The fluorescence emission (λ_{em}) of **2a** and **2b** was observed at 432 nm (Figure 2.4). The fluorescence signal of lactone **2b,** which lacks an allyl group, was much lower than that of lactone **2a**, which contains an allyl group. We hence proceeded to use **1**, which has an allyl group for our analysis.

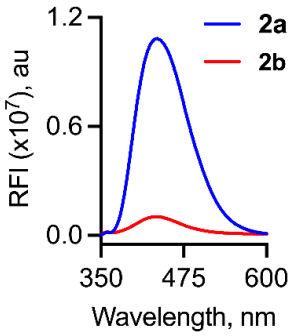

Figure 2.4. The fluorescence spectra for compounds **2a** and **2b** (5 μM) were measured in PBS (pH 7.4) (λ_{ex} = 320 nm; λ_{em} = 432 nm).

2.2.4. Stability and reactivity of 2a

Since lactone **2a** has an allyl group (electrophilic group), we tested out the stability and reactivity of **2a** towards nucleophilic attack by biologically relevant nucleophiles. The lactone **2a** (10 μM) was reacted with 100 equivalents of biologically relevant nucleophiles for 2 h in 7.4 pH PBS for 2 h at 37 ˚C. The fluorescence signal of **2a** (λ_{ex} = 320 nm; λ_{em} = 432 nm) remained intact in the presence of the nucleophiles, suggesting that the lactone was stable toward nucleophilic attack by common cellular nucleophiles (Figure 2.5).

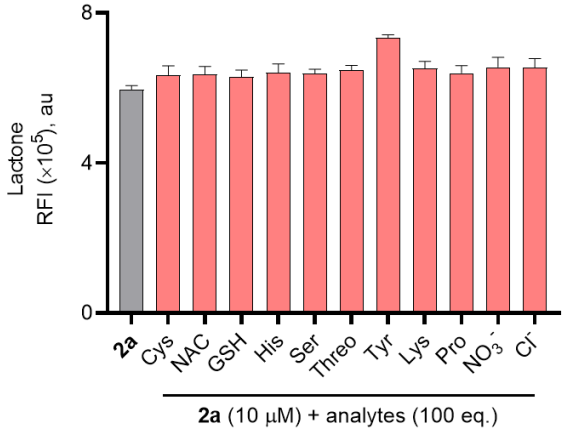

Figure 2.5. Stability and reactivity of **2a** (10 μM) towards nucleophiles (100 equiv.) for 120 min. Cys: cysteine; NAC: *N*- acetylcysteine; GSH: glutathione; His: histidine; Ser: serine; Threo: threonine; Tyr: tyrosine; Lys: lysine; Pro: proline; NO_3^-: sodium nitrate; Cl^-: sodium chloride. Results are expressed as mean ± SD (n =3/group).

2.2.5. Formation of 2a from 1 upon activation by esterase

First, in order to ascertain the ability of the persulfide donor **1** to generate lactone **2a** in the presence of esterase (Es), fluorescence-based experiments were performed.

2.2.5.1. Release of 2a from 1 by fluorescence and mass spectrometry analysis

Compound **1** (20 μM) was treated with Es (1 U/mL) in PBS (pH 7.4), and the fluorescence intensity corresponding to the **2a** formation was monitored The compound was itself weakly fluorescent, but the addition of Es (1 U/mL) led to a significant increase in fluorescence intensity (48-fold) attributable to the formation of **2a** (λ_{ex} = 320 nm; λ_{em} = 432 nm) after incubation for 1 h in PBS (pH 7.4) (Figure 2.6).

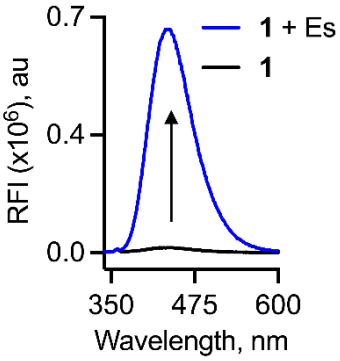

Figure 2.6. Monitoring the formation of lactone **2a** from **1** by fluorescence (λ_{ex} = 330 nm; λ_{em} = 432 nm) at 20 μM without or with Es (1 U/mL) in pH 7.4 buffer at 37 °C.

The formation of **2a** was independently confirmed by mass spectrometry analysis (expected, m/z = 253.0859, $[M+H]^+$; observed, m/z = 253.0864) (Figure 2.7).

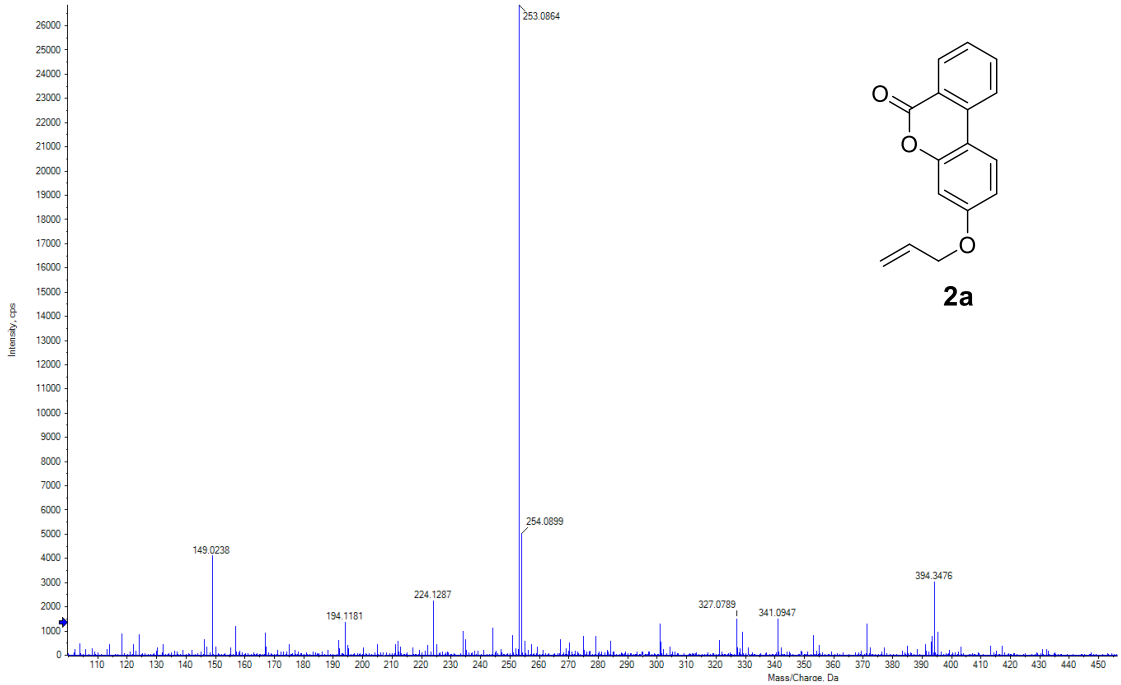

Figure 2.7. Mass spectrometry analysis of **1** (10 μM) upon incubation with Es (2.5 U/mL) for 30 min. For **2a** (expected, m/z =253.0859, $[M+H]^+$; observed, m/z = 253.0864).

2.2.5.2. Concentration-dependent release of 2a

Next, the concentration-dependent release of **2a** from **1** was studied. The fluorescence signal enhancement (λ_{ex} = 320 nm; λ_{em} = 432 nm) corresponding to **2a** formation from varying concentrations of **1** (0-20 µM) was monitored in the presence of Es (1 U/mL). The dose-dependent studies demonstrated that the fluorescence corresponding to **2a** formation gradually increased over time and plateaued after 1 h (Figure 2.8).

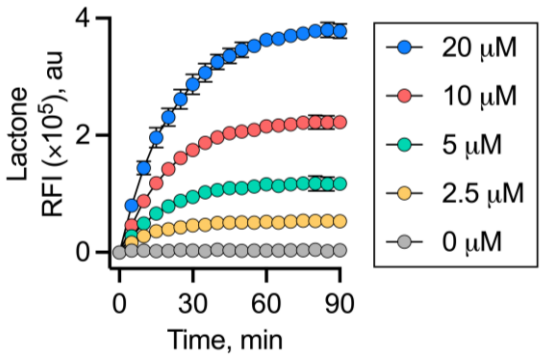

Figure 2.8. Concentration-dependent release of lactone **2a** from **1** (0-20 µM) by fluorescence (λ_{ex} = 330 nm; λ_{em} = 432 nm) with Es (1 U/mL) in pH 7.4 buffer at 37 °C.

Further, the curve fitting for the **2a** formation to a first-order exponential equation yielded rate constants ranging from 0.047 to 0.073 min^{-1}(Table 2.1).

Table 2.1. Rate constants and rates of **2a** formation and persulfide generation from **1**

1 Conc. (µM)	**2a** formation ($\times 10^{-1}$ min^{-1})	Persulfide generation ($\times 10^{-1}$ min^{-1})		Rate of **2a** formation (µM min^{-1})	Rate of persulfide generation (µM min^{-1})	
		SSP2	mBBr		SSP2	mBBr
2.5	0.73	0.17	0.18	0.18	0.04	0.05
5	0.56	0.24	0.22	0.28	0.12	0.11
10	0.51	0.23	0.25	0.51	0.24	0.25
20	0.47	0.27	0.35	0.94	0.55	0.70

2.2.5.3. Formation of 2a in cell lysates

Next, we tested the ability of **1** to be cleaved under cell culture conditions using a similar fluorescence-based assay. Compound **1** with varying concentrations (0-10 µM) was incubated with the N2a cell lysates, and the fluorescence signal corresponding to the **2a** formation (λ_{ex} =

320 nm; λ_{em} = 432 nm) was monitored. In cell lysates, a dose-dependent enhancement in the fluorescence signal was observed corresponding to the formation of **2a** (Figure 2.9).

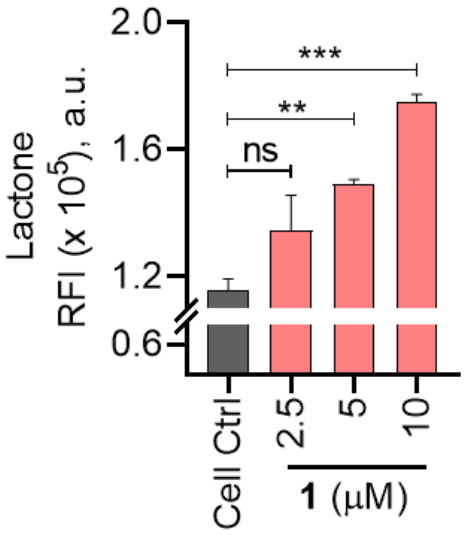

Figure 2.9. Compound **1** was incubated in N2a cell lysate (1 mg/mL) for 2 hours; cell ctrl refers to untreated cell lysate. Fluorescence measurement (λ_{ex} = 320 nm; λ_{em} = 432 nm) was carried out by varying concentrations of **1**. Results are expressed as mean ± SD (n =3/group). *p*-value was determined by using Two-way ANOVA relative to the cell ctrl. (** $p \leq 0.002$; *** $p \leq 0.001$ and ns indicates not significant).

Overall, these results supported that **1** underwent the lactonization to produce **2a** upon activation by esterase.

2.2.6. Persulfide detection

Once it was established that compound **1** can be cleaved by esterase and release lactone **2a** under physiological conditions, we next attempted to detect the release of the persulfide. Persulfides are highly reactive species, which makes their detection quite challenging. The most commonly used method is to leverage its nucleophilicity and trap it as an adduct by reacting it with an electrophile and using a turn-on persulfide-sensitive fluorescent probe. So, a series of experiments were conducted to directly trap the persulfide release from **1** using an electrophilic trapping agent (monobromobimane: **mBBr**) and persulfide-specific fluorescent probes (**SSP2**).

2.2.6.1. mBBr-based persulfide detection

The electrophilic trapping agent monobromobimane (mBBr)-based fluorescence enhancement assay was used,[14] where persulfide generated from compound **1** will react with mBBr and form a fluorescent **NAC-SS-bimane** adduct (λ_{ex} = 380 nm; λ_{em} = 455 nm) as depicted in Scheme 2.5.

Upon co-incubation of compound **1** (100 µM) with Es (1 U/mL) and **mBBr** (100 µM), a distinct time-dependent increase in fluorescence signal (λ_{ex} = 380 nm; λ_{em} = 455 nm) corresponding to the **NAC-SS-bimane** was observed over 60 min (Figure 2.10.A). The formation of **NAC-SS-bimane** adduct (expected, m/z = 408.0658, $[M+Na]^+$; observed, m/z = 408.0663) was further confirmed by MS analysis (Figure 2.11). Additionally, a dose-dependent study of **1** (0-100 µM) with Es (1 U/mL) and mBBr (100 µM) showed a good linear relationship (R^2 = 0.98) (Figure 2.10.B).

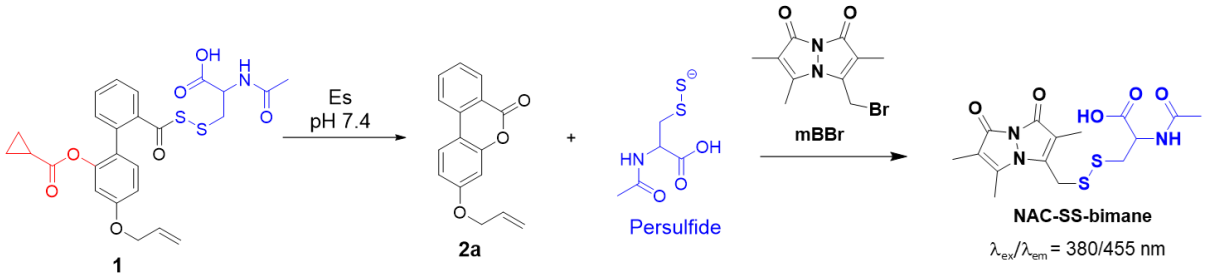

Scheme 2.5. Formation of the **NAC-SS-bimane** adduct when **1** incubated with Es and mBBr.

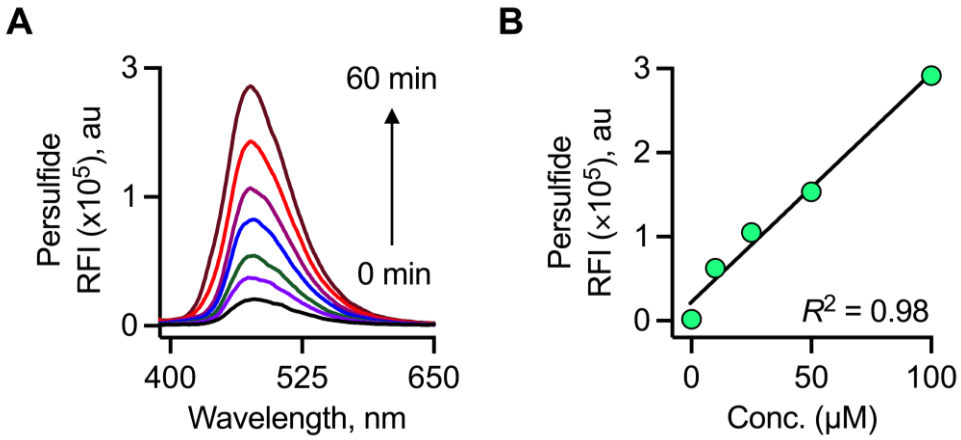

Figure 2.10. Detection of persulfide released from (A) **1** (100 µM) over 60 min and (B) **1** (0-100 µM) in a concentration-dependent manner following treatment with Es (1 U/mL) and mBBr (100 µM) after 60 min.

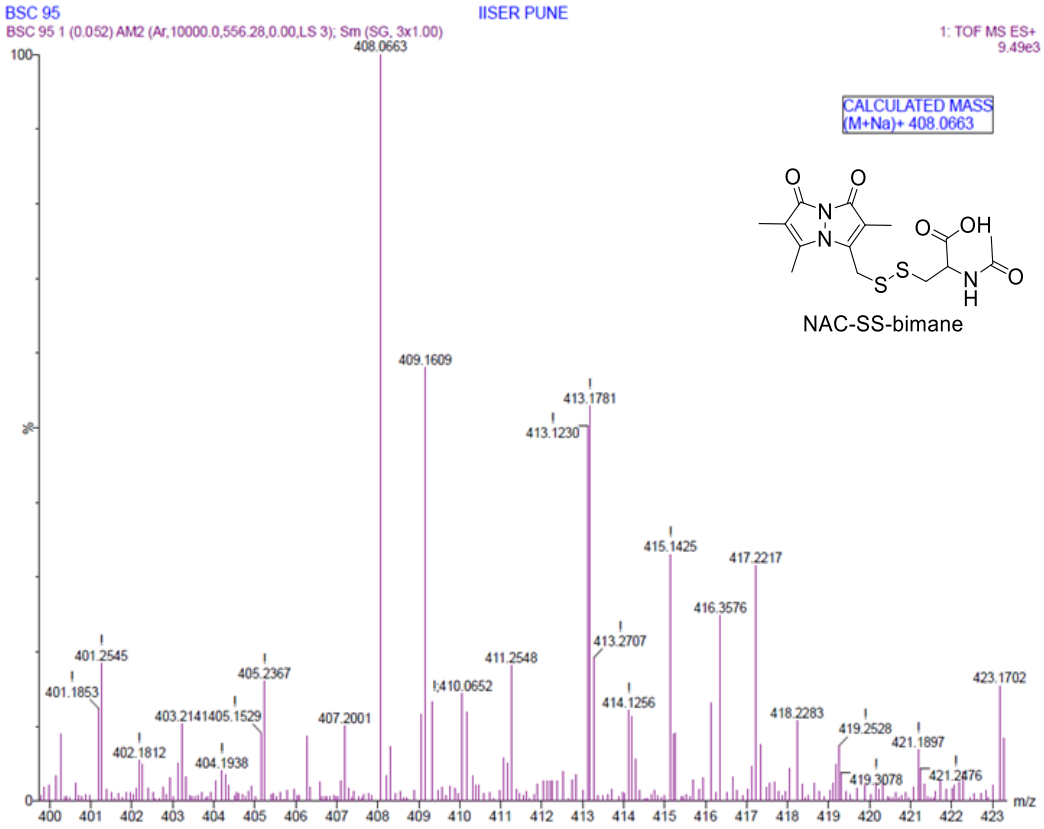

Figure 2.11. Mass of the **NAC-SS-bimane** adduct formation when **1** incubated with Es and mBBr (expected, m/z = 408.0658, $[M+Na]^+$; observed, m/z = 408.0663).

2.2.6.2. Sulfane sulfur detection using SSP2

Independently, we also measured the rate of persulfide generation from **1** using a well-established fluorogenic sulfane sulfur probe (**SSP2**).[32] The persulfide released from compound **1** will react with the **SSP2** probe and release highly fluorescent fluorescein (λ_{ex} = 482 nm; λ_{em} = 518 nm), as shown in Scheme 2.6.

When the varying concentrations of compound **1** (0-20 μM) was co-incubated with Es (1 U/mL) and **SSP2** (10 μM), a significant dose-dependent enhancement in the fluorescence intensity (λ_{ex} = 482 nm; λ_{em} = 518 nm), corresponding to the generation of sulfane sulfur was observed over a period of 90 min (Figure 2.12).

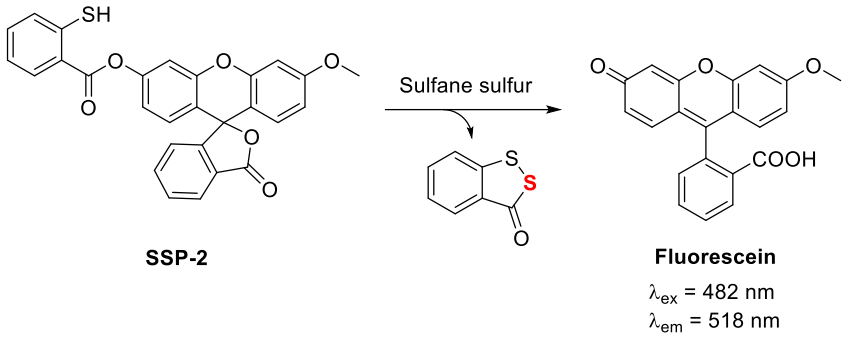

Scheme 2.6. Release of fluorescein upon reaction of sulfane sulfur with **SSP2**.

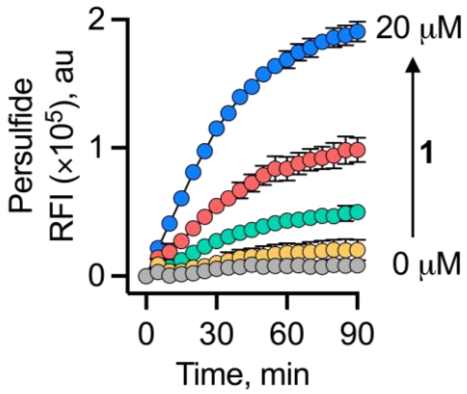

Figure 2.12. Monitoring the release of persulfide generated upon co-treatment of Es (1 U/mL) and **SSP2** (10 μM) with varied concentrations of **1** (0-20 μM) over 90 min.

So, the persulfide generation was monitored using two independent assays. Under these experimental conditions, the rate of persulfide formation in both **mBBr** and **SSP2** assays showed an excellent correlation (R^2 = 0.99) (Figure 2.13 and Table 2.1).

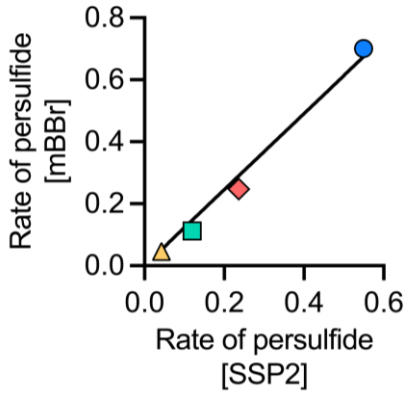

Figure 2.13. Correlation between the rate of persulfide formation from **1** (△ 2.5 μM; □ 5 μM; ◊ 10 μM and ○ 20 μM) in **mBBr** and **SSP2** assays.

2.2.7. Concomitant release of persulfide and lactone 2a

The time course for the formation of **2a** and NAC persulfide at various concentrations of **1** was independently monitored by a change in fluorescence signal. When followed over 90 min, the time courses of these events were similar (Figures 2.8 and 2.12). The rate for **2a** formation was found to be marginally higher in magnitude (2-3 fold) than the rate of persulfide generation (Table 2.1). This is expected since lactonization (k_{2a}) occurs at a faster rate compared to the rate of formation of NAC persulfide covalent adducts (k_{SSP2} for SSP2 assay) that occurs through a two-step process rather than a single step as shown in Scheme 2.7.

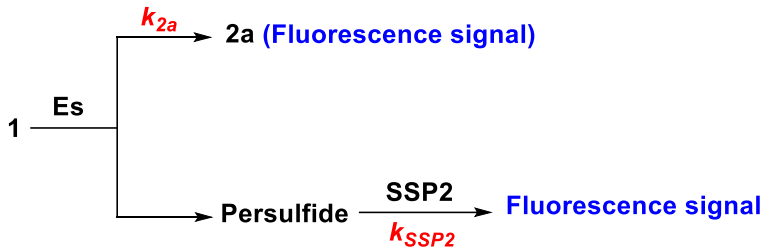

Scheme 2.7. Formation of **2a** (k_{2a}) and persulfide detection using **SSP2** (k_{SSP2}) from **1** upon activation by esterase.

To establish a correlation between the lactone (**2a**) and persulfide formation (**SSP2**) from **1**, the maximum fluorescence change at 90 min was considered as the plateau was reached. These fluorescence values were normalized and then plotted. An excellent correlation between the two parameters was observed, suggesting that the release of fluorophore **2a** and NAC persulfide occur nearly concurrently following esterase-mediated cleavage of **1** and subsequent lactonization (Figure 2.14).

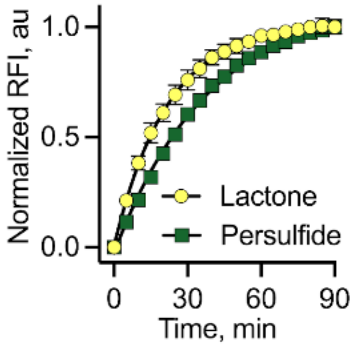

Figure 2.14. Correlation between change in fluorescence corresponding to the formation of lactone **2a** and persulfide formed upon incubation of **1** (20 μM) with Es (1 U/mL) and **SSP2** (10 μM).

Similarly, the rates of persulfide generation as determined by SSP2 and rates of **2a** formation (Table 2.1) from the varying concentrations of **1** were compared. A good linear correlation between the rates of persulfide and **2a** formation was observed (R^2 = 0.99) at concentrations ranging from 2.5 to 20 μM (Figure 2.15).

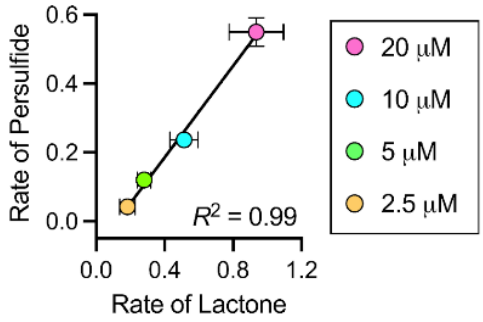

Figure 2.15. Correlation between the rates of lactone and persulfide formation upon treatment of **1** (2.5, 5, 10, and 20 μM) with Es (1 U/mL) in the presence of **SSP2** (10 μM)**.**

Taken together, these data show that the fluorescence signal produced can be used as a proxy for persulfide production.

2.2.8. Persulfide and H_2S Measurement using LC/MS analysis

Persulfides can also be detected by reacting it with a suitable electrophile. *N*-(4-hydroxyphenethyl)-2-iodoacetamide (**HPE-IAM**) has been previously reported as an effective persulfide alkylating agent due to its mild electrophilic nature.[33] Persulfides, being unstable, can undergo disproportionation to form polysulfides ($RS(S)_nH$) and hydrogen polysulfides (H_2S_n), which can react with **HPE-IAM** and hence be detected as HPE-IAM adducts as well using LC/MS (Scheme 2.8).

Compound **1** (50 μM) was incubated in the presence of Es (1 U/mL) and **HPE-IAM** (10 mM) in PBS pH 7.4. After the incubation for 60 minutes, the samples were subjected to LC/MS analysis. A new peak attributable to the persulfide adduct at 12.5 min, **NAC-SS-HPE-AM** (expected, m/z = 373.0886 $[M + H]^+$; observed, m/z = 373.0891), was observed, indicating the release of NAC persulfide (Figures 2.16 and 2.17). Under these conditions, we also observe **Bis-S-HPE-AM** (expected, m/z = 389.1530 $[M + H]^+$; observed, m/z = 389.1537) presumably due to the reaction of HPE-IAM with H_2S formed by the decomposition of NAC persulfide through disproportionation (Figures 2.16 and 2.18).

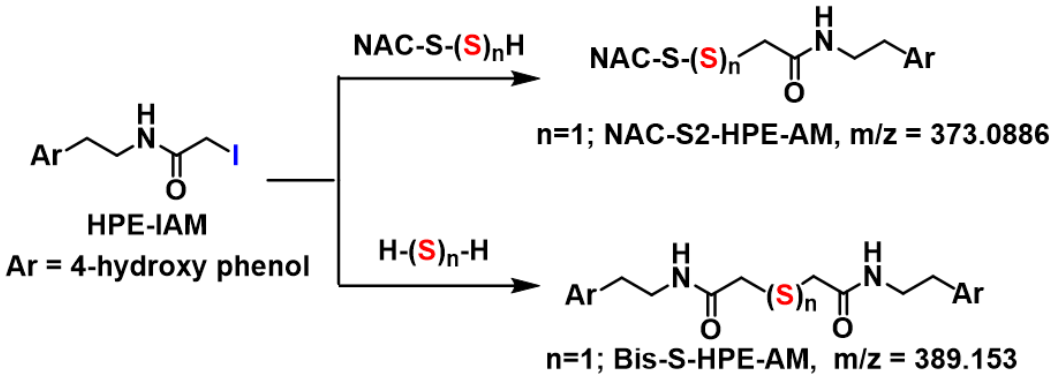

Scheme 2.8. LC/MS study. Reaction scheme showing detection of persulfides/polysulfides and hydrogen sulfide/polysulfides as their HPE-AM and bis-S-HPE-AM adducts, respectively. (Ar = 4-hydroxyphenyl).

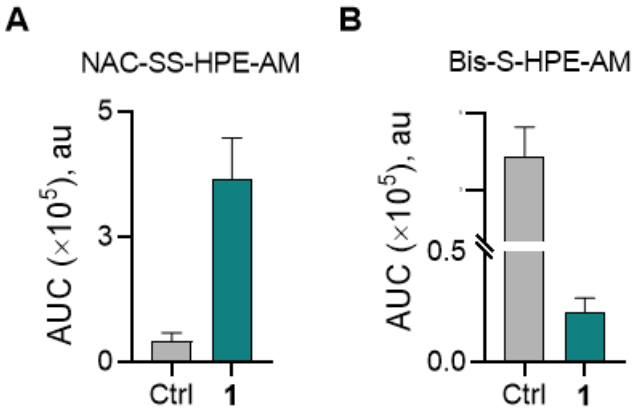

Figure 2.16. LC/MS study. (A) Persulfide **(NAC-SS-HPE-AM)** and (B) H_2S **(Bis-S-HPE-AM)** formation were measured by the detection of trapped HPE-IAM species from **1** and ctrl. The ctrl was prepared by reacting 200 μM NAC, 200 μM **DEA/NO** (sodium 2-(*N*, *N*-diethylamino)-diazenolate-2-oxide) and 200 μM NaSH at room temperature for 20 min[34]. Results are expressed as mean ± SD (n =3/group).

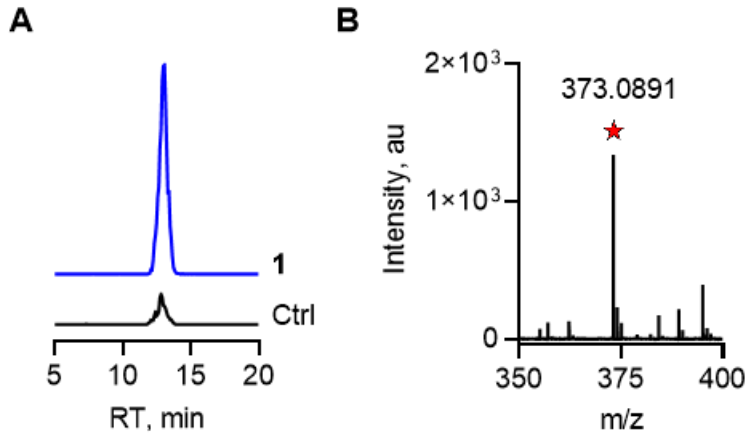

Figure 2.17. A) Extracted ion chromatograms from an LC/MS analysis of **NAC-SS-HPE-AM** formation from **1** and ctrl; (B) Mass spectra for **NAC-SS-HPE-AM** (expected, m/z = 373.0886 $[M + H]^+$; observed, m/z = 373.0891).

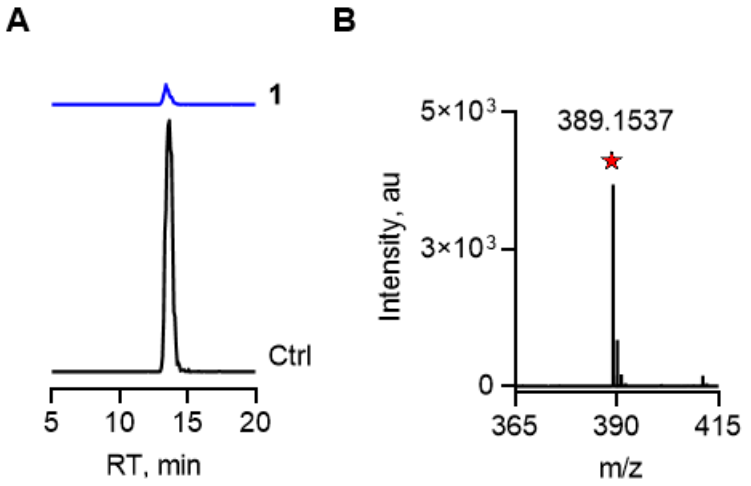

Figure 2.18. A) Extracted ion chromatograms from an LC/MS analysis of **Bis-S-HPE-AM** formation from **1** and ctrl ; (B) Mass spectra for **Bis-S-HPE-AM** (expected, m/z = 389.1530 $[M + H]^+$; observed, m/z = 389.1537).

From the above data, it can be concluded that compound **1** reacts with esterase to generate persulfides as well as H_2S.

2.2.9. H_2S Measurement

As compound **1** was also able to generate H_2S as a decomposition by-product of persulfide, we measured H_2S formation using lead acetate and a colorimetric methylene blue assay.

2.2.9.1. H_2S measurement using lead acetate assay

Firstly, H_2S release was studied using the lead acetate assay. In this assay, H_2S released from **1** was trapped by $Pb(OAc)_2$ soaked paper, and a black spot of lead sulfide (PbS) was formed on the paper (Scheme 2.9).

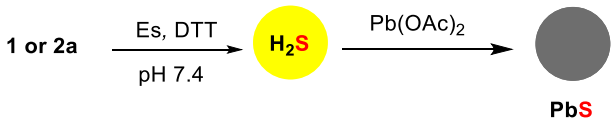

Scheme 2.9. Lead acetate assay for the detection of H_2S from **1** and **2a**.

In this assay, 200 μM of **1** or **2a** were incubated with Es (1 U/mL) and DTT (10 mM) in PBS (pH 7.4) at 37 °C. The assay was performed in a 96-well plate, which was covered with 10% $Pb(OAc)_2$ soaked paper, and the reaction was incubated for 3 h. A black spot for PbS was observed for **1**, indicating H_2S formation, whereas, as expected, negative control **2a** failed to produce H_2S (Figure 2.19).

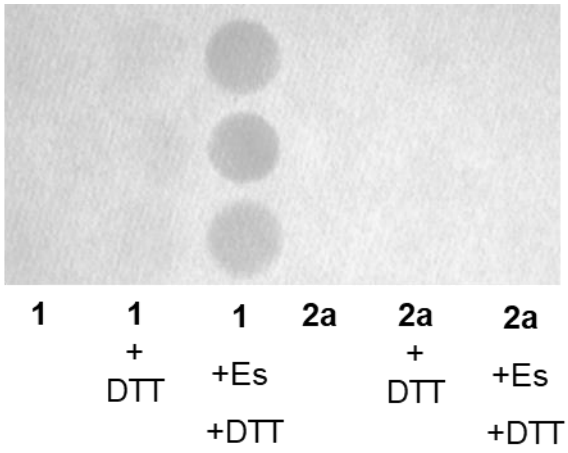

Figure 2.19. Lead acetate assay for H_2S generation from **1** (200 μM) in the presence of Es and DTT for 3 h. **2a** was used as a negative control.

2.2.9.2. Methylene blue assay for H_2S measurement

Along with the lead acetate assay for H_2S measurement, a standard methylene blue (MB) colorimetric assay was performed with compound **1** as shown in Scheme 2.10.[35]

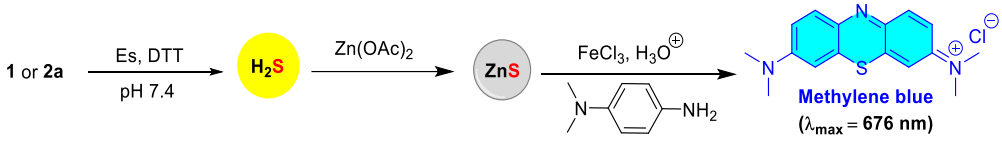

Scheme 2.10. Methylene blue assay protocol for the measurement of H_2S from **1** and **2a**.

In this assay, 200 μM of **1** or **2a** were incubated with Es (1 U/mL), **Zn(OAc)$_2$** (400 μM), and **DTT** (10 mM) in PBS (pH 7.4) at 37 °C for 3 h. Next, aliquots from the reaction mixtures were treated with methylene blue reagents and mixed. The final reaction mixture was then transferred to the 96-well plate, and absorbance at 676 nm was recorded. Similar to the lead acetate assay, a signal for the H_2S generation from **1** was observed, whereas, as expected, no signal from negative control **2a** was observed (Figure 2.20).

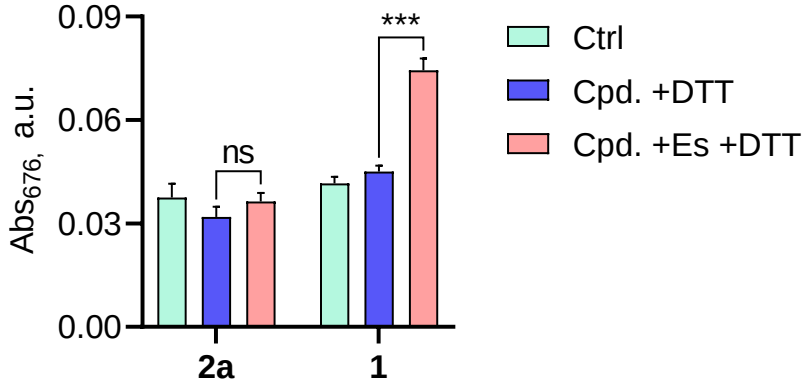

Figure 2.20. Methylene blue assay for H_2S generation from **1** in the presence of Es and DTT for 3 h. Results are expressed as mean ± SD (n =3/group). *p*-value was determined by using Two-way ANOVA relative to w/o Es. (***$p \leq 0.001$ and ns indicates not significant). **2a** was used as a negative control.

Overall, this data suggests that compound **1** was able to generate H_2S in the presence of esterase under reducing conditions.

2.2.10. MTT assay for cell viability of 1

MTT assay is commonly used to determine the cytotoxicity of the compound by measuring the cell's viability. Live cells are known to release higher amounts of mitochondrial reductases than unhealthy/dead cells. These reductases in the presence of co-factor NADH (Nicotinamide adenine dinucleotide hydrogen) react with the yellow-colored **MTT** dye (3-(4,5-dimethylthiazol-2-yl)-2,5-diphenyl tetrazolium bromide) and gets converted to pink colored formazan dye (Scheme 2.11). The absorbance of the formazan dye was monitored at 570 nm to determine the cell viability. Mouse embryonic fibroblast (MEF) cells were treated with varying concentrations of **1** and incubated for 24 h, following which cell viability was measured. Compound **1** was found to be well tolerated by MEF cells up to 100 μM (Figure 2.21).

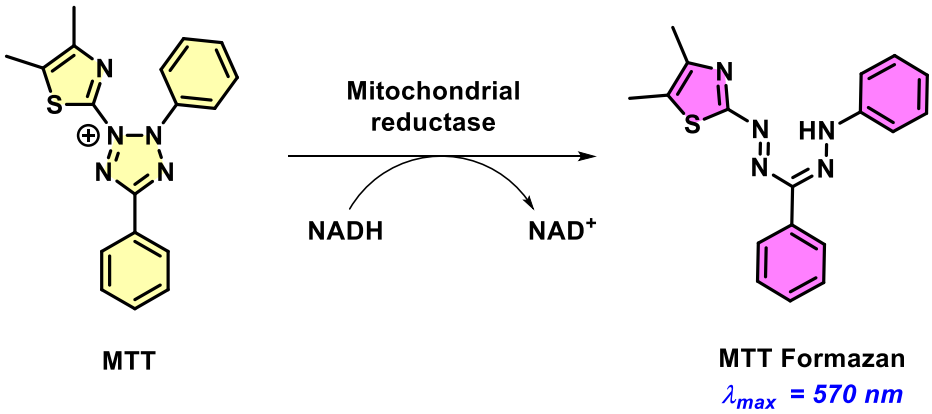

Scheme 2.11. MTT assay for cell viability. The formation of pink-colored formazan dye from yellow-colored MTT in the presence of cellular reductases and NADH.

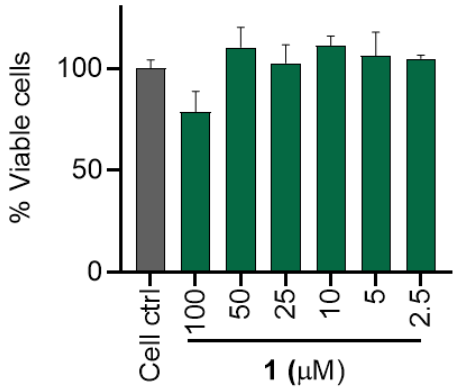

Figure 2.21. Cell viability assay was conducted on MEF cells with compound **1** for 24 h.

2.2.11. Two-photon confocal microscopy

As compound **1** generates persulfide as well as fluorogenic lactone **2a**, we evaluated the intracellular activation of **1** using confocal microscopy. Since **2a** belongs to a class of fluorophores that are compatible with two-photon imaging, it has more advantages over one-photon imaging, such as deep tissue penetration, decreased light scattering, and less photo-bleaching. [36] So, we performed two-photon imaging in MEF cells with compound **1**. MEF cells were treated with 50 μM of **1** for 4 h, followed by two-photon confocal imaging. The fluorescence signal attributable to **2a** formation from **1** was observed (λ_{ex} = 700 nm; λ_{em} = 432 nm) (Figure 2.22). Together, these results support that compound **1** is able to generate **2a** in the presence of cellular esterase.

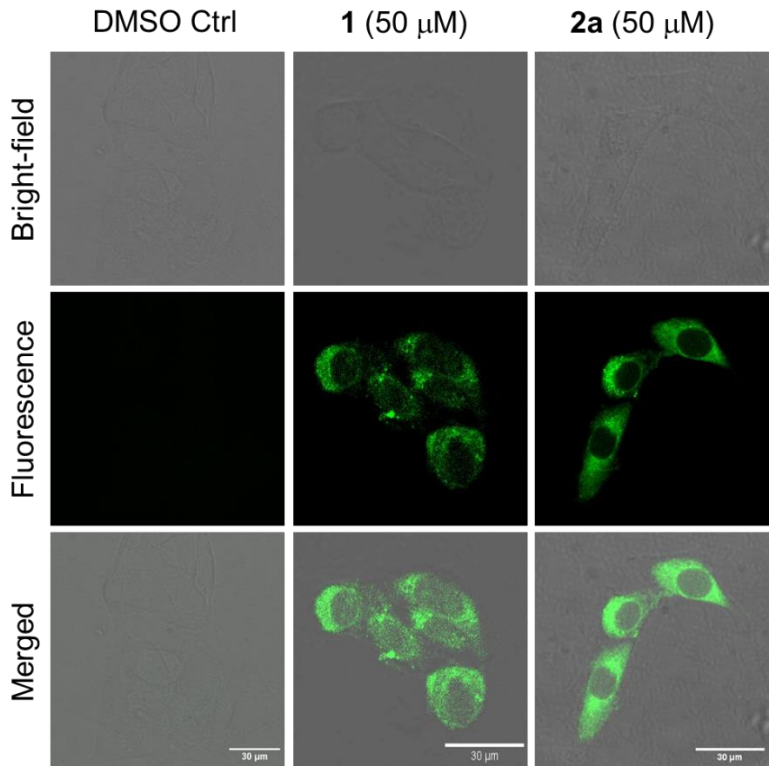

Figure 2.22. Two-photon confocal microscopy images of MEF cells treated with **1** and **2a** (50 μM). The excitation and emission channels were 700 nm and 432 nm, respectively. Scale bar is 30 μm.

2.2.13. ROS quenching using DCF-DA assay

Lastly, the ability of persulfide donor **1** to protect the cells from the cytotoxicity induced by oxidative stress was evaluated in MEF cells. The oxidative stress in MEF cells was induced by a cell-permeable ROS generator, **MGR-1** (Scheme 2.12).[37] To understand if **1** acted through diminishing ROS levels, a standard **H_2-DCF-DA** assay was performed in MEF cells (Scheme 2.13).

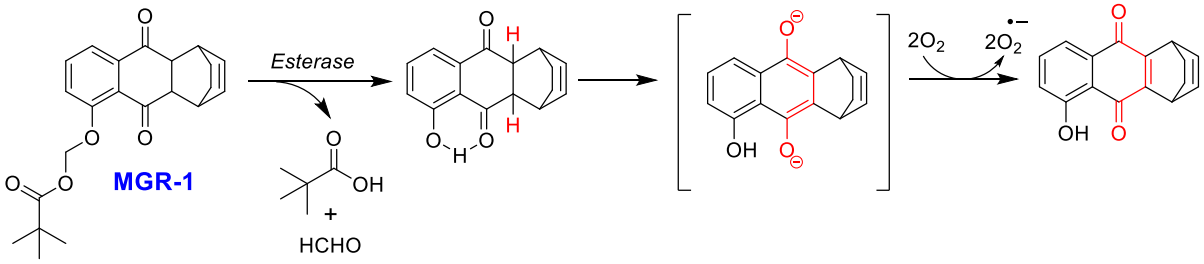

Scheme 2.12. Structure and generation of ROS from **MGR-1**.

The MEF cells were treated with 25 or 50 μM of **1** for 4 h, followed by exposure to **MGR-1** (15 μM) for 1 h, and finally, the **DCF-DA** probe (10 μM) was added for 10 min, and the cells were imaged using microscopy. As expected, an enhanced fluorescence signal was observed in **MGR-1**-treated cells, and in the cells pre-treated with compound **1**, a dose-dependent reduction in the fluorescence intensity was observed. This data supports the cytoprotective effect of compound **1** (Figure 2.23).

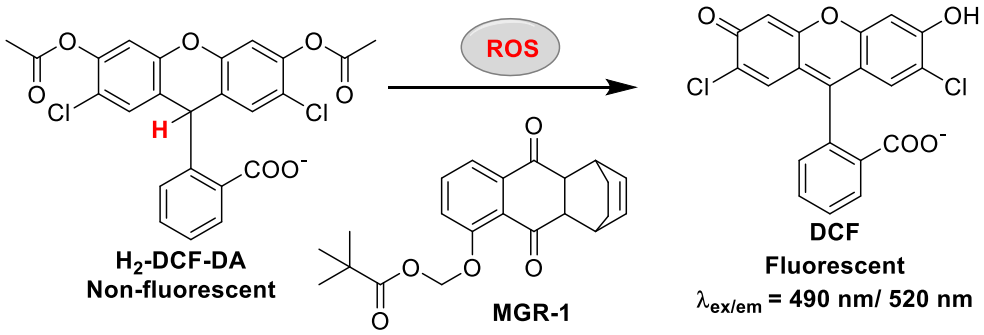

Scheme 2.13. Detection of ROS generated from **MGR-1** using **H₂-DCF-DA**.

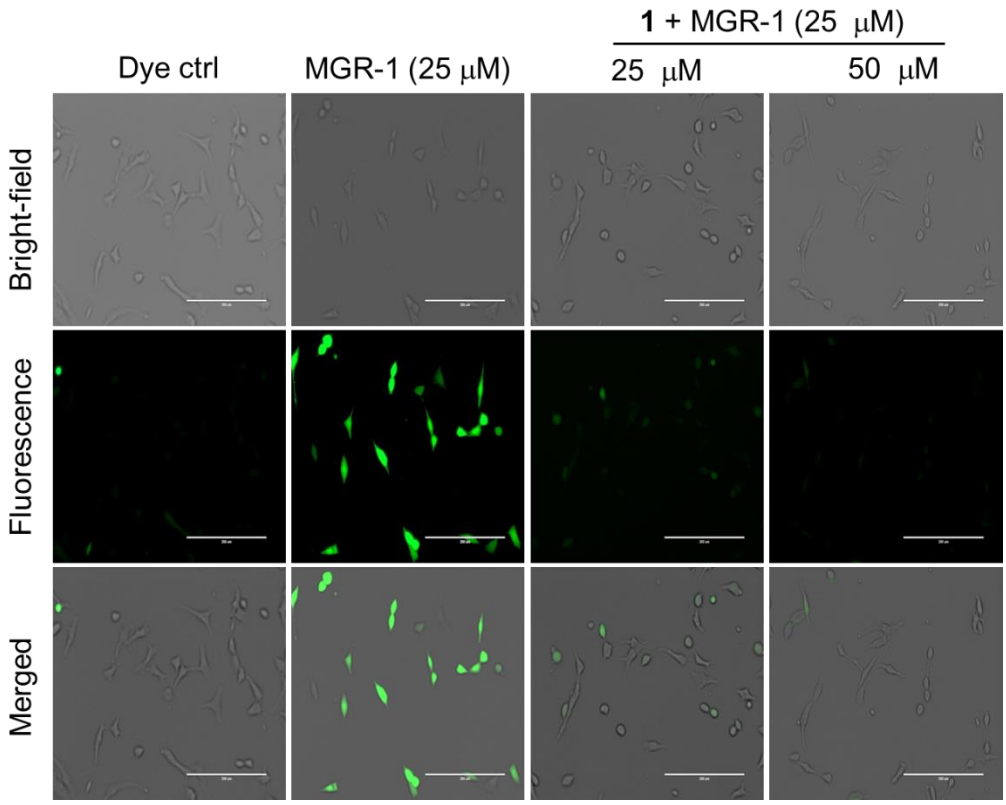

Figure 2.23. MEF cells were treated with varying concentrations of **1** (25 μM and 50 μM) for 4 h, followed by treatment with **MGR-1** (25 μM) for 1 h. Intracellular ROS levels were detected using DCF dye (10 μM). The cells were imaged in the 20× GFP filter. Scale bar is 200 μm.

2.3. Summary

In summary, using a latent fluorophore strategy, we report a new probe **1** embedded with N-acetylcysteine persulfide that is cleaved by esterase to produce a persulfide as well as a fluorescence reporter **2a** without any electrophilic byproducts. Firstly, the photophysical properties, stability, and reactivity of lactone **2a** were evaluated. The lactone **2a** was stable towards biologically relevant nucleophiles, suggesting its non-electrophilic nature. Next, the formation of fluorophore lactone **2a** from **1** was monitored using fluorescence-based experiments. A significant enhancement in the fluorescence intensity attributable to **2a** formation (λ_{ex} = 320 nm; λ_{em} = 432 nm) was observed upon activation of **1** by esterase, and the formation of **2a** was independently confirmed from MS analysis. Next, the persulfide release from **1** was detected using an electrophilic trapping agent (monobromobimane: **mBBr**) and persulfide-specific fluorescent probes (**SSP2**). Both the independent fluorescent assays exhibited an excellent correlation. Next, the rates of lactone **2a** and persulfide generation (**SSP2**) were compared, and an excellent correlation was observed, suggesting the release of fluorophore and NAC persulfide occur nearly concurrently following esterase-mediated cleavage and subsequent lactonization. This fluorescence signal of lactone can be used as a proxy signal for the persulfide generation, which eliminates the need for secondary assays for the detection of persulfides. Next, an additional LC-MS experiment was conducted to validate the persulfide generation and H_2S from **1** using **HPE-IAM** as an electrophilic trapping agent. H_2S generation was independently verified using lead acetate and methylene blue assays. Further, the intracellular activation of **1** to release **2a** was monitored using two-photon confocal microscopy. The cytoprotection, i.e., ROS quenching ability of **1**, was demonstrated using the standard DCF-DA assay in MEF cells.

2.4. Experimental protocols

2.4.1. General methods

All the chemicals and solvents were purchased from commercial sources and used as received unless stated otherwise. Column chromatography was performed using silica gel-Rankem (60–120 mesh) as stationary phase. Preparative high-performance liquid chromatography (HPLC) was done using Combiflash EZ prep UV using a Kromasil®C-18 preparative column (250 mm × 21.2 mm, 5 μm). ^{1}H and ^{13}C spectra were recorded on a JEOL 400 MHz (or 100 MHz for ^{13}C) or a Bruker 400 MHz (or 100 MHz for ^{13}C) spectrometer unless otherwise specified using either residual solvent signals ($CDCl_3$ δH = 7.26 ppm, δC = 77.2 ppm), or as an internal tetramethylsilane (δH = 0.00, δC = 0.0). Chemical shifts (δ) are reported in ppm and coupling constants (*J*) in Hz. The following abbreviations are used: m (multiplet), s (singlet), d (doublet), t (triplet), ddt (doublet of doublet of triplet) and dq (doublet of quartet). High-resolution mass spectra were obtained from HRMS-ESI-Q-Time of Flight LC/MS. FT-IR spectra were recorded using a BRUKER-ALPHA FT-IR spectrometer and reported in cm^{-1}. All measurements were done using a LC/MS method in the positive ion mode using high-resolution multiple reaction monitoring (MRM-HR) analysis on a Sciex X500R quadrupole time-of-flight (QTOF) mass spectrometer fitted with an Exion UHPLC system. Photometric measurements were performed using an Ensight Multimode Plate Reader (PerkinElmer). Fluorometric measurements were performed using a Thermo Scientific Varioscan microplate reader and a HORIBA Scientific Fluoromax-4 spectrofluorometer.

2.4.2. Synthesis and characterization

Compounds **2a**,[30,31] **2b**,[30] and **9**[15] were synthesized following previously reported protocols, and each compound's analytical data was consistent with reported values.

4-(allyloxy)-2'-(hydroxymethyl)-[1,1'-biphenyl]-2-ol (3):

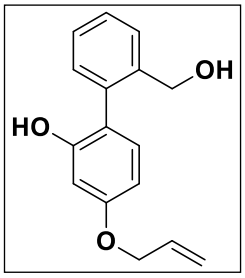

Lithium aluminium hydride (LAH) pellets (1.8g, 47.5 mmol) were added to a solution of compound **2a** (4g, 15.8 mmol) in dry THF (50 mL) at 0 ˚C under N_2 atmosphere. After 15 min, following the consumption of starting material by TLC, the reaction was quenched with ice-cold water (30 mL), and the resulting solution was extracted with EtOAc (3 × 10 mL). The combined organic phase was washed with brine, dried over Na_2SO_4, and evaporated under reduced pressure. The crude product was then recrystallized with $CHCl_3$ to give the

desired compound **3** (1.63 g, 94%) as white colored solid. FT-IR (ν_{max}, cm^{-1}): 3273, 1616; ^1H NMR (400 MHz, $CDCl_3$) δ 7.53 – 7.51 (m, 1H), 7.43 – 7.37 (m, 2H), 7.25 – 7.23 (m, 1H), 7.02 – 6.99 (m, 1H), 6.58 – 6.57 (m, 2H), 6.08 (ddt, *J* = 17.2, 10.6, 5.3 Hz, 1H), 5.99 (s, 1H), 5.46 (dq, *J* = 17.2, 1.6 Hz, 1H), 5.32 (dq, *J* = 10.5, 1.4 Hz, 1H), 4.55 (dt, *J* = 5.3, 1.5 Hz, 2H), 4.50 (s, 2H), 2.26 (s, 1H); ^{13}C NMR (100 MHz, $CDCl_3$): δ 159.7, 154.0, 139.2, 136.5, 133.3, 131.5, 131.4, 129.4, 128.7, 128.6, 120.5, 118.0, 107.7, 102.9, 69.0, 63.9; HRMS (ESI-TOF) for $C_{16}H_{16}O_3[M+H]^+$: Calcd., 257.1172, Found, 257.1177.

4-(allyloxy)-2'-(((*tert*-butyldimethylsilyl)oxy)methyl)-[1,1'-biphenyl]-2-ol (4):

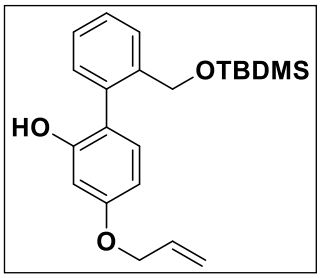

To a solution of **3** (0.256 g, 1.0 mmol) in anhydrous DCM (20 mL), imidazole (0.147 g, 2.2 mmol) was added at rt under N_2 atmosphere. After stirring for 1 h at rt the ice bath was used to bring down the temperature to 0 ˚C, and TBDMS-Cl (0.331 g, 2.2 mmol) was added to it. After 10 min , the reaction was brought back to RT and stirred for another 2 h. After the consumption of the starting material, as monitored by TLC, the organic solvent was evaporated under reduced pressure, diluted with water, and the aqueous solution was extracted with EtOAc (3 × 10 mL). The combined organic layer was washed with brine, dried over Na_2SO_4, filtered and the filtrate was concentrated to give a crude compound. This crude was further purified by column chromatography using silica gel (60 - 120) with 8% EtOAc/hexane as the eluent to obtain **4** (0.304 g, 87%) as a pale-yellow liquid. FT-IR (ν_{max}, cm^{-1}): 2928, 2856, 1618; ^1H NMR (400 MHz, $CDCl_3$) δ 7.52 (dd, *J* = 7.4, 1.8 Hz, 1H), 7.36 (td, *J* = 6.8, 1.7 Hz, 2H), 7.3 - 7.21 (m, 1H), 7.00 (d, *J* = 8.3 Hz, 1H), 6.59 (dt, *J* = 8.3, 2.5 Hz, 2H), 6.09 (ddt, *J* = 17.2, 10.6, 5.3 Hz, 1H), 5.45 (dq, *J* = 17.2, 1.6 Hz, 1H), 5.31 (dq, *J* = 10.5, 1.4 Hz, 1H), 4.56 (dt, *J* = 5.3, 1.5 Hz, 2H), 4.50 (s, 2H), 0.91 (s, 9H), 0.07 (s, 6H); ^{13}C NMR (100 MHz, $CDCl_3$): δ 172.7, 158.8, 148.8, 139.7, 134.7, 132.9, 131.3, 130.1, 127.6, 126.4, 126.3, 117.9, 112.4, 108.9, 69.1, 62.7, 29.7, 18.3, 12.8, -5.4; HRMS (ESI-TOF) for $C_{22}H_{30}O_3Si[M+Na]^+$: Calcd., 393.1856, Found, 393.1863.

4-(allyloxy)-2'-(((*tert*-butyldimethylsilyl)oxy)methyl)-[1,1'-biphenyl]-2-yl cyclopropanecarboxylate (5):

A solution of **4** (0.24 g, 0.6 mmol) and cyclopropane carboxylic acid (CPCA) (0.084 g, 1.0 mmol) were taken in DCM (20 mL). To the above reaction mixture DMAP (0.008 g, 0.064 mmol) was added and stirred for 15 min. To the reaction mixture, DCC (0.147g, 0.71 mmol)

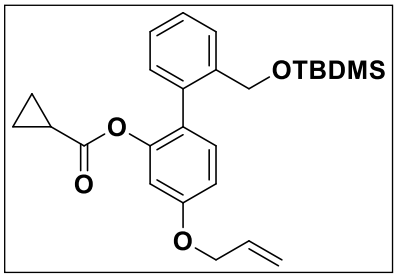

was added under N_2 atmosphere and the reaction was stirred at rt for overnight. Upon completion of the reaction, as monitored by TLC solvent was evaporated, diluted with 10 mL of water, extracted with EtOAc (3 × 20 mL). The combined organic layer was washed with brine, dried over Na_2SO_4, filtered and filtrate was concentrated to give a crude compound. This crude was further purified by column chromatography using silica gel (60 - 120) with 6% EtOAc/hexane as the eluent to obtain **5** (0.261 g, 92%) as a yellow liquid. FT-IR (ν_{max}, cm^{-1}): 2928, 2856, 1751, 1617; ^1H NMR (400 MHz, $CDCl_3$): δ 7.58 (dd, *J* = 7.7, 0.7 Hz, 1H), 7.36 (td, *J* = 7.6, 1.4 Hz, 1H), 7.23 (d, *J* = 6.2 Hz, 1H), 7.16 (d, *J* = 8.5 Hz, 1H), 7.09 (dd, *J* = 7.6, 1.2 Hz, 1H), 6.84 (dd, *J* = 8.5, 2.6 Hz, 1H), 6.72 (d, *J* = 2.5 Hz, 1H), 6.08 (ddt, *J* = 17.2, 10.6, 5.3 Hz, 1H), 5.44 (dq, *J* = 17.3, 1.6 Hz, 1H) , 5.32 (dq, *J* = 10.5, 1.4 Hz, 1H), 4.57 (dt, *J* = 5.3, 1.5 Hz, 2H), 4.50 (d, *J* = 7.0 Hz, 2H), 1.51-1.45 (m, 1H), 0.90 (s, 9H), 0.70 (d, *J* = 8.0 Hz, 4H), 0.00 (s, 6H); ^{13}C NMR (100 MHz, $CDCl_3$): δ 172.8, 158.9, 148.9, 139.9, 134.8, 133.1, 131.4, 130.2, 127.7, 126.6, 126.5, 126.2, 118.0, 112.5, 109.1, 69.2, 62.8, 26.1, 18.5, 13.0, 8.5, -5.2; HRMS (ESI-TOF) for $C_{24}H_{34}O_4Si[M+Na]^+$: Calcd., 461.2123, Found, 461.2119.

4-(allyloxy)-2'-(hydroxymethyl)-[1,1'-biphenyl]-2-yl cyclopropanecarboxylate (6):

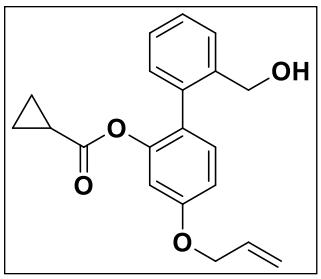

To a well-stirred solution of **5** (0.24 g, 0.5 mmol) in H_2O:THF (1:1 v/v, 20 mL), AcOH (60 mL) was added and the reaction was stirred at rt for 18 h. Once the starting material was completely consumed, as monitored by TLC, the reaction mixture was extracted with EtOAc (3 × 20 mL). The combined organic layer was washed with brine, dried over Na_2SO_4, filtered and the filtrate was concentrated to give a crude product. This crude was further purified by column chromatography using silica gel (60 - 120) with 15% EtOAc/hexane as the eluent to obtain **6** (0.091 g, 52%) as a yellow liquid. FT-IR (ν_{max}, cm^{-1}): 3434, 1742, 1616; ^1H NMR (400 MHz, $CDCl_3$): δ 7.53 (dd, *J* = 7.7, 1.1 Hz, 1H), 7.37 (td, *J* = 7.5, 1.4 Hz, 1H), 7.28 (td, *J* = 7.5, 1.4 Hz, 1H), 7.17 – 7.13 (m, 2H), 6.86 (dd, *J* = 8.5, 2.6 Hz, 1H), 6.72 (d, *J* = 2.5 Hz, 1H), 6.07 (ddt, *J* = 17.2, 10.6, 5.3 Hz, 1H), 5.44 (dq, *J* = 17.3, 1.6 Hz, 1H), 5.31 (dq, *J* = 10.5, 1.4 Hz, 1H), 4.56 (dt, *J* = 5.3, 1.5 Hz, 3H), 4.38 (d, *J* = 12.2 Hz, 1H), 1.52-1.47 (m, 1H), 0.70 (d, *J* = 8.0 Hz, 4H); ^{13}C NMR (100 MHz, $CDCl_3$): δ 173.4, 159.1, 149.1, 139.7, 135.8, 133.0, 131.6, 130.7, 129.0, 128.2, 127.2, 126.2, 118.1, 112.6, 109.0, 69.2,

63.1, 34.0, 12.9, 8.9, 8.8; HRMS (ESI-TOF) for $C_{20}H_{20}O_4[M+Na]^+$: Calcd., 347.1254, Found, 347.1259.

4-(allyloxy)-2'-formyl-[1,1'-biphenyl]-2-yl cyclopropanecarboxylate (7):

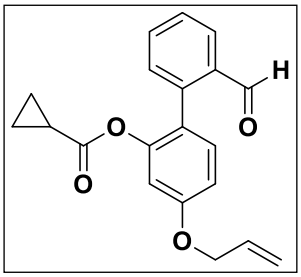

To a stirred solution of **6** (0.05 g, 0.15 mmol) in DCM (10 mL) at room temperature, PCC (0.07 g, 0.31 mmol) was added in to it under inert atmosphere. The reaction was stirred at rt for 40 min. The reaction mixture was filtered through celite and the filtrate was evaporated. The residue was further purified by column chromatography using silica gel (60-120) with 10% EtOAc/hexane as eluent, to provide **7** (0.038 g, 76%) as yellowish coloured solid. FT-IR (ν_{max}, cm^{-1}): 2921, 1750, 1694, 1616; ^1H NMR (400 MHz, $CDCl_3$) δ 9.84 (d, *J* = 0.7 Hz, 1H), 7.99 (dd, *J* = 7.8, 1.1 Hz, 1H), 7.61 (td, *J* = 7.5, 1.5 Hz, 1H), 7.48 (t, *J* = 7.6 Hz, 1H), 7.32 (dd, *J* = 7.7, 0.8 Hz, 1H), 7.25 (d, *J* = 8.9 Hz, 1H), 6.91 (dd, *J* = 8.5, 2.5 Hz, 1H), 6.76 (d, *J* = 2.5 Hz, 1H), 6.07 (ddt, *J* = 17.2, 10.6, 5.3 Hz, 1H), 5.45 (dq, *J* = 17.3, 1.6 Hz, 1H), 5.33 (dq, *J* = 10.5, 1.4 Hz, 1H), 4.57 (dt, *J* = 5.3, 1.5 Hz, 2H), 1.53 – 1.46 (m, 1H), 0.72 (d, 4H); ^{13}C NMR (100 MHz, $CDCl_3$): δ 192.5, 172.7, 159.8, 149.3, 140.8, 134.1, 133.7, 132.8, 131.5, 128.1, 127.0, 118.3, 113.0, 109.1, 69.3, 12.8, 9.0, 8.8; HRMS (ESI-TOF) for $C_{20}H_{18}O_4[M+Na]^+$: Calcd., 345.1097, Found, 345.1102.

4'-(allyloxy)-2'-((cyclopropanecarbonyl)oxy)-[1,1'-biphenyl]-2-carboxylic acid (8):

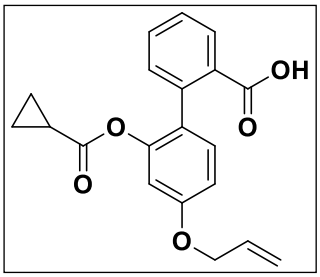

A solution of **7** (0.520 g, 1.61 mmol) was taken in dry ACN (30 mL) under N_2 atmosphere, and KH_2PO_4 (0.074 g, 0.53 mmol) was added and stirred for 15 min. To the reaction mixture, 30% H_2O_2 (1.3 mL, 16.66 mmol) and $NaClO_2$ (0.332 g, 3.66 mmol) were added and stirred at room temperature for 2 h. Upon the completion of reaction, as monitored by TLC the solvent was evaporated under reduced pressure. The reaction mixture was diluted with 10 mL of water and extracted with EtOAc (3 × 20 mL). The combined organic layer was washed with brine, dried over Na_2SO_4, filtered and the filtrate was concentrated under reduced pressure to give a crude compound. The residue was further purified by column chromatography using silica gel (60-120) with 30% EtOAc/hexane as eluent, to give **8** (0.486 g, 89%) as bright yellow colored solid. FT-IR (ν_{max}, cm^{-1}): 2922, 1745, 1699, 1618; ^1H NMR (400 MHz, $CDCl_3$): δ 7.84 (d, *J* = 7.7 Hz, 1H), 7.51 (td, *J* = 7.5, 1.2 Hz, 1H), 7.42 (td, *J* = 7.6, 1.1 Hz, 1H), 7.27 (d, *J* = 6.5 Hz, 1H), 7.21 (d, *J* = 8.5 Hz, 1H), 6.88 (dd, *J* = 8.5, 2.5 Hz, 1H),

6.73 (d, *J* = 2.5 Hz, 1H), 6.06 (ddt, *J* = 17.2, 10.6, 5.3 Hz, 1H), 5.44 (dd, *J* = 17.3, 1.4 Hz, 1H), 5.32 (dd, *J* = 10.5, 1.2 Hz, 1H), 4.57 (d, *J* = 5.3, 1.5 Hz, 2H), 1.65 – 1.57 (m, 1H), 0.80 (d, 4H); ^{13}C NMR (100 MHz, $CDCl_3$): δ 174.6, 170.3, 159.7, 148.2, 136.2, 132.8, 132.5, 131.4, 131.3, 130.9, 130.3, 127.9, 125.9, 118.3, 113.2, 108.8, 69.3, 13.0, 9.7, 9.2; HRMS (ESI-TOF) for $C_{20}H_{18}O_5[M+Na]^+$: Calcd., 361.1046, Found, 361.1050.

_N_-acetyl-S-((4'-(allyloxy)-2'-((cyclopropanecarbonyl)oxy)-[1,1'-biphenyl]-2-carbonyl)thio)cysteine (1)[16]:

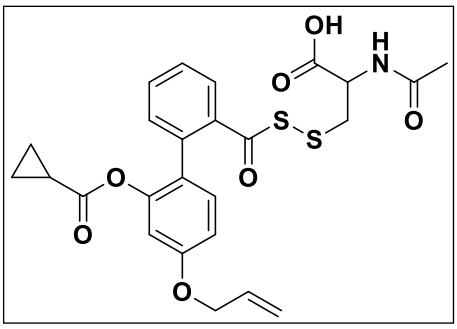

A mixture of compound **8** (0.1 g, 0.28 mmol), lawesson's reagent (0.057 g, 0.14 mmol), and dry toluene (6 mL), was charged to a pressure tube and heated at 120 ^{o}C for 3 h. After consumption of the starting material, as monitored by TLC, the solvent was evaporated under reduced pressure. The reaction mixture was diluted with DCM (10 mL), washed with 1 N HCl and brine, and dried over Na_2SO_4. The filtrate was concentrated under reduced pressure to give a crude oily compound (**10**) which was carried forward to the next step without further purification. The oily product was dissolved in $CHCl_3$ (10 mL), **9** (**NAC-SS-Py**) (0.078 g, 0.28 mmol) was added under N_2 atmosphere at rt. The solution was stirred for 8 h. Once the starting material was completely consumed, as monitored by TLC, the solvent was evaporated under reduced pressure to give the crude compound. The residue was purified by preparative HPLC using Kromasil®C-18 column at ambient temperature under the gradient elution with H_2O: ACN (40:60, v/v) as mobile phase at a flow rate of 12 mL/min to afford pure product **1** (0.027 g, 18%) as a brownish solid. FT-IR (ν_{max}, cm^{-1}): 3348, 2922, 2855, 1736, 1707, 1647, 1618; ^{1}H NMR (400 MHz, $CDCl_3$): δ 7.78 (d, *J* = 7.6 Hz, 1H), 7.72 (s, 1H), 7.58 (t, *J* = 7.1 Hz, 1H), 7.45 (t, *J* = 7.3 Hz, 1H), 7.33 (d, *J* = 7.6 Hz, 1H), 7.21 (d, *J* = 8.5 Hz, 1H), 6.86 (dd, *J* = 8.5, 2.4 Hz, 1H), 6.69 (d, *J* = 2.5 Hz, 1H), 6.06 (ddt, *J* = 17.2, 10.6, 5.3 Hz, 1H), 5.42 (dd, *J* = 17.3, 1.1 Hz, 1H), 5.30 (dd, *J* = 10.5, 1.2 Hz, 1H), 4.54 (d, *J* = 5.2 Hz, 2H), 3.44 (s, 1H), 2.96 (d, *J* = 12.3 Hz, 1H), 1.96 (s, 3H), 1.61 - 1.54 (m, 1H), 0.78 (d, *J* = 6.7 Hz, 4H); ^{13}C NMR (100 MHz, $CDCl_3$): δ 173.0, 171.7, 159.7, 136.2, 136.1, 132.8, 132.3, 131.5, 128.3, 127.9, 125.3, 118.2, 109.0, 69.2, 52.5, 41.8, 22.6, 12.9, 9.1; HRMS (ESI-TOF) for $C_{25}H_{25}NO_7S_2[M+H]^+$: Calcd., 516.1145, Found, 516.1150.

2.4.3. Photophysical properties

2.4.3.1. Measurement of absorbance

Stock solutions of **2a** and **2b** (10 mM) in DMSO were prepared. The solution was prepared by adding 100 μM of **2a** or **2b** (10 μL, 10 mM) with 990 μL phosphate buffer saline (10 mM, pH 7.4) into a cuvette. UV/vis spectra were recorded using a SHIMADZU, UV-2600 UV-Vis spectrophotometer at room temperature.

2.4.3.2. Measurement of fluorescence

Stock solutions of **2a** and **2b** (10 mM) in DMSO were prepared. The solution was prepared by adding 5 μM of **2a** or **2b** (0.5 μL, 10 mM) with 990 μL phosphate buffer saline (10 mM, pH 7.4) into a cuvette. Fluorescence spectra were recorded by using a HORIBA Scientific Fluoromax-4 spectrofluorometer at room temperature.

2.4.4. Stability and reactivity of 2a towards nucleophiles

Stock solution of **2a** (0.5 mM) in DMSO was prepared. Stock solutions of 10 mM of L-cysteine (Cys), *N*- acetyl cysteine (NAC), L-glutathione (GSH), L-histidine (His), L-threonine (Threo), L-serine (Ser), L-lysine (Lys), L-proline (Pro), sodium chloride (NaCl), and sodium nitrate ($NaNO_3$) were prepared in de-ionised water. Stock solution of 10 mM of L-tyrosine (Tyr) was prepared in DMSO. The reaction mixture was prepared by adding 10 μM of **2a** (4 μL, 0.5 mM), with or without 100 eq. of nucleophiles (20 μL, 10 mM stock) and the volume was adjusted to 200 μL using phosphate buffer saline (10 mM, pH 7.4) in a 96-well plate and then incubated for 120 min at 37 ˚C. The fluorescence (λ_{ex} = 320 nm and λ_{em} = 432 nm) was measured using an Ensight Multimode Plate Reader (PerkinElmer).

2.4.5. Monitoring the release of 2a upon esterase activation of 1

(A) Fluorometric analysis

Stock solutions of **1** (10 mM), **2a** (10 mM) in DMSO, and porcine liver esterase (100 U/mL; Sigma Aldrich, E3019) in phosphate buffer saline (10 mM, pH 7.4) were prepared. The reaction mixture was prepared by adding 10 μM of **1** (10 μL, 1 mM), with or without 1 U/mL Es (esterase;10 μL, 100 U/mL stock) and the volume was adjusted to 1000 μL using phosphate buffer saline (10 mM, pH 7.4) in a 1.5 mL eppendorf tube and incubated for 60 min at 37 ˚C then transferred into a micro-fluorescence cell (Hellma, path length 1.0 cm). Fluorescence spectra (λ_{ex} = 320 nm and λ_{em} = 432 nm) were recorded using HORIBA Scientific Fluoromax-4 spectrofluorometer with an excitation and an emission slit width of 2 nm.

(B) Fluorescence-based analysis

Stock solutions of **1** (0.5 mM) in DMSO and porcine liver esterase (10 U/mL; Sigma Aldrich, E3019) in phosphate buffer saline (10 mM, pH 7.4) were prepared. The reaction mixture was prepared by adding 10 μM of **1** (4 μL, 0.5 mM) with or without 1 U/mL esterase (20 μL, 10 U/mL stock) and the volume was adjusted to 200 μL using phosphate buffer saline (10 mM, pH 7.4) in a 96-well plate and then incubated for 120 min at 37 ˚C. The fluorescence (λ_{ex} = 320 nm and λ_{em} = 432 nm) was measured using an Ensight Multimode Plate Reader (PerkinElmer).

Stock solutions of **1** or **2a** (0.125, 0.25, 0.5, 1 mM) in DMSO and porcine liver esterase (10 U/mL; Sigma Aldrich, E3019) in phosphate buffer saline (10 mM, pH 7.4) were prepared. The reaction mixture was prepared by varying concentrations (0-20 μM) of **1** (4 μL from respective stocks (0.125-1 mM)), with or without 1 U/mL esterase (20 μL, 10 U/mL stock) and the volume was adjusted to 200 μL using phosphate buffer saline (10 mM, pH 7.4) in a 96-well plate. The time-dependent fluorescence increment (λ_{ex} = 320 nm and λ_{em} = 432 nm) was recorded at 37 ˚C for a period of 120 min using an Ensight Multimode Plate Reader (PerkinElmer).

2.4.6. Persulfide measurement using monobromobimane (mBBr) [13]

(A) Fluorometric analysis

i) Time-dependent fluorescence analysis

Stock solutions of **1** (10 mM), monobromobimane (**mBBr**, 10 mM) in DMSO, and porcine liver esterase (100 U/mL; Sigma Aldrich, E3019) in phosphate buffer saline (10 mM, pH 7.4) were prepared. The reaction mixture was prepared by adding 100 μM of **1** (10 μL, 10 mM), 100 μM of **mBBr** (10 μL, 10 mM), with or without 1 U/mL esterase (10 μL, 100 U/mL stock), and the volume was adjusted to 1000 μL using phosphate buffer saline (10 mM, pH 7.4) in a 1.5 mL eppendorf tube and then transferred into a micro-fluorescence cell (Hellma, path length 1.0 cm). Fluorescence spectra (λ_{ex} = 380 nm and λ_{em} = 455 nm) were recorded over 60 min using a HORIBA Scientific Fluoromax-4 spectrofluorometer with an excitation and an emission slit width of 1 nm.

ii) Concentration-dependent fluorescence analysis

Stock solutions of **1** (10 mM), monobromobimane (**mBBr**, 10 mM) in DMSO, and porcine liver esterase (100 U/mL; Sigma Aldrich, E3019) in phosphate buffer saline (10 mM, pH 7.4) were prepared. The reaction mixture was prepared by varying concentrations (0-100 μM) of **1**

(1-10 μL from 10 mM), with or without 1 U/mL esterase (20 μL, 10 U/mL stock), and the volume was adjusted to 1000 μL using phosphate buffer saline (10 mM, pH 7.4) in a 1.5 mL eppendorf tube. The reactions were incubated for 60 min at 37 ˚C and then transferred into a micro-fluorescence cell (Hellma, path length 1.0 cm). Fluorescence spectra (λ_{ex} = 380 nm and λ_{em} = 455 nm) were recorded using a HORIBA Scientific Fluoromax-4 spectrofluorometer with an excitation and an emission slit width of 1 nm.

(B) Fluorescence-based analysis

Concentration-dependent fluorescence analysis

Stock solutions of **1** (0.25, 0.5, 1, 2 mM), **mBBr** (2 mM) in DMSO, and porcine liver esterase (10 U/mL; Sigma Aldrich, E3019) in phosphate buffer saline (10 mM, pH 7.4) were prepared. The reaction mixture was prepared by varying concentrations (0-20 μM) of **1** (2 μL from respective stocks (0.25-2 mM)), **mBBr** (2 μL, 2 mM stock), with or without 1 U/mL esterase (20 μL, 10 U/mL stock) and the volume was adjusted to 200 μL using phosphate buffer saline (10 mM, pH 7.4) in a 96-well plate. The time-dependent fluorescence increment (λ_{ex} = 380 nm and λ_{em} = 455 nm) was recorded at 37 ˚C for a period of 120 min using an Ensight Multimode Plate Reader (PerkinElmer).

2.4.7. Sulfane sulfur measurement using SSP2[32]

(A) Fluorometric analysis

Stock solutions of **1** (10 mM), **SSP2** (10 mM) in DMSO, and porcine liver esterase (100 U/mL; Sigma Aldrich, E3019) in phosphate buffer saline (10 mM, pH 7.4) were prepared. The reaction mixture was prepared by adding 100 μM of **1** (10 μL, 10 mM), 50 μM of **SSP2** (5 μL, 10 mM), with or without 1 U/mL of esterase (10 μL, 100 U/mL stock) and the volume was adjusted to 1000 μL using phosphate buffer saline (10 mM, pH 7.4) in a 1.5 mL eppendorf tube and then transferred into a micro-fluorescence cell (Hellma, path length 1.0 cm). Fluorescence spectra (λ_{ex} = 482 nm and λ_{em} = 518 nm) were recorded over 120 min using a HORIBA Scientific Fluoromax-4 spectrofluorometer with an excitation and an emission slit width of 1 nm.

(B) Fluorescence-based analysis

Stock solutions of **1** (0.25, 0.5, 1, 2 mM), **SSP2** (1 mM) in DMSO, and porcine liver esterase (10 U/mL; Sigma Aldrich, E3019) in phosphate buffer saline (10 mM, pH 7.4) were prepared.

The reaction mixture was prepared by varying concentrations (0-20 μM) of **1** (2 μL from respective stocks (0.25-2 mM)), **SSP2** (2 μL, 1 mM stock), with or without 1 U/mL esterase (20 μL, 10 U/mL stock) and the volume was adjusted to 200 μL using phosphate buffer saline (10 mM, pH 7.4) in a 96-well plate. The time-dependent fluorescence increment (λ_{ex} = 482 nm and λ_{em} = 518 nm) was recorded at 37 ˚C for a period of 120 min using an Ensight Multimode Plate Reader (PerkinElmer).

2.4.8. Persulfide/polysulfide measurement from 1 using LC/MS

Stock solutions of **1** (10 mM) and **HPE-IAM** (100 mM) were prepared in DMSO. A stock solution of porcine liver esterase (100 U/mL; Sigma Aldrich, E3019) was prepared in PBS pH 7.4. The reaction mixture for **1** was prepared by adding 50 μM of **1** (2 μL, 10 mM stock) along with 10 mM **HPE-IAM** (4 μL, 100 mM) and 1 U/mL esterase (4 μL, 100 U/mL stock). The volume was adjusted to 400 μL using 10 mM PBS, pH 7.4, and the reaction mixture was incubated at 37 °C. 100 μL aliquots of the reaction mixture were taken at pre-determined time points, and the reaction was quenched by adding 100 μL of acetonitrile. The samples were centrifuged at 10, 000 x *g* for 10 minat 4 ˚C, the supernatant was collected and assessed thereafter by LC/MS. All measurements were done using a previously established LC/MS method[38] with slight modification. All measurements were done using the following protocol: Acetonitrile (A) and 0.1% formic acid in water (B) were used as the mobile phase. A multistep gradient was used with the flow rate of 0.2 mL/min starting with 0:100 → 0 min 0:100 to 5:95 → 0.10 -1 min, 5:95 to 90:10→ 1 - 15 min, 90:10 to 0:100 → 15 – 15.10 min, and 0:100 → 15 – 22 min. Measurements were carried out in the positive ion mode using high-resolution multiple reaction monitoring (MRM- HR) analysis on a Sciex X500R quadrupole time-of-flight (QTOF) mass spectrometer fitted with an Exion UHPLC system using a Kinetex 2.6 mm hydrophilic interaction liquid chromatography (HILIC) column with 100 Å particle size, 150 mm length and 3 mm internal diameter (Phenomenex). Nitrogen was the nebulizer gas, with the nebulizer pressure set at 50 psi, declustering potential = 80 V, entrance potential = 10 V, collision energy = 20 V, and collision exit potential = 5 V. The MRM-HR mass spectrometry parameters for measuring compounds are: m/z precursor ion mass $(M + H)^+$: 516.1145 (**1**), 305.9985 (**HPE-IAM**), 373.0891 (**NAC-SS-HPE-AM**), 389.1530 (**Bis-S-HPE-AM**).

2.4.9. Lead acetate assay for the H_2S detection from 1

Firstly, lead acetate paper was prepared by soaking Whatman filter paper with 10 % (w/v) lead acetate solution and dried. Stock solutions of **1** (10 mM), **2a** (10 mM) in DMSO, and porcine liver esterase (100 U/mL; Sigma Aldrich, E3019) in phosphate buffer saline (10 mM, pH 7.4) were prepared. Dithiothreitol (**DTT**, 10 mM) was prepared in deionized water.

Lead acetate assay was performed in a 96-well plate (with lid). The reaction samples were prepared by sequentially adding 200 μM of **1 or 2a** (14 μL from 10 mM), 10 mM of **DTT** (7 μL, 10 mM stock), with or without 1 U/mL esterase (7 μL, 100 U/mL stock), and the volume was adjusted to 700 μL using phosphate buffer saline (10 mM, pH 7.4) in a 1.5 mL Eppendorf tube. Aliquoted 200 μL from each reaction (in triplicate) in a 96-well plate, covered with 10 % lead acetate-soaked paper followed by the lid, sealed, and placed in a static incubator maintained at 37 ˚C for 3 h. After 3 h, lead acetate paper was carefully removed, and the image was taken using Syngene G-Box Chemi-XRQ.

2.4.10. Methylene blue assay for the H_2S detection from 1

General protocol: The methylene blue assay was conducted as previously reported with some modifications.[33,37] Stock solutions of **1** (10 mM), **2a** (10 mM) in DMSO, and porcine liver esterase (100 U/mL; Sigma Aldrich, E3019) in phosphate buffer saline (10 mM, pH 7.4) were prepared. Dithiothreitol (**DTT**, 100 mM), **NaSH** (100 mM), and **$Zn(OAc)_2.2H_2O$** (40 mM) were prepared in deionized water. Stock solution of **$FeCl_3$** (30 mM) was prepared in 1.2 M HCl, and *N*, *N*–dimethyl-*p*-phenylenediamine sulfate (**DMPPDA**) (20 mM) was prepared in 7.2 M HCl.

The reaction samples were prepared by sequentially adding 400 μM **$Zn(OAc)_2.2H_2O$** (10 μL, 40 mM stock), varying concentrations of **1** or **2a** from 25-100 μM (10 μL from respective stocks (1-4 mM)) with or without 1 U/mL esterase (10 μL, 100 U/mL stock) and the volume was adjusted to 1000 μL using phosphate buffer saline (10 mM, pH 7.4) in a 1.5 mL eppendorf tube and placed in a static incubator maintained at 37 ˚C.

207 μL aliquot of the reaction mixture was taken at pre-determined time points and 10 mM **DTT** (23 μL, 100 mM stock) was added, from which 200 μL was added to a 1.5 mL eppendorf containing equal volumes (200 μL) of **$FeCl_3$**, **DMPPDA** and incubated at 37 ˚C for 30 min in dark, to allow the formation of the methylene blue dye. An aliquot of 150 μL was transferred to a 96-well plate and the absorbance values were recorded at 676 nm using a microplate reader (Thermo Scientific VarioskanFlash).

2.4.11. Cell viability assay for 1

Mouse embryonic fibroblasts (MEF) cells were seeded at a concentration of 1×10^4 cells/well overnight in a 96-well plate in complete DMEM medium supplemented with 5% FBS (fetal bovine serum) and 1% antibiotic solution in an atmosphere of 5% CO_2 at 37 ˚C. Cells were exposed to varying concentrations of compound **1** prepared as a DMSO stock solution so that the final concentration of DMSO was 0.5%. The cells were incubated for 24 h at 37 ˚C. A 0.5 mg/mL stock solution of 3-(4, 5-dimethylthiazol-2-yl)-2, 5-diphenyl tetrazolium bromide (**MTT**) was prepared in DMEM and 100 μL of the resulting solution was added to each well. After 4 h incubation, the media was removed carefully, and 100 μL of DMSO was added. Spectrophotometric analysis of each well using a microplate reader (Thermo Scientific Varioscan) at 570 nm was carried out to estimate cell viability.

2.4.12. Detection of 2a release in N2a cell lysate

N2a cells were cultured in a 10 cm plates in complete DMEM medium supplemented with 5% FBS (fetal bovine serum) and 1% antibiotic solution in an atmosphere of 5% CO_2 at 37 ˚C. When the cells were 70% confluent, old media was removed and the cells were washed with serum free DMEM media. The cells were trypsinized and subsequently resuspended in DMEM. The cells were harvested by centrifugation at 1000 rpm/min at 4 ˚C. Pellets were washed twice with PBS (1x), resuspended in PBS (1x, 2 mL), and transferred to a microcentrifuge tube. Cells were lysed by sonication using a 130 W ultrasonic processor (VX 130W) with a stepped microtip for 2 min (with 3 sec. ON and 3 sec. OFF pulse, 60% amplitude) under ice-cold conditions. The total protein concentration of the whole cell lysate was determined by Bradford assay and further adjusted to 1 mg/mL with PBS (1×).

Stock solutions of **1** and **2a** (0.05 mM, 0.125 mM, 0.25 mM, 0.5 mM) independently in DMSO and a 1 mg/mL stock solution of cell lysate in phosphate buffer saline (10 mM, pH 7.4) were prepared. The reaction mixture was prepared by adding 1 μM, 2.5 μM, 5 μM and 10 μM **1** or **2a** (2 μL from 0.05 mM, 0.125 mM, 0.25 mM, 0.5 mM) independently along with cell lysate (98 μL, 1 mg/mL) in 96-well plate and incubated at 37 ˚C. The fluorescence corresponding to **2a** release (excitation at 320 nm; emission at 432 nm) was measured for 3 h using an Ensight Multimode Plate Reader (PerkinElmer).

2.4.13. Confocal imaging of MEF cells with 1

MEF cells were seeded at 1×10^5 cells/well in a 6-well Corning plate (on cover slip) overnight in Dulbecco's modified Eagle's medium (DMEM) supplemented with 10% FBS (fetal bovine serum) and 1% antibiotic solution in an atmosphere of 5% CO_2 at 37 ˚C. After incubation, the media was removed, and the cells were washed with 1 mL of PBS. Then 1 mL of fresh DMEM media was added along with 50 μM of **1**/**2a**, and the cells were incubated for 4 h at 37 ˚C. After 4 h, the media was removed, cells were washed twice with 1 mL of PBS, and then cells were imaged on a Carl Zeiss LSM710 laser scanning confocal microscope (700 nm for two-photon) with a 63x oil immersion objective. Images were analyzed by ImageJ software.

2.4.14. ROS quenching in MEF cells with 1

MEF cells were seeded at 1×10^5 cells/well in a 6-well Corning plate overnight in Dulbecco's modified Eagle's medium (DMEM) supplemented with 10% FBS (fetal bovine serum) and 1% antibiotic solution in an atmosphere of 5% CO_2 at 37 ˚C. The old media was removed, and the cells were washed with 1 mL of PBS. Then 1 mL of fresh DMEM media was added along with 25 and 50 μM of **1**, and the cells were incubated for 4 h at 37 ˚C. After 4 h, the media was removed, cells were washed with 1 mL of PBS and treated with **MGR-1** (25 μM) for 1 h. After **MGR-1** treatment, the media was removed, cells were washed with 1× PBS and then treated cells with **H_2DCF-DA-probe** (10 μM) and cells were incubated further for 10 min at 37 ˚C. The cells were washed twice with 1 mL of PBS and then were imaged on an EVOS fluorescence microscope using a 20x GFP filter.

2.5. NMR spectra of compounds

^{1}H NMR spectra of **1**

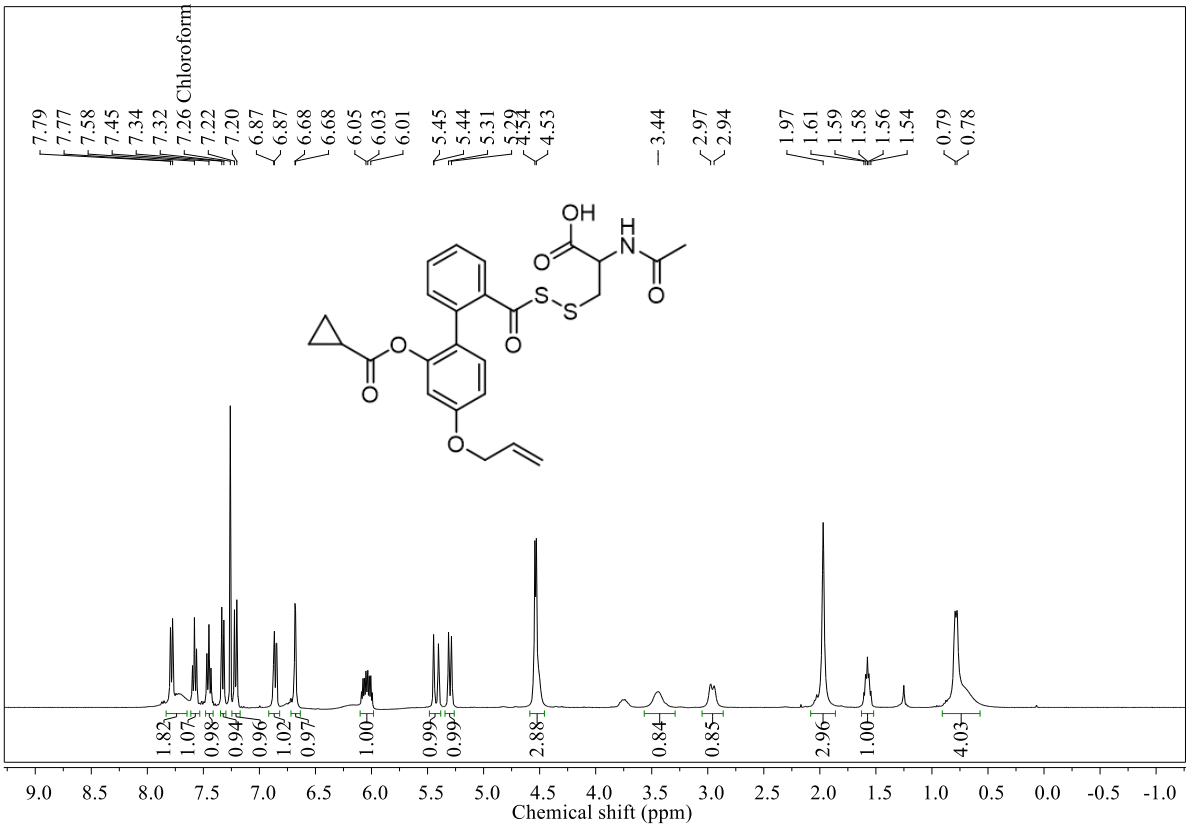

^{13}C NMR spectra of **1**

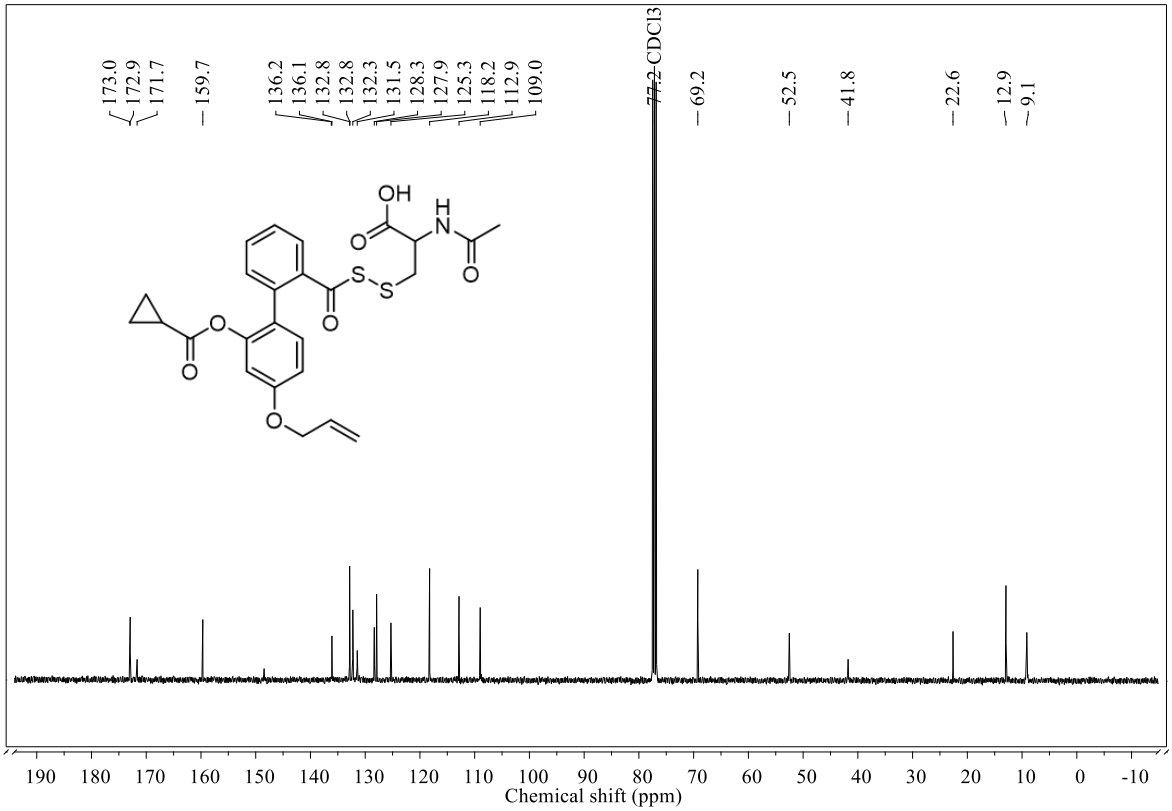

^{1}H NMR spectra of **3**

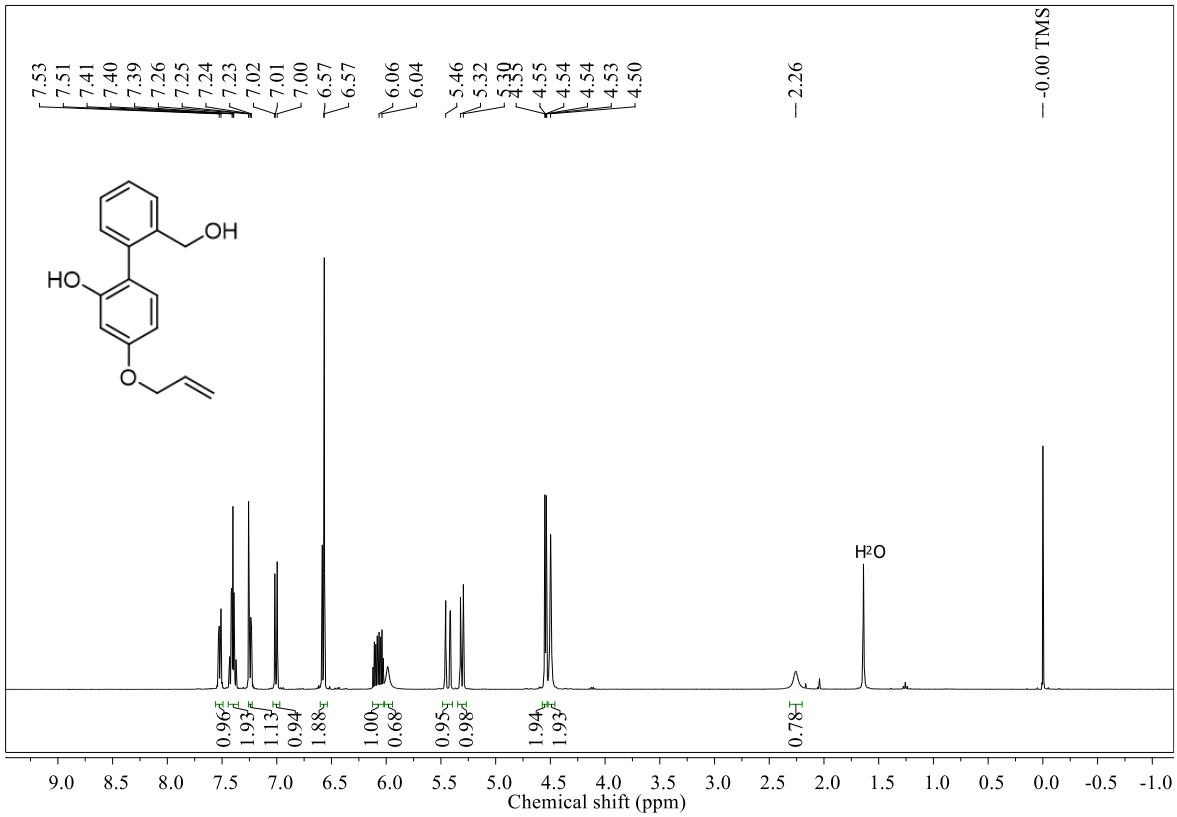

^{13}C NMR spectra of **3**

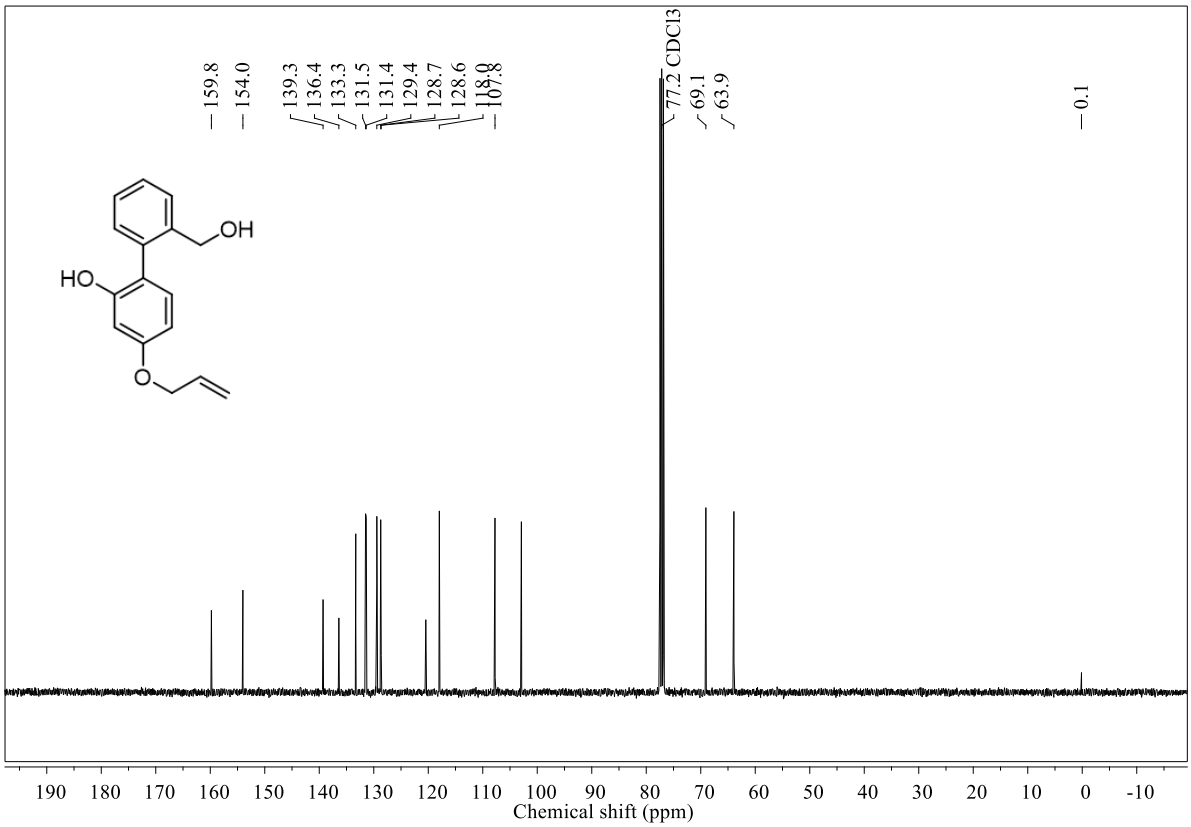

^{1}H NMR spectra of **4**

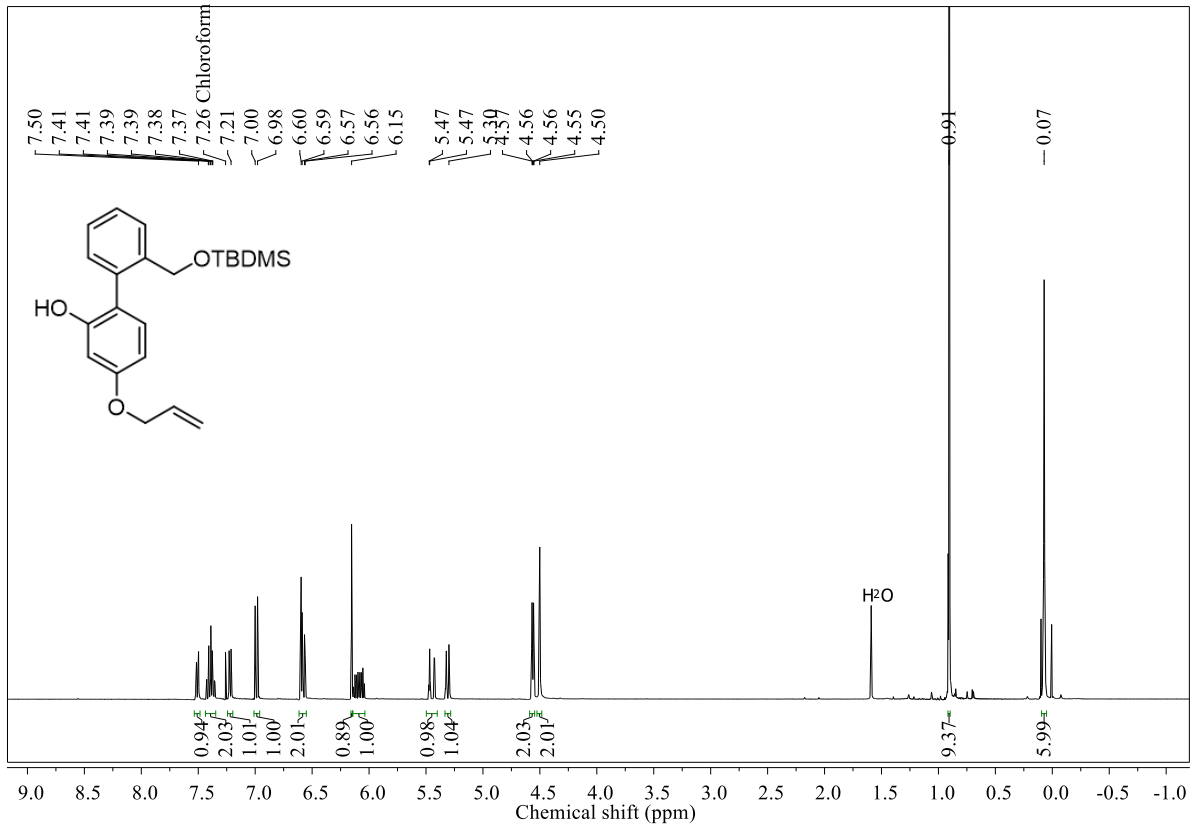

^{13}C NMR spectra of **4**

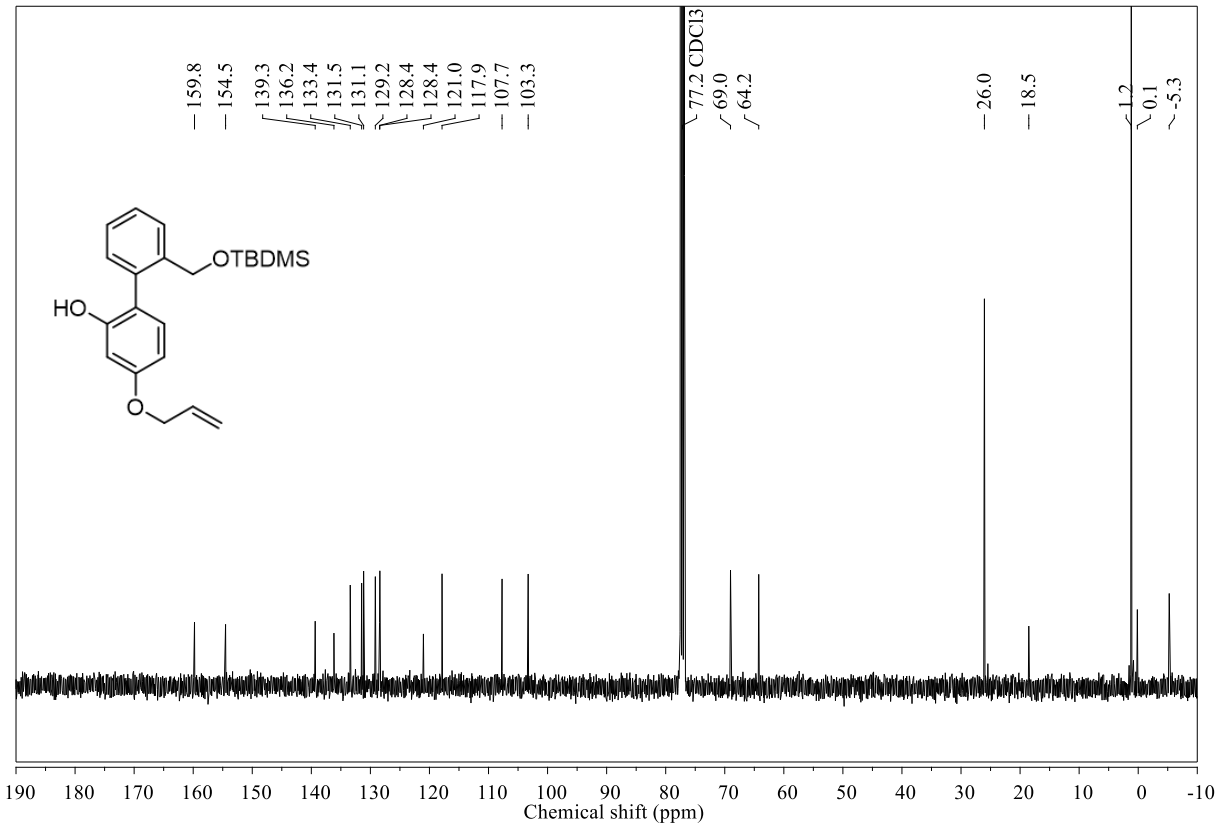

^{1}H NMR spectra of **5**

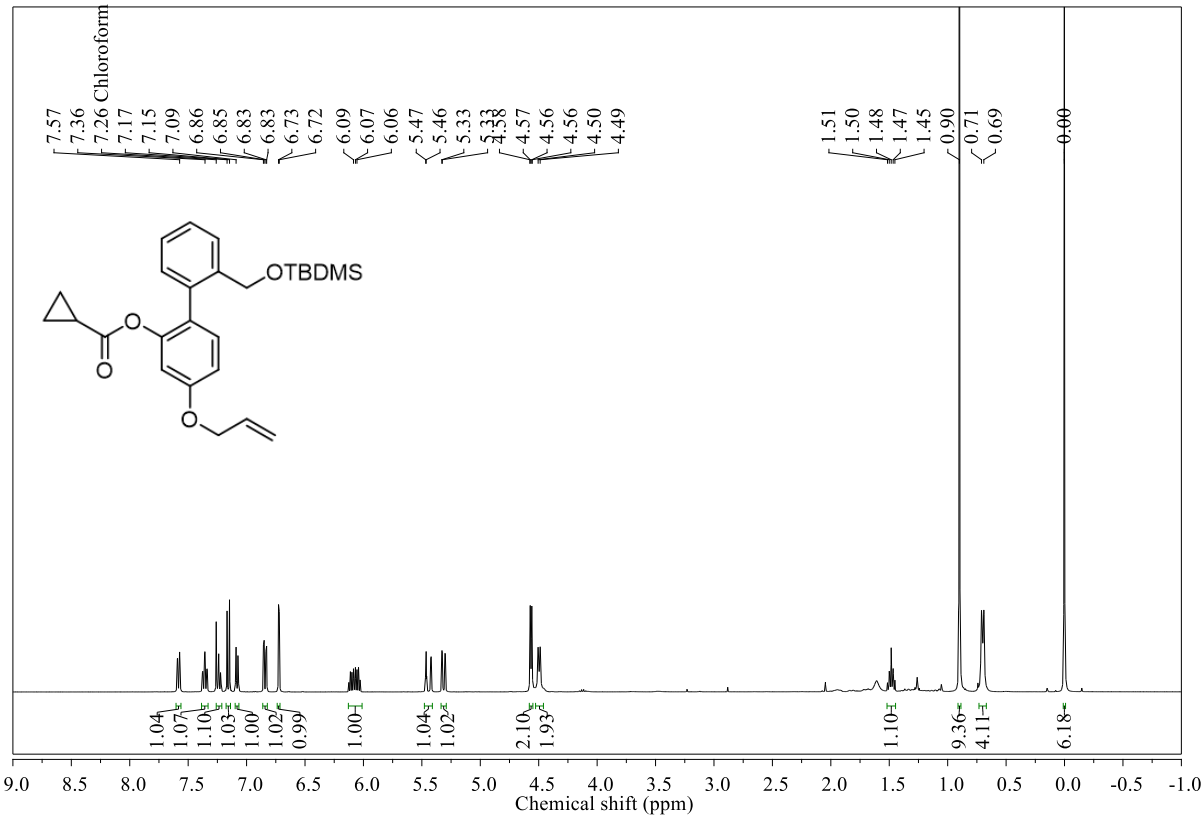

^{13}C NMR spectra of **5**

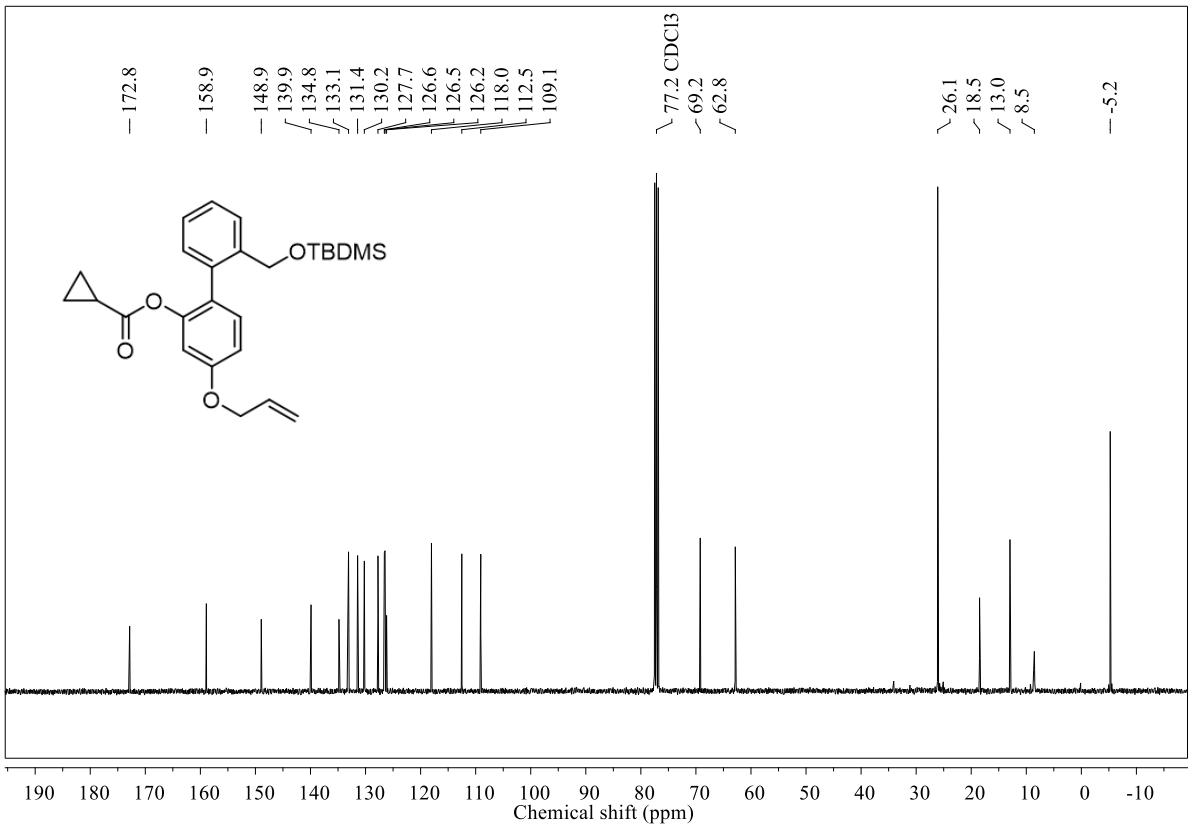

^{1}H NMR spectra of **6**

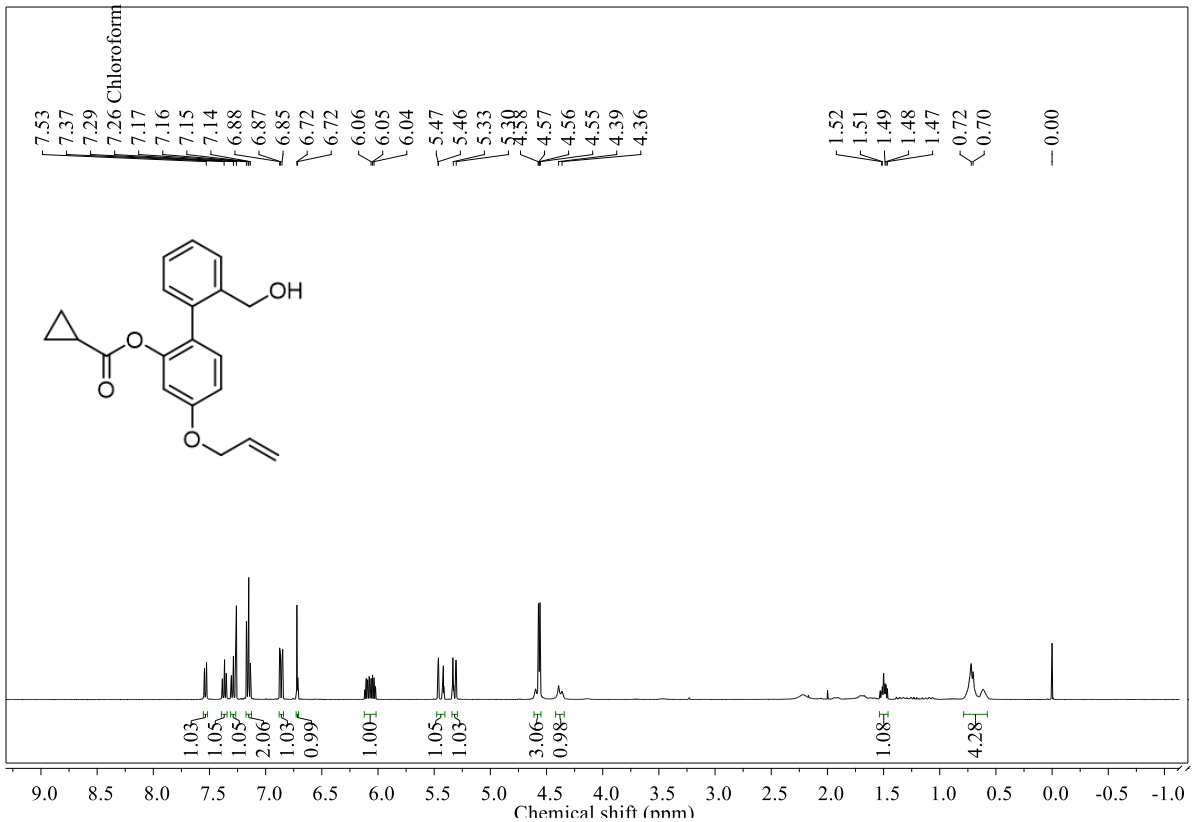

^{13}C NMR spectra of **6**

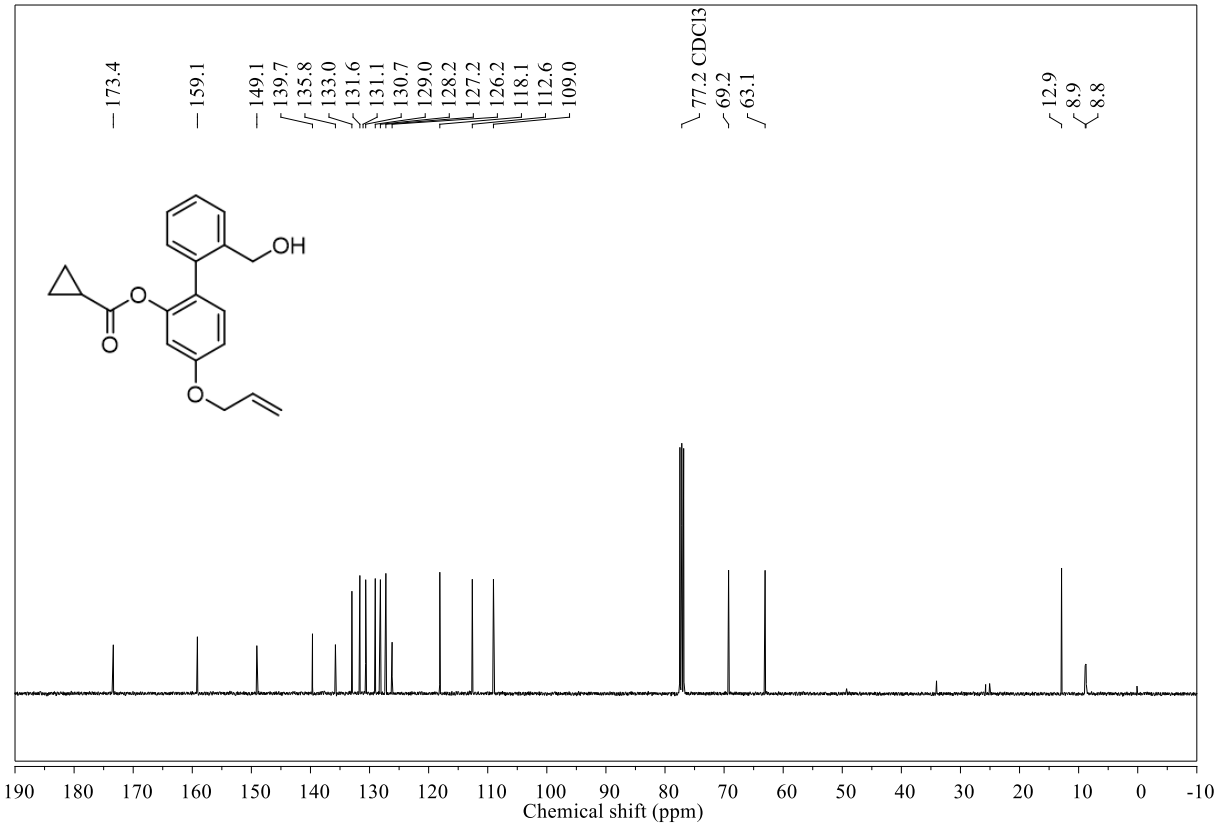

^{1}H NMR spectra of **7**

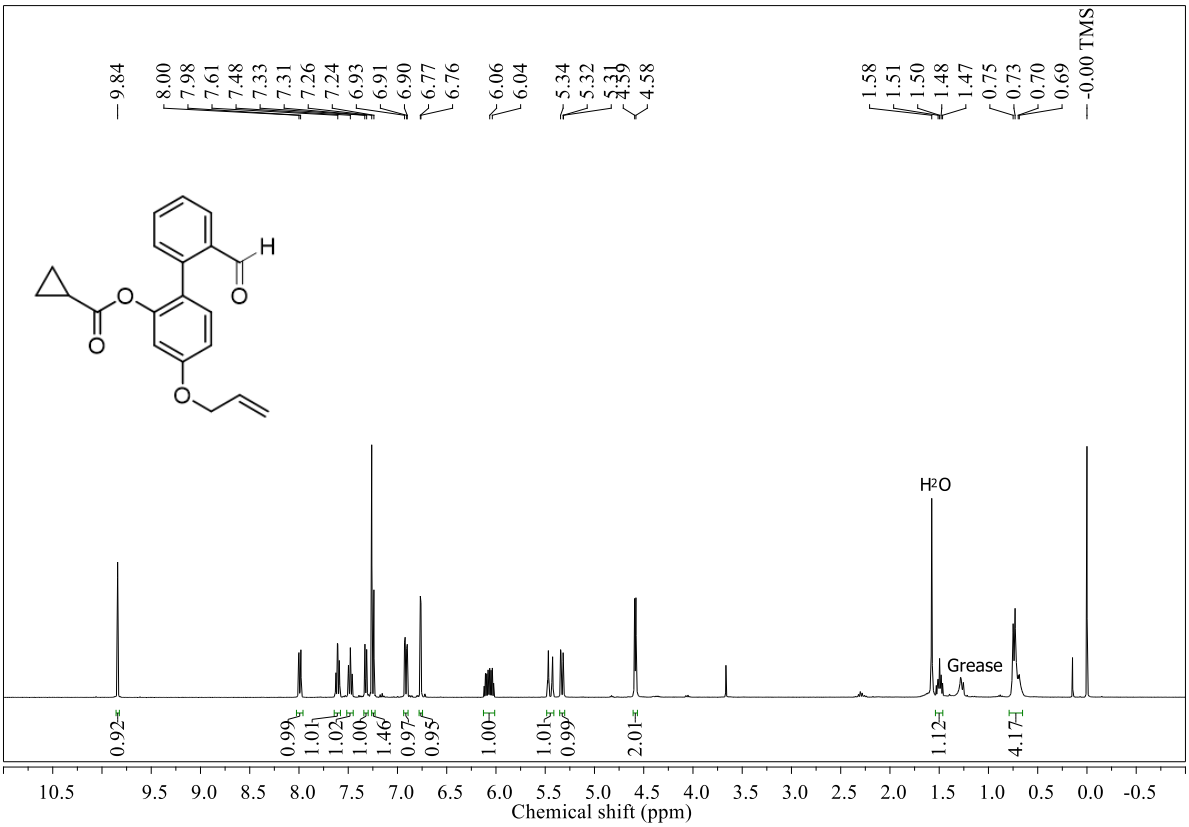

^{13}C NMR spectra of **7**

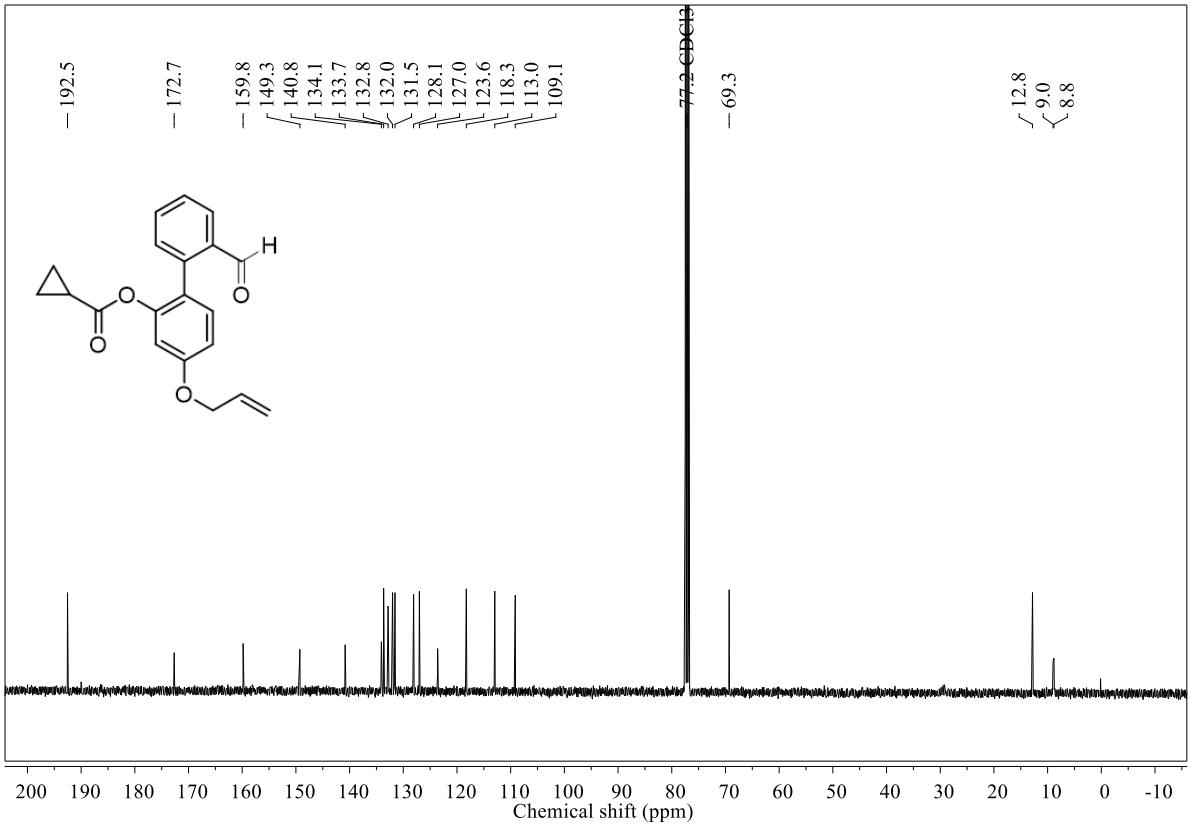

^{1}H NMR spectra of **8**

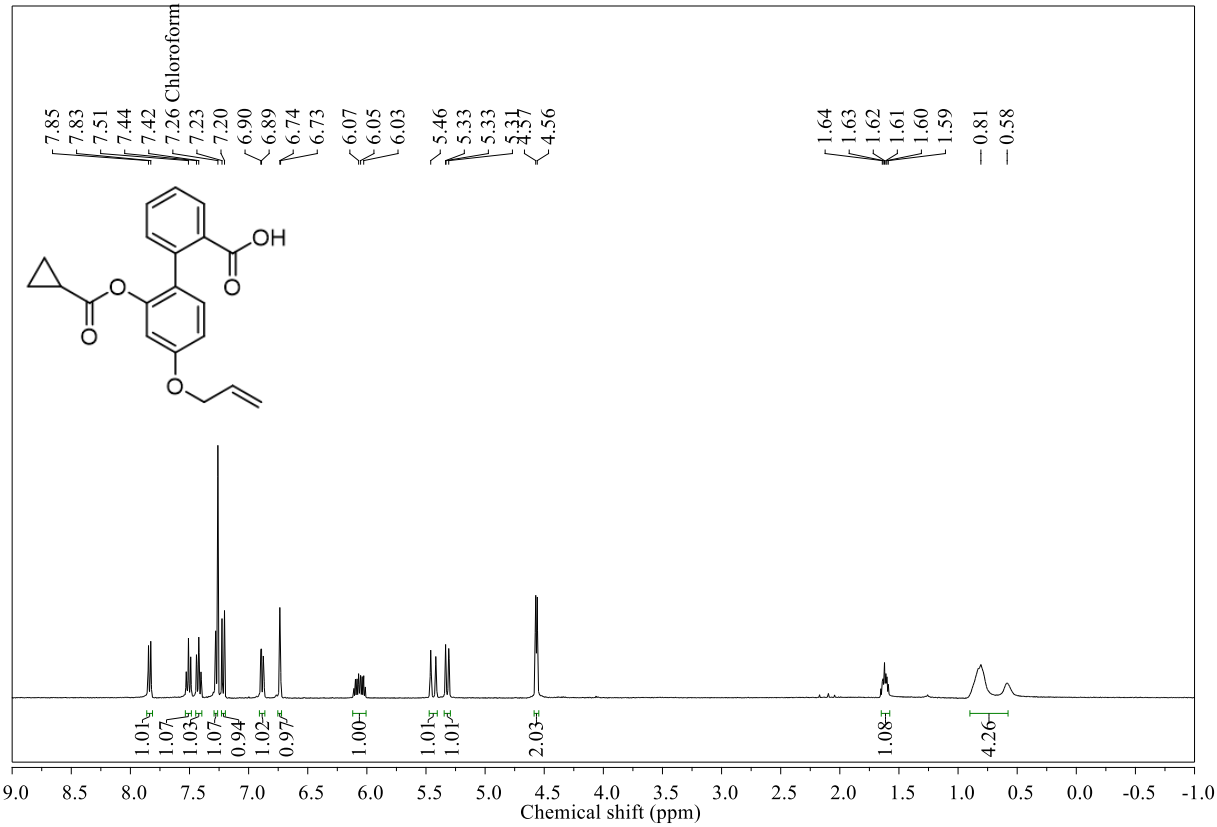

^{13}C NMR spectra of **8**

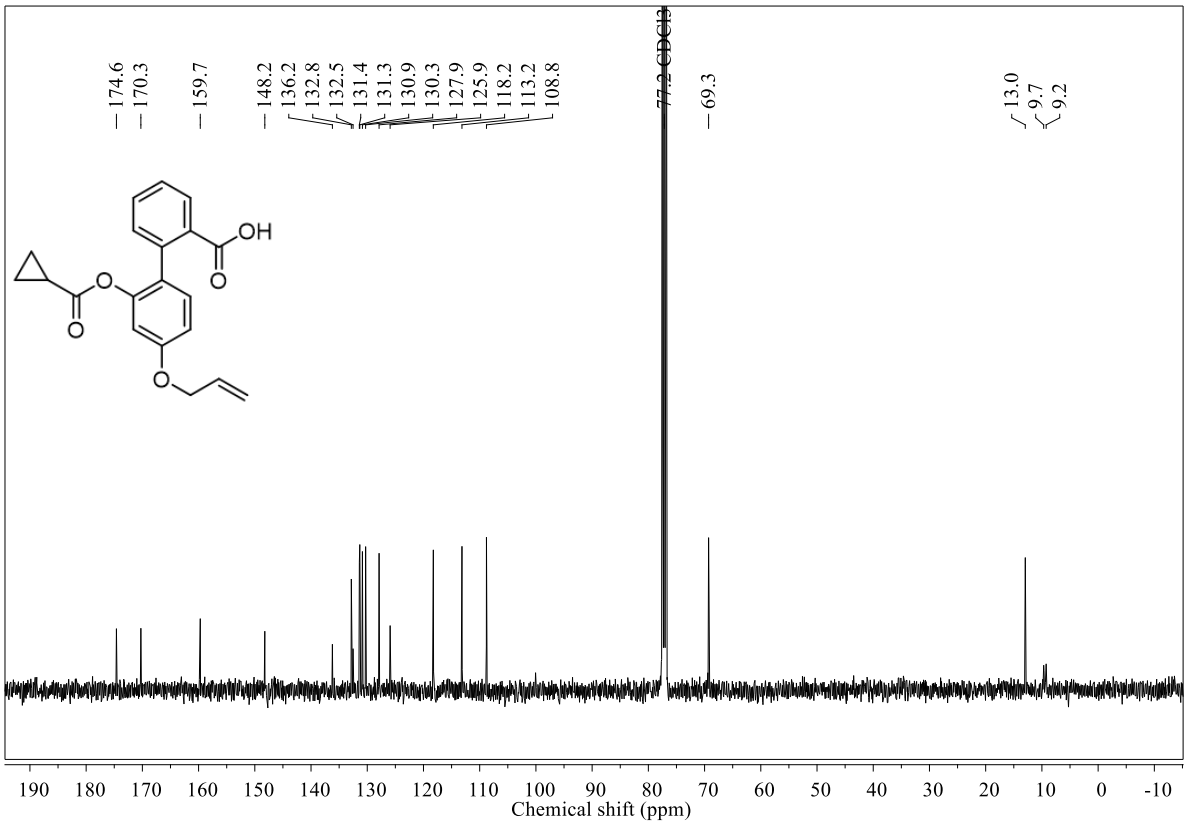

2.6. References

(1) Park, C. M.; Weerasinghe, L.; Day, J. J.; Fukuto, J. M.; Xian, M. Persulfides: Current Knowledge and Challenges in Chemistry and Chemical Biology. *Mol. Biosyst.* **2015**, *11* (7), 1775–1785.

(2) Filipovic, M. R.; Zivanovic, J.; Alvarez, B.; Banerjee, R. Chemical Biology of H 2 S Signaling through Persulfidation. *Chem. Rev.* **2018**, *118* (3), 1253–1337.

(3) Kaspar, J. W.; Niture, S. K.; Jaiswal, A. K. Nrf2:INrf2 (Keap1) Signaling in Oxidative Stress. *Free Radic. Biol. Med.* **2009**, *47* (9), 1304–1309.

(4) Koike, S.; Ogasawara, Y.; Shibuya, N.; Kimura, H.; Ishii, K. Polysulfide Exerts a Protective Effect against Cytotoxicity Caused by t -Buthylhydroperoxide through Nrf2 Signaling in Neuroblastoma Cells. *FEBS Lett.* **2013**, *587* (21), 3548–3555.

(5) Yang, G.; Zhao, K.; Ju, Y.; Mani, S.; Cao, Q.; Puukila, S.; Khaper, N.; Wu, L.; Wang, R. Hydrogen Sulfide Protects Against Cellular Senescence via S -Sulfhydration of Keap1 and Activation of Nrf2. *Antioxid. Redox Signal.* **2013**, *18* (15), 1906–1919.

(6) Mustafa, A. K.; Gadalla, M. M.; Sen, N.; Kim, S.; Mu, W.; Gazi, S. K.; Barrow, R. K.; Yang, G.; Wang, R.; Snyder, S. H. HS Signals through Protein S-Sulfhydration. *Sci. Signal.* **2009**, *2* (96).

(7) Nasi, S.; Ehirchiou, D.; Chatzianastasiou, A.; Nagahara, N.; Papapetropoulos, A.; Bertrand, J.; Cirino, G.; So, A.; Busso, N. The Protective Role of the 3-Mercaptopyruvate Sulfurtransferase (3-MST)-Hydrogen Sulfide (H2S) Pathway against Experimental Osteoarthritis. *Arthritis Res. Ther.* **2020**, *22* (1), 49.

(8) Zheng, Y.; Yu, B.; Li, Z.; Yuan, Z.; Organ, C. L.; Trivedi, R. K.; Wang, S.; Lefer, D. J.; Wang, B. An Esterase-Sensitive Prodrug Approach for Controllable Delivery of Persulfide Species. *Angew. Chemie Int. Ed.* **2017**, *56* (39), 11749–11753.

(9) Yuan, Z.; Zheng, Y.; Yu, B.; Wang, S.; Yang, X.; Wang, B. Esterase-Sensitive

Glutathione Persulfide Donor. *Org. Lett.* **2018**, *20* (20), 6364–6367.

(10) Dillon, K. M.; Carrazzone, R. J.; Wang, Y.; Powell, C. R.; Matson, J. B. Polymeric Persulfide Prodrugs: Mitigating Oxidative Stress through Controlled Delivery of Reactive Sulfur Species. *ACS Macro Lett.* **2020**, *9* (4), 606–612.

(11) Dillon, K. M.; Morrison, H. A.; Powell, C. R.; Carrazzone, R. J.; Ringel-Scaia, V. M.; Winckler, E. W.; Council-Troche, R. M.; Allen, I. C.; Matson, J. B. Targeted Delivery of Persulfides to the Gut: Effects on the Microbiome. *Angew. Chemie Int. Ed.* **2021**, *60* (11), 6061–6067.

(12) Bora, P.; Sathian, M. B.; Chakrapani, H. Enhancing Cellular Sulfane Sulfur through β-Glycosidase-Activated Persulfide Donors: Mechanistic Insights and Oxidative Stress Mitigation. *Chem. Commun.* **2022**, *58* (18), 2987–2990.

(13) Chaudhuri, A.; Venkatesh, Y.; Das, J.; Gangopadhyay, M.; Maiti, T. K.; Singh, N. D. P. One- and Two-Photon-Activated Cysteine Persulfide Donors for Biological Targeting. *J. Org. Chem.* **2019**, *84* (18), 11441–11449.

(14) Chaudhuri, A.; Venkatesh, Y.; Jena, B. C.; Behara, K. K.; Mandal, M.; Singh, N. D. P. Real-Time Monitoring of a Photoactivated Hydrogen Persulfide Donor for Biological Entities. *Org. Biomol. Chem.* **2019**, *17* (39), 8800–8805.

(15) Powell, C. R.; Dillon, K. M.; Wang, Y.; Carrazzone, R. J.; Matson, J. B. A Persulfide Donor Responsive to Reactive Oxygen Species: Insights into Reactivity and Therapeutic Potential. *Angew. Chemie Int. Ed.* **2018**, *57* (21), 6324–6328.

(16) Hankins, R. A.; Suarez, S. I.; Kalk, M. A.; Green, N. M.; Harty, M. N.; Lukesh, J. C. An Innovative Hydrogen Peroxide-Sensing Scaffold and Insight Towards Its Potential as an ROS-Activated Persulfide Donor. *Angew. Chemie Int. Ed.* **2020**, *59* (49), 22238–22245.

(17) Bora, P.; Chauhan, P.; Manna, S.; Chakrapani, H. A Vinyl-Boronate Ester-Based Persulfide Donor Controllable by Hydrogen Peroxide, a Reactive Oxygen Species

(ROS). *Org. Lett.* **2018**, *20* (24), 7916–7920.

(18) Wang, Y.; Dillon, K. M.; Li, Z.; Winckler, E. W.; Matson, J. B. Alleviating Cellular Oxidative Stress through Treatment with Superoxide-Triggered Persulfide Prodrugs. *Angew. Chemie Int. Ed.* **2020**, *59* (38), 16698–16704.

(19) Kang, J.; Xu, S.; Radford, M. N.; Zhang, W.; Kelly, S. S.; Day, J. J.; Xian, M. O→S Relay Deprotection: A General Approach to Controllable Donors of Reactive Sulfur Species. *Angew. Chemie Int. Ed.* **2018**, *57* (20), 5893–5897.

(20) Khodade, V. S.; Pharoah, B. M.; Paolocci, N.; Toscano, J. P. Alkylamine-Substituted Perthiocarbamates: Dual Precursors to Hydropersulfide and Carbonyl Sulfide with Cardioprotective Actions. *J. Am. Chem. Soc.* **2020**, *142* (9), 4309–4316.

(21) Xu, Y.; Xu, B.; Wang, J.; Jin, H.; Xu, S.; Wang, G.; Zhen, L. Peroxynitrite-Promoted Persulfide Prodrugs with Protective Potential against Paracetamol Poisoning. *Chem. – A Eur. J.* **2022**, No. Figure 1.

(22) Thompson, D. C.; Thompson, J. A.; Sugumaran, M.; Moldéus, P. Biological and Toxicological Consequences of Quinone Methide Formation. *Chem. Biol. Interact.* **1993**, *86* (2), 129–162.

(23) Ali, K.; Mishra, P.; Kumar, A.; Reddy, D. N.; Chowdhury, S.; Panda, G. Reactivity vs. Selectivity of Quinone Methides: Synthesis of Pharmaceutically Important Molecules, Toxicity and Biological Applications. *Chem. Commun.* **2022**, *58* (42), 6160–6175.

(24) Dillon, K. M.; Matson, J. B. A Review of Chemical Tools for Studying Small Molecule Persulfides: Detection and Delivery. *ACS Chem. Biol.* **2021**, *16* (7), 1128–1141.

(25) Fallah, A.; Noshadi, B.; Gazi, M.; Gülcan, H. O. Urolithin A and B Derivatives as ON-OFF Selective Fluorescent Sensors for Iron(III). *J. Fluoresc.* **2020**, *30* (1), 113–120.

(26) Liu, W.; Liu, H.; Peng, X.; Zhou, G.; Liu, D.; Li, S.; Zhang, J.; Wang, S. Hypoxia-Activated Anticancer Prodrug for Bioimaging, Tracking Drug Release, and Anticancer

Application. *Bioconjug. Chem.* **2018**, *29* (10), 3332–3343.

(27) Caswell, M.; Schmir, G. L. Formation and Hydrolysis of Lactones of Phenolic Acids. *J. Am. Chem. Soc.* **1980**, *102* (14), 4815–4821.

(28) Tejasri S. Synthesis and Evaluation of Small Molecule Hydrogen Sulfide Donors. **2017**, 1–42.

(29) Kumar, A. S. Design and Development of a Triggerable Biphenyl Based Novel Persulfide Donor Department of Chemistry. **2020**, 1–49.

(30) Franks, A. T.; Franz, K. J. A Prochelator with a Modular Masking Group Featuring Hydrogen Peroxide Activation with Concurrent Fluorescent Reporting. *Chem. Commun.* **2014**, *50* (77), 11317–11320.

(31) Krzeszewski, M.; Vakuliuk, O.; Gryko, D. T. Color-Tunable Fluorescent Dyes Based on Benzo[c]Coumarin. *European J. Org. Chem.* **2013**, *2013* (25), 5631–5644.

(32) Chen, W.; Liu, C.; Peng, B.; Zhao, Y.; Pacheco, A.; Xian, M. New Fluorescent Probes for Sulfane Sulfurs and the Application in Bioimaging. *Chem. Sci.* **2013**, *4* (7), 2892–2896.

(33) Hamid, H. A.; Tanaka, A.; Ida, T.; Nishimura, A.; Matsunaga, T.; Fujii, S.; Morita, M.; Sawa, T.; Fukuto, J. M.; Nagy, P.; Tsutsumi, R.; Motohashi, H.; Ihara, H.; Akaike, T. Polysulfide Stabilization by Tyrosine and Hydroxyphenyl-Containing Derivatives That Is Important for a Reactive Sulfur Metabolomics Analysis. *Redox Biol.* **2019**, *21*, 101096.

(34) Ida, T.; Sawa, T.; Ihara, H.; Tsuchiya, Y.; Watanabe, Y.; Kumagai, Y.; Suematsu, M.; Motohashi, H.; Fujii, S.; Matsunaga, T.; Yamamoto, M.; Ono, K.; Devarie-Baez, N. O.; Xian, M.; Fukuto, J. M.; Akaike, T. Reactive Cysteine Persulfides and S-Polythiolation Regulate Oxidative Stress and Redox Signaling. *Proc. Natl. Acad. Sci.* **2014**, *111* (21), 7606–7611.

(35) Sharma, A. K.; Nair, M.; Chauhan, P.; Gupta, K.; Saini, D. K.; Chakrapani, H. Visible-Light-Triggered Uncaging of Carbonyl Sulfide for Hydrogen Sulfide (H 2 S) Release. *Org. Lett.* **2017**, *19* (18), 4822–4825.

(36) McFadden, P. D.; Frederick, K.; Argüello, L. A.; Zhang, Y.; Vandiver, P.; Odegaard, N.; Loy, D. A. UV Fluorescent Epoxy Adhesives from Noncovalent and Covalent Incorporation of Coumarin Dyes. *ACS Appl. Mater. Interfaces* **2017**, *9* (11), 10061–10068.

(37) Kelkar, D. S.; Ravikumar, G.; Mehendale, N.; Singh, S.; Joshi, A.; Sharma, A. K.; Mhetre, A.; Rajendran, A.; Chakrapani, H.; Kamat, S. S. A Chemical–Genetic Screen Identifies ABHD12 as an Oxidized-Phosphatidylserine Lipase. *Nat. Chem. Biol.* **2019**, *15* (2), 169–178.

(38) Zhang, T.; Ono, K.; Tsutsuki, H.; Ihara, H.; Islam, W.; Akaike, T.; Sawa, T. Enhanced Cellular Polysulfides Negatively Regulate TLR4 Signaling and Mitigate Lethal Endotoxin Shock. *Cell Chem. Biol.* **2019**, *26* (5), 686-698.e4.

(39) Yadav, P. K.; Yamada, K.; Chiku, T.; Koutmos, M.; Banerjee, R. Structure and Kinetic Analysis of H2S Production by Human Mercaptopyruvate Sulfurtransferase. *J. Biol. Chem.* **2013**, *288* (27), 20002–20013.

Chapter 3. Development of Esterase-Triggered Persulfide Generator *via* 3-MST Pathway

3.1. Introduction

In **Chapter 2,** the development of the small molecule for the real-time monitoring of the persulfide generation was described. However, compound **1** was associated with certain limitations, such as the challenging synthesis, and disulfide bonds are susceptible to reaction with the thiols, leading to non-specific reactions. To overcome these limitations, the strategy of developing a tool in order to generate persulfide enzymatically was considered.

One of the important enzymes involved in persulfide biogenesis is the H_2S-producing enzyme, 3-mercaptopyruvate sulfurtransferase (3-MST), a member of the sulfurtransferase family, and is ubiquitously expressed in mammalian tissues.[1] 3-MST utilizes 3-mercaptopyruvate (3-MP) as the natural substrate and accepts the sulfur from it to form a transient persulfide intermediate in its active site cysteine and an enolate of pyruvate as the byproduct (Figure 3.1).[2,3] The sulfur from the persulfide intermediate can be transferred to target proteins or reduced by thioredoxin (Trx) to produce H_2S (Figure 3.1).[4]

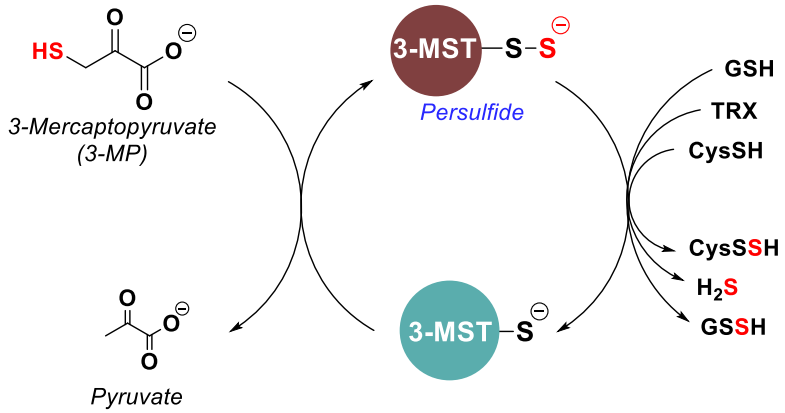

Figure 3.1. Reaction mechanism for turnover of 3-mercaptopyruvate (3-MP) by 3-mercaptopyruvate sulfurtransferase (3-MST) to form a transient 3-MST persulfide intermediate and pyruvate as the byproduct. The 3-MST persulfide can undergo reduction to generate H_2S or transfer the sulfur to other acceptor proteins or small-molecule thiol.

The natural substrate for 3-MST, 3-MP, generates H_2S spontaneously through non-enzymatic mechanisms, which can be a potential limitation for its use.[5] To address this, an artificial substrate with structural features similar to 3-MP, a phenacyl thiol-based compound that has a sulfur donor and an enolizable ketone, was developed in our lab, which facilitates the formation of 3-MST persulfide and further feeds into the biosynthetic machinery for total cellular

persulfidation and H_2S generation. (Figure 3.2).[6] Due to the propensity of thiols to undergo aerial oxidation, phenacyl thiol was protected as the thioacetate to improve stability and longer shelf life. The thioacetate can be easily deprotected by the widely prevalent enzyme esterase. Using this approach, a library of artificial substrates was developed and evaluated for H_2S and persulfide generation. Their antioxidant and anti-inflammatory properties were further validated in both cellular and animal models.[6]

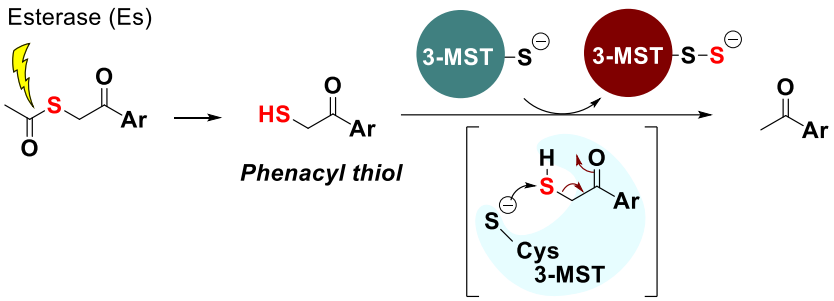

Figure 3.2. 3-MST artificial substrate similar to 3-MP was designed, which, upon turnover by 3-MST, feeds into the biosynthetic machinery of the cell to induce persulfidation and generate ketone as a byproduct.

Leveraging the biphenyl-based NAC persulfide donor **1**, an esterase-sensitive 3-MST artificial substrate donor **11** was developed, which generates the lactone **2a** and the artificial substrate **13** in the presence of Es (Scheme 3.1). Then **13** gets turned over by 3-MST to generate 3-MST persulfide.

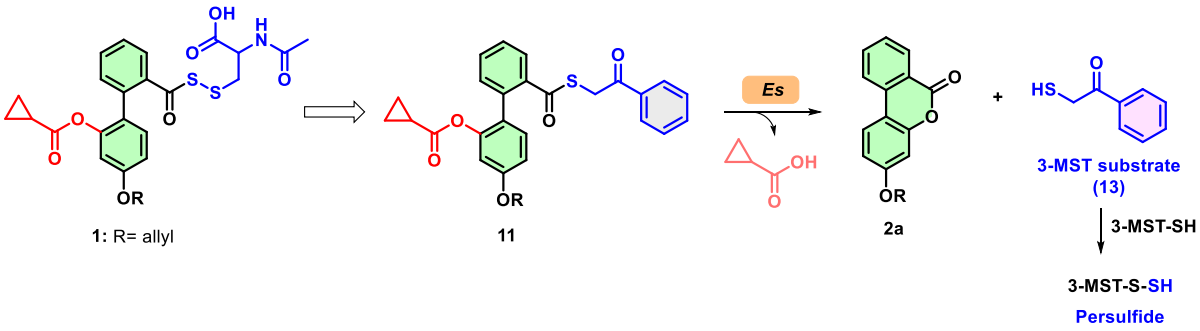

Scheme 3.1. Design of biphenyl-based esterase-sensitive 3-MST artificial substrate donor.

3.2. Results and discussion

3.2.1. Synthesis

The carboxylic acid compound **8** was reacted with freshly prepared phenacyl thiol (**13**) in the presence of DCC and DMAP. The thioester **11** was isolated in 20% yield (Scheme 3.2).

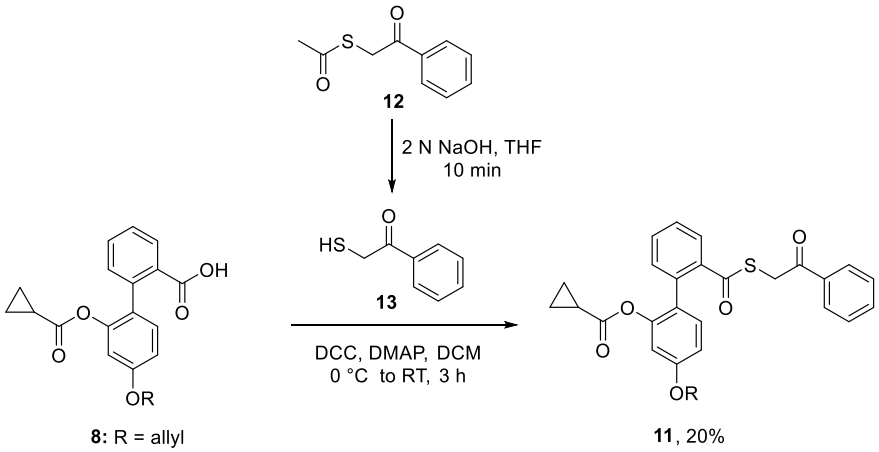

Scheme 3.2. Synthesis of biphenyl-based esterase-sensitive 3-MST artificial donor **11**.

3.2.2. Activation of 11 and detection of 2a and 13

The compound **11**, upon activation by esterase (Es), generates the lactone **2a** and 3-MST artificial substrate **13** in a single step. The fluorophore lactone **2a** formation can be monitored by a fluorescence-based experiment (λ_{ex} = 320 nm; λ_{em} = 432 nm). In addition, **2a** and **13** can be directly detected by HPLC analysis. **13** reacts with 3-MST enzyme and produces 3-MST persulfide, which can be detected by sulfane sulfur probe **SSP2**. Persulfidated 3-MST can transfer the sulfhydryl group to the thiol acceptor, **GSH**, and produce the GSSH and H_2S, which can be monitored by LC/MS using **HPE-IAM**, as described in the previous chapter. Also, the 3-MST persulfide in the presence of the reducing condition (**DTT**) produces H_2S, which can be detected by lead acetate, methylene blue assay, or by trapping it with an **HPE-IAM** (Scheme 3.3).

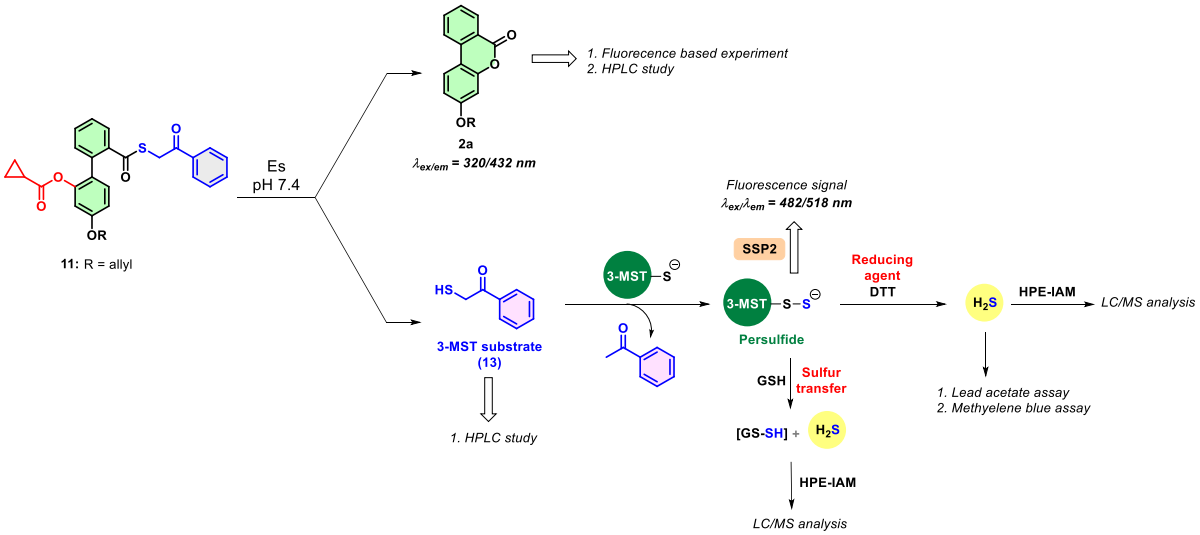

Scheme 3.3. Tools for detection of lactone **2a** and 3-MST persulfide **13** from **11** in the presence of Es. Further detection of persulfide, sulfur transfer, and H_2S detection generated from **13**.

3.2.3. Formation of 2a from 11 upon activation by esterase

Firstly, the ability of compound **11** to generate lactone **2a** in the presence of esterase (Es), fluorescence-based experiments were performed.

3.2.3.1. Release of 2a from 11 by fluorimetry analysis

Compound **11** (10 μM) was treated with Es (1 U/mL) in PBS (pH 7.4), and the fluorescence intensity corresponding to the **2a** formation was monitored. As expected, without Es, no fluorescence signal was observed, but the addition of Es (1 U/mL) led to an enhancement in the fluorescence signal corresponding to the **2a** formation (λ_{ex} = 320 nm; λ_{em} = 432 nm) (Figure 3.3).

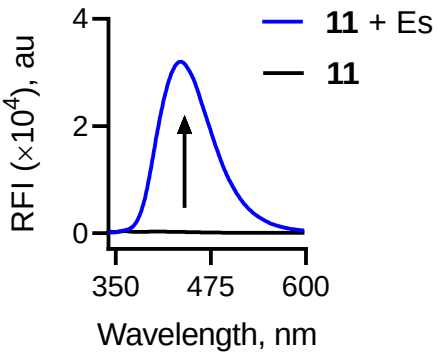

Figure 3.3. Monitoring the formation of lactone (**2a**) from **11** (10 μM) by fluorescence (λ_{ex} = 320 nm; λ_{em} = 432 nm) with or without Es (1 U/mL) in pH 7.4 PBS at 37 °C.

3.2.3.2. Concentration-dependent release of 2a

Next, the concentration-dependent release of **2a** from **11** was studied. The enhancement in the fluorescence signal (λ_{ex} = 320 nm; λ_{em} = 432 nm) attributable to the **2a** formation from varying concentrations of **11** (0-20 μM) was monitored in the presence of Es (1 U/mL). A dose-dependent increase in the fluorescence signal corresponding to **2a** was observed over time, and the signal plateaued after 30 min (Figure 3.4.A). Further, the curve fitting for the lactone formation to a first-order exponential equation yielded rate constants ranging from 0.10 to 0.15 min^{-1}.

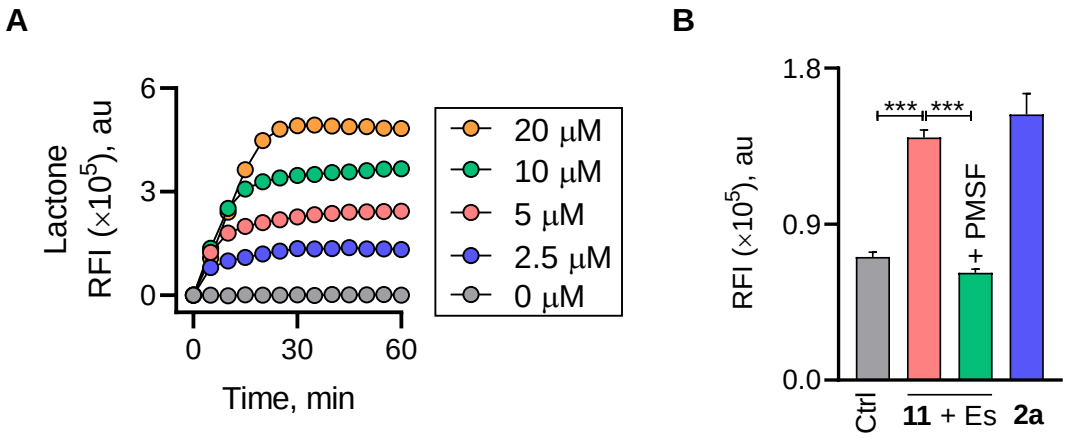

Figure 3.4. Monitoring the formation of lactone (**2a**) from **11** by fluorescence (A) in a concentration-dependent manner (0-20 μM) with Es (1 U/mL) in pH 7.4 buffer at 37 °C and (B) at **11** (10 μM) with and without Es (1 U/mL) inhibitor PMSF (1 mM) in PBS (pH 7.4) at 37 °C after 60 min; ctrl refers to **11** alone; +PMSF (phenylmethanesulfonyl fluoride) refers to pre-treatment of Es with PMSF followed by compound treatment. Statistical significance was carried out using One-way ANOVA (*** $p \leq 0.001$).

Based on the fluorescence experiment, the quantitative yield of the **2a** was observed when **11** was incubated with Es for 1 h (Figure 3.4.B). On the other hand, the yield of **2a** from the persulfide donor **1** was found to be lower (40-50 %) due to hydrolysis of the perthioester in the presence of esterase, further halting the lactonization reaction. In a control experiment, an esterase inhibitor, PMSF (phenylmethanesulfonyl fluoride), was used to study the role of the enzyme.[7] Pretreatment with PMSF resulted in a diminished fluorescence signal from **11,** corresponding to the formation of **2a** (Figure 3.4.B). Hence, cleavage by Es is an important prerequisite for the lactone formation.

Overall, these results suggest that compound **11** produced the fluorophore lactone **2a** upon activation by esterase.

3.2.4. HPLC studies

Next, to assess the stability of **11** in the buffer and the byproduct formation from **11**, HPLC experiments were performed.

3.2.4.1. Stability of 11

Compound **11** alone remained stable during incubation in pH 7.4 PBS for 2 h at 37 °C, as determined by HPLC analysis (Figure 3.5).

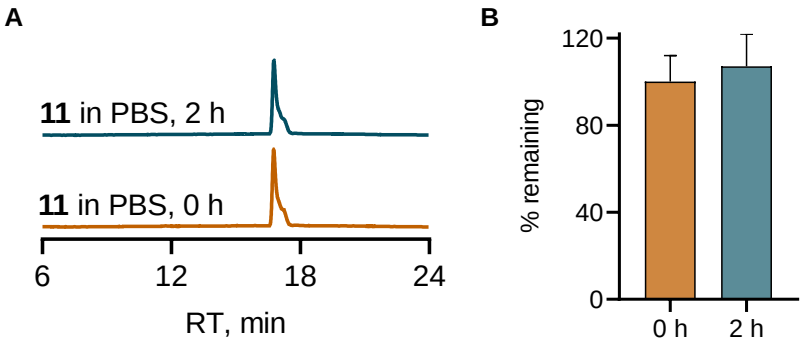

Figure 3.5. Stability of **11** in pH 7.4 PBS. (A) HPLC traces of stability of **11** in pH 7.4 PBS buffer (10 mM) at 37 °C. (B) Area under the curve (AUC) corresponding to the **11** at 3.6 min and remaining in the buffer after 2 h of incubation (Abs = 250 nm).

3.2.4.2. Decomposition of 11 in the presence of esterase

Next, the decomposition of **11** in the presence of Es was studied. Compound **11** was treated with 1U/mL Es in pH 7.4 PBS, and the HPLC profiles were recorded at different time points (Abs = 250 nm). Complete disappearance of **11** (RT 16.7 min) was observed within 60 min (Figure 3.6 and Figure 3.7.A). Along with the disappearance of **11**, the formation of **2a** (RT 14.9 min) and **13** (RT 10.0 min) was observed (Figure 3.6).

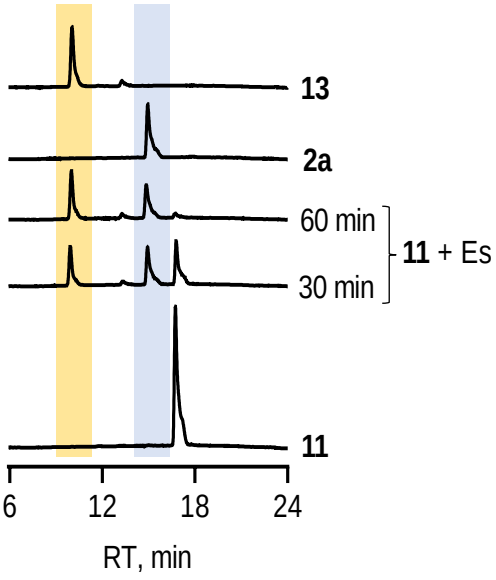

Figure 3.6. HPLC traces for decomposition of **11** (25 μM) and formation of **2a** and **13** in the presence of Es (1 U/mL) (Abs = 250 nm) over 60 min.

The quantitative formation of lactone **2a** was revealed by HPLC analysis (Figure 3.7.B). This result is well aligned with the fluorescence data that was recorded with **11** in the presence of Es. Also, quantitative 3-MST artificial substrate **13** formation was observed (Figure 3.7.C). Overall, HPLC results showed the efficient conversion of **11** in the presence of Es, to form **2a** as well as phenacyl thiol **13**.

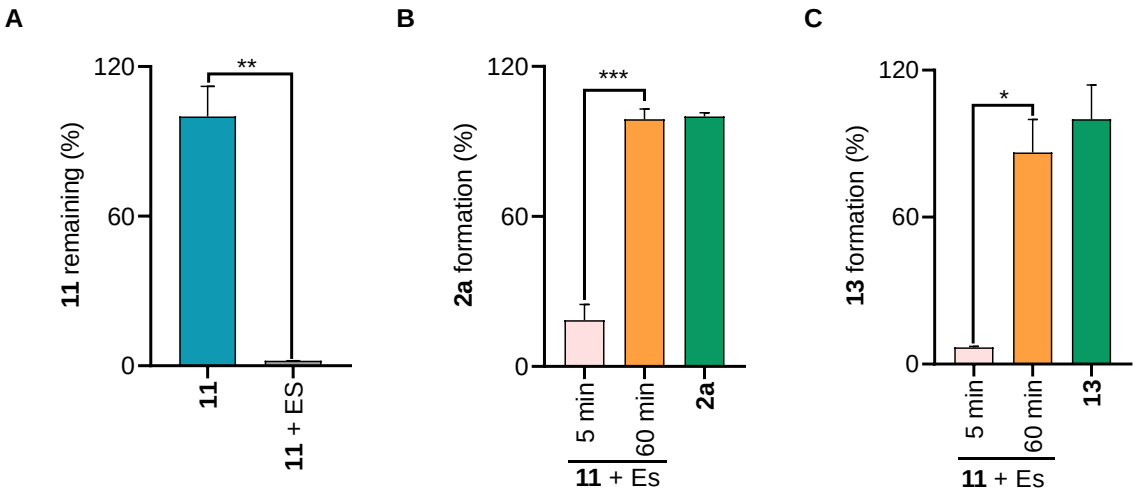

Figure 3.7. Area under the curve (AUC) for the peak corresponding to the (A) **11** remaining, (B) formation of **2a,** and (C) formation of **13** from **11** as monitored by HPLC. (Abs = 250 nm). Statistical significance was carried out using One-way ANOVA(*$p < 0.033$, **$p < 0.002$, *** $p \leq 0.001$).

3.2.5. Selectivity study of 11 towards esterase

Next, the selectivity of **11** towards activation by esterase was investigated in the presence of several biologically relevant nucleophiles, reductants, and oxidants. The compound **11** was incubated in a buffer and treated with 100 equivalents of biologically relevant species, and the fluorescence signal corresponding to the formation of **2a** (λ_{ex} = 320 nm; λ_{em} = 432 nm) was monitored. Compound **11** generates **2a** only in the presence of Es, and no significant levels of **2a** formation were observed in the presence of biologically relevant nucleophiles, oxidants, and reductants (Figure 3.8), suggesting the selectivity of **11** towards activation by esterase.

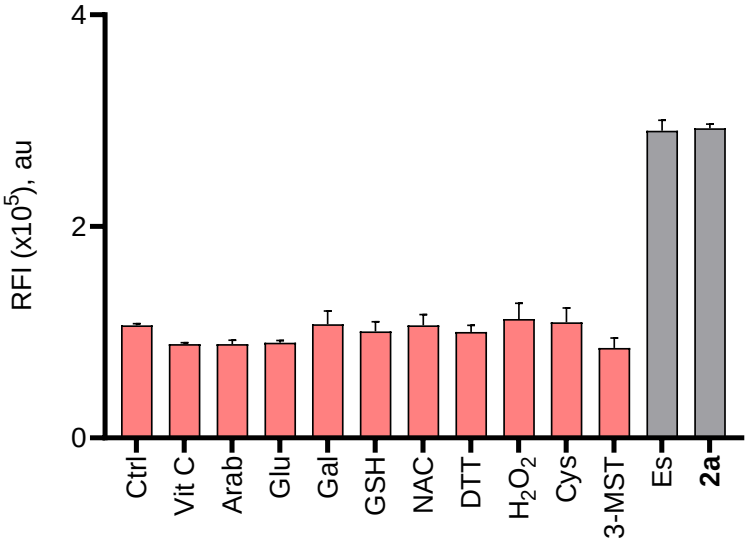

Figure 3.8. Fluorescence response of **11** (10 μM) to various biological analytes (100 equiv.) in pH 7.4 PBS after 60 min at 37 °C. Ctrl: **11** alone; Vit C: ascorbic acid; Arab: arabinose; Glu: glucose; Gal: galactose; GSH: glutathione; NAC: *N*- acetylcysteine; DTT: dithiothreitol; H_2O_2: hydrogen peroxide; Cys: cysteine;3-MST: 3-mercaptopyruvate sulfurtransferase (10 μM); Es: esterase (1 U/mL). Results are expressed as mean ± SD (n =3/group).

3.2.6. Sulfane sulfur detection from 11 using SSP2

3-MST reacts with the phenacyl thiol **13**, leading to the formation of 3-MST persulfide. A reported turn-on fluorescence probe, **SSP2**, as described in **Chapter 2**, was used to assess the persulfide formation.[8] In this assay, compound **11** (10 μM) was incubated with Es (1 U/mL) and *b*3-MST (1 μM) for 60 min at 37 °C. At a pre-determined time point, the **SSP2** probe was added and incubated, and finally, the fluorescence signal for sulfane sulfur generation (λ_{ex} = 482 nm; λ_{em} = 518 nm) was monitored. A strong fluorescence response was observed for **11** in the presence of Es and 3-MST, which indicates significant sulfane sulfur formation (Figure 3.9). As **DTT** was known to reduce sulfane sulfur, the fluorescence signal for sulfane sulfur formation was significantly reduced for the DTT-treated group (Figure 3.9).

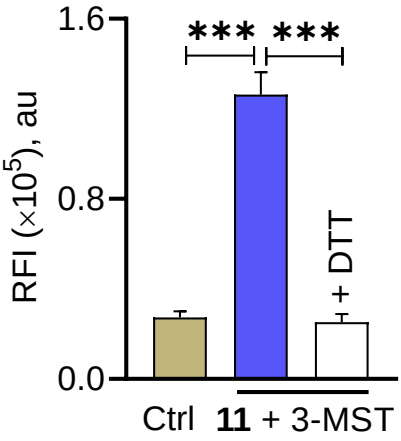

Figure 3.9. Sulfane sulfur detection with **11** (10 μM) in the presence of *b*3-MST (1 μM), Es (1 U/mL), using **SSP2** (5 μM) based fluorescent assay. Ctrl: **11** only. +DTT: addition of **DTT**. λ_{ex} = 482 nm and λ_{em} = 518 nm. Statistical significance was carried out using One-way ANOVA (*** $p \leq 0.001$).

3.2.7. H_2S generation from 11 in the presence of 3-MST and DTT

Next, compound **11** was tested for its ability to generate H_2S in the presence of Es and 3-MST under reducing conditions (**DTT**) using a lead acetate assay and a colorimetric methylene blue assay.[6]

3.2.7.1. H_2S measurement using lead acetate assay

Firstly, H_2S release was studied using the lead acetate assay. In this assay, H_2S released from compound **11** was trapped by **Pb(OAc)$_2$** soaked paper, and a black spot of lead sulfide (PbS) was formed on the paper (Scheme 3.4).

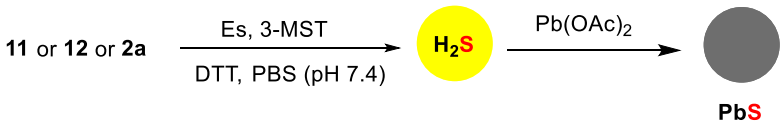

Scheme 3.4. Detection of H_2S *via* lead acetate assay.

In this assay, 100 μM of **11** was incubated with Es (1 U/mL), *b*3-MST (1 μM), and **DTT** (10 mM) in PBS (pH 7.4) at 37 °C. The assay was performed in a 96-well plate, which was covered with 10% $Pb(OAc)_2$ soaked paper, and the reaction was incubated for 2 h. Using a similar protocol, **12** was used as a positive control, and **2a** was used as a negative control for this assay.

An intense black spot for PbS was observed for both **11** and **12**, indicating H_2S formation. As expected, negative control **2a** failed to produce H_2S in the presence of *b*3- MST(Figure 3.10). Only compound control did not show a significant amount of H_2S production.

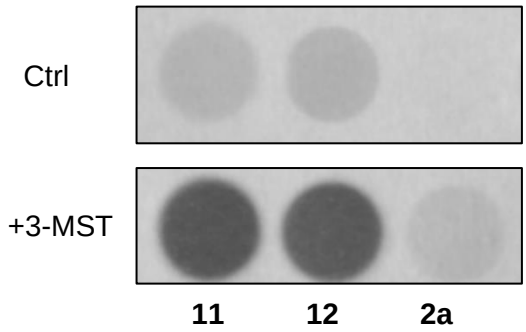

Figure 3.10. H_2S detection from compounds (**11**, **12**, and **2a** at 100 μM) in the presence of *b*3-MST (1 μM), Es (1 U/mL), and **DTT** (10 mM) for 2 h using lead acetate assay. Ctrl represents only compounds. +3-MST refers to the incubation with 3-MST. **12** was used as a positive control, and **2a** as a negative control.

3.2.7.2. Methylene blue assay for H_2S measurement

Along with the lead acetate assay for H_2S measurement, a standard methylene blue (MB) colorimetric assay was performed with compound **11,** as shown in Scheme 3.5.

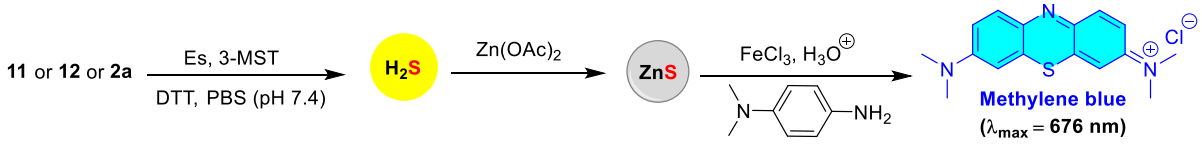

Scheme 3.5. Detection of H_2S *via* methylene blue assay.

In this assay, 100 μM of **11** was incubated with Es (1 U/mL), *b*3-MST (1 μM), **Zn(OAc)$_2$** (400 μM), and **DTT** (10 mM) in PBS (pH 7.4) at 37 °C for 2 h. Using a similar protocol, **12** was used as a positive control, and **2a** was used as a negative control for this assay. Next, aliquots from the reaction mixtures were treated with methylene blue reagents and mixed. The final reaction mixture was then transferred to the 96-well plate, and absorbance at 676 nm was recorded. Similar to the lead acetate assay, a signal for the H_2S generation from both **11** and **12** was observed, whereas, as expected, no signal from negative control **2a** was observed (Figure 3.11). As anticipated, compound control did not produce significant H_2S in the absence of 3-MST.

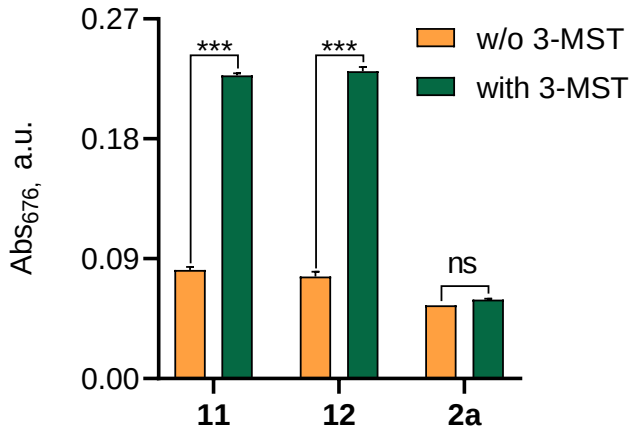

Figure 3.11. H_2S detection of compounds (**11**, **12**, and **2a** at 100 μM)in the presence of b3-MST (1 μM), Es (1 U/mL), and **DTT** (10 mM) for 2 h using methylene blue assay. Results are expressed as mean ± SD (n =3/group). **12** was used as a positive control, and **2a** as a negative control. Statistical significance was carried out using One-way ANOVA (*** $p \leq 0.001$).

Overall, this data suggests that compound **11** was able to generate H_2S in the presence of esterase and 3-MST under reducing conditions.

3.2.8. Sulfur transfer from 11 using LC/MS

Upon establishing that the artificial substrate **13** generated from **11** is turned over by 3-MST to form the 3-MST persulfide as an intermediate, the formation of persulfide/polysulfide was next evaluated by leveraging the ability of 3-MST persulfide to transfer the sulfane sulfur to a small molecule acceptor thiol such as **GSH**. GSH, upon reacting with 3-MST-SS^- will form GSH persulfide (GS-SH) and H_2S as a by-product. These reactive species were reacted with an electrophilic trapping agent (**HPE-IAM**),[9] and the corresponding HPE-IAM adducts were detected using LC/MS analysis (Scheme 3.6).

Compound **11** (50 μM) was incubated with Es (1 U/mL) and *b*3-MST (5 μM) and then with **GSH** (1 mM) and finally with **HPE-IAM** (10 mM) in PBS pH 7.4 at 37 °C. Finally, the samples were subjected to LC/MS analysis. A peak for the formation of the **GSS-HPE-AM** adduct (expected m/z = 517.1420; observed m/z = 517.1429) was observed at 7.3 min, indicating the formation of GSSH (Figure 3.12). Under these conditions, we also observe **Bis-S-HPE-AM** (expected m/z = 389.1530; observed m/z = 389.1537), presumably due to the reaction of HPE-IAM with H_2S formed by the reaction GS-SH and GSH. (Figure 3.13).

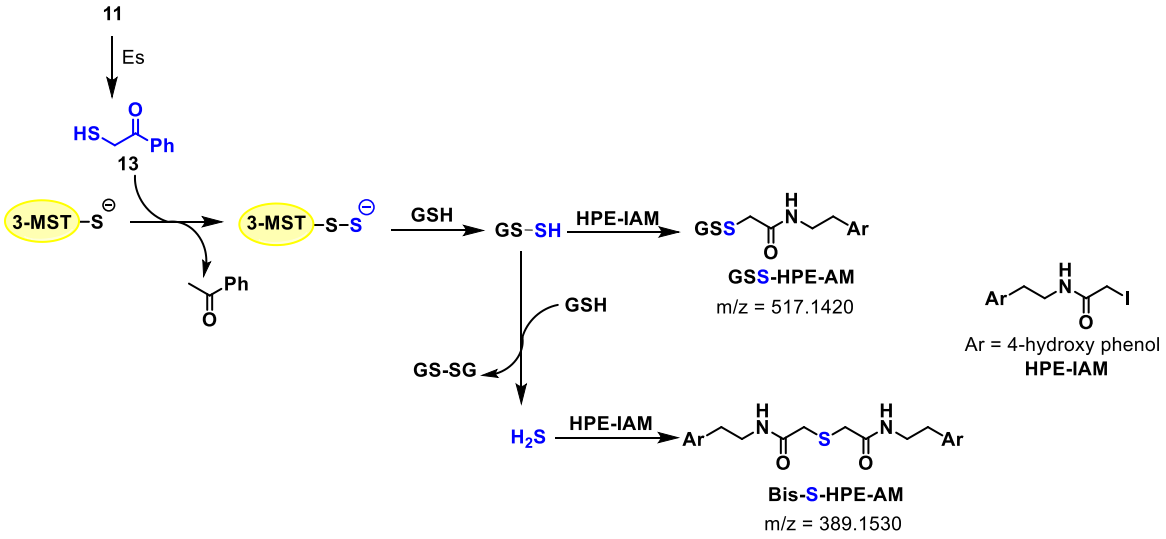

Scheme 3.6. LC/MS study. Reaction scheme showing the formation and detection of persulfides/polysulfides and hydrogen sulfide/polysulfides as their **HPE-AM** and **Bis-S-HPE-AM** adducts from **11**, respectively. Ar = 4-hydroxyphenyl.

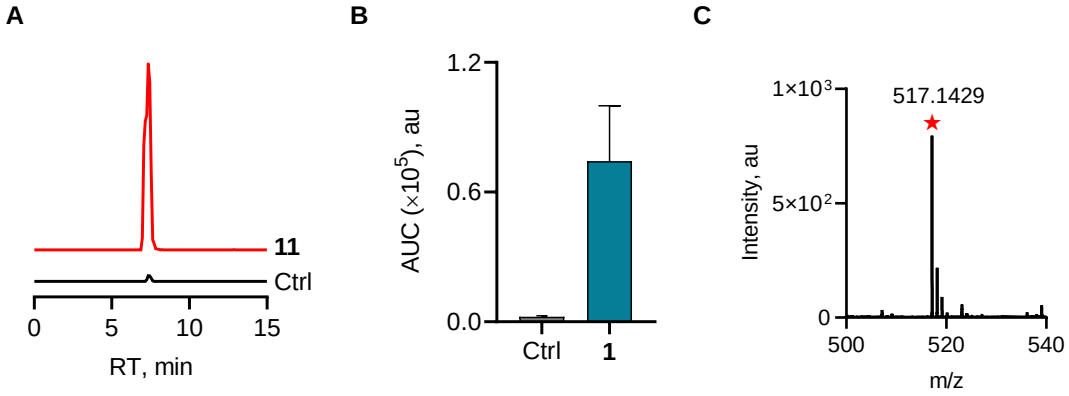

Figure 3.12. LC/MS study. (A) Extracted ion chromatograms from an LC/MS analysis of **GSS-HPE-AM** formation from **11** and ctrl, (B) GSSH **(GSS-HPE-AM)** formation was measured by the detection of trapped HPE-IAM species from **11** and ctrl, and (C) Mass spectra for **GSS-HPE-AM** (expected, m/z = 517.1420 $[M + H]^+$; observed, m/z = 517.1429).The ctrl was prepared by reacting 200 μM **GSH**, 200 μM, **DEA/NO** (sodium 2-(N, N-diethylamino)-diazenolate-2-oxide), and 200 μM **NaSH** at room temperature for 20 min.[10] Results are expressed as mean ± SD (n =3/group).

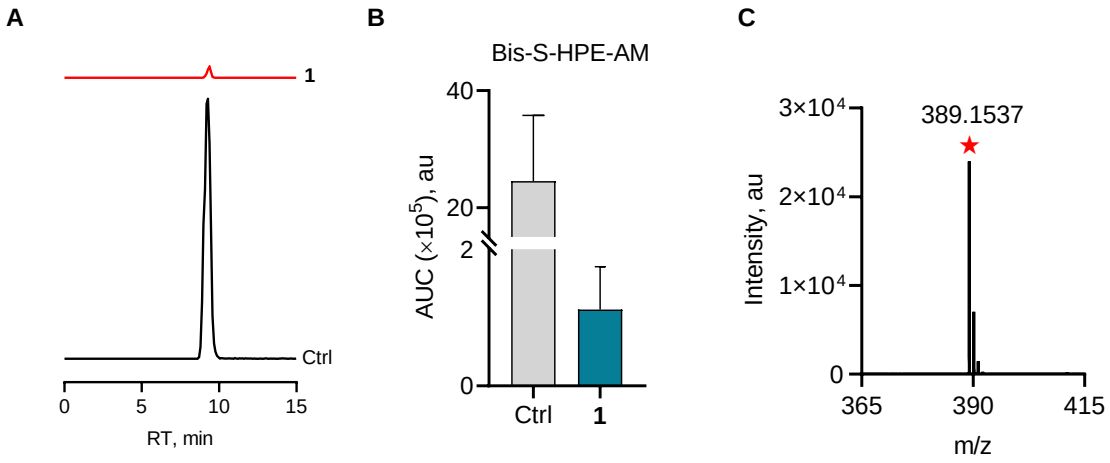

Figure 3.13. LC/MS study. (A) Extracted ion chromatograms from an LC/MS analysis of **Bis-S-HPE-AM** formation from **11** and ctrl, (B) H_2S **(Bis-S-HPE-AM**) formation was measured by the detection of trapped HPE-IAM species from **11** and ctrl, and (C) Mass spectra for **Bis-S-HPE-AM** (expected, m/z = 389.1530 $[M + H]^+$; observed, m/z = 389.1537). The ctrl was prepared by reacting 200 μM **GSH**, 200 μM, **DEA/NO** (sodium 2-(N, N-diethylamino)-diazenolate-2-oxide), and 200 μM **NaSH** at room temperature for 20 min. Results are expressed as mean ± SD (n =3/group).

3.2.9. MTT assay for cell viability of 11

The cytotoxicity of compound **11** was evaluated using a standard MTT assay to estimate the cell viability. Mouse embryonic fibroblast (MEF) cells were treated with varying concentrations of **11** and incubated for 24 h, following which cell viability was measured. Compound **11** was found to be well tolerated by MEF cells up to 100 μM (Figure 3.14).

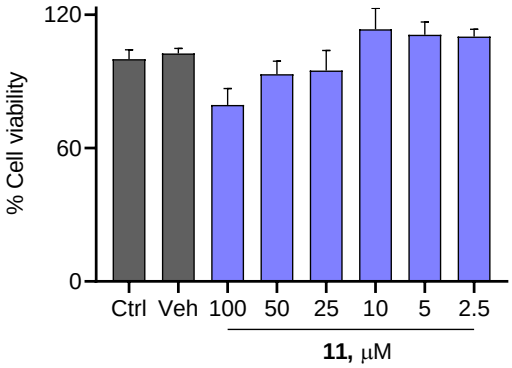

Figure 3.14. Cell viability assay was conducted on MEF (Mouse Embryonic Fibroblast) cells with compound **11** for 24 h. Results are expressed as mean ± SD (n =3/group).

3.2.10. Cytoprotection in chondrocytes

Since H_2S and sulfane sulfur are known to mitigate oxidative stress, the H_2S and sulfane sulfur releasing ability of compound **11** to protect the cells from cytotoxicity induced by oxidative stress was measured. The chondrocytes (C28/I2 cells) are the model cell line used to study osteoarthritis (OA), the most common joint disease, and is characterized by a gradual loss of articular cartilage and joint hypertrophy.[11] Chronic inflammation and oxidative stress contribute to the onset and progression of OA.[12,13] We first measured the cytotoxicity of **11** in the chondrocyte C28/I2 cells using WST-8 assay. Similar to **MTT**, yellow-colored **WST-8** gets converted to orange-colored formazan dye in the presence of the reductase and cofactor NADH (Scheme 3.7). The **WST-8** formazan dye was monitored at 450 nm to determine the cell viability. The chondrocytes were treated with varying concentrations of **11** and found that the compound was well tolerated by cells up to 100 µM (Figure 3.15). (Chondrocytes data was provided by Dr. Rachit Agarwal's Lab, Department of Bioengineering, IISc Bangalore).

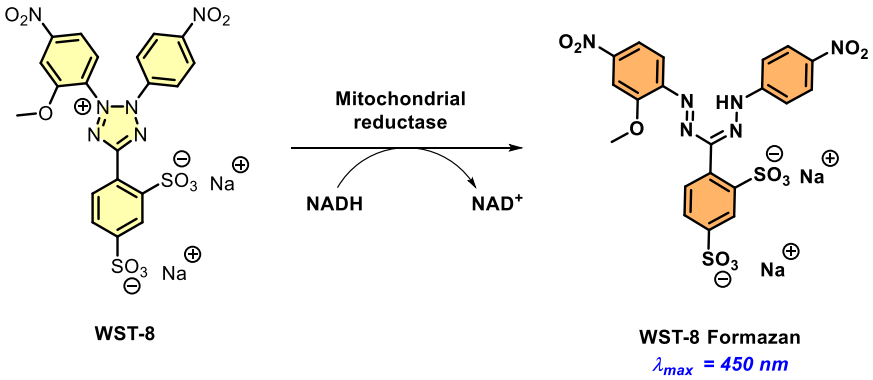

Scheme 3.7. WST-8 assay for cell viability. The formation of orange-colored formazan dye from yellow-colored **WST-8** in the presence of cellular reductases and NADH.

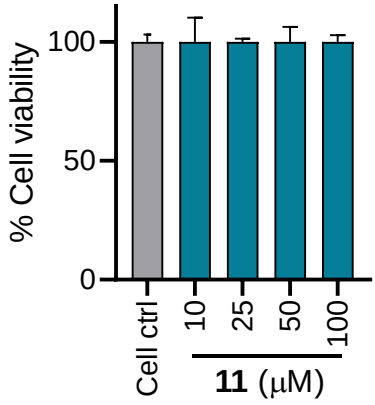

Figure 3.15. Cell viability assay conducted on C28/I2 cells. Cells were treated with varying concentrations of compound **11** for 24 h. All data are presented as mean ± SD (n = 3/group).

Next, we determined the cytoprotective effects of **11** in C28/I2 cells against oxidative stress induced by a cell-permeable ROS generator **MGR-1**, as explained in **Chapter 2**.[14] Cells were preincubated with varying concentrations of **11** (0 –100 μM) for 3 h and then were exposed to **MGR-1** (15 μM), after which the cell viability was assessed. As expected, exposure of cells to **MGR-1** resulted in a reduction in viable cells. Pre-treatment of cells with **11** demonstrated significant protective effects from **MGR-1** induced oxidative stress in a concentration-dependent manner (Figure 3.16).

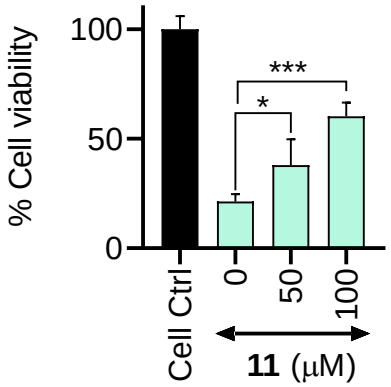

Figure 3.16. Cytoprotective activity conducted on C28/I2 cells. Cells were treated with varying concentrations of **11**, followed by treatment with **MGR-1** (15 μM). All data are presented as mean ± SD (n = 3/group). Statistical significance was established relative to **MGR-1** using One-way ANOVA (* $p < 0.033$, *** $p \leq 0.001$).

3.3. Summary

In summary, using the biphenyl system and lactonization as a key step, an esterase-sensitive 3-MST artificial substrate generator **11** was developed. Upon activation by esterase, **11** produces the fluorescent lactone **2a** and **13**. The formation of lactone **2a** and **13** from **11** was monitored using fluorescence-based experiments and HPLC. Next, the sulfane sulfur formation from **11** in the presence of Es and 3-MST was measured using fluorescent probe **SSP2**. Furthermore, efficient H_2S release from **11** was detected using lead acetate and methylene blue assay. Next, an LC-MS experiment was conducted to validate the transfer of sulfane sulfur generated from **11** under 3-MST conditions to small molecule thiol, **GSH**, using **HPE-IAM**. Mitigation of the oxidative stress by **11** was demonstrated in chondrocytes.

3.4. Experimental protocols

3.4.1 General methods

All the chemicals and solvents were purchased from commercial sources and used as received unless stated otherwise. Column chromatography was performed using silica gel-Rankem (60–120 mesh) as the stationary phase. Preparative high-performance liquid chromatography (HPLC) was done using Combiflash EZ prep UV using a Kromasil®C-18 preparative column (250 mm × 21.2 mm, 5 μm). ^{1}H and ^{13}C spectra were recorded on a JEOL 400 MHz (or 100 MHz for ^{13}C) or a Bruker 400 MHz (or 100 MHz for ^{13}C) spectrometer unless otherwise specified using either residual solvent signals ($CDCl_3$ δH = 7.26 ppm, δC = 77.2 ppm), or as an internal tetramethylsilane (δH = 0.00, δC = 0.0). Chemical shifts (δ) are reported in ppm and coupling constants (*J*) in Hz. The following abbreviations are used: m (multiplet), s (singlet), d (doublet), t (triplet), ddt (doublet of doublet of triplet) and dq (doublet of quartet). High-resolution mass spectra were obtained from HRMS-ESI-Q-Time of Flight LC/MS. FT-IR spectra were recorded using a BRUKER-ALPHA FT-IR spectrometer and reported in cm^{-1}. All measurements were done using a LC/MS method in the positive ion mode using high-resolution multiple reaction monitoring (MRM-HR) analysis on a Sciex X500R quadrupole time-of-flight (QTOF) mass spectrometer fitted with an Exion UHPLC system. Photometric measurements were performed using an Ensight Multimode Plate Reader (PerkinElmer). Fluorometric measurements were performed using a Thermo Scientific Varioscan microplate reader and a HORIBA Scientific Fluoromax-4 spectrofluorometer.

3.4.2. Synthesis and characterization

Compounds **12**,[15] **2a,**[16] and **8**[16] were synthesized following previously reported protocols, and each compound's analytical data was consistent with reported values.

4-(allyloxy)-2'-(((2-oxo-2-phenylethyl)thio)carbonyl)-[1,1'-biphenyl]-2-yl cyclopropanecarboxylate (11):

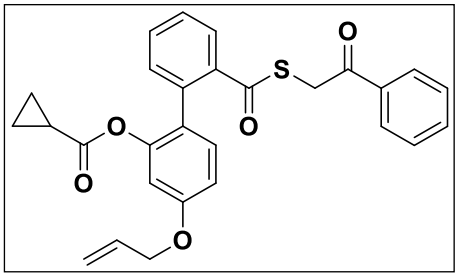

A solution of **8** (0.1 g, 0.29 mmol) was taken in DCM (5 mL). To the reaction mixture, DCC (0.068 g, 0.32 mmol) and DMAP (0.008 g, 0.059 mmol) were added under N_2 atmosphere, and the reaction was stirred for 1 h at 0 ^{o}C. A solution of freshly prepared phenacyl thiol **13** (0.09 g, 0.59 mmol) in DCM (2 mL) was added to the above reaction mixture and stirred at rt for 3 h

until the complete consumption of the starting material, as monitored by TLC. The solvent from the reaction mixture was evaporated, diluted residue with water (10 mL), and extracted with EtOAc (3 × 20 mL). The combined organic layer was washed with brine, dried over Na_2SO_4, and filtered, and the filtrate was concentrated to give a crude compound. The crude residue was further purified by column chromatography using silica gel (100-200) with 4% EtOAc/hexane as eluant to provide **11** (0.028 g, 20%) as a yellowish sticky liquid. FT-IR (ν_{max}, cm^{-1}): 3308, 2958, 2917, 2850, 1730, 1700, 1678, 1617; ^{1}H NMR (400 MHz, $CDCl_3$): δ 7.97 (dd, *J* = 8.3, 1.2 Hz, 2H), 7.89 (dd, *J* = 7.8, 1.1 Hz, 1H), 7.61 - 7.51 (m, 2H), 7.49 - 7.40 (m, 3H), 7.28 (dd, *J* = 7.6, 1.1 Hz, 1H), 7.22 (d, *J* = 8.5 Hz, 1H), 6.84 (dd, *J* = 8.5, 2.5 Hz, 1H), 6.66 (d, *J* = 2.5 Hz, 1H), 6.07 (ddt, *J* = 17.6, 10.6, 5.3 Hz, 1H), 5.43 (dq, *J* = 17.2, 1.5 Hz, 1H), 5.30 (dq, *J* = 10.5, 1.4 Hz, 1H), 4.53 (dt, *J* = 5.3, 1.5 Hz, 2H), 4.46 (s, 2H), 1.62 - 1.56 (m, 1H), 0.74 (d, *J* = 8.0 Hz, 4H); ^{13}C NMR (100 MHz, $CDCl_3$): δ 193.7, 191.7, 173.0, 159.3, 148.5, 137.4, 136.0, 135.6, 133.8, 133.1, 132.1, 131.1, 128.8, 128.7, 128.4, 127.7, 125.9, 118.0, 112.6, 108.9, 69.1, 37.2, 12.9, 9.0; HRMS (ESI-TOF) for $C_{28}H_{24}O_5S[M+Na]^+$: Calcd., 495.1237, Found, 495.1241.

3.4.3. Monitoring the release of 2a upon esterase activation of 11

(A) Fluorometric analysis:

Stock solutions of **11** (10 mM), **2a** (10 mM) in DMSO, and porcine liver esterase (Es, 100 U/mL; Sigma Aldrich, E3019) in phosphate buffer saline (10 mM, pH 7.4) were prepared. The reaction mixture was prepared by adding 10 μM of **11** (10 μL, 1 mM), with or without 1 U/mL Es (esterase;10 μL, 100 U/mL stock) and the volume was adjusted to 1000 μL using phosphate buffer saline (10 mM, pH 7.4) in a 1.5 mL eppendorf tube and incubated for 60 min at 37 ˚C then transferred into a micro-fluorescence cell (Hellma, path length 1.0 cm). Fluorescence spectra (λ_{ex} = 320 nm and λ_{em} = 432 nm) were recorded using a HORIBA Scientific Fluoromax-4 spectrofluorometer.

(B) Fluorescence-based analysis:

Stock solutions of **11** (0.5 mM) in DMSO and porcine liver esterase (10 U/mL; Sigma Aldrich, E3019) in phosphate buffer saline (10 mM, pH 7.4) were prepared. The reaction mixture was prepared by adding 10 μM of **11** (4 μL, 0.5 mM) with or without 1 U/mL esterase (20 μL, 10 U/mL stock), and the volume was adjusted to 200 μL using phosphate buffer saline (10 mM,

pH 7.4) in a 96-well plate and then incubated for 60 min at 37 ˚C. The fluorescence (λ_{ex} = 320 nm and λ_{em} = 432 nm) was measured using an Ensight Multimode Plate Reader (PerkinElmer).

Stock solutions of **11** or **2a** (0.125, 0.25, 0.5, 1 mM) in DMSO and porcine liver esterase (10 U/mL; Sigma Aldrich, E3019) in phosphate buffer saline (10 mM, pH 7.4) were prepared. The reaction mixture was prepared by varying concentrations (0-20 μM) of **1** (4 μL from respective stocks (0.125-1 mM)), with or without 1 U/mL esterase (20 μL, 10 U/mL stock), and the volume was adjusted to 200 μL using phosphate buffer saline (10 mM, pH 7.4) in a 96-well plate. The time-dependent fluorescence increment (λ_{ex} = 320 nm and λ_{em} = 432 nm) was recorded at 37 ˚C for a period of 120 min using an Ensight Multimode Plate Reader (PerkinElmer).

Stock solutions of **PMSF** (100 mM) in isopropanol and esterase (100 U/mL) in phosphate buffer saline (PBS), pH 7.4, were prepared. The reaction mixture was prepared by adding 1 mM of **PMSF** (7 μL, 100 mM) along with 1 U/mL esterase (70 μL, 1 U/mL stock), and the volume was adjusted to 700 μL using phosphate buffer saline (10 mM, pH 7.4) in a 96-well plate. Measurements were carried out after incubation for 30 min at 37 ˚C.

Stock solutions of **11** (0.5 mM) in DMSO and esterase (1 U/mL, pre-treated with **PMSF**) in phosphate buffer saline (10 mM, pH 7.4) were prepared independently. Measurements were carried out by using the above-described protocol.

3.4.4. Stability assessment of 11 by HPLC

A stock solution of **11** (10 mM) was prepared independently in DMSO. In a typical reaction, compound 50 μM **11** (5 μL, 10 mM stock) was added to 995 μL of phosphate buffer saline (10 mM, pH 7.4), and the reaction mixture was incubated at 37 ºC. Aliquots were taken at determined time points (0 h and 2 h), diluted with an equal amount of acetonitrile, and then injected in an HPLC instrument attached to a UV detector (absorbance at 250 nm). Phenomenex Luna C-18 reverse phase column, 100 Å particle size and 5 μM pore size (250 × 4.6 mm) was used. The mobile phase was water: acetonitrile with a multistep gradient starting at 35:65 → 0 min, 35:65 to 35:65 → 0 - 2 min, 35:65 to 20:80 → 2 - 5 min, 20:80 to 10:90 → 5 - 8 min, 10:90 to 5:95 → 8 - 11 min, 5:95 to 10:90 → 11 - 14 min, 10:90 to 20:80 → 14 - 17 min, 20:80 to 35:65 → 17 - 20 min, 35:65 to 35:65 → 20 - 24 min was used at a flow rate of 0.5 mL/min.

3.4.5. Decomposition of 11 in the presence of esterase using HPLC

Stock solutions of **11** (10 mM), **12** (10 mM), and **2a** (10 mM) were prepared in DMSO. Porcine liver esterase (100 U/mL) in phosphate buffer saline (10 mM, pH 7.4) was prepared. The reaction mixture was prepared by adding 50 μM of **11** (5 μL, 10 mM) with or without 1 U/mL Es (10 μL, 100 U/mL stock), and the volume was adjusted to 1 mL using phosphate buffer saline (10 mM, pH 7.4) in an Eppendorf then incubated for 120 min at 37 ˚C on thermomixer (300 rpm). 200 μL aliquots of the reaction mixture were taken at pre-determined time points, and the reaction was quenched by adding 200 μL of acetonitrile. The samples were centrifuged at 10000 x g for 5 min at 4 ˚C; the supernatant was collected and injected (50 μL) in high-performance liquid chromatography (HPLC) attached with a UV detector (absorbance at 250 nm). Phenomenex Luna C-18 reverse phase column, 100 Å particle size and 5 μm pore size (250 × 4.6 mm) was used. The mobile phase was water: acetonitrile with a multistep gradient starting at 35:65 → 0 min, 35:65 to 35:65 → 0 - 2 min, 35:65 to 20:80 → 2 - 5 min, 20:80 to 10:90 → 5 - 8 min, 10:90 to 5:95 → 8 - 11 min, 5:95 to 10:90 → 11 - 14 min, 10:90 to 20:80 → 14 - 17 min, 20:80 to 35:65 → 17 - 20 min, 35:65 to 35:65 → 20 - 24 min was used at a flow rate of 0.5 mL/min.

3.4.6. Selectivity studies of 11

Stock solutions of **11** and **2a** (1 mM) and porcine liver esterase (100 U/mL) were prepared in DMSO and phosphate buffer saline (10 mM, pH 7.4), respectively. Stock solutions of GSH (10 mM), Cys (10 mM), vitamin-C (10 mM), arabinose (10 mM), glucose (10 mM), galactose (10 mM), *N*- acetylcysteine (NAC, 10 mM), DTT (10 mM), and H_2O_2 (30%, 10 mM) in phosphate buffer were prepared independently from commercial sources. A stock solution of 285 μM 3-MST was used.

The reaction mixture was prepared by adding 10 μM of **11** (2 μL, 1 mM), with or without 1 U/mL esterase (2 μL, 100 U/mL stock), and the volume was adjusted to 200 μL using phosphate buffer saline (10 mM, pH 7.4)) in a 96-well plate and then incubated for 60 min at 37 ˚C. Similarly, a reaction mixture of 10 μM of **11** (2 μL, 1 mM), with or without 100 μM (10 eq.) of various analytes (2 μL, 10 mM stock), was prepared, and the volume was adjusted to 200 μL using phosphate buffer saline (10 mM, pH 7.4) in a 96-well plate and then incubated for 60 min at 37 ˚C. The fluorescence (λ_{ex} = 320 nm and λ_{em} = 432 nm) was measured using an Ensight Multimode Plate Reader (PerkinElmer).

3.4.7. Sulfane sulfur measurement from 11 using SSP2

Stock solutions of **11** (10 mM), **12** (10 mM), **2a** (10 mM), and **SSP2** (5 mM) were prepared in DMSO. Porcine liver esterase (100 U/mL) in phosphate buffer saline (10 mM, pH 7.4) was prepared. Individual reaction samples were prepared for **11**, **12**, and **2a**. To 3-MST (1 μM), compound (10 μM) and Es (1 U/mL) were added. Volume was adjusted to 400 μL using 10 mM PBS pH 7.4 buffer. The reaction was incubated for 1 h at 37 °C.

A reaction was set up for compound control. Individual reaction samples were prepared for **11**, **12**, and **2a**. The reaction mixtures were prepared by adding compound (10 μM) with Es (1 U/mL), and the volume was adjusted to 400 μL using 10 mM PBS pH 7.4 buffer. The reaction was incubated for 1 h at 37 °C.

A reaction was set up for enzyme control. The reaction mixtures were prepared by 3-MST (10 μM), 4 μL of DMSO, Es (1 U/mL), and the volume was adjusted to 400 μL using 10 mM PBS pH 7.4 buffer. The reaction was incubated for 1 h at 37 °C.

A similar reaction was set up for **DTT** control. Individual reaction samples were prepared for **11**, **12**, and **2a**. The reaction mixtures were prepared by adding compound (10 μM) with Es (1 U/mL) and 3-MST (1 μM). The volume was adjusted to 360 μL using 10 mM PBS pH 7.4 buffer. The reaction was incubated for 1 h at 37 °C. Finally, the reaction mixture was treated with 10 mM DTT (40 μL of 100 mM stock) and further incubated at 37 °C for 1 h.

The above treatment groups were finally incubated with 5 μM **SSP2** (4 μL, 5 mM) at 37 °C for 10 min in the dark. 100 μL aliquot of each sample was transferred to a 96-well plate, and the fluorescence was recorded (λ_{ex} = 482 nm; λ_{em} = 518 nm) using an Ensight Multimode Plate Reader (PerkinElmer).

3.4.8. Lead acetate assay for the H_2S detection from 11

The lead acetate assays were conducted as previously reported, with some modifications. Firstly, lead acetate paper was prepared by soaking Whatman filter paper with 10 % (w/v) lead acetate solution and dried. 392 μM stock of wild-type (wt) *b*3-MST was used for lead acetate assay. Stocks of all compounds (**11**, **12**, and **2a**) (10 mM) were prepared in DMSO. Porcine liver esterase (100 U/mL) in phosphate buffer saline (10 mM, pH 7.4) was prepared. Dithiothreitol (**DTT**, 10 mM) was prepared in deionized water.

Lead acetate assay was performed in a 96-well plate (with lid). Individual reaction samples were prepared for **11**, **12**, and **2a**. Compound (100 μM) was subsequently added to Es (1U/mL),

wt 3-MST (1 μM) and DTT (10 mM). The final volume was adjusted to 200 μL using 10 mM phosphate buffer saline (PBS) pH 7.4 buffer, covered with 10% lead acetate-soaked paper, sealed, and incubated at 37 °C.

A similar protocol was followed for the substrate controls. Individual reaction samples were prepared for **11**, **12**, and **2a**. Compound (100 μM) was subsequently added to Es(1 U/mL) and DTT (10 mM). The final volume was adjusted to 200 μL using 10 mM PBS pH 7.4 buffer, covered with 10% lead acetate-soaked paper, sealed, and incubated at 37 °C.

A separate experiment was conducted to test the enzyme controls. DMSO (1%), Esterase (1 U/mL), *b*3-MST (0.5 μM), and **DTT** (10 mM) were sequentially added. The final volume was adjusted to 200 μL using 10 mM PBS pH 7.4 buffer, covered with 10% lead acetate-soaked paper, sealed, and incubated at 37 °C.

Lead acetate paper was carefully taken out at predetermined time points, and an image was captured using Syngene G-Box Chemi-XRQ.

3.4.9. Methylene blue assay for the H_2S detection from 11

General protocol: The methylene blue assays were conducted as previously reported with some modifications. Briefly, 392 μM stock of wt *b*-3MST was used for the methylene blue assay. 10 mM stocks of all compounds (**11**, **12**, and **2a**) were prepared in DMSO. Porcine liver esterase (100 U/mL) in phosphate buffer saline (10 mM, pH 7.4) was prepared. Dithiothreitol (**DTT**, 100 mM), **NaSH** (100 mM), and **$Zn(OAc)_2.2H_2O$** (40 mM) were prepared in deionized water. Stock solutions of **$FeCl_3$** (30 mM) and *N*, *N*–dimethyl-p-phenylenediamine sulfate (**DMPPDA**) (20 mM) were prepared in 1.2 M HCl and 7.2 M HCl, respectively.

Individual reaction samples were prepared for **11**, **12**, and **2a**. Compound (100 μM) was added to Es (1 U/mL), **$Zn(OAc)_2.2H_2O$** (400 μM), *b*3-MST(1 μM), and **DTT** (10 mM). The final volume was adjusted to 0.5 mL using 10 mM PBS pH 7.4 buffer and incubated at 37 °C.

A similar protocol was followed for the substrate controls. Individual reaction samples were prepared for **11**, **12**, and **2a**. Compound (100 μM) was added to Es (1 U/mL), **$Zn(OAc)_2.2H_2O$** (400 μM), and **DTT** (10 mM). The final volume was adjusted to 0.5 mL using 10 mM PBS pH 7.4 buffer and incubated at 37 °C.

A separate experiment was conducted to test the enzyme controls. DMSO (1%), Esterase (1 U/mL), *b*3-MST(0.5 μM), and **DTT** (10 mM) were sequentially added. The final volume was adjusted to 0.5 mL using 10 mM PBS pH 7.4 buffer and incubated at 37 °C.

At predetermined time points, equal volumes (200 μL) of **$FeCl_3$**, **DMPPDA**, and aliquots from the above reaction samples were mixed, and the resulting solution was incubated at 37 °C for 30 min in dark to allow the formation of the methylene blue dye. An aliquot of 150 μL was transferred to a 96-well plate, and the absorbance values were recorded at 676 nm using a microplate reader (Thermo Scientific VarioskanFlash).

3.4.10. Sulfur transfer detection from 11 using LC/MS

Stock solutions of **11** (10 mM) and **HPE-IAM** (100 mM) were prepared in DMSO. A stock solution of porcine liver esterase (100 U/mL; Sigma Aldrich, E3019) was prepared in PBS pH 7.4 and). A stock solution of **GSH** (10 mM) was prepared in DI water. The reaction mixture was prepared by adding 50 μM of **11** (1.5 μL, 10 mM stock), 1 U/mL esterase (3 μL, 100 U/mL stock), and 5 μM of 3-MST (19.5 μL, 77 μM stock). The volume was adjusted to 300 μL using 10 mM PBS, pH 7.4, and the reaction mixture was incubated for 60 min at 37 °C. 1 mM **GSH** (30 μL of 10 mM) was then added and incubated at 37 °C for 30 min, followed by 10 mM **HPE-IAM** (30 μL of 100 mM) and further incubation for 15 min at 37 °C. Finally, the reaction was quenched by adding 300 μL of acetonitrile. Similarly, control reactions were set up for the **11** or **HPE-IAM** alone and 3-MST only. The samples were centrifuged at 10,000 x g for 10 min at 4 ˚C; the supernatant was collected and assessed thereafter by LC/MS. All measurements were done using a previously established LC/MS method[17] with slight modification. All measurements were done using the following protocol: Acetonitrile (A) and 0.1% formic acid in water (B) were used as the mobile phase. A multistep gradient was used with the flow rate of 0.2 mL/min starting with 0:100 → 0 min 0:100 to 5:95 → 0.10 -1 min, 5:95 to 90:10→ 1 - 15 min, 90:10 to 0:100 → 15 – 15.10 min, and 0:100 → 15 – 22 min. Measurements were carried out in the positive ion mode using high-resolution multiple reaction monitoring (MRM-HR) analysis on a Sciex X500R quadrupole time-of-flight (QTOF) mass spectrometer fitted with an Exion UHPLC system using a Kinetex 2.6 mm hydrophilic interaction liquid chromatography (HILIC) column with 100 Å particle size, 150 mm length and 3 mm internal diameter (Phenomenex). Nitrogen was the nebulizer gas, with the nebulizer pressure set at 50 psi, declustering potential = 80 V, entrance potential = 10 V, collision energy = 20 V, and collision exit potential = 5 V. The MRM-HR mass spectrometry parameters for measuring compounds are: m/z precursor ion mass $(M + H)^+$: 473.1417 (**1**), 305.9985 (**HPE-IAM**), 517.1420 (**GSS-HPE-AM**), 389.1530 (**Bis-S-HPE-AM**).

3.4.11. Cell viability assay for 11

MEF cells: Mouse embryonic fibroblasts (MEF) cells were seeded at a concentration of 1×10^4 cells/well overnight in a 96-well plate in complete DMEM medium supplemented with 5% FBS (fetal bovine serum) and 1% antibiotic solution in an atmosphere of 5% CO_2 at 37 ˚C. Cells were exposed to varying concentrations of compound **11** prepared as a DMSO stock solution so that the final concentration of DMSO was 0.5%. The cells were incubated for 24 h at 37 ˚C. A 0.5 mg/mL stock solution of 3-(4, 5-dimethylthiazol-2-yl)-2, 5-diphenyl tetrazolium bromide (**MTT**) was prepared in DMEM and 100 µL of the resulting solution was added to each well. After 4 h incubation, the media was removed carefully and 100 µL of DMSO was added. Spectrophotometric analysis of each well using a microplate reader (Thermo Scientific Varioscan) at 570 nm was carried out to estimate cell viability.

C28/I2 cells: Cell metabolic activity was assessed using the water-soluble tetrazolium salt-8 (**WST-8**) proliferation assay Kit (Cayman). Human chondrocytes, C28/I2 cells, were seeded overnight in a 24-well plate at a concentration of 6000 cells/well in complete DMEM medium (Gibco) supplemented with 5% FBS (fetal bovine serum: Sigma Aldrich) and 1% antibiotic solution (Thermo Fisher Scientific). The cells were incubated with different concentrations of **11** prepared as a DMSO stock solution, resulting in a final DMSO concentration of 0.1%.

A stock solution of WST-8 containing 2 µL of WST-8 developer reagent and 2 µL of electron mediator solution per 96 µL of complete DMEM was prepared. After 24 hours, the cells were washed with 1x PBS, and 100 µL of the WST-8 solution was added to each well. After a 1-hour incubation, the cell metabolic activity was estimated by measuring the absorbance at 450 nm using a microplate reader (Tecan Spark). (**Note:** All the experiments with C28/I2 cells were conducted at Dr. Rachit Agarwal's Lab, IISc Bangalore)

3.4.12. Protection from oxidative stress

C28/I2 cells were seeded overnight in a 24-well plate at a concentration of 6000 cells/well in complete DMEM medium (Gibco) supplemented with 5% FBS (fetal bovine serum: Sigma Aldrich) and 1% antibiotic solution (Thermo Fisher Scientific). The cells were pre-treated for 3 hours with various concentrations of **11**, which were prepared as a DMSO stock solution to achieve a final DMSO concentration of 0.1%. Following this pre-treatment, **MGR-1** was added to the cells at different concentrations and incubated for 24 hours.

A stock solution of **WST-8** containing 2 µL of **WST-8** developer reagent and 2 µL of electron mediator solution per 96 µL of complete DMEM was prepared. After 24 hours of treatment, the cells were washed with 1x PBS, and 100 µL of the **WST-8** solution was added to each well. After a 1-hour incubation, the cell metabolic activity was estimated by measuring the absorbance at 450 nm using a microplate reader (Tecan Spark).

3.5. NMR spectra of compound

^{1}H NMR spectra of **11**

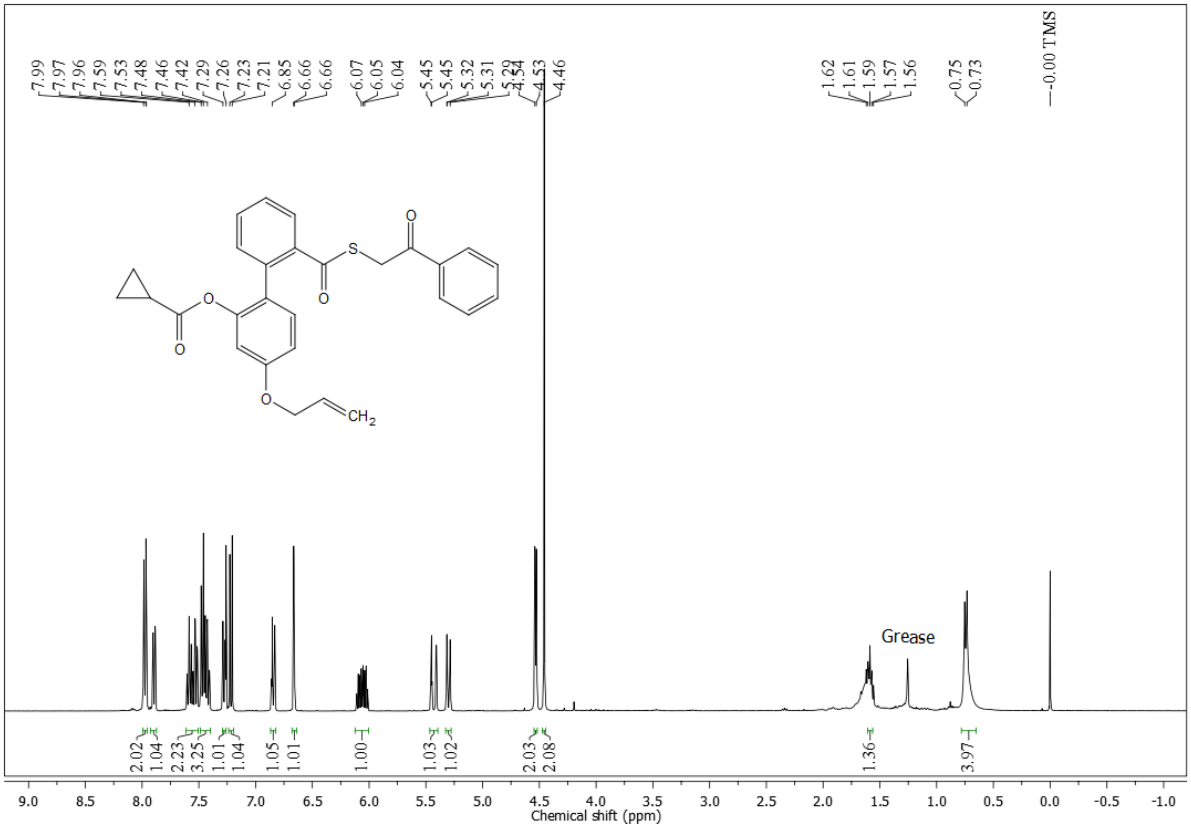

^{13}C NMR spectra of **11**

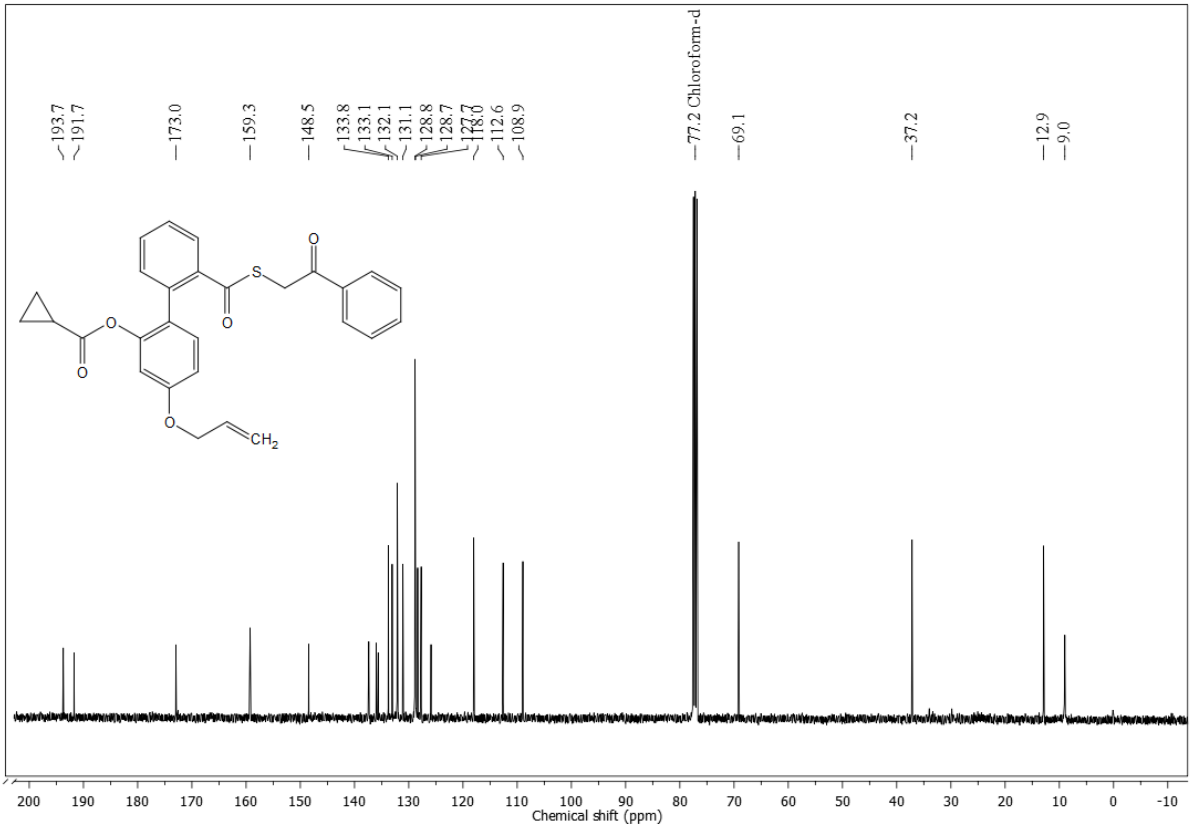

3.6. References

(1) Nagahara, N. Multiple Role of 3-mercaptopyruvate Sulfurtransferase: Antioxidative Function, H 2 S and Polysulfide Production and Possible SO x Production. *Br. J. Pharmacol.* **2018**, *175* (4), 577–589.

(2) Yadav, P. K.; Yamada, K.; Chiku, T.; Koutmos, M.; Banerjee, R. Structure and Kinetic Analysis of H2S Production by Human Mercaptopyruvate Sulfurtransferase. *J. Biol. Chem.* **2013**, *288* (27), 20002–20013.

(3) Nagahara, N.; Yoshii, T.; Abe, Y.; Matsumura, T. Thioredoxin-Dependent Enzymatic Activation of Mercaptopyruvate Sulfurtransferase. *J. Biol. Chem.* **2007**, *282* (3), 1561–1569.

(4) Kimura, Y.; Koike, S.; Shibuya, N.; Lefer, D.; Ogasawara, Y.; Kimura, H. 3-Mercaptopyruvate Sulfurtransferase Produces Potential Redox Regulators Cysteine- and Glutathione-Persulfide (Cys-SSH and GSSH) Together with Signaling Molecules H2S2, H2S3 and H2S. *Sci. Rep.* **2017**, *7* (1), 10459.

(5) Coletta, C.; Módis, K.; Szczesny, B.; Brunyánszki, A.; Oláh, G.; Rios, E. C. S.; Yanagi, K.; Ahmad, A.; Papapetropoulos, A.; Szabo, C. Regulation of Vascular Tone, Angiogenesis and Cellular Bioenergetics by the 3-Mercaptopyruvate Sulfurtransferase/H2S Pathway: Functional Impairment by Hyperglycemia and Restoration by Dl-α-Lipoic Acid. *Mol. Med.* **2015**, *21* (1), 1–14.

(6) Bora, P.; Manna, S.; Nair, M. A.; Sathe, R. R. M.; Singh, S.; Sreyas Adury, V. S.; Gupta, K.; Mukherjee, A.; Saini, D. K.; Kamat, S. S.; Hazra, A. B.; Chakrapani, H. Leveraging an Enzyme/Artificial Substrate System to Enhance Cellular Persulfides and Mitigate Neuroinflammation. *Chem. Sci.* **2021**, *12* (39), 12939–12949.

(7) Smith, P. C.; McDonagh, A. F.; Benet, L. Z. Effect of Esterase Inhibition on the Disposition of Zomepirac Glucuronide and Its Covalent Binding to Plasma Proteins in the Guinea Pig. *J. Pharmacol. Exp. Ther.* **1990**, *252* (1), 218–224.

(8) Chen, W.; Liu, C.; Peng, B.; Zhao, Y.; Pacheco, A.; Xian, M. New Fluorescent Probes for Sulfane Sulfurs and the Application in Bioimaging. *Chem. Sci.* **2013**, *4* (7), 2892–2896.

(9) Hamid, H. A.; Tanaka, A.; Ida, T.; Nishimura, A.; Matsunaga, T.; Fujii, S.; Morita, M.; Sawa, T.; Fukuto, J. M.; Nagy, P.; Tsutsumi, R.; Motohashi, H.; Ihara, H.; Akaike, T. Polysulfide Stabilization by Tyrosine and Hydroxyphenyl-Containing Derivatives That Is Important for a Reactive Sulfur Metabolomics Analysis. *Redox Biol.* **2019**, *21*, 101096.

(10) Ida, T.; Sawa, T.; Ihara, H.; Tsuchiya, Y.; Watanabe, Y.; Kumagai, Y.; Suematsu, M.; Motohashi, H.; Fujii, S.; Matsunaga, T.; Yamamoto, M.; Ono, K.; Devarie-Baez, N. O.; Xian, M.; Fukuto, J. M.; Akaike, T. Reactive Cysteine Persulfides and S-Polythiolation Regulate Oxidative Stress and Redox Signaling. *Proc. Natl. Acad. Sci.* **2014**, *111* (21), 7606–7611.

(11) Martel-Pelletier, J. Pathophysiology of Osteoarthritis. *Osteoarthr. Cartil.* **1998**, *6* (6), 374–376

(12) Ansari, M. Y.; Ahmad, N.; Haqqi, T. M. Oxidative Stress and Inflammation in Osteoarthritis Pathogenesis: Role of Polyphenols. *Biomed. Pharmacother.* **2020**, *129*, 110452.

(13) Liu, L.; Luo, P.; Yang, M.; Wang, J.; Hou, W.; Xu, P. The Role of Oxidative Stress in the Development of Knee Osteoarthritis: A Comprehensive Research Review. *Front. Mol. Biosci.* **2022**, *9*.

(14) Kelkar, D. S.; Ravikumar, G.; Mehendale, N.; Singh, S.; Joshi, A.; Sharma, A. K.; Mhetre, A.; Rajendran, A.; Chakrapani, H.; Kamat, S. S. A Chemical–Genetic Screen Identifies ABHD12 as an Oxidized-Phosphatidylserine Lipase. *Nat. Chem. Biol.* **2019**, *15* (2), 169–178.

(15) Heredia, A. A.; Soria-Castro, S. M.; Bouchet, L. M.; Oksdath-Mansilla, G.; Barrionuevo, C. A.; Caminos, D. A.; Bisogno, F. R.; Argüello, J. E.; Peñéñory, A. B. Stereoselective One-Pot Synthesis of β-Alkylsulfide Enol Esters. Base-Triggered Rearrangement under Mild Conditions. *Org. Biomol. Chem.* **2014**, *12* (33), 6516.

(16) Choudhary, B. S.; Kumar, T. A.; Vashishtha, A.; Tejasri, S.; Kumar, A. S.; Agarwal, R.; Chakrapani, H. An Esterase-Cleavable Persulfide Donor with No Electrophilic Byproducts and a Fluorescence Reporter. *Chem. Commun.* **2024**, *60* (13), 1727–1730

(17) Zhang, T.; Ono, K.; Tsutsuki, H.; Ihara, H.; Islam, W.; Akaike, T.; Sawa, T. Enhanced Cellular Polysulfides Negatively Regulate TLR4 Signaling and Mitigate Lethal Endotoxin Shock. *Cell Chem. Biol.* **2019**, *26* (5), 686-698.e4.

In **Chapters 2** and **3**, the development of esterase-activated persulfide generators was described. As esterase is ubiquitous, delivery of persulfide is not selective towards a particular cell type. Designing a tool for specific persulfide generation is desirable to overcome the limitations associated with the esterase-based strategy. In order to achieve this goal, a ROS-activated (H_2O_2) persulfide generator was considered to leverage the elevated ROS levels as a trigger to enhance the specificity of activation and release of the active species (Figure 4.1.1).

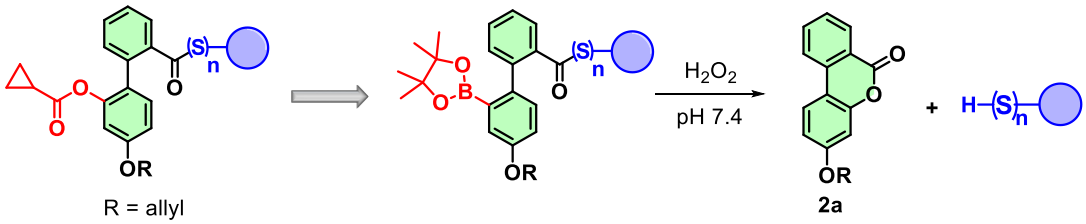

Figure 4.1.1. Development of biphenyl-based ROS-activated persulfide generators.

The well-known boronate ester group was used as a trigger to develop the ROS-activated persulfide generators. However, the attempts to develop biphenyl-based ROS-activated persulfide generators were unsuccessful due to the synthesis difficulty and complexity. An alternate strategy for persulfide generators with non-electrophilic byproduct formation was considered.

Lukesh and co-workers have developed an H_2O_2 responsive persulfide generator **RAH393** (Scheme 4.1.1).[1] Upon activation by H_2O_2, the phenolate undergoes intramolecular cyclization to release *N*-acetyl cysteamine persulfide and an innocuous lactone by-product.

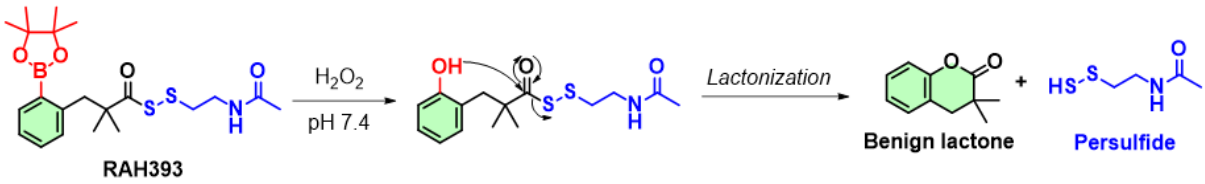

Scheme 4.1.1. ROS-activated persulfide donor **RAH393**, sensitive to H_2O_2.

The scope and utility of the **RAH393** scaffold in order to develop a persulfide generator (**Chapter 4.1**) or masked drugs (**Chapter 4.2**) were investigated (Figure 4.1.2).

Figure 4.1.2. ROS-activated persulfide donors, sensitive to H_2O_2.

Chapter 4.1. Development of ROS-activated Persulfide Generator Through 3-MST Pathway

4.1.1. Introduction

Using the **RAH393** scaffold, a ROS-activated 3-MST artificial substrate **14** was developed. Upon activation by H_2O_2, compound **14** generates the 3-MST artificial substrate **13** and benign lactone **15** as a byproduct (Scheme 4.1.2).

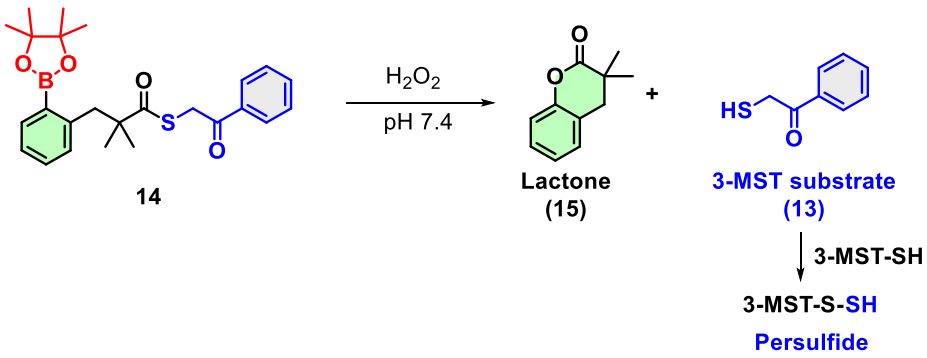

Scheme 4.1.2. Design of ROS-activated 3-MST artificial substrate donor.

4.1.2. Results and Discussion

4.1.2.1. Synthesis

Compound **14** was synthesized in 5 steps.[1] Ethyl-isobutyrate was activated using freshly prepared LDA and reacted with 2-bromobenzyl bromide to give compound **16** in 81% yield. Miyaura borylation of **16** gave **17** in 67% yield. The ethyl ester group in **17** was hydrolyzed under basic conditions to yield the carboxylic acid compound **18** in 86% yield. The carboxylic

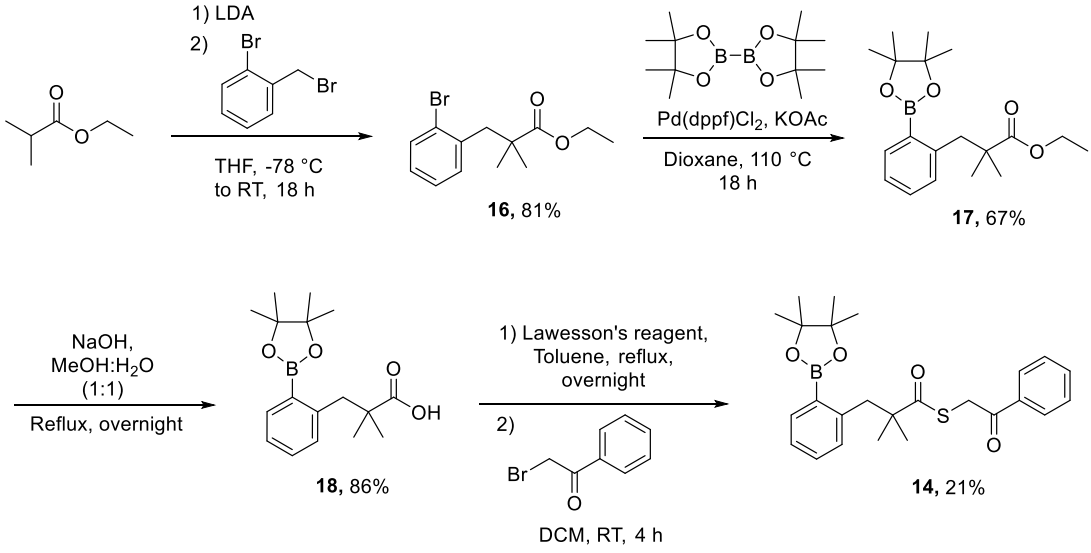

Scheme 4.1.3. Synthesis of ROS-activated 3-MST substrate **14**.

acid 1**8** was converted to its corresponding thiocarboxylic acid **19** using Lawesson's reagent, and the crude was reacted with phenacyl bromide to provide the desired compound **14** in 21% yield (Scheme 4.1.3).

4.1.2.2. Activation of 14 and detection of 13 and 15

Compound **14**, in the presence of H_2O_2, generates lactone **15** and phenacyl thiol **13** in a single step. Both **13** and **15** can be directly detected by LC/MS analysis. **13** reacts with 3-MST and produces 3-MST persulfide, which can be detected by sulfane sulfur probe **SSP2**. Persulfidated 3-MST can transfer the sulfhydryl group to the thiol acceptor, **GSH**, and produce the GS-SH and H_2S, which can be monitored by LC/MS using **HPE-IAM**, as described in the previous chapters. Also, the 3-MST persulfide in the presence of **DTT** produces H_2S, which can be detected by lead acetate, methylene blue assay, or by trapping it with an **HPE-IAM** (Scheme 4.1.4).

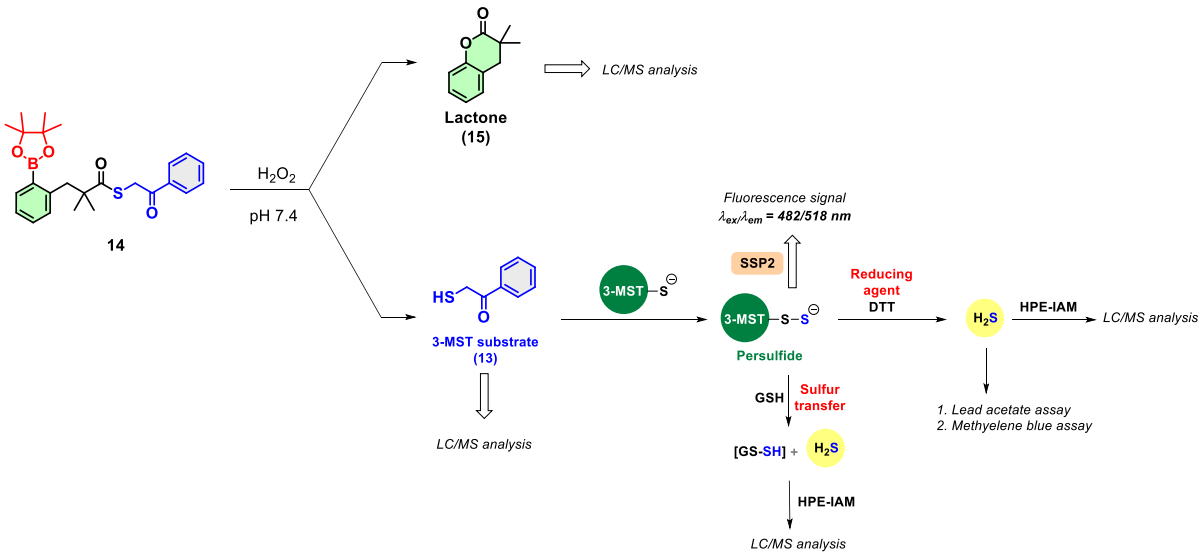

Scheme 4.1.4. Tools for detection of lactone **15** and 3-MST artificial substrate **13** from **14** in the presence of H_2O_2. Further detection of persulfide, sulfur transfer, and H_2S generated from **13** through 3-MST pathway.

4.1.2.3. Activation of 14 in the presence of H_2O_2

4.1.2.3.1. TLC-based experiment to study the decomposition of 14 in the presence of H_2O_2

Firstly, to assess the activation of **14** in the presence of H_2O_2 to generate lactone **15** and phenacyl thiol **13**, a TLC-based experiment was performed (Scheme 4.1.5.A). Also, the authentic phenacyl thiol **13** was generated from **12** in the presence of Es (Scheme 4.1.5.B).

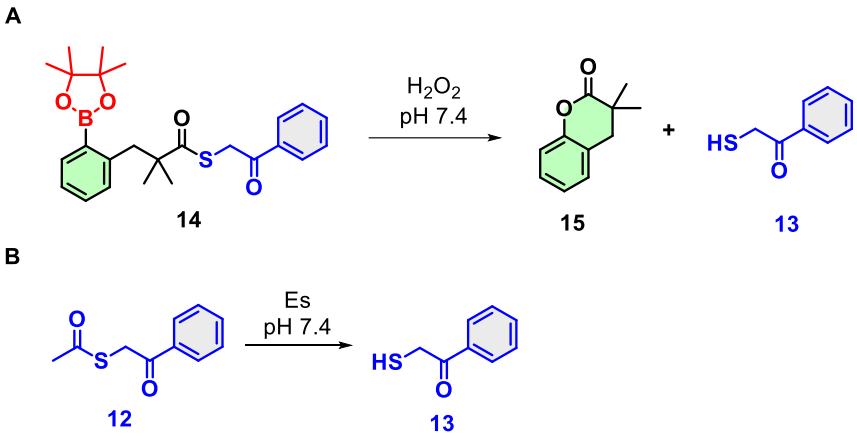

Scheme 4.1.5. (A) Activation of **14** in the presence of H_2O_2 produces lactone **15** and phenacyl thiol **13**. (B) Formation of the phenacyl thiol **13** from **12** in the presence of Es.

Compound **14** (200 μM) was treated with 100 equiv. of H_2O_2 in pH 7.4 PBS containing 100 μM diethylenetriaminepentaacetic acid (DTPA) at 37 °C. At pre-determined time points, the EtOAc extraction was done, and the EtOAc layer was spotted on a TLC plate. Along with this, an EtOAc layer obtained from compound control alone for **14**, **15**, and the **12** + Es reaction was also spotted on TLC. TLC was run in 10% EtOAc/hexane, and the formation of **13** and **15** was monitored. Under the experimental conditions, **14** underwent H_2O_2-mediated cleavage to produce the lactone **15** (in lane b) and phenacyl thiol **13** (in lane b), which have the same R_f as the authentic lactone **15** (in lane c) and the phenacyl thiol **13** (in lane d) generated from **12** **(**Figure 4.1.3.A). Also, the almost disappearance of **14** in the presence of H_2O_2 was observed within 120 min **(**Figure 4.1.3.B).

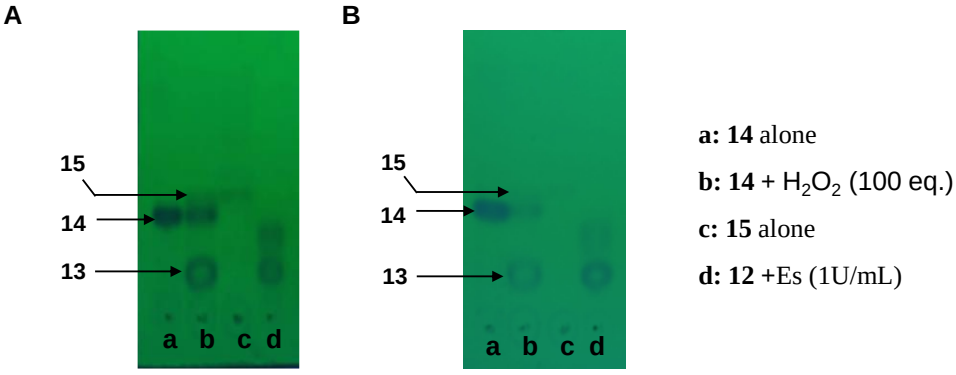

Figure 4.1.3. TLC experiment using 10% EtOAc/Hexane as eluant. Decomposition of **14** in the presence of H_2O_2 to generate lactone **15** and phenacyl thiol **13** after (A) 60 min and (B) 120 min, respectively.

Overall, the TLC experiment data suggest that **14** underwent lactonization to produce **13** and **15** in the presence of H_2O_2.

4.1.2.3.2. LC/MS analysis

Next, to validate the formation of lactone **15** and phenacyl thiol **13** from **14** in the presence of H_2O_2, an LC/MS experiment was performed (Scheme 4.1.6).

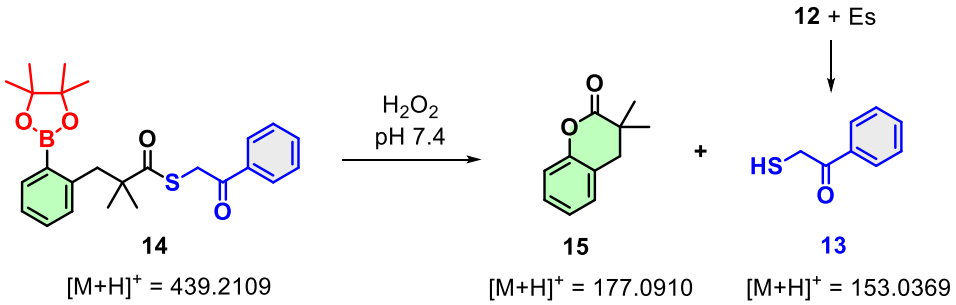

Scheme 4.1.6. LC/MS analysis for the decomposition of **14** in the presence of H_2O_2 to generate lactone **15** and phenacyl thiol **13**.

Compound **14** (100 μM) was treated with 100 equiv. of H_2O_2 in pH 7.4 PBS containing 100 μM diethylenetriaminepentaacetic acid (DTPA), and the LC/MS was recorded at different time points. A peak for the formation of the phenacyl thiol **13** (expected m/z = 153.0369 $[M + H]^+$; observed m/z = 153.0365) was observed at 13.6 min (Figure 4.1.4). Similarly, another peak corresponding to the formation of lactone **15** (expected m/z = 177.0910 $[M + H]^+$; observed m/z = 177.0904) was observed at 12.6 min (Figure 4.1.5).

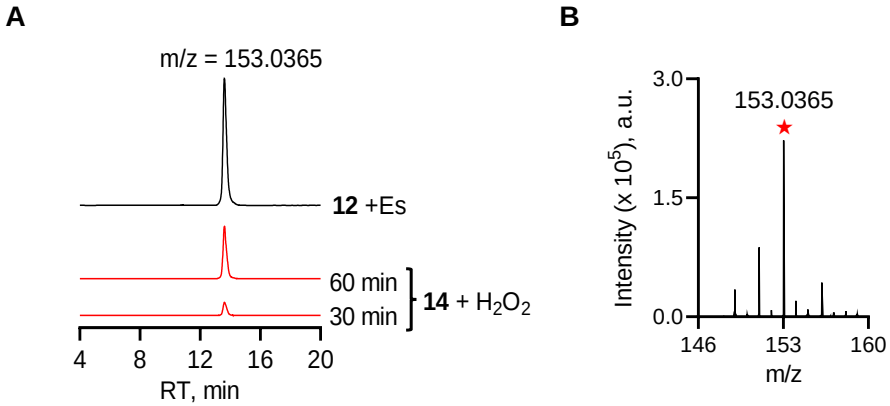

Figure 4.1.4. LC/MS study. (A) Extracted ion chromatograms for the formation of phenacyl thiol **13** and (B) Mass spectra for **13** (expected m/z = 153.0369 $[M + H]^+$; observed m/z = 153.0365) from **14** in the presence of H_2O_2.

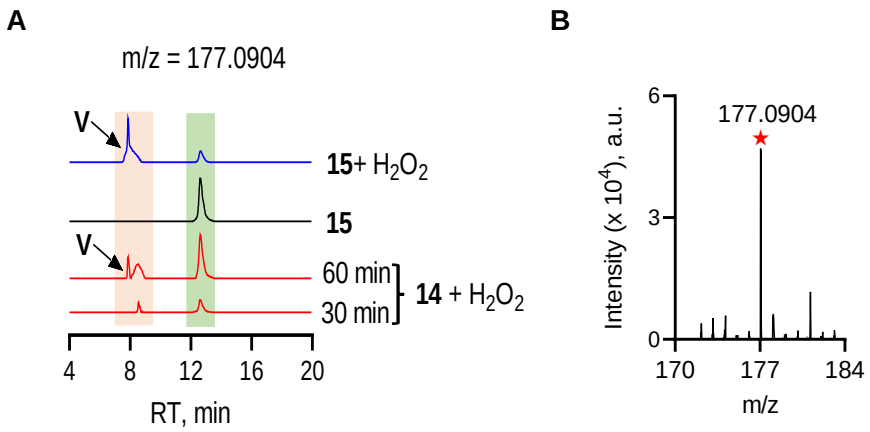

Figure 4.1.5. LC/MS study. (A) Extracted ion chromatograms for the formation of lactone **15** and (B) Mass spectra for **15** (expected m/z = 177.0910 $[M + H]^+$; observed m/z = 177.0904), from **14** in the presence of H_2O_2.

Along with the peak for the authentic lactone, a broad peak with the same mass was observed around 8.0 min, which increased over the period (Figure 4.1.5.A). Due to the presence of excess H_2O_2 in the reaction, we hypothesize that the lactone **15** formed further decomposes to form different intermediates, as depicted in Scheme 4.1.7. Intermediate **II** gets protonated due to the formic acid present in the water, an eluant in the LC/MS, leading to the formation of intermediate **V**, which is the open form of lactone having a similar mass as lactone **15** (Scheme 4.1.7 and Figure 4.1.5.A). Also, in a control reaction where lactone **15** was treated with H_2O_2, a similar broad peak was observed (Figure 4.1.5.A), further confirming the formation of the cleaved lactone.

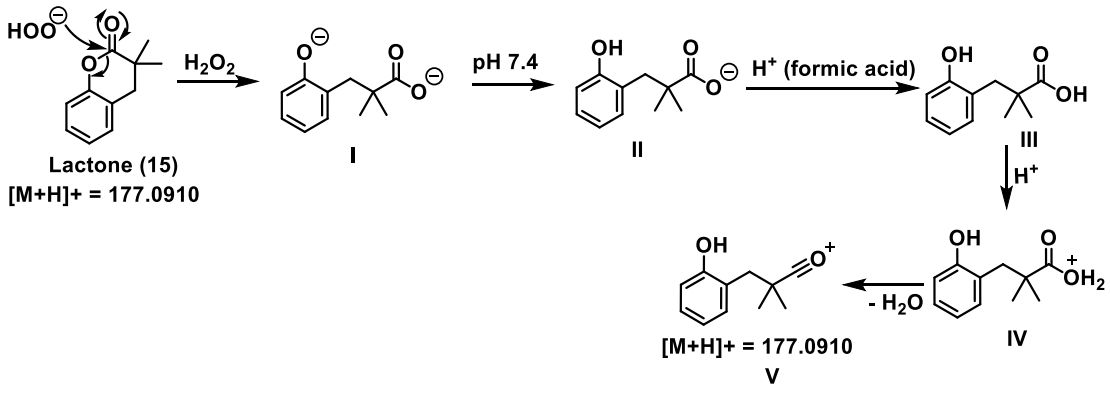

Scheme 4.1.7. Lactone **15** in the presence of excess H_2O_2.

Additionally, the carboxylate intermediate **II** was confirmed independently by HRMS analysis (expected, m/z = 193.0865 $[M-H]^-$; observed, m/z = 193.0865) (Figure 4.1.6).

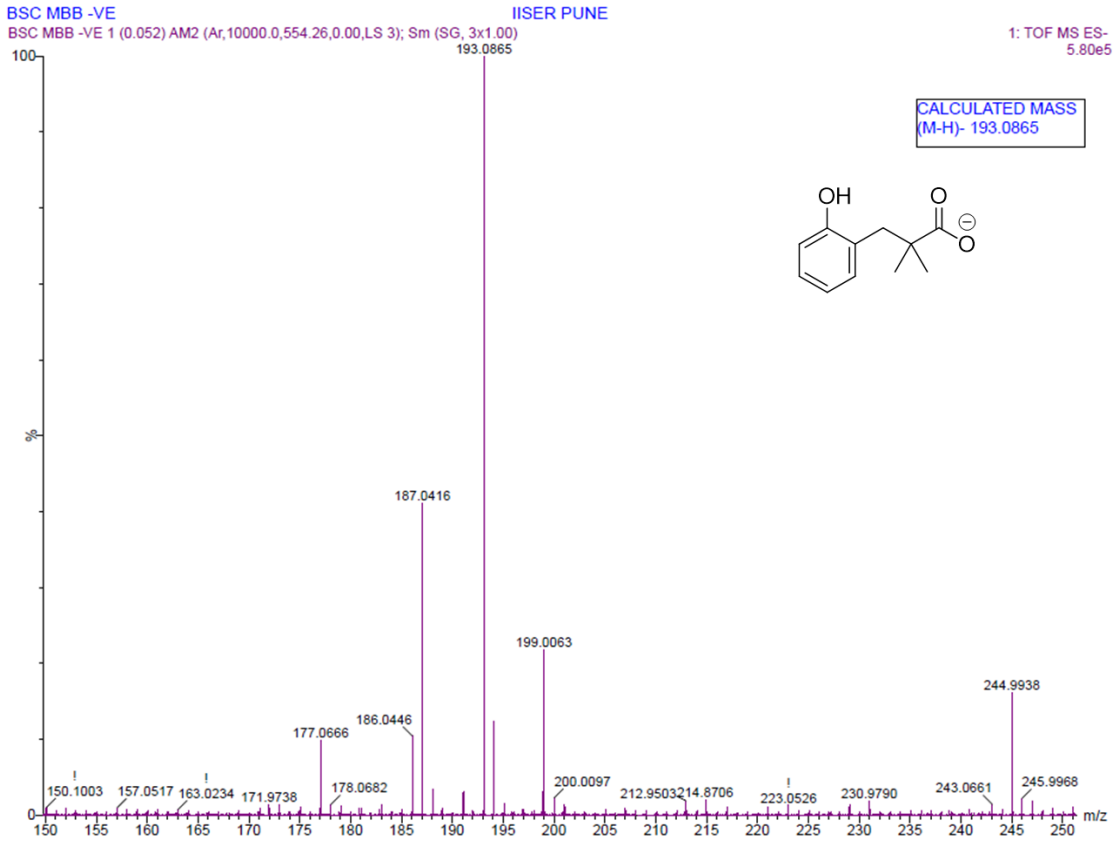

Figure 4.1.6. Mass spectrometry analysis for the formation of carboxylate intermediate of lactone **II** from **14** in the presence of H_2O_2. For **II** (expected, m/z = 193.0865 $[M-H]^-$; observed, m/z = 193.0865).

4.1.2.3.3. Trapping of 13 using mBBr

Next, to further validate the formation of phenacyl thiol **13**, an electrophilic trapping experiment using **mBBr** was conducted (Scheme 4.1.8). Upon co-incubation of the **14** with H_2O_2 and **mBBr** in pH 7.4 PBS containing 100 μM diethylenetriaminepentaacetic acid (DTPA), the formation of **Thiol-mBB** adduct (expected, m/z = 343.1116 $[M + H]^+$; observed, m/z = 343.1111) was observed by MS analysis (Figure 4.1.7).

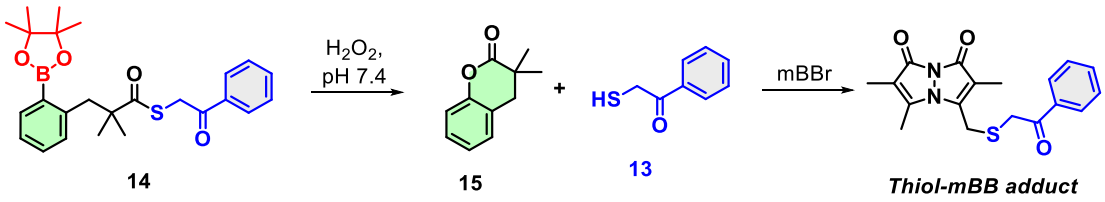

Scheme 4.1.8. Formation of the **Thiol-mBB** adduct when **14 (**100 μM) is incubated with 100 equivalents of H_2O_2 and **mBBr** (100 μM).

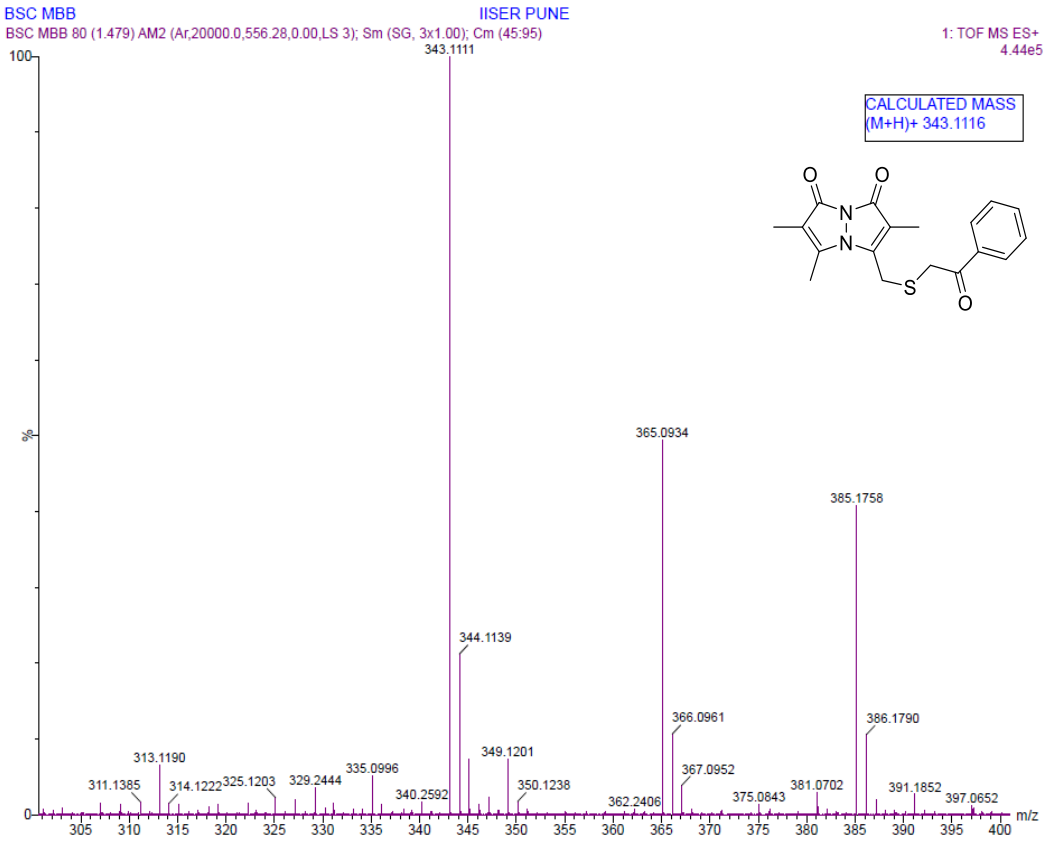

Figure 4.1.7. Mass spectrometry analysis for the formation of **thiol-mBB** adduct from **14** in the presence of H_2O_2. For **thiol-mBB** adduct (expected, m/z = 343.1116 $[M + H]^+$; observed, m/z = 343.1111).

Overall, the LC/MS analysis suggests that **14** underwent lactonization to produce **13** and **15** upon activation by H_2O_2.

4.1.2.4. Sulfane sulfur detection from 14 using SSP2

As described in **Chapter 3**, sulfane sulfur detection from **14** in the presence of H_2O_2 and 3-MST, turn-on fluorescence probe **SSP2** was used (Scheme 4.1.9).[2] In this assay, compound **14** (100 μM) was incubated with 100 equiv. of H_2O_2 in pH 7.4 PBS containing 100 μM diethylenetriaminepentaacetic acid (DTPA) for 60 min at 37 °C. Then, the excess H_2O_2 was quenched using the catalase enzyme, which is known to convert H_2O_2 into water and molecular oxygen. Further, the reaction mixture was treated with *b*3-MST (10 μM) for 30 min, and then the **SSP2** probe (50 μM) was added and incubated, and finally, the fluorescence signal for sulfane sulfur generation (λ_{ex} = 482 nm; λ_{em} = 518 nm) was monitored. A strong fluorescence

response was observed for **14** in the presence of H_2O_2 and 3-MST, which indicates significant sulfane sulfur formation (Figure 4.1.8).

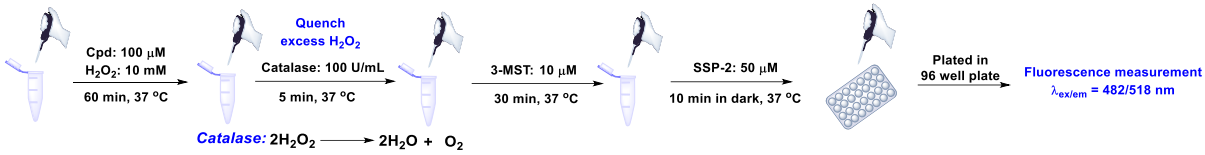

Scheme 4.1.9. Sulfane sulfur detection using **SSP2**.

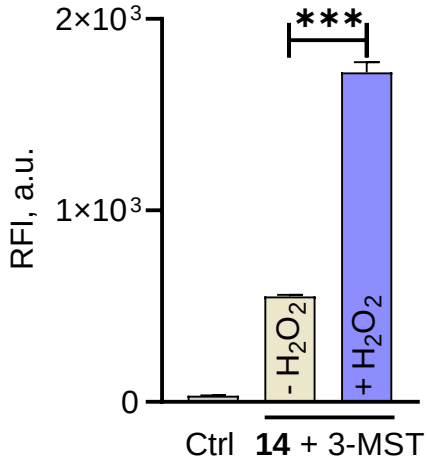

Figure 4.1.8. Sulfane sulfur detection with **14** (100 μM) in the presence of *b*3-MST (10 μM), H_2O_2 (10 mM) using **SSP2** (50 μM) based fluorescent assay (λ_{ex} = 482 nm and λ_{em} = 518 nm). Ctrl: **14** only; + H_2O_2 or -H_2O_2: presence or absence of H_2O_2. Statistical significance was measured using One-way ANOVA (*** $p \leq 0.001$).

4.1.2.5. H_2S generation from 14 in the presence of 3-MST and DTT

Next, compound **14** was tested for its ability to generate H_2S in the presence of H_2O_2 and 3-MST under reducing conditions (**DTT**) using a lead acetate assay and a colorimetric methylene blue assay.[3] In both these assays, quenching of excess H_2O_2 by catalase was carried out as described above in section 4.1.2.4.

4.1.2.5.1. H_2S measurement using lead acetate assay

Firstly, H_2S release was studied using the lead acetate assay. In this assay, H_2S released from compound **14** was trapped by **Pb(OAc)$_2$** soaked paper, and a black spot of lead sulfide (PbS) was formed on the paper (Scheme 4.1.10).

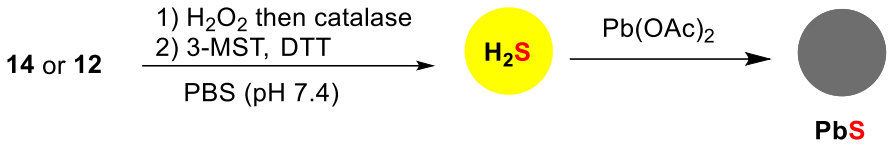

Scheme 4.1.10. Detection of H_2S *via* lead acetate assay.

In this assay, 100 μM of **14** was incubated with 100 equiv. of H_2O_2 in pH 7.4 PBS containing 100 μM diethylenetriaminepentaacetic acid (DTPA) for 60 min at 37 °C, followed by catalase for 5 min. Further, the reaction mixture was treated with *b*3-MST (1 μM) and 10 mM **DTT**. The assay was performed in a 96-well plate, which was covered with 10% $Pb(OAc)_2$ soaked paper, and the reaction was incubated for 2 h. Using a similar protocol, **12** was used as a positive control for this assay, and the reaction was set with 1U/mL Es. A black spot for PbS was observed for both **14** and **12**, indicating H_2S formation. (Figure 4.1.9). The reaction of **14** without H_2O_2 did not show a significant amount of H_2S production.

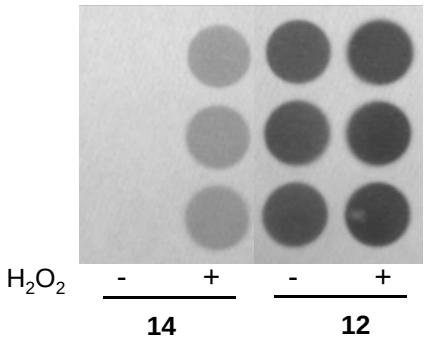

Figure 4.1.9. H_2S detection from compounds (**14** and **12** at 100 μM) in the presence of *b*3-MST (1 μM), H_2O_2 (10 mM), and **DTT** (10 mM) for 2 h using lead acetate assay. + H_2O_2 or - H_2O_2: presence or absence of H_2O_2. **12** was used as a positive control.

As compound **14** has a thioester functional group, which is prone to cleaved by esterase or biothiol such as **GSH**. To assess the stability and selectivity of **14**, lead acetate was performed in the presence of Es and **GSH**.

Using a similar lead acetate assay protocol, compound **14** was treated with either 100 equiv. of H_2O_2 or 100 equiv. of **GSH** or 1U/mL Es in pH 7.4 PBS containing 100 μM diethylenetriaminepentaacetic acid (DTPA) at 37 °C for 2 h. The black spot corresponding to the H_2S formation was observed from **14** in the H_2O_2 reaction. No signal for H_2S formation from the GSH reaction was observed. However, a low-intensity signal for PbS formation was observed from the Es reaction, indicating the cleavage of the thioester group (Figure 4.1.10).

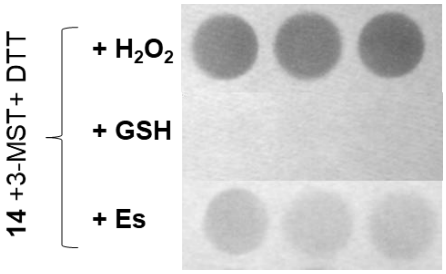

Figure 4.1.10. H_2S detection from compound **14** at 100 µM in the presence of 100 equiv. of H_2O_2 or **GSH** or 1U/mL Es, *b*3-MST (1 µM) **DTT** (10 mM) for 2 h using lead acetate assay.

Additionally, a TLC-based experiment with compound **14,** to assess the cleavage of the thioester group to generate the acid **18** and phenacyl thiol **13** in the presence of Es was performed (Scheme 4.1.11) as described in Section 4.1.2.3.1.

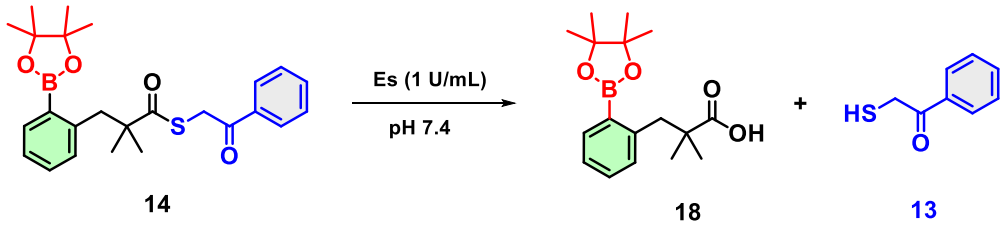

Scheme 4.1.11. Cleavage of **14** in the presence of Es, produces acid **18** and phenacyl thiol **13**.

From the TLC experiment, cleavage of compound **14** in the presence of Es to generate acid **18** and phenacyl thiol **13** was not observed over a period of 60 min.

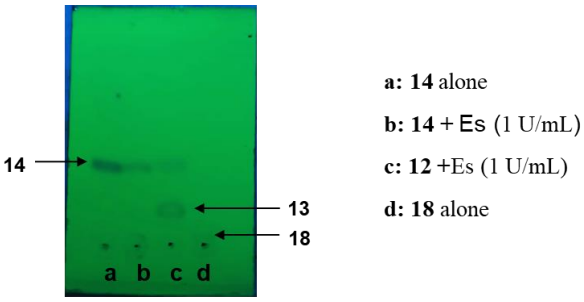

Figure 4.1.11. TLC experiment using 10% EtOAc/Hexane as eluant. Decomposition of **14** in the presence of Es to generate acid **18** and phenacyl thiol **13** after 60 min.

4.1.2.5.2. Methylene blue assay for H_2S measurement

Along with the lead acetate assay for H_2S measurement, a standard methylene blue (MB) colorimetric assay was performed with compound **14,** as depicted in Scheme 4.1.12.

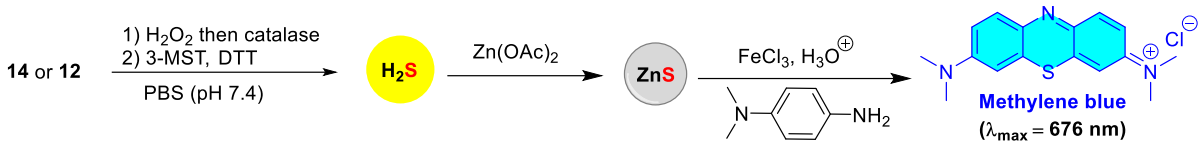

Scheme 4.1.12. Detection of H_2S *via* methylene blue assay.

In this assay, 100 µM of **14** was incubated with 100 equiv. of H_2O_2 in pH 7.4 PBS containing 100 µM diethylenetriaminepentaacetic acid (DTPA) for 60 min at 37 °C, followed by catalase for 5 min. Further, the reaction mixture was treated with *b*3-MST (1 µM), **Zn(OAc)$_2$** (400 µM), and **DTT** (10 mM) at 37 °C for 2 h. Using a similar protocol, **12** was used as a positive control for this assay, and the reaction was set up with 1U/mL Es. Next, aliquots from the reaction mixtures were treated with methylene blue reagents and mixed. The final reaction mixture was then transferred to the 96-well plate, and absorbance at 676 nm was recorded. Similar to the lead acetate assay, a signal for the H_2S generation from both **14** and **12** was observed (Figure 4.1.12). As anticipated, the reaction of **14** without H_2O_2 did not produce significant H_2S.

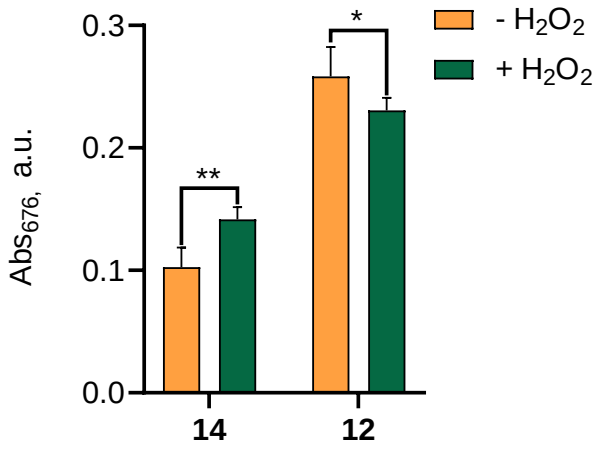

Figure 4.1.12. H_2S detection of compounds (**14** and **12** at 100 µM)in the presence of *b*3-MST (1 µM), H_2O_2 (10 mM), and **DTT** (10 mM) for 2 h using methylene blue assay. Results are expressed as mean ± SD (n =3/group). **12** was used as a positive control. Statistical significance was carried out using One-way ANOVA (*p < 0.033, **p < 0.002).

4.1.2.6. Sulfur transfer from 14 using LC/MS

After establishing that phenacyl thiol **13** generated from **14** is turned over by 3-MST to form the 3-MST persulfide as an intermediate, the formation of persulfide/polysulfide was next evaluated by exploiting the ability of 3-MST persulfide to transfer the sulfane sulfur to a small

molecule acceptor thiol such as **GSH**.[3] GSH, upon reaction with 3-MST-SS$^-$ will form GSH persulfide (GS-SH) and H_2S as a by-product. These reactive species were reacted with an electrophilic trapping agent (**HPE-IAM**),[4] and the corresponding HPE-IAM adducts were detected using LC/MS analysis (Scheme 4.1.13).

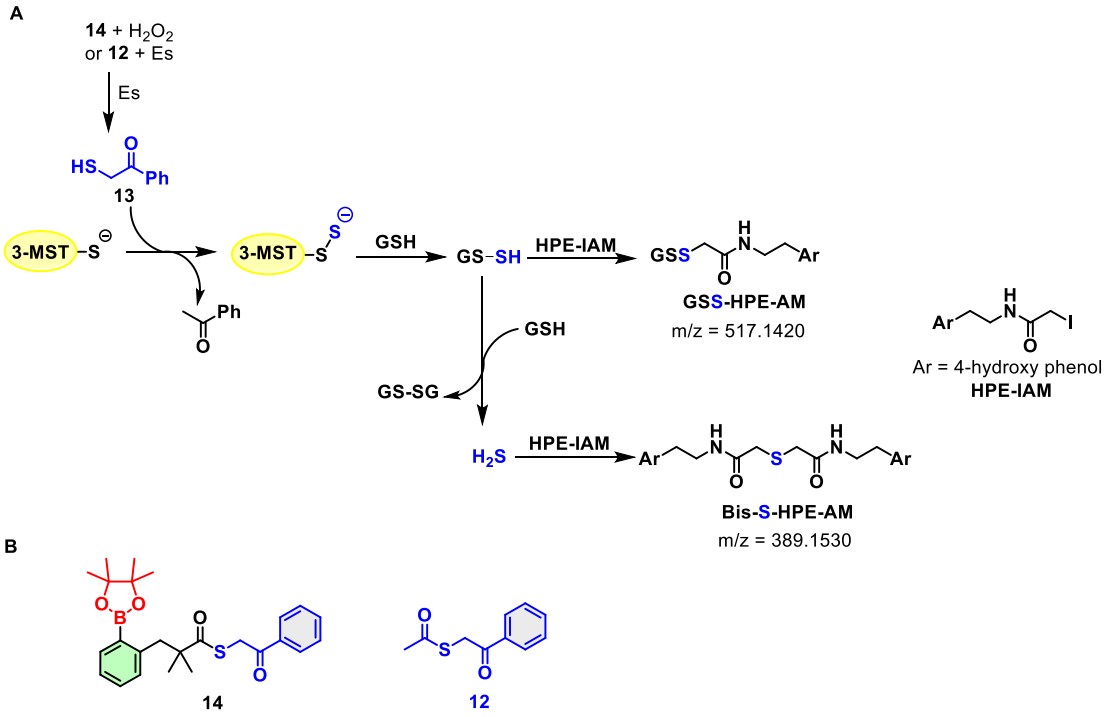

Scheme 4.1.13. (A) LC/MS study. Reaction scheme showing the formation and detection of persulfides/polysulfides and hydrogen sulfide/polysulfides as their HPE-AM and Bis-S-HPE-AM adducts from **14** and **12**, respectively. (B) Structures of compounds **12** and **14**.

Compound **14** (100 µM) was incubated with H_2O_2 (10 mM) in pH 7.4 PBS containing 100 µM diethylenetriaminepentaacetic acid (DTPA) for 60 min at 37 °C. and then treated with catalase for 5 min. Further, the reaction mixture was treated with *b*3-MST (25 µM) and **GSH** (1 mM) and finally with **HPE-IAM** (5 mM) at 37 °C. Using similar reaction conditions, **12** was used as a positive control for this assay, and the reaction was set up with 1U/mL. Finally, the samples were subjected to LC/MS analysis. A peak for the formation of the **GSS-HPE-AM** adduct (expected m/z = 517.1420; observed m/z = 517.1429) was observed at 4.3 min, indicating the formation of GSSH (Figure 4.1.13). Under these conditions, we also observe **Bis-S-HPE-AM** (expected m/z = 389.1530; observed m/z = 389.1537), presumably due to the reaction of HPE-IAM with H_2S formed by the reaction of GS-SH and GSH. (Figure 4.1.14).

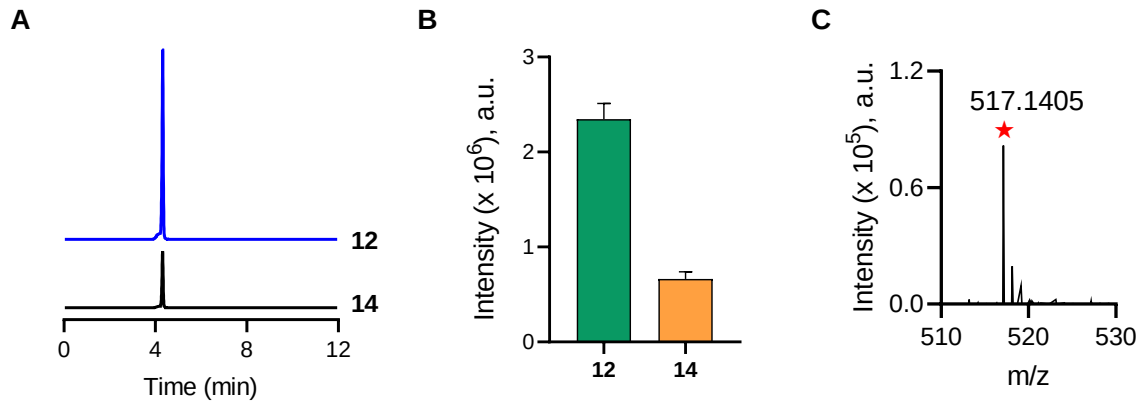

Figure 4.1.13. LC/MS study. (A) Extracted ion chromatograms from an LC/MS analysis of **GSS-HPE-AM** formation from **12** and **14**, (B) GSSH (**GSS-HPE-AM**) formation was measured by the detection of trapped HPE-IAM species from **12** and **14**, and (C) Mass spectra for **GSS-HPE-AM** (expected, m/z = 517.1420 $[M + H]^+$; observed, m/z = 517.1405). Results are expressed as mean ± SD (n =3/group).

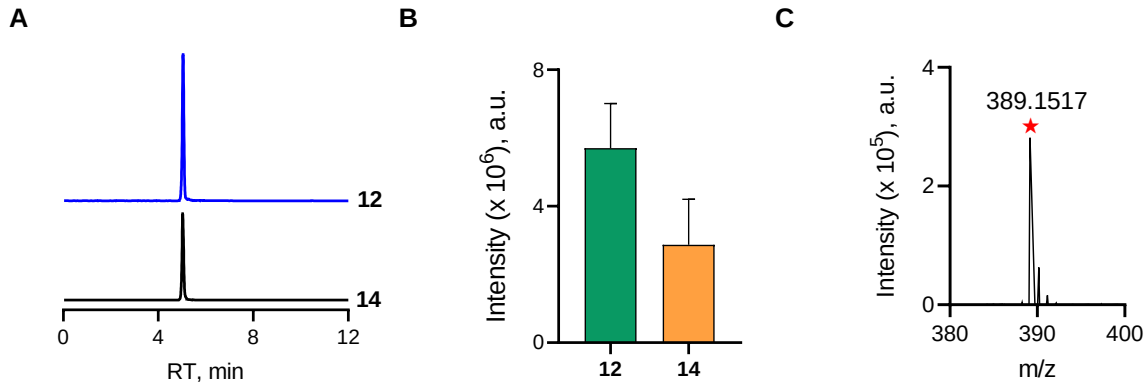

Figure 4.1.14. LC/MS study. (A) Extracted ion chromatograms from an LC/MS analysis of **Bis-S-HPE-AM** formation from **12** and **14**, (B) H_2S **(Bis-S-HPE-AM**) formation was measured by the detection of trapped HPE-IAM species from **12** and **14**, and (C) Mass spectra for **Bis-S-HPE-AM** (expected, m/z = 389.1530 $[M + H]^+$; observed, m/z = 389.1517). **12** was used as a positive control. Results are expressed as mean ± SD (n =3/group).

4.1.2.7. MTT assay for cell viability of 14

Next, the cytotoxicity of compound **14** was evaluated using a standard **MTT** assay to estimate the cell viability. Mouse embryonic fibroblast (MEF) cells were treated with varying concentrations of **14** and incubated for 24 h, following which cell viability was measured. Compound **14** was found to be well tolerated by MEF cells up to 100 µM (Figure 4.1.15).

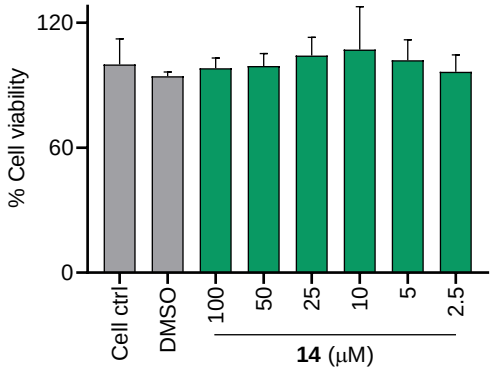

Figure 4.1.15. Cell viability assay was conducted on MEF (Mouse Embryonic Fibroblast) cells with compound **14** for 24 h. Results are expressed as mean ± SD (n =3/group).

4.1.2.8. *In vivo* anti-inflammatory study

Persulfides and polysulfides have been reported to exhibit anti-inflammatory properties.[5,6] To investigate this, a mouse endotoxin shock model was utilized, where **LPS** was used as an endotoxin, which is known to enhance the pro-inflammatory cytokines (TNF-α, IL-6, etc.) *via* toll-like receptors (Figure 4.1.16).[6]

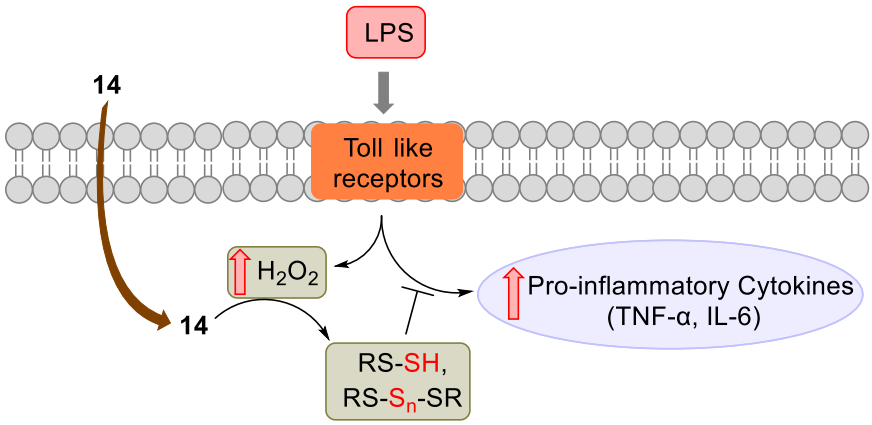

Figure 4.1.16. LPS-induced pro-inflammatory cytokines and anti-inflammatory properties of persulfide and polysulfides.

The C57BL/6J mice were administered with compound **14** (20 mg/kg) for 1 hour, followed by 5 mg/kg lipopolysaccharide (**LPS**) administration and an additional dose of compound **14** (20 mg/kg).[3] After overnight treatment, the mice were sacrificed, and the organs were harvested (Figure 4.1.17.A). The proinflammatory cytokines from the brain tissue of these mice were measured. In the control group treated with **LPS** alone, cytokines TNF-α and IL-6 were significantly elevated compared to vehicle-treated mice. However, in the group pre-treated

with compound **14**, a marked decrease in the levels of cytokines was observed (Figure 4.1.17.B). Overall, these results indicate that compound **14** exhibited good *in vivo* anti-inflammatory property.

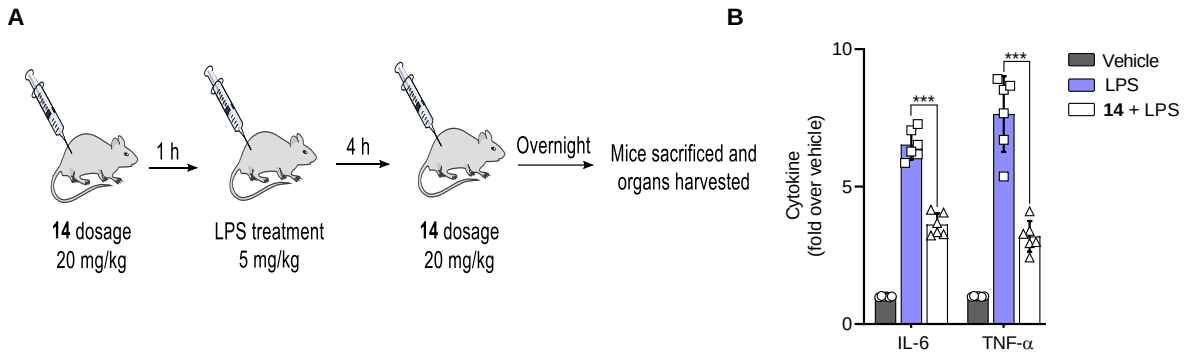

Figure 4.1.17. (A) Protocol used for the LPS-induced mouse endotoxin shock model, and (B) Pro-inflammatory cytokines, TNF-α, and IL-6 measurement using a standard ELISA assay. All data are presented as mean ± SD (n = 6 per group). Statistical significance was carried out using One-way ANOVA (***p < 0.001 *vs.* LPS). The LPS experiment was performed with the help of Simran Gupta (Prof. Harinath Chakrapani Lab, IISER Pune).

4.1.3. Summary

In summary, based on the trimethyl lock strategy, a ROS-activated 3-MST artificial substrate **14** was developed. Upon activation by H_2O_2, **14** produces the 3-MST artificial substrate **13** and a benign lactone **15**. Firstly, the formation of lactone **15** and phenacyl thiol **13** from **14** was monitored using LC/MS analysis. Also, the formation of **13** from **14** was independently confirmed using the mBBr trapping HRMS experiment. Next, the sulfane sulfur formation from **14** in the presence of H_2O_2 and 3-MST was measured using fluorescent probe SSP2. Furthermore, the H_2S release from **14** was detected using lead acetate and methylene blue assay. Next, an LC/MS experiment was conducted to validate the transfer of sulfane sulfur generated from **14** in the presence of H_2O_2 and 3-3-MST conditions to GSH using HPE-IAM. Compound **14** demonstrated good *in vivo* anti-inflammatory property in the endotoxin (LPS) shock mouse model.

4.1.4. Experimental protocols

4.1.4.1. General methods

All the chemicals and solvents were purchased from commercial sources and used as received unless stated otherwise. Column chromatography was performed using silica gel-Rankem (60–120 mesh) as stationary phase. Preparative high-performance liquid chromatography (HPLC) was done using Combiflash EZ prep UV using a Kromasil®C-18 preparative column (250 mm × 21.2 mm, 5 μm). ^{1}H and ^{13}C spectra were recorded on a JEOL 400 MHz (or 100 MHz for ^{13}C) or a Bruker 400 MHz (or 100 MHz for ^{13}C) spectrometer unless otherwise specified using either residual solvent signals ($CDCl_3$ δH = 7.26 ppm, δC = 77.2 ppm), or as an internal tetramethylsilane (δH = 0.00, δC = 0.0). Chemical shifts (δ) are reported in ppm and coupling constants (*J*) in Hz. The following abbreviations are used: m (multiplet), s (singlet), d (doublet), t (triplet), ddt (doublet of doublet of triplet) and dq (doublet of quartet). High-resolution mass spectra were obtained from HRMS-ESI-Q-Time of Flight LC/MS. FT-IR spectra were recorded using a BRUKER-ALPHA FT-IR spectrometer and reported in cm^{-1}. All measurements were done using a LC/MS method in the positive ion mode using high-resolution multiple reaction monitoring (MRM-HR) analysis on a Sciex X500R quadrupole time-of-flight (QTOF) mass spectrometer fitted with an Exion UHPLC system. Photometric measurements were performed using an Ensight Multimode Plate Reader (PerkinElmer). Fluorometric measurements were performed using a Thermo Scientific Varioscan microplate reader and a HORIBA Scientific Fluoromax-4 spectrofluorometer.

4.1.4.2. Synthesis and Characterization

Compounds **12**[7] and **15**[1] were synthesized following the previously reported protocols, and the analytical data of the compounds were consistent with reported values.

Ethyl 3-(2-bromophenyl)-2,2-dimethylpropanoate (16)[1]:

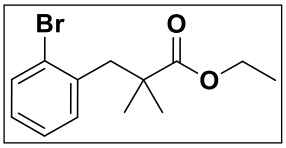

To a solution of diisopropylamine (1.12 mL, 8.00 mmol) in anhydrous THF (15 mL) at −78 °C was added *n*-butyllithium in hexanes (5.00 mL of a 1.6 M solution, 8.00 mmol) and the resulting mixture was stirred under nitrogen for 15 minutes. Then ethyl isobutyrate (0.581 g, 5.00 mmol) dissolved in THF (5 mL) was added dropwise and stirred under nitrogen for 30 minutes. Next, 2-bromobenzylbromide (0.5 g, 2.00 mmol) dissolved in anhydrous tetrahydrofuran (5 mL) was added dropwise, and the mixture was allowed to warm to room temperature overnight. Upon

completion of the reaction, as monitored by TLC, the reaction mixture was quenched with deionized water and extracted with DCM (3 × 20 mL). The combined organic layer was washed with brine, dried over Na_2SO_4, and filtered, and the filtrate was concentrated to give a crude compound. The resulting oil was purified by column chromatography using silica gel (60 - 120) with 2% EtOAc/hexane as the eluent to obtain **16** (0.466 g, 81%) as a yellow oil. FT-IR (ν_{max}, cm^{-1}): 1723; ^1H NMR (400 MHz, $CDCl_3$): δ 7.54 (dd, *J* = 8.0, 1.1 Hz, 1H), 7.23 – 7.11 (m, 2H), 7.09 – 7.02 (m, 1H), 4.14 (q, *J* = 7.1 Hz, 2H), 3.12 (s, 2H), 1.23 (s, 9H); ^{13}C NMR (100 MHz, $CDCl_3$): δ 177.6, 138.1, 133.1, 131.6, 128.1, 127.1, 126.2, 60.7, 44.3, 44.2, 25.1, 14.3; HRMS (ESI-TOF) for $C_{13}H_{17}BrO_2$ $[M+H]^+$: Calcd., 285.0490, Found, 285.0497.

Ethyl 2,2-dimethyl-3-(2-(4,4,5,5-tetramethyl-1,3,2-dioxaborolan-2-yl)phenyl)propanoate (17)[1]:

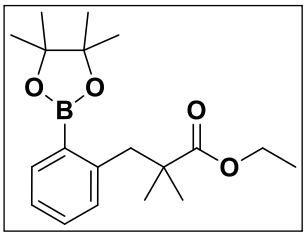

To a solution of **16** (1.0 g, 3.51 mmol) in degassed 1,4-dioxane (20 mL) was added bis(pinacolato)diboron (1.78 g, 7.01 mmol), $Pd(dppf)Cl_2$ (0.286 g, 0.35 mmol), and potassium acetate (1.38 g, 14.03 mmol) and the reaction mixture was refluxed for 18 h under nitrogen atmosphere. Upon completion of the reaction, as monitored by TLC, the solvent was evaporated, diluted with 20 mL of water, and extracted with DCM (3 × 20 mL). The combined organic layer was washed with brine, dried over Na_2SO_4, filtered, and the filtrate was concentrated to give a crude oil. This crude was further purified by column chromatography using silica gel (60 - 120) with 4% EtOAc/hexane as the eluent to obtain **17** (0.775 g, 67%) as a yellow liquid. FT-IR (ν_{max}, cm^{-1}): 1726, 1598; ^1H NMR (400 MHz, $CDCl_3$): δ 7.77 (dd, *J* = 7.4, 1.3 Hz, 1H), 7.31 (td, *J* = 7.5, 1.6 Hz, 1H), 7.19 (td, *J* = 7.4, 1.1 Hz, 1H), 7.10 (d, *J* = 7.6 Hz, 1H), 4.11 (q, *J* = 7.1 Hz, 2H), 3.29 (s, 2H), 1.35 (s, 12H), 1.22 (t, *J* = 7.1 Hz, 3H), 1.13 (s, 6H); ^{13}C NMR (100 MHz, $CDCl_3$): δ 178.3, 144.7, 135.9, 130.5, 130.4, 125.7, 83.7, 60.4, 43.9, 43.7, 25.1, 24.8, 14.3; ^{11}B NMR (128 MHz, $CDCl_3$) δ 32.00; HRMS (ESI-TOF) for $C_{19}H_{29}BO_4$ $[M+H]^+$: Calcd., 355.2056, Found, 355.2060.

2,2-dimethyl-3-(2-(4,4,5,5-tetramethyl-1,3,2-dioxaborolan-2-yl)phenyl)propanoic acid (18):

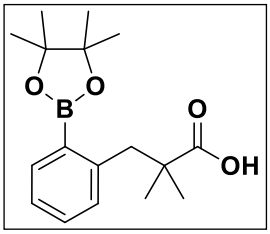

To a solution of **17** (0.523 g, 1.57 mmol) in MeOH/H_2O (3: 1 v/v, 10 mL), NaOH (0.252 g, 6.30 mmol) was added. The reaction mixture was refluxed overnight. Upon completion of the reaction, as monitored by TLC, the reaction mixture was quenched with 1N HCl and the resulting solution was extracted with DCM (3 × 15 mL). The combined organic layer was washed with brine, dried over Na_2SO_4, and filtered, and the filtrate was concentrated to give a crude compound. The crude product was purified by column chromatography using silica gel (60 - 120) with 10% EtOAc/hexane as the eluent to obtain **18** (0.425 g, 86%) as a white solid. FT-IR (ν_{max}, cm^{-1}): 1697, 1598; ^1H NMR (400 MHz, $CDCl_3$): δ 7.78 (dd, *J* = 7.5, 1.1 Hz, 1H), 7.31 (td, *J* = 7.5, 1.5 Hz, 1H), 7.19 (td, *J* = 7.4, 1.1 Hz, 1H), 7.23-7.19 (m, 1H), 3.34 (s, 2H), 1.35 (s, 12H), 1.13 (s, 6H); ^{13}C NMR (100 MHz, $CDCl_3$): δ 184.2, 144.3, 136.0, 130.6, 130.5, 128.2, 125.8, 83.7, 43.8, 43.3, 25.1, 24.7; ^{11}B NMR (128 MHz, $CDCl_3$) δ 31.78; HRMS (ESI-TOF) for $C_{17}H_{25}BO_4$ $[M+Na]^+$: Calcd., 327.1743, Found, 327.1746.

S-(2-oxo-2-phenylethyl) 2,2-dimethyl-3-(2-(4,4,5,5-tetramethyl-1,3,2-dioxaborolan-2-yl)phenyl)propanethioate (14):

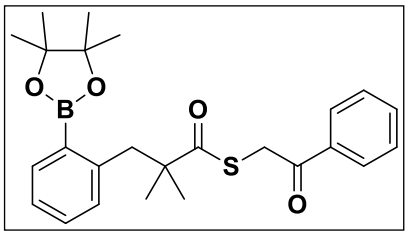

A mixture of compound **18** (0.071 g, 0.23 mmol), Lawesson's reagent (0.047 g, 0.12 mmol), and dry toluene (5 mL) was charged to a pressure tube and heated at 120 °C and stirred overnight. After consumption of the starting material, as monitored by TLC, the solvent was evaporated under reduced pressure. The reaction mixture was diluted with DCM (10 mL), washed with 1 N HCl and brine, and dried over Na_2SO_4. The filtrate was concentrated under reduced pressure to give a crude oily compound **19** carried forward to the next step without further purification. The oily product was dissolved in DCM (5 mL), and phenacyl bromide (0.046 g, 0.23 mmol) was added under N_2 atmosphere at rt. The solution was stirred for 4 h. Once the starting material was completely consumed, as monitored by TLC, the solvent was evaporated under reduced pressure to give a crude compound. The residue was purified by column chromatography using silica gel (60-120) with 5% EtOAc/hexane as eluent to give **14** (0.021 g, 21%) as a white solid. FT-IR (ν_{max}, cm^{-1}): 1735, 1679, 1598; ^1H NMR (400 MHz, $CDCl_3$): δ 8.04-8.01 (m, 2H), 7.79 (dd, *J* = 7.4, 1.3 Hz, 1H), 7.63 – 7.56 (m, 1H), 7.49 (t, *J* = 7.4 Hz, 2H), 7.29 (td, *J* = 7.5, 1.6

Hz, 1H), 7.20 (td, *J* = 7.4, 1.1 Hz, 1H), 7.10 (d, *J* = 7.6 Hz, 1H), 4.36 (s, 2H), 3.35 (s, 2H), 1.34 (s, 12H), 1.20 (s, 6H); ^{13}C NMR (100 MHz, $CDCl_3$): 205.6, 194.1, 143.7, 136.1, 135.9, 133.7, 130.9, 130.5, 128.9, 128.7, 125.9, 83.7, 51.2, 43.6, 36.4, 29.8, 25.1, 24.6; ^{11}B NMR (128 MHz, $CDCl_3$) δ 31.64; HRMS (ESI-TOF) for $C_{25}H_{31}BO_4S$ $[M+Na]^+$: Calcd., 461.1933, Found, 461.1933.

4.1.4.3. TLC-based assay to study the decomposition of 14 in the presence of H_2O_2

Stock solutions of **14** (10 mM), **15** (10 mM), and **12** (10 mM) in DMSO and H_2O_2 (100 mM) in deionized water were prepared. A stock solution of porcine liver esterase (100 U/mL; Sigma Aldrich, E3019) was prepared in PBS pH 7.4. The reaction samples were prepared by adding 100 μM of **14** (10 μL, 10 mM) with or without 10 mM H_2O_2 (100 μL, 100 mM), and the volume was adjusted to 1000 μL using 10 mM PBS (pH 7.4) buffer containing 100 μM DTPA. Along with this, **13** was prepared by adding 100 μM of **12** (10 μL, 10 mM stock) with 1 U/mL esterase (10 μL, 100 U/mL stock), and the volume was adjusted to 1000 μL using 10 mM PBS (pH 7.4) containing 100 μM diethylenetriaminepentaacetic acid (DTPA). The control reaction was prepared by adding 100 μM of 100 μM of **15** (10 μL, 10 mM stock), and the volume was adjusted to 1000 μL using 10 mM PBS (pH 7.4) containing 100 μM diethylenetriaminepentaacetic acid (DTPA). Finally, the reaction mixtures were incubated at 37 °C. At predetermined time points, 200 μL aliquots were taken and extracted with 100 μL ethyl acetate. Then, the organic layer was spotted on a TLC plate and run using 10% ethyl acetate/hexane as a mobile phase.

4.1.4.4. Decomposition of 14 using LC/MS

Stock solutions of **12, 14**, and **15** (10 mM) in DMSO and H_2O_2 (100 mM) in DI water were prepared. A stock solution of porcine liver esterase (100 U/mL; Sigma Aldrich, E3019) was prepared in PBS pH 7.4. The reaction mixture for **14** was prepared by adding 100 μM of **14** (4 μL, 10 mM stock) along with 10 mM H_2O_2 (40 μL, 100 mM), and the volume was adjusted to 400 μL using 10 mM PBS (pH 7.4) buffer containing 100 μM DTPA. The control reactions of **12** and **15** were prepared by adding 100 μM of **12** or **15** (4 μL, 10 mM stock), and the volume was adjusted to 400 μL using 10 mM PBS (pH 7.4) containing 100 μM diethylenetriaminepentaacetic acid (DTPA). The **13** reaction mixture was prepared by adding 100 μM of **12** (4 μL, 10 mM stock) with 1 U/mL esterase (4 μL, 100 U/mL stock), and the volume was adjusted to 400 μL using 10 mM PBS (pH 7.4) containing 100 μM DTPA. The

reaction mixtures were incubated at 37 °C. The different sets of reactions were set up for the different time points. After the incubation at the time points, the reaction mixture samples were centrifuged at 10000 x g for 10 min at 4 °C; the supernatant was collected and assessed thereafter by LC-MS. All measurements were done using the following protocol: Acetonitrile (A) and 0.1% formic acid in water (B) were used as the mobile phase. A multistep gradient (H_2O: ACN) was used with the flow rate of 0.5 mL/min starting with 40:60 → 0 – 2 min, 40:60 to 30:70 → 2 – 5 min, 30:70 to 05:95 → 5 – 10 min, 05:95 to 00:100 → 10 – 12 min, 00:100 to 05:95 → 12 – 14 min, 05:95 to 30:70 → 14 – 17 min, 30:70 to 40:60 → 17 – 18 min, and 40:60 → 18 – 21 min. Measurements were carried out in the positive ion mode using Agilent 6545 Quadrupole Time-Of-Flight (QTOF) LC-MS/MS with a Phenomenex®C-18 reverse phase column (250 mm × 4.6 mm, 5 μm). All LC/MS runs were performed using an ESI source with the following MS parameters: drying and sheath gas temperature = 320 °C; drying and sheath gas flow rate = 10L/min; fragmentor voltage = 150 V; capillary voltage = 4 kV; nebulizer (ion source gas) pressure = 45 Ψ and nozzle voltage = 1 kV. For the analysis of compounds from the reaction mixture, a curated library was employed in the form of a Personal Compound Database Library (PCDL), and the peaks were validated based on relative retention times and MS/MS fragments obtained.

4.1.4.5. mBBr thiol trapping experiment

Stock solutions of **14** (10 mM), monobromobimane (**mBBr**, 10 mM) in DMSO, and H_2O_2 (100 mM) in deionized water were prepared. The reaction mixture was prepared by adding 100 μM of **14** (10 μL, 10 mM), 100 μM of **mBBr** (10 μL, 10 mM), with H_2O_2 (100 μL, 100 mM stock), and the volume was adjusted to 1000 μL using phosphate buffer saline (10 mM, pH 7.4) containing 100 μM DTPA in a 1.5 mL Eppendorf tube. The reaction was incubated for 120 min at 37 ˚C, and the reaction mixture was evaporated under nitrogen and subjected to High-Resolution Mass Spectrometry (HRMS) analysis.

4.1.4.6. Sulfane sulfur measurement from 14 using SSP2

Stock solutions of **14** (10 mM), **12** (10 mM), and **SSP2** (5 mM) were prepared in DMSO. Stock solutions of H_2O_2 (100 mM), Catalase (10000 U/mL), porcine liver esterase (ES, 100 U/mL), and Dithiothreitol (**DTT**, 100 mM) were prepared in deionized water.

The reaction mixture was prepared by adding 100 μM of **14** (4 μL, 10 mM), 10 mM H_2O_2 (40 μL, 100 mM stock), and incubated for 1 h at 37 °C. After 1 h, excess H_2O_2 in the reaction mixture was quenched by adding 100 U/mL catalase (4 μL, 10000 U/mL stock) and incubated

for 5 min at 37 ˚C, followed by the addition of 10 μM *b*3-MST (10.2 μL, 392 μM stock). The reaction mixture was further incubated for 30 min at 37 ˚C, and the final volume of the reaction mixture was adjusted to 400 μL using 10 mM PBS (pH 7.4) containing 100 μM DTPA in a 1.5 mL Eppendorf tube.

A similar control reaction was set up for compound **14** without H_2O_2**.** The reaction mixture was prepared by adding 100 μM of **14** (4 μL, 10 mM), 10 μM *b*3-MST (10.2 μL, 392 μM stock). and incubated for 30 min at 37 ˚C, and the final volume of the reaction mixture was adjusted to 400 μL using 10 mM PBS (pH 7.4) containing 100 μM DTPA in a 1.5 mL Eppendorf tube.

A reaction was set up for compound **12**. The reaction mixture was prepared by adding 100 μM of **12** (4 μL, 10 mM), 1 U/mL ES (4 μL, 100 U/mL stock), with or without 10 mM H_2O_2 (40 μL, 100 mM stock) and incubated for 1 h at 37 °C. After 1 h, 10 μM *b*3-MST (10.2 μL, 392 μM stock) was added, and the reaction mixture was further incubated for 30 min at 37 ˚C, and the final volume of the reaction mixture was adjusted to 400 μL using 10 mM PBS (pH 7.4) containing 100 μM DTPA in a 1.5 mL Eppendorf tube.

The above treatment groups were finally incubated with 50 μM of **SSP2** (4 μL, 5 mM) for 10 min at 37 °C in the dark. 100 μL aliquot of each reaction mixture (in triplicate) was transferred to a 96-well plate, and the fluorescence was recorded (λ_{ex} = 482 nm and λ_{em} = 518 nm) using an Ensight Multimode Plate Reader (PerkinElmer).

4.1.4.7. Lead acetate assay for the H_2S detection from 14

Firstly, lead acetate paper was prepared by soaking Whatman filter paper with 10 % (w/v) lead(II) acetate solution and dried. Stock solutions of **14** (10 mM) and **12** (10 mM) were prepared in DMSO. Stock solutions of H_2O_2 (100 mM), Catalase (10000 U/mL), porcine liver esterase (ES, 100 U/mL), and Dithiothreitol (**DTT**, 100 mM) were prepared in deionized water.

Lead acetate assay was performed in a 96-well plate (with lid). The reaction mixture was prepared by adding 100 μM of **14** (7 μL, 10 mM), with 10 mM H_2O_2 (70 μL, 100 mM stock), and incubated for 1 h at 37 °C. After 1 h, excess H_2O_2 in the reaction mixture was quenched by adding 100 U/mL catalase (7 μL, 10000 U/mL stock) and incubated for 5 min at 37 ˚C, followed by the addition of 1 μM *b*3-MST (1.79 μL, 392 μM stock) and 10 mM of **DTT** (70 μL, 100 mM stock), and the volume was adjusted to 700 μL using 10 mM PBS (pH 7.4) containing 100 μM diethylenetriaminepentaacetic acid (DTPA) in a 1.5 mL Eppendorf tube.

A similar control reaction was set up for **14** without H_2O_2**.** The reaction mixture was prepared by adding 100 μM of **14** (7 μL, 10 mM), 1 μM *b*-3MST (1.78 μL, 392 μM stock), and 10 mM of **DTT** (70 μL, 100 mM stock), and the volume was adjusted to 700 μL using 10 mM PBS (pH 7.4) containing 100 μM DTPA in a 2.0 mL Eppendorf tube. A similar reaction was set up with the GSH (100 equiv.) or Es (1 U/mL) in the selectivity assessment assay.

A similar reaction was set up for **12**. The reaction mixture was prepared by adding 100 μM of **12** (7 μL, 10 mM), 1 U/mL ES (7 μL, 100 U/mL stock), and incubated for 10 min at 37 °C, followed by the addition of 10 mM H_2O_2 (70 μL, 100 mM stock), further incubated for 1 h at 37 °C. After 1 h, excess H_2O_2 in the reaction mixture was quenched by adding 100 U/mL catalase (7 μL, 10000 U/mL stock) and incubated for 5 min at 37 ˚C, followed by the addition of 1 μM *b*3-MST (1.79 μL, 392 μM stock) and 10 mM of **DTT** (70 μL, 100 mM stock), and the volume was adjusted to 700 μL using 10 mM PBS (pH 7.4) containing 100 μM DTPA in a 1.5 mL Eppendorf tube.

A similar control reaction was set up for **12** without H_2O_2**.** The reaction mixture was prepared by adding 100 μM of **12** (7 μL, 10 mM), 1 U/mL ES (7 μL, 100 U/mL stock), 1 μM *b*-3MST (1.78 μL, 392 μM stock), and 10 mM of **DTT** (70 μL, 100 mM stock), and the volume was adjusted to 700 μL using 10 mM PBS (pH 7.4) containing 100 μM DTPA in a 2.0 mL Eppendorf tube.

Aliquoted 200 μL from each reaction (in triplicate) in a 96-well plate, covered with 10 % lead acetate-soaked paper followed by the lid, sealed, and placed in a static incubator maintained at 37 ˚C for 2 h. After 2 h, lead acetate paper was carefully removed, and the image was taken using Syngene G-Box Chemi-XRQ.

4.1.4.8. Methylene blue assay for the H_2S detection from 14

The methylene blue assay was conducted as previously reported with some modifications. Stock solutions of **14** (10 mM) and **12** (10 mM) were prepared in DMSO. Stock solutions of H_2O_2 (100 mM), Catalase (10000 U/mL), porcine liver esterase (ES, 100 U/mL), Dithiothreitol (**DTT**, 100 mM), and **$Zn(OAc)_2.2H_2O$** (40 mM) were prepared in deionized water. Stock solutions of **$FeCl_3$** (30 mM) in 1.2 M HCl and *N, N*–dimethyl-p-phenylenediamine sulfate (**DMPPDA**) (20 mM) were prepared in 7.2 M HCl.

The reaction mixture was prepared by adding 400 μM **$Zn(OAc)_2.2H_2O$** (15 μL, 40 mM stock), 100 μM of **14** (15 μL, 10 mM), with 10 mM H_2O_2 (150 μL, 100 mM stock), and incubated for

1 h at 37 °C. After 1 h, excess H_2O_2 in the reaction mixture was quenched by adding 100 U/mL catalase (15 μL, 10000 U/mL stock) and incubated for 5 min at 37 ˚C, followed by the addition of 1 μM *b*3-MST (3.83 μL, 392 μM stock) and 10 mM of **DTT** (150 μL, 100 mM stock), and the volume was adjusted to 1500 μL using 10 mM PBS (pH 7.4) containing 100 μM DTPA in a 2.0 mL Eppendorf tube.

A similar control reaction was set up for compound **14** without H_2O_2**.** The reaction mixture was prepared by adding 400 μM $Zn(OAc)_2.2H_2O$ (15 μL, 40 mM stock), 100 μM of **14** (15 μL, 10 mM), 1 μM *b*3-MST (3.83 μL, 392 μM stock), and 10 mM of **DTT** (150 μL, 100 mM stock), and the volume was adjusted to 1500 μL using 10 mM PBS (pH 7.4) containing 100 μM DTPA in a 2.0 mL Eppendorf tube.

A similar reaction was set up for **12**. The reaction mixture was prepared by adding 400 μM $Zn(OAc)_2.2H_2O$ (15 μL, 40 mM stock), 100 μM of **12** (15 μL, 10 mM), 1 U/mL ES (7 μL, 100 U/mL stock), and incubated for 10 min at 37 °C, followed by the addition of 10 mM H_2O_2 (150 μL, 100 mM stock), further incubated for 1 h at 37 °C. After 1 h, excess H_2O_2 in the reaction mixture was quenched by adding 100 U/mL catalase (15 μL, 10000 U/mL stock) and incubated for 5 min at 37 ˚C, followed by the addition of 1 μM *b*3-MST (3.83 μL, 392 μM stock) and 10 mM of **DTT** (150 μL, 100 mM stock), and the volume was adjusted to 1500 μL using 10 mM PBS (pH 7.4) containing 100 μM DTPA in a 2.0 mL Eppendorf tube.

A similar control reaction was set up for compound **12** without H_2O_2**.** The reaction mixture was prepared by adding 400 μM **$Zn(OAc)_2.2H_2O$** (15 μL, 40 mM stock), 100 μM of **12** (15 μL, 10 mM), 1 U/mL ES (7 μL, 100 U/mL stock), 1 μM *b*3-MST (3.83 μL, 392 μM stock), and 10 mM of **DTT** (150 μL, 100 mM stock), and the volume was adjusted to 1500 μL using 10 mM PBS (pH 7.4) containing 100 μM DTPA in a 2.0 mL Eppendorf tube.

200 μL aliquot of the reaction mixture was taken at pre-determined time points and added to a 1.5 mL Eppendorf containing equal volumes (200 μL) of **$FeCl_3$**, **DMPPDA,** and incubated at 37 ˚C for 30 min in the dark, to allow the formation of the methylene blue dye. An aliquot of 150 μL was transferred to a 96-well plate, and the absorbance values were recorded at 676 nm using a microplate reader (Thermo Scientific VarioskanFlash).

4.1.4.9. Sulfur transfer measurement from 14 using LC/MS

Stock solutions of **14** (10 mM)**, 12** (10 mM), and **HPE-IAM** (100 mM) were prepared in DMSO. A stock solution of porcine liver esterase (100 U/mL; Sigma Aldrich, E3019) was prepared in PBS pH 7.4. Stock solutions of **GSH** (10 mM), catalase (10000 U/mL), and H_2O_2 (100 mM) were prepared in DI water. The reaction mixture was prepared by adding 100 μM of **14** (2 μL, 10 mM stock), 100 equiv. of H_2O_2 (20 μL, 100 mM stock), and the reaction mixture was incubated for 1 h at 37 °C, followed by 100 U/mL catalase treatment (2 μL, 10000 U/mL stock) for 5 min. Then, 25 μM of 3-MST (12.75 μL, 392 μM stock) was added to the reaction mixture and incubated for 30 min, followed by the addition of 10 mM **GSH** (20 μL, 100 mM stock) for 30 min at 37 °C. The volume was adjusted to 200 μL using 10 mM PBS (pH 7.4) containing 100 μM DTPA in a 2.0 mL Eppendorf tube. Finally, 5 mM **HPE-IAM** (10 μL,100 mM stock) was added and further incubated for 30 min at 37 °C. Finally, the reaction was quenched by adding 200 μL of acetonitrile. Similarly, a control reaction for **12** was set up in the presence of Es (1 U/mL). The samples were centrifuged at 10,000 x g for 10 min at 4 ˚C; the supernatant was collected and assessed thereafter by LC/MS. All measurements weredone using a previously established LC/MS method with slight modification. All measurements were done using the following protocol: Acetonitrile (A) and 0.1% formic acid in water (B) were used as the mobile phase. A multistep gradient was used with the flow rate of 0.2 mL/min starting with 0:100 → 0 min 0:100 to 5:95 → 0.10 -1 min, 5:95 to 90:10→ 1 - 15 min, 90:10 to 0:100 → 15 – 15.10 min, and 0:100 → 15 – 22 min. Measurements were carried out in the positive ion mode using Agilent 6545 Quadrupole Time-Of-Flight (QTOF) LC-MS/MS with a Phenomenex®C-18 reverse phase column (250 mm × 4.6 mm, 5 μm). All LC-MS runs were performed using an ESI source with the following MS parameters: drying and sheath gas temperature = 320 °C; drying and sheath gas flow rate = 10L/min; fragmentor voltage = 150 V; capillary voltage = 4 kV; nebulizer (ion source gas) pressure = 45 Ψ and nozzle voltage = 1 kV. For the analysis of compounds from the reaction mixture, a curated library was employed in the form of a Personal Compound Database Library (PCDL), and the peaks were validated based on relative retention times and MS/MS fragments obtained.

4.1.4.10. Cell viability assay for 14

Mouse embryonic fibroblasts (MEF) cells were seeded at a concentration of 1×10^4 cells/well overnight in a 96-well plate in complete DMEM medium supplemented with 5% FBS (fetal bovine serum) and 1% antibiotic solution in an atmosphere of 5% CO_2 at 37 ˚C. Cells were

exposed to varying concentrations of compound **14** prepared as a DMSO stock solution so that the final concentration of DMSO was 0.5%. The cells were incubated for 24 h at 37 ˚C. A 0.5 mg/mL stock solution of 3-(4, 5-dimethylthiazol-2-yl)-2, 5-diphenyl tetrazolium bromide (**MTT**) was prepared in DMEM and 100 μL of the resulting solution was added to each well. After 4 h incubation, the media was removed carefully and 100 μL of DMSO was added. Spectrophotometric analysis of each well using a microplate reader (Thermo Scientific Varioscan) at 570 nm was carried out to estimate cell viability.

4.1.4.11. Mice study

All mouse studies described in the manuscript received formal approval from the Indian Institute of Science Education and Research, Pune-Institutional Animal Ethics Committee (protocol no: IISER Pune IAEC/2023_01/05), constituted as per the guidelines outlined by the Committee for the Purpose of Control and Supervision of Experiments on Animals (CPCSEA), Government of India. All mice were maintained at the National Facility for Gene Function in Health and Disease (NFGFHD) at IISER Pune, supported by a grant from the Department of Biotechnology, Govt. of India (BT/INF/22/SP17358/2016). All mice used in the study were generated by breeding wild-type C57BL/6J mice and had *ad libitum* access to water and food. All mice used for the experiment were age and gender-matched. For the experiment where neuroinflammation was studied, an intraperitoneal injection of lipopolysaccharide (**LPS**) in 1× PBS (vehicle) at a dose of 5 mg/kg body weight was used to generate systemic inflammation. Test compound **14** was also injected intraperitoneally in two doses – the first at 20 mg/kg body weight 1 h before the **LPS** administration and the second dose of 20 mg/kg body weight 4 h after the 5 mg/kg **LPS** administration, following which the mice were kept overnight.

Measurement of cytokines:

Mice were deeply anesthetized with isoflurane and euthanized by cervical dislocation. The brains of the mice were dissected within 15 seconds post decapitation, divided into two sagittal equal halves, weighed, washed with cold phosphate buffer saline (PBS), and flash frozen in liquid nitrogen. The cytokines were measured using protocols described previously.[3,8] One-half of the brains were re-suspended in 2 mL cold 1× PBS and homogenized using Dounce homogenization. The protein in each sample was estimated using Bradford assay and was finally adjusted to 1 mg/mL in each sample. The cytokines in each sample were measured using an ELISA kit.

4.1.5. NMR spectra of compounds

^{1}H NMR spectra of **14**

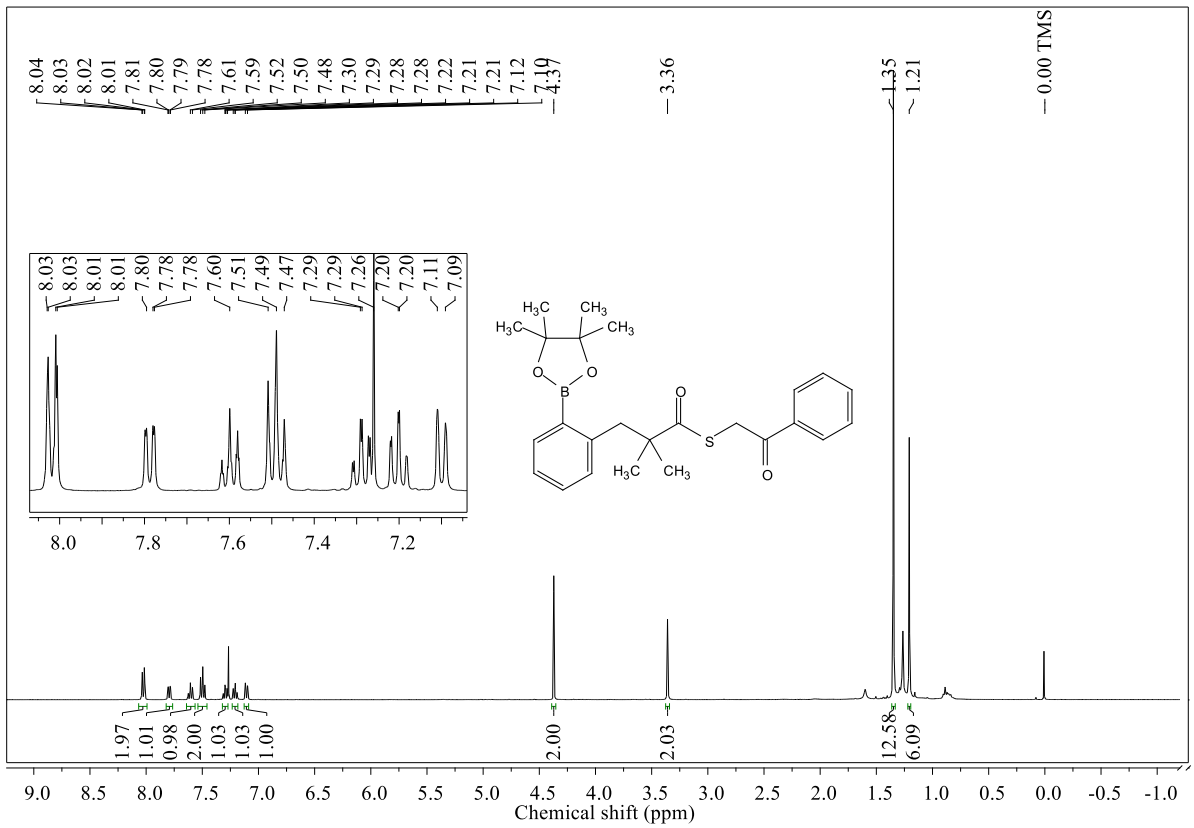

^{13}C NMR spectra of **14**

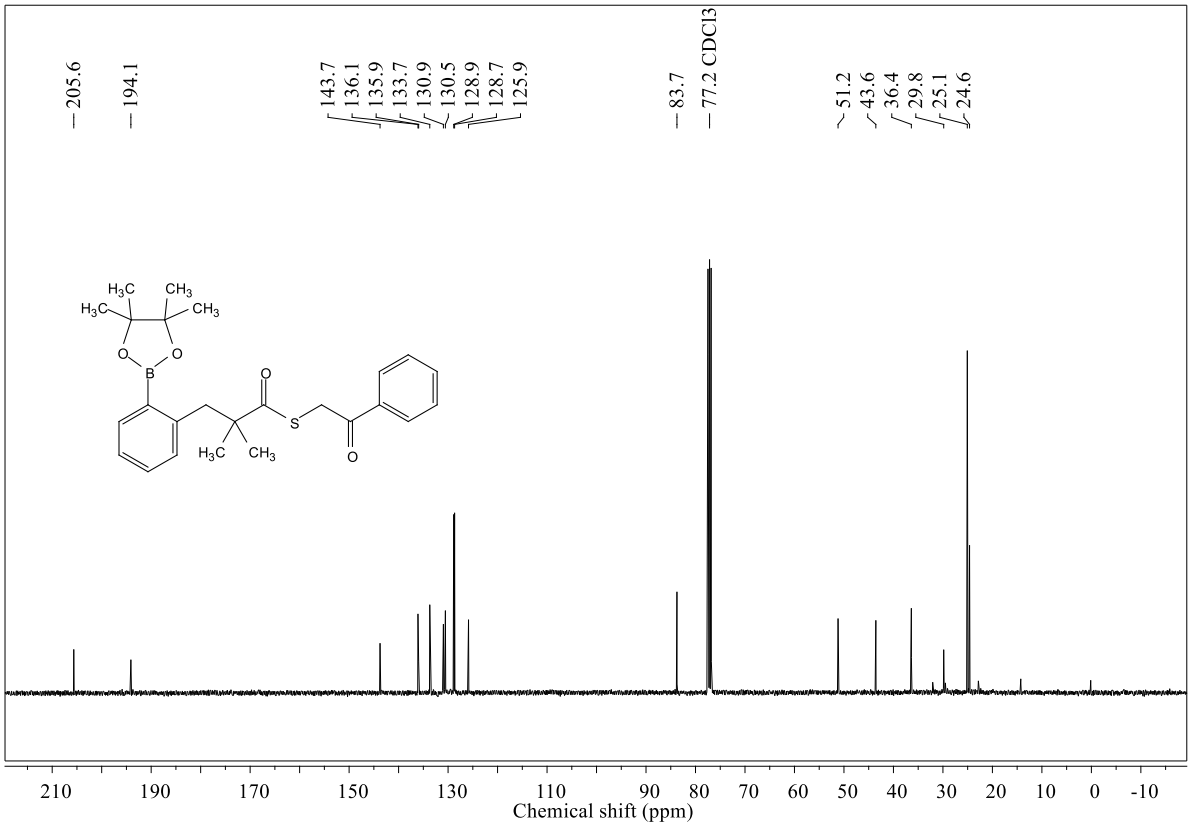

^{11}B NMR spectra of **14**

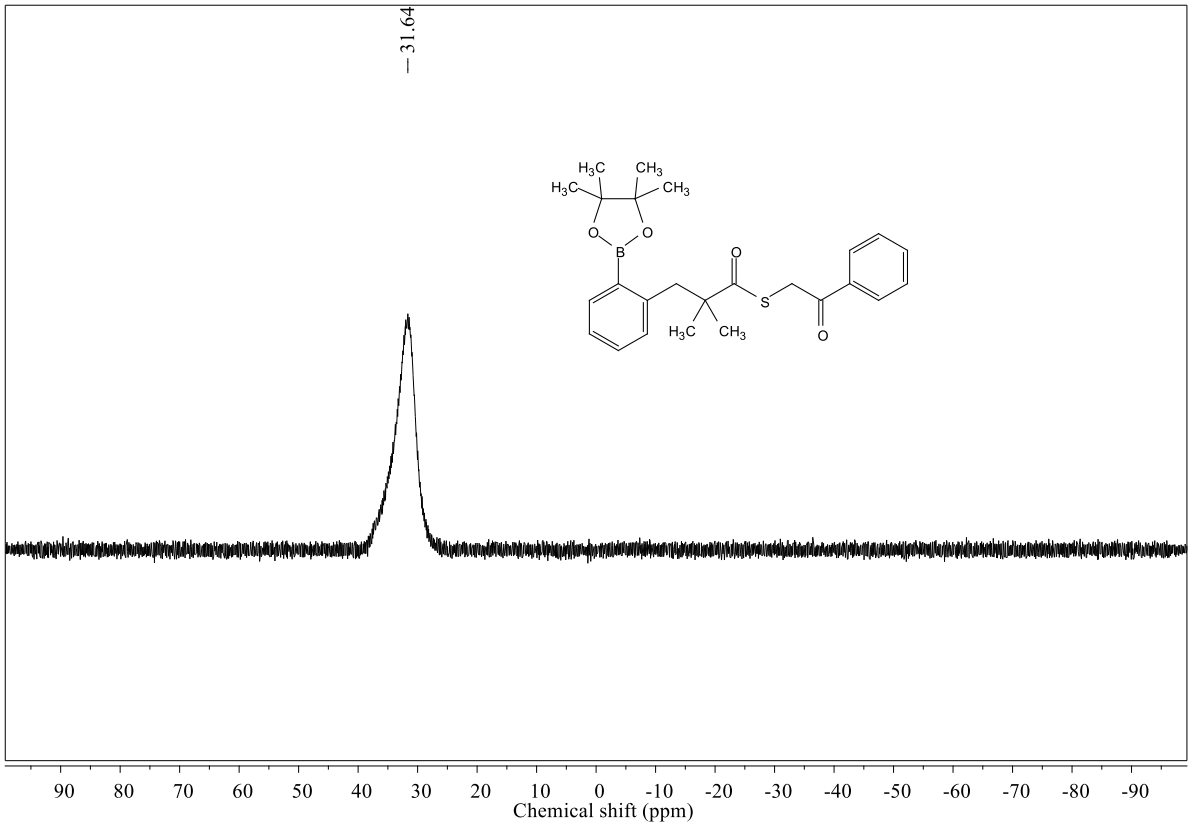

^{1}H NMR spectra of **15**

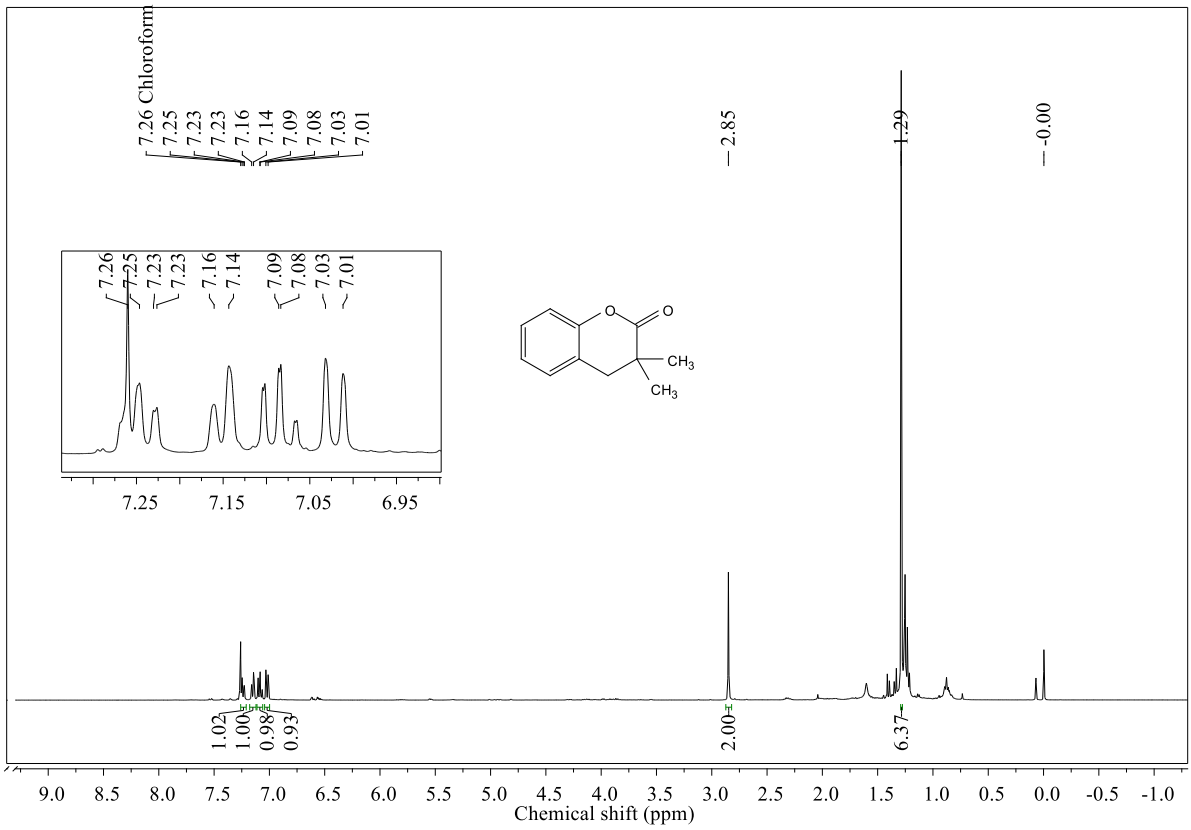

^{1}H NMR spectra of **16**

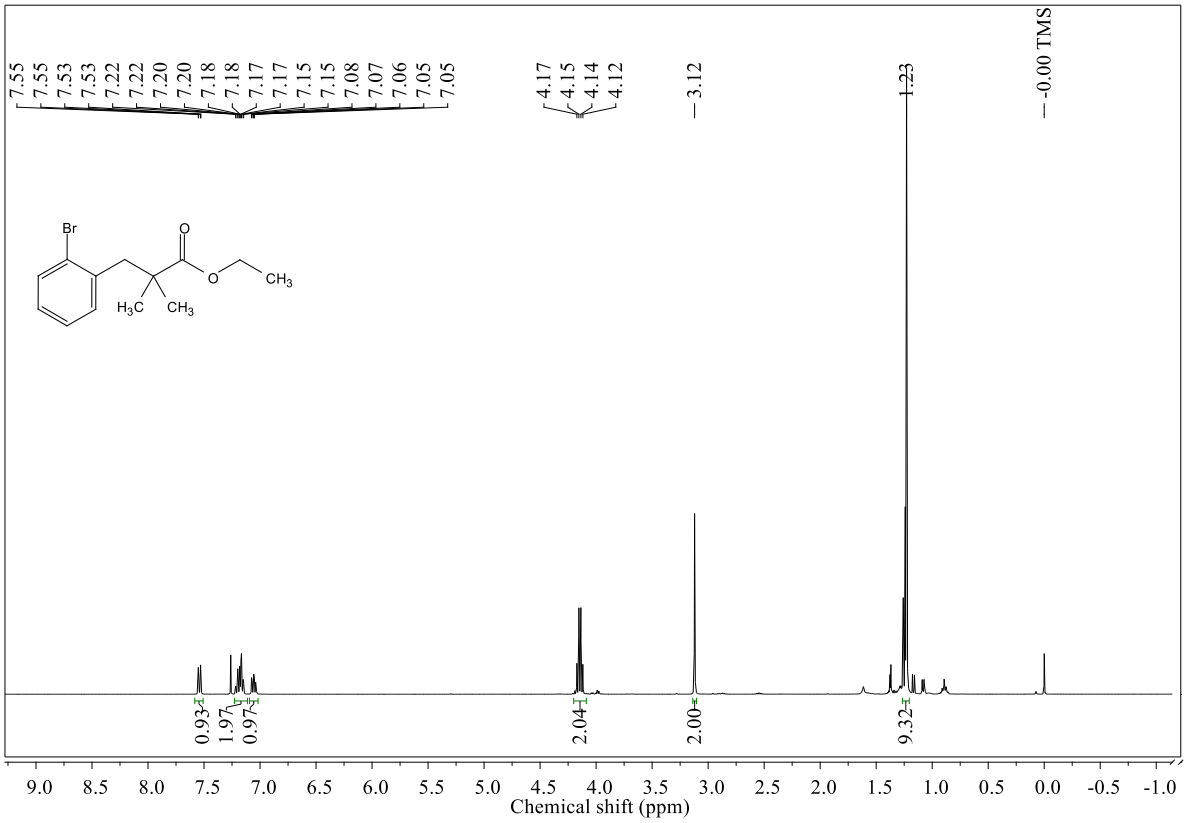

^{13}C NMR spectra of **16**

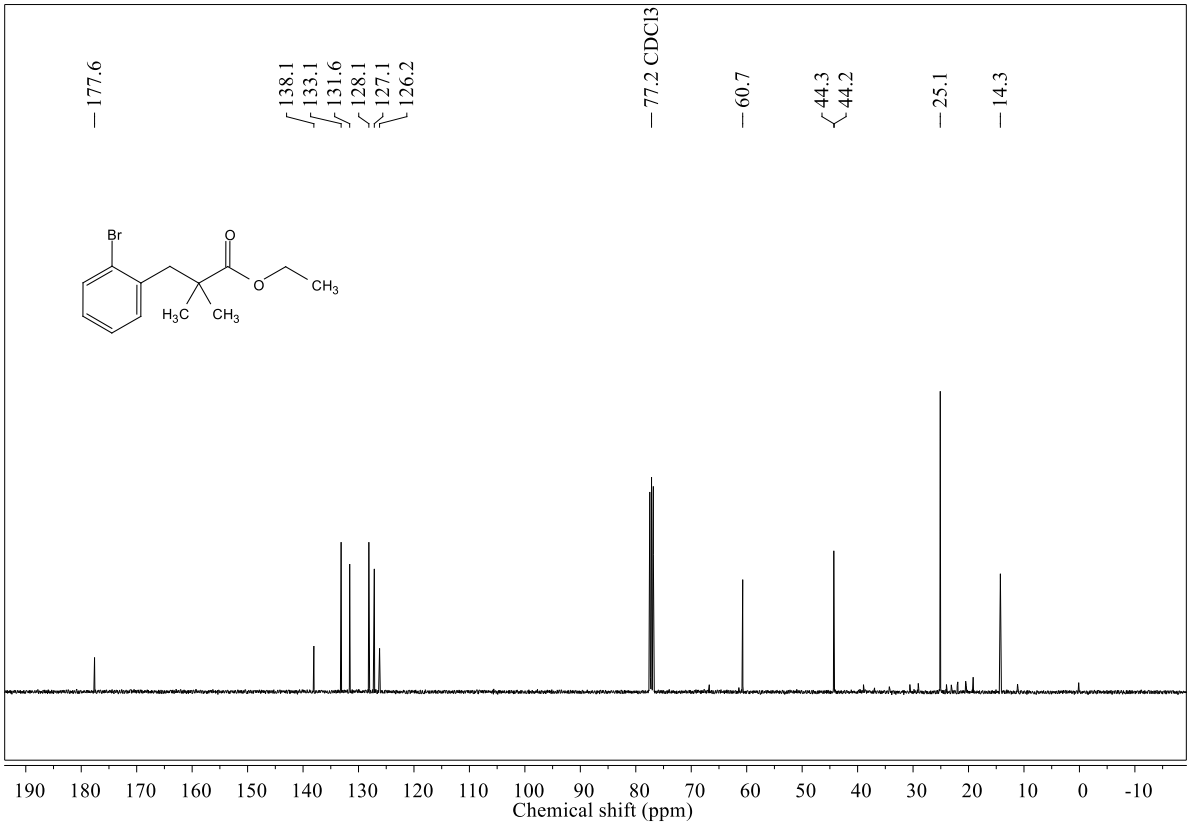

^{1}H NMR spectra of **17**

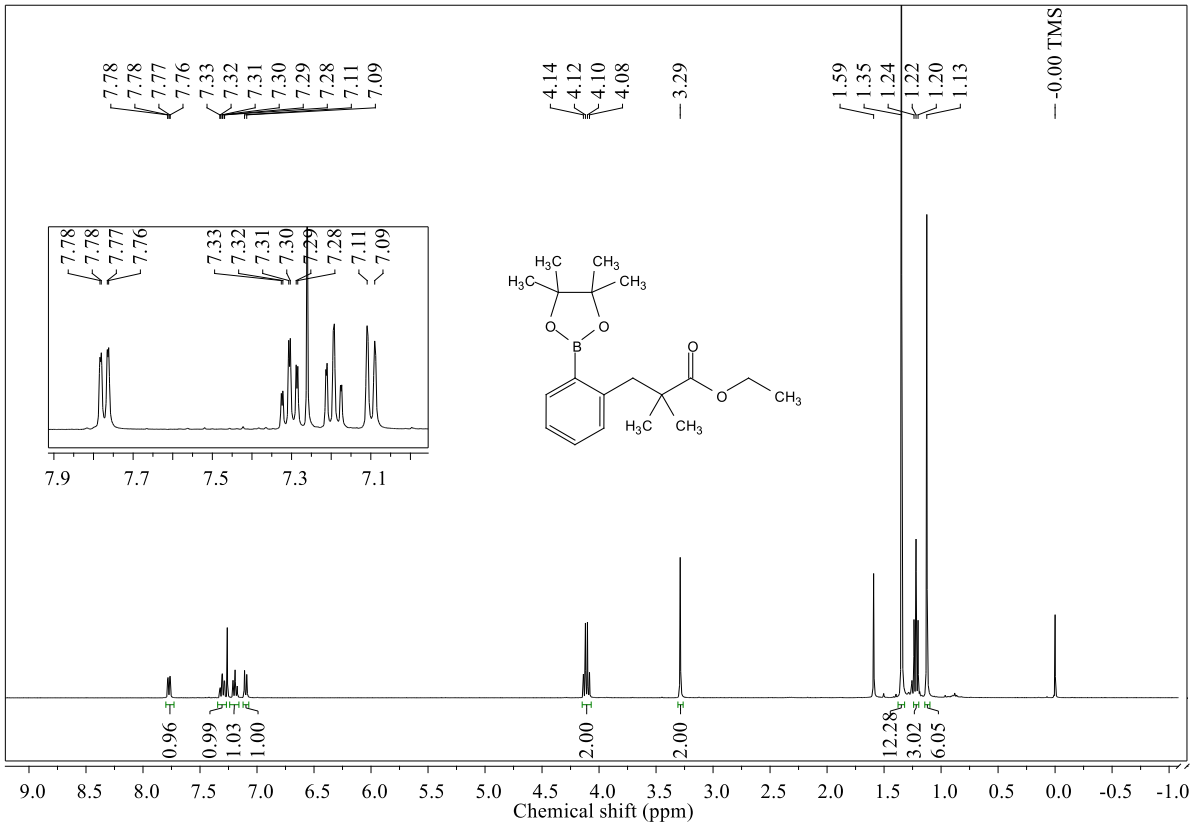

^{13}C NMR spectra of **17**

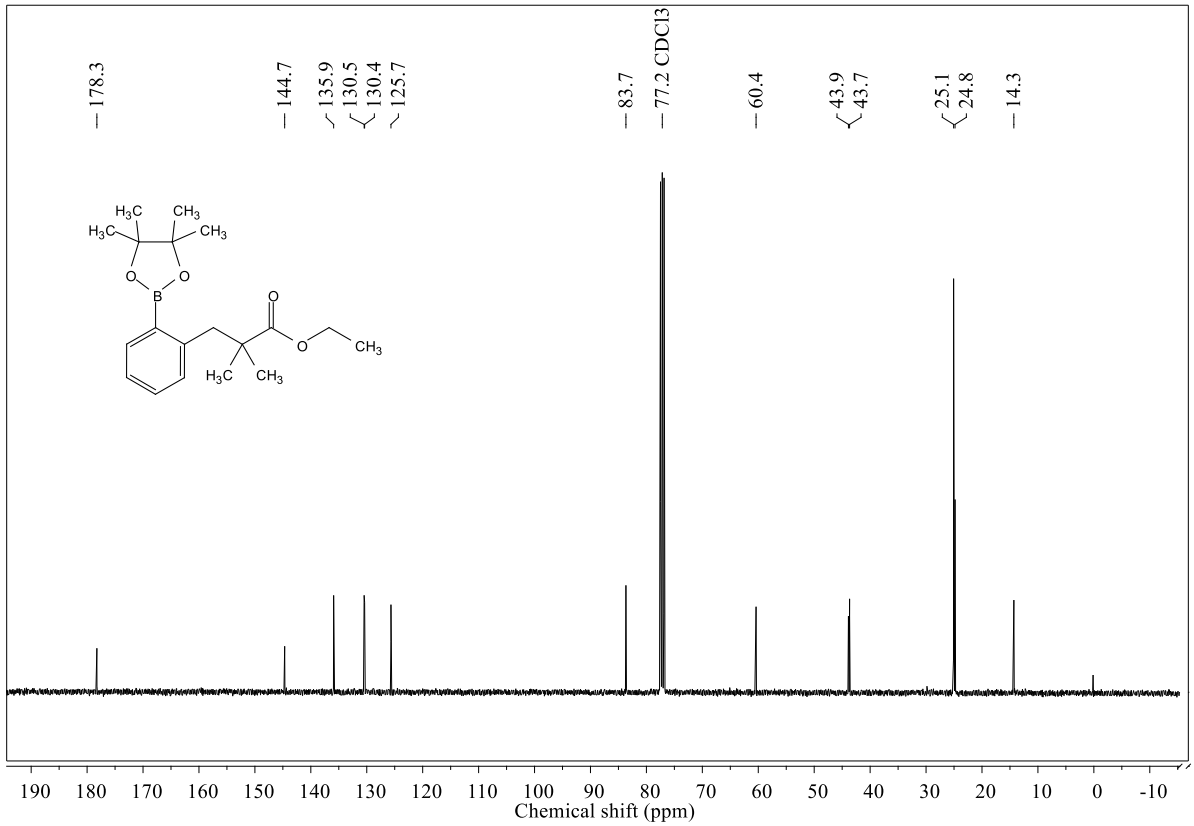

^{11}B NMR spectra of **17**

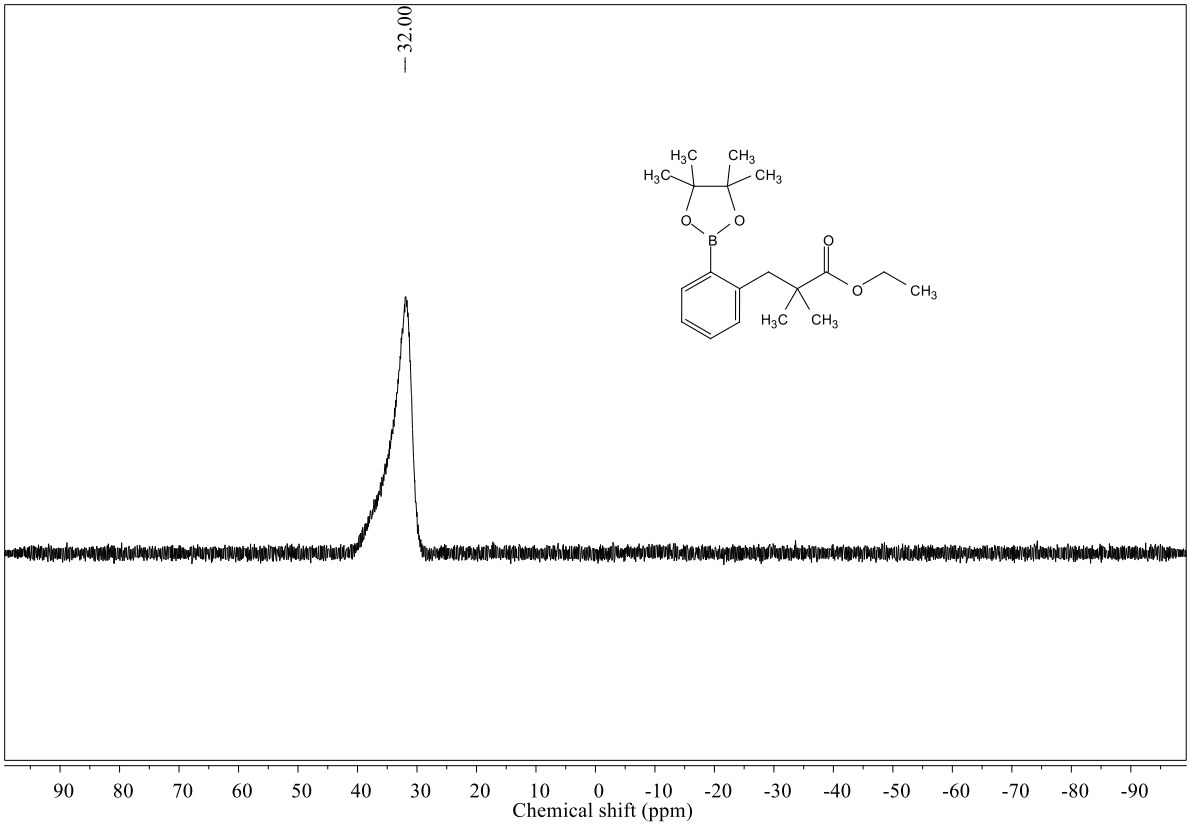

^{1}H NMR spectra of **18**

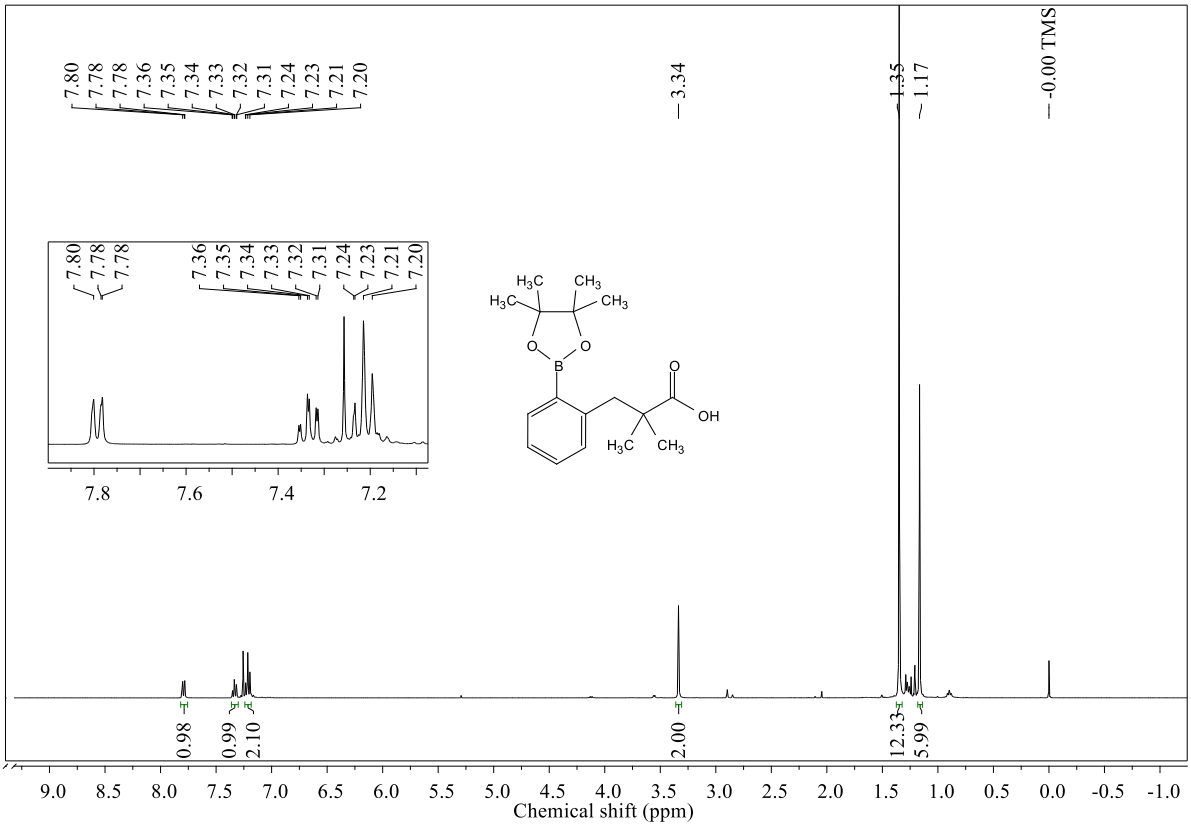

^{13}C NMR spectra of **18**

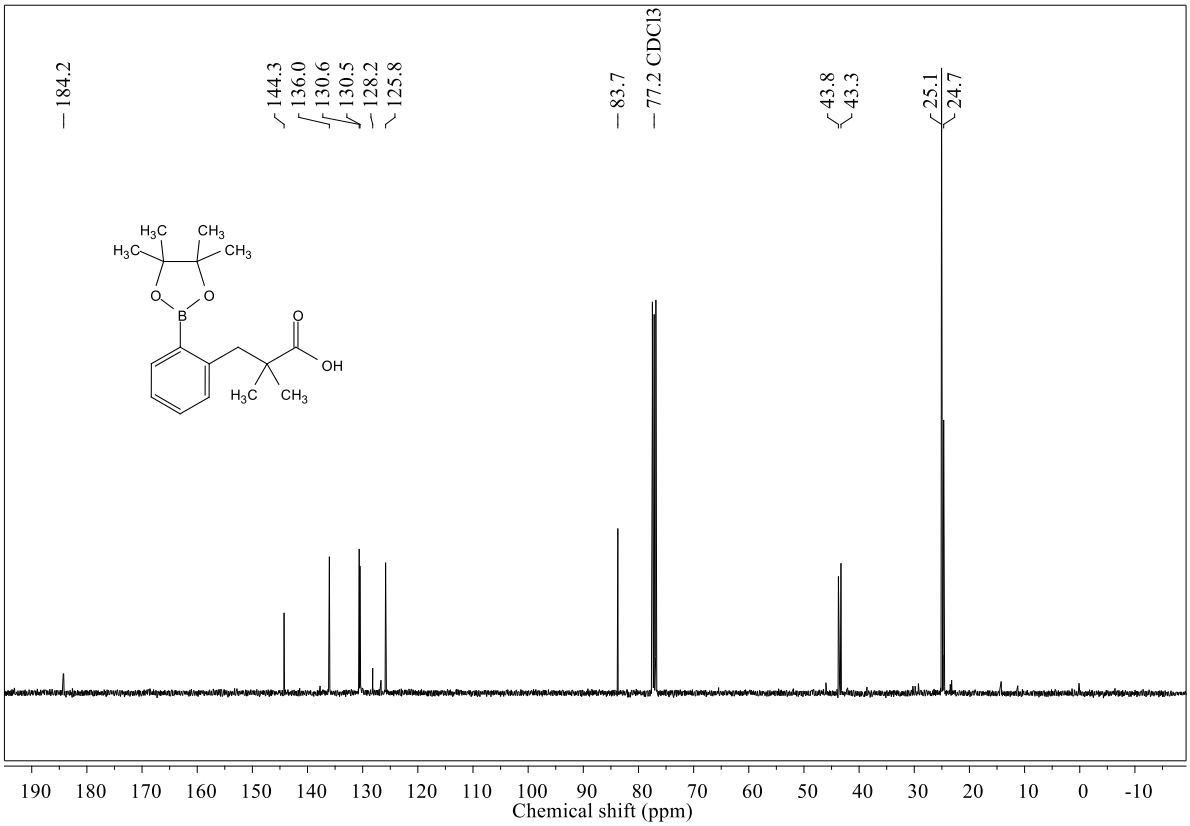

^{11}B NMR spectra of **18**

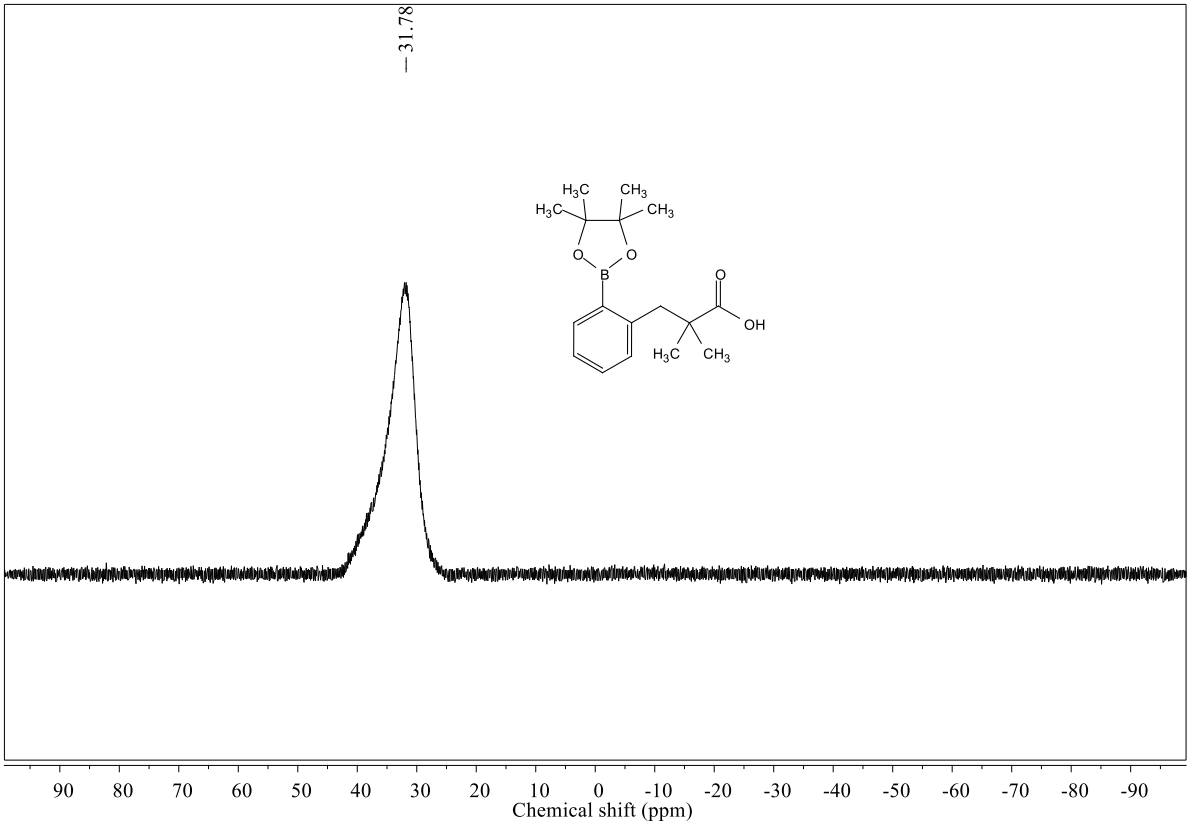

4.1.6. References

(1) Hankins, R. A.; Suarez, S. I.; Kalk, M. A.; Green, N. M.; Harty, M. N.; Lukesh, J. C. An Innovative Hydrogen Peroxide-Sensing Scaffold and Insight Towards Its Potential as an ROS-Activated Persulfide Donor. *Angew. Chemie Int. Ed.* **2020**, *59* (49), 22238–22245.

(2) Chen, W.; Liu, C.; Peng, B.; Zhao, Y.; Pacheco, A.; Xian, M. New Fluorescent Probes for Sulfane Sulfurs and the Application in Bioimaging. *Chem. Sci.* **2013**, *4* (7), 2892–2896.

(3) Bora, P.; Manna, S.; Nair, M. A.; Sathe, R. R. M.; Singh, S.; Sreyas Adury, V. S.; Gupta, K.; Mukherjee, A.; Saini, D. K.; Kamat, S. S.; Hazra, A. B.; Chakrapani, H. Leveraging an Enzyme/Artificial Substrate System to Enhance Cellular Persulfides and Mitigate Neuroinflammation. *Chem. Sci.* **2021**, *12* (39), 12939–12949.

(4) Hamid, H. A.; Tanaka, A.; Ida, T.; Nishimura, A.; Matsunaga, T.; Fujii, S.; Morita, M.; Sawa, T.; Fukuto, J. M.; Nagy, P.; Tsutsumi, R.; Motohashi, H.; Ihara, H.; Akaike, T. Polysulfide Stabilization by Tyrosine and Hydroxyphenyl-Containing Derivatives That Is Important for a Reactive Sulfur Metabolomics Analysis. *Redox Biol.* **2019**, *21*, 101096.

(5) Du, J.; Huang, Y.; Yan, H.; Zhang, Q.; Zhao, M.; Zhu, M.; Liu, J.; Chen, S. X.; Bu, D.; Tang, C.; Jin, H. Hydrogen Sulfide Suppresses Oxidized Low-Density Lipoprotein (Ox-LDL)-Stimulated Monocyte Chemoattractant Protein 1 Generation from Macrophages via the Nuclear Factor KB (NF-KB) Pathway. *J. Biol. Chem.* **2014**, *289* (14), 9741–9753.

(6) Zhang, T.; Ono, K.; Tsutsuki, H.; Ihara, H.; Islam, W.; Akaike, T.; Sawa, T. Enhanced Cellular Polysulfides Negatively Regulate TLR4 Signaling and Mitigate Lethal Endotoxin Shock. *Cell Chem. Biol.* **2019**, *26* (5), 686-698.e4.

(7) Heredia, A. A.; Soria-Castro, S. M.; Bouchet, L. M.; Oksdath-Mansilla, G.; Barrionuevo, C. A.; Caminos, D. A.; Bisogno, F. R.; Argüello, J. E.; Peñéñory, A. B. Stereoselective One-Pot Synthesis of β-Alkylsulfide Enol Esters. Base-Triggered Rearrangement under Mild Conditions. *Org. Biomol. Chem.* **2014**, *12* (33), 6516.

(8) Kelkar, D. S.; Ravikumar, G.; Mehendale, N.; Singh, S.; Joshi, A.; Sharma, A. K.; Mhetre, A.; Rajendran, A.; Chakrapani, H.; Kamat, S. S. A Chemical–Genetic Screen Identifies ABHD12 as an Oxidized-Phosphatidylserine Lipase. *Nat. Chem. Biol.* **2019**, *15* (2), 169–178.

Chapter 4.2. Design and Development of ROS-triggered WR1065 Donor

4.2.1. Introduction

In previous **Chapter 4.1,** the development of the ROS-activated persulfide generator was discussed. Next, this strategy was extended for the development of the ROS-triggered prodrug (Figure 4.2.1), which produces lactone **15** and the active drug upon activation by H_2O_2. In order to achieve this goal, the known thiol-based radioprotectant **WR-1065**, the active form of the drug amifostine, was considered.

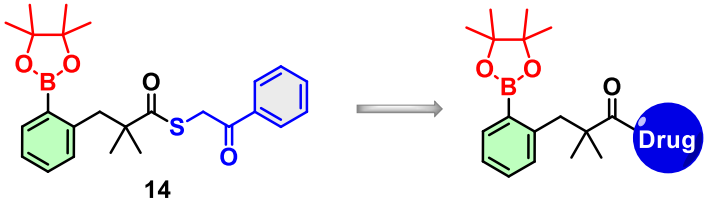

Figure 4.2.1. Development of ROS-triggered prodrug.

Amifostine (**WR-2721**), is a clinically approved cancer chemotherapeutic and radioprotective drug. It is an organic thiophosphate drug (**WR-2721**) which, on hydrolysis by alkaline liver phosphatase (ALP), gives active thiol **WR-1065** (Figure 4.2.2.A).[1,2]

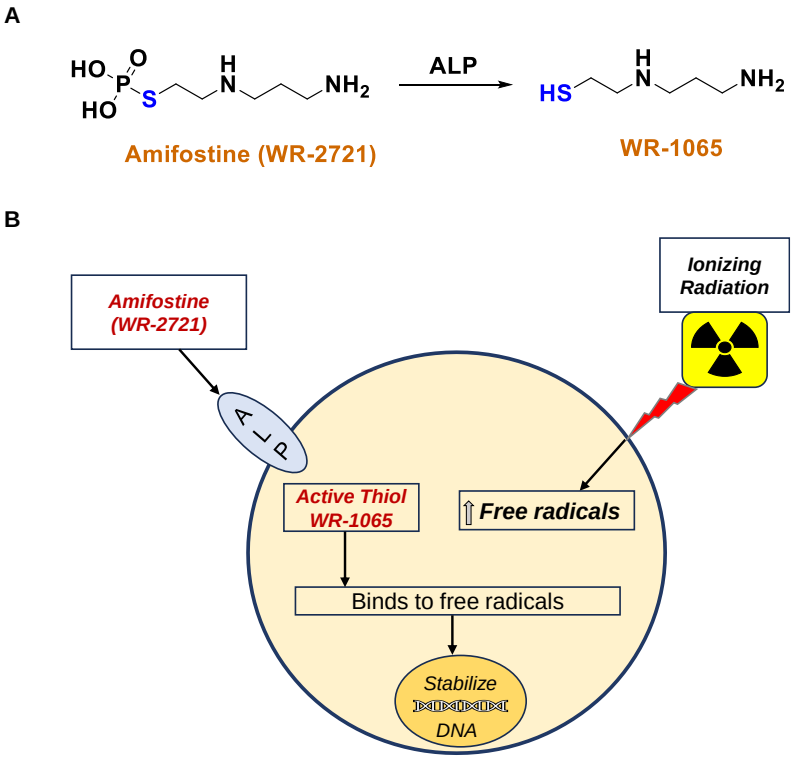

Figure 4.2.2. (A) Activation of amifostine (**WR-2721**) by Alkaline phosphatase (ALP) to generate the active thiol **WR-1065**, and (B) Mechanism of action amifostine to protect cells from radiation-induced damage by quenching the free radicals.

The active form **WR-1065** elicits cytoprotective effects by detoxifying cytotoxic drugs, scavenging free radicals formed by radiation, and participating in DNA repair pathways (Figure 4.2.2.B).[3,4] This selectivity arises because normal tissues can metabolize the drug more effectively than tumor tissues. Additionally, amifostine is therapeutically recommended to abate *cis*-platin-induced nephrotoxicity, decrease xerostomia, and reduce neutropenia-related fever.[5] However, amifostine has been associated with certain adverse effects, such as hypotension, vomiting, and nausea.[6]

By leveraging the ROS scaffold, a ROS-triggered **WR-1065** donor **20** was developed. Upon activation by H_2O_2, compound **20** generates the active thiol **WR-1065** and benign lactone **15** as a byproduct (Scheme 4.2.1).

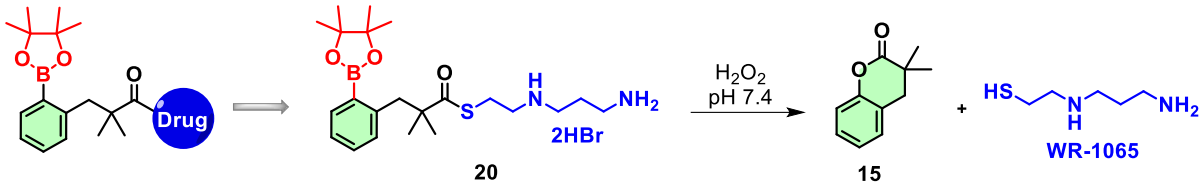

Scheme 4.2.1. Design of the ROS-triggered **WR-1065** donor.

4.2.2. Results and Discussion

4.2.2.1. Synthesis

The commercially available 1,3-diamino alcohol was subjected to Cbz-protection using a reported protocol to yield the compound **21** in 46% yield.[7] Then, compound **21** was reacted with CBr_4 and PPh_3 to produce the bromide precursor **22** in 42% yield (Scheme 4.2.2).[8]

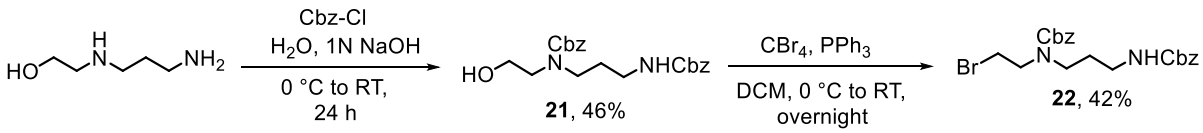

Scheme 4.2.2. Synthesis of the bromide precursor **22**.

Next, the desired molecule, **20**, was synthesized in three steps. The previously synthesized carboxylic acid derivative in **Chapter 4.1** was converted into the thiocarboxylic acid **19** using Lawesson's reagent[9] and then reacted with the bromide compound **22** in the presence of the Et_3N to yield the Cbz-protected **WR-1065** compound **23** in 19% yield. Finally, using a reported protocol with some modification,[7] the Cbz group was deprotected using HBr/AcOH to produce the ROS-activated **WR-1065** donor **20** as a hydrobromide salt in 45% yield (Scheme 4.2.3).

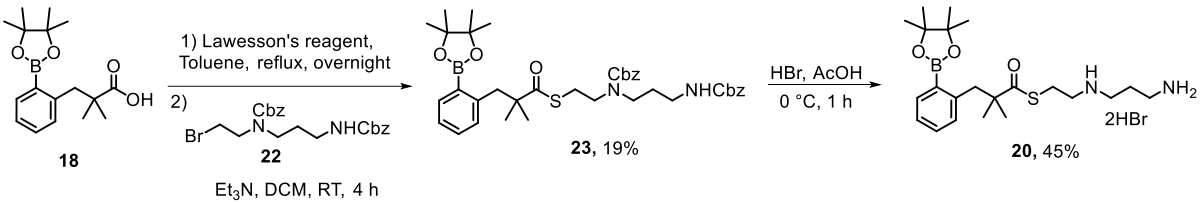

Scheme 4.2.3. Synthesis of ROS-triggered **WR-1065** donor **20**.

4.2.2.2. Activation of 20 in the presence of H_2O_2

An electrophilic trapping experiment using **mBBr** was conducted to trap the thiol **WR-1065**, upon activation of **20** in the presence of H_2O_2, as discussed in the previous **Chapter 4.1** (Scheme 4.2.4).

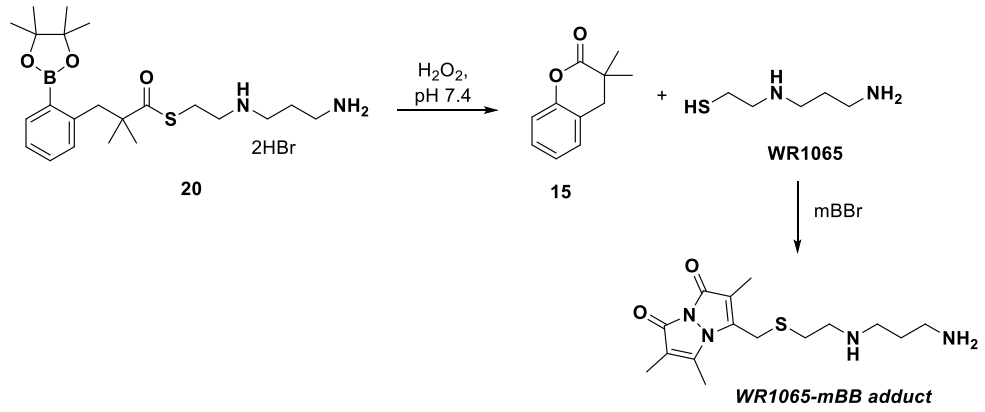

Scheme 4.2.4. Formation of the **WR1065-mBB** adduct when **20 (**100 μM) co-incubated with 100 equiv. of H_2O_2 and **mBBr** (100 μM).

In this assay, the compound **20** (100 μM) was co-incubated with 100 equiv. of H_2O_2 and 100 μM **mBBr** in pH 7.4 PBS containing 100 μM diethylenetriaminepentaacetic acid (DTPA). The mass corresponding to the formation of **WR1065-mBB** adduct (expected, m/z = 325.1693 $[M + H]^+$; observed, m/z = 325.3272) was observed by MALDI analysis (Figure 4.2.3).

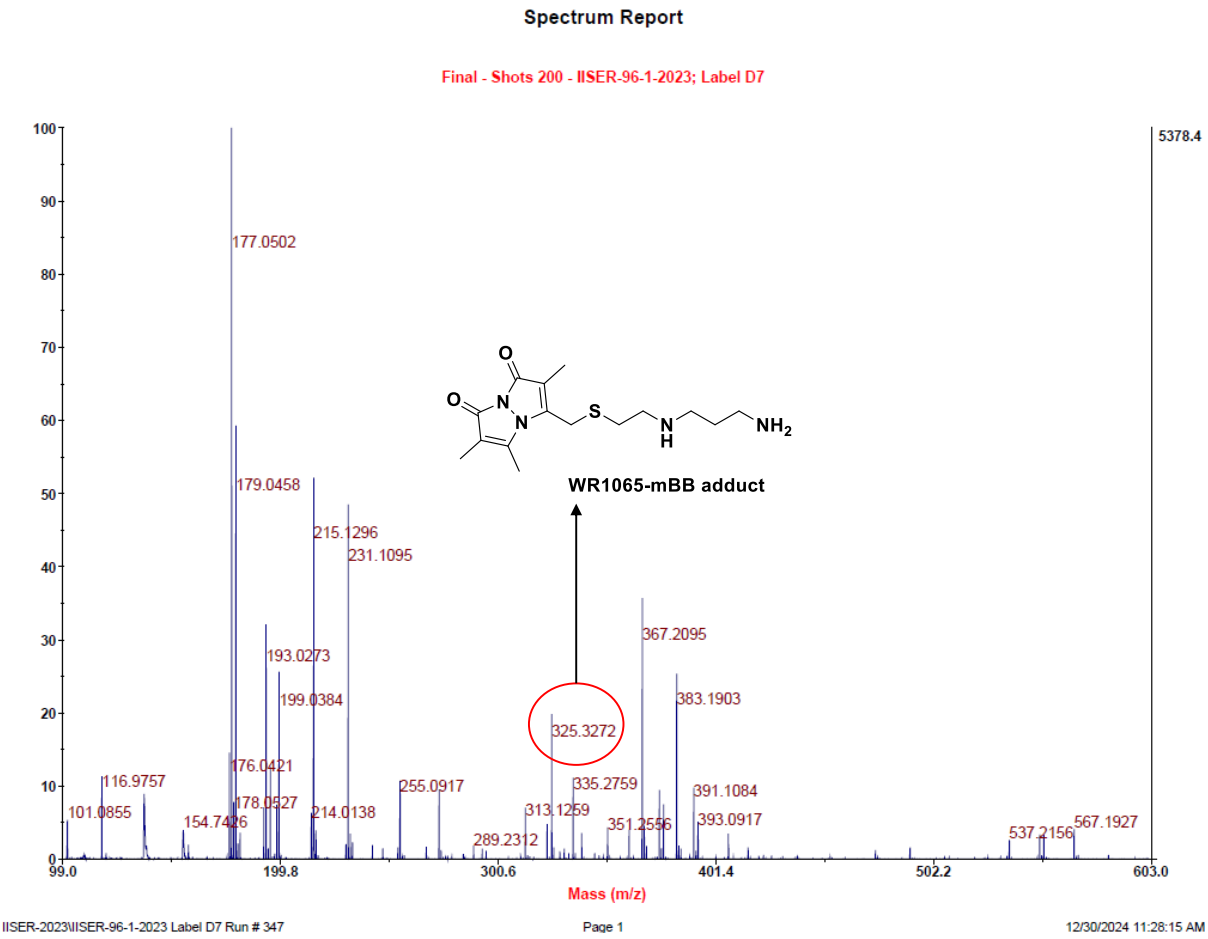

Figure 4.2.3. MALDI analysis for the formation of **WR1065-mBB** from **20** in the presence of H_2O_2 and mBBr. For **WR1065-mBB** (expected, m/z = 325.1693 $[M + H]^+$; observed, m/z = 325.3272).

Overall, MALDI analysis suggests, compound **20** was able to generate the lactone **15** and the thiol **WR-1065** in the presence of H_2O_2.

4.2.3. Summary and outlook

In summary, using the ROS scaffold, a ROS-triggered **WR-1065** donor **20** was developed. Upon activation by H_2O_2, **20** produces active drug **WR-1065** and a benign lactone **15**. Further experiments to evaluate and validate the activation of **20** in the presence of H_2O_2 are in progress.

4.2.4. Experimental protocols

4.2.4.1 General methods

All the chemicals and solvents were purchased from commercial sources and used as received unless stated otherwise. Column chromatography was performed using silica gel-Rankem (60–120 mesh) as the stationary phase. Preparative high-performance liquid chromatography (HPLC) was done using Combiflash EZ prep UV using a Kromasil®C-18 preparative column (250 mm × 21.2 mm, 5 μm). ^{1}H and ^{13}C spectra were recorded on a JEOL 400 MHz (or 100 MHz for ^{13}C) or a Bruker 400 MHz (or 100 MHz for ^{13}C) spectrometer unless otherwise specified using either residual solvent signals ($CDCl_3$ δH = 7.26 ppm, δC = 77.2 ppm), (CD_3OD δH = 3.34 ppm, δC = 49.8 ppm) or as an internal tetramethylsilane (δH = 0.00, δC = 0.0). Chemical shifts (δ) are reported in ppm and coupling constants (*J*) in Hz. The following abbreviations are used: m (multiplet), s (singlet), d (doublet), t (triplet), ddt (doublet of doublet of triplet) and dq (doublet of quartet). High-resolution mass spectra were obtained from HRMS-ESI-Q-Time of Flight LC/MS. FT-IR spectra were recorded using a BRUKER-ALPHA FT-IR spectrometer and reported in cm^{-1}.

4.2.4.2 Synthesis and Characterization

Compounds **18**[9] and **21**[7] were synthesized following previously reported protocols, and each compound's analytical data was consistent with reported values.

Benzyl (3-(((benzyloxy)carbonyl)amino)propyl)(2-bromoethyl)carbamate (22):

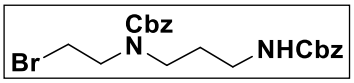

To a stirred solution of **21** (0.375 g, 0.97 mmol) and carbon tetrabromide (0.515 g, 1.55 mmol) in DCM (10 mL) at 0 ºC, PPh_3 (0.445 g, 1.70 mmol) dissolved in 3 mL DCM was added into it under N_2 atmosphere. The reaction was stirred at 0 ºC to rt overnight. Upon completion of the reaction, as monitored by TLC, the reaction mixture was diluted with water (15 mL), and the aqueous layer was washed with DCM (3 × 10 mL). The combined organic layer was washed with brine, dried over Na_2SO_4, and filtered, and the filtrate was concentrated to give a crude compound. The crude product was purified by column chromatography using silica gel (60 - 120) with 10% EtOAc/hexane as the eluent to obtain **22** (0.185 g, 42%) as a white solid. FT-IR (ν_{max}, cm^{-1}): 2924, 1703; ^{1}H NMR (400 MHz, $CDCl_3$) δ 7.35 (m, 10H), 5.14 – 5.09 (m, 4H), 3.60 – 3.37 (m, 6H), 3.18 – 3.16 (m, 2H), 1.75 – 1.69 (m, 2H); ^{13}C NMR (100 MHz, $CDCl_3$) δ 156.6, 129.2, 128.9, 128.8 128.6, 128.5, 128.4, 128.2, 128.2, 128.0, 67.7, 66.7, 49.8, 45.7, 45.4, 44.7, 37.7,

33.7, 28.9, 28.4; HRMS (ESI-TOF) for $C_{21}H_{26}BrN_2O_4$ $[M+H]^+$: Calcd., 449.1076, Found, 449.1071.

S-(2-(((benzyloxy)carbonyl)(3-(((benzyloxy)carbonyl)amino)propyl)amino)ethyl)2,2-dimethyl-3-(2-(4,4,5,5-tetramethyl-1,3,2-dioxaborolan-2-yl)phenyl)propanethioate (23):

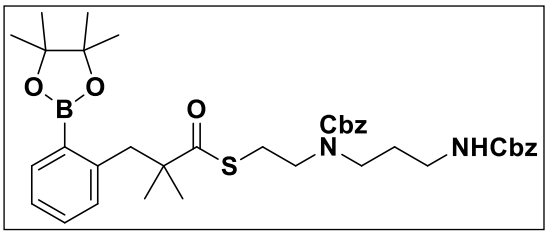

A mixture of compound **18** (0.101 g, 0.33 mmol), Lawesson's reagent (0.067 g, 0.16 mmol), and dry toluene (5 mL) was charged to a pressure tube and heated at 120 ^oC and stirred overnight. After consumption of the starting material, as monitored by TLC, the solvent was evaporated under reduced pressure. The reaction mixture was diluted with DCM (10 mL), washed with 1 N HCl and brine, and dried over Na_2SO_4. The filtrate was concentrated under reduced pressure to give a crude oily compound **19** carried forward to the next step without further purification. The oily product was dissolved in DCM (5 mL), and Et_3N (70 μL, 0.49 mmol) was added under N_2 atmosphere at rt. Then, a solution of bromide **21** (0.149 g, 0.33 mmol) was added dropwise to the reaction mixture and stirred for 4 h. Once the starting material was completely consumed, as monitored by TLC, the solvent was evaporated under reduced pressure to give a crude compound. The residue was purified by preparative HPLC using Kromasil®C-18 column at ambient temperature under the gradient elution with H_2O: ACN (0:100, v/v) as mobile phase at a flow rate of 12 mL/min to afford pure product **23** (0.044 g, 19%) as a sticky solid FT-IR (ν_{max}, cm^{-1}): 2925, 1720, 1702; ^1H NMR (400 MHz, $CDCl_3$) δ 7.78 (dd, *J* = 7.4, 1.3 Hz, 1H), 7.33 (m,11H), 7.20 (dd, *J* = 7.4, 6.5 Hz, 1H), 7.07 (d, *J* = 7.2 Hz, 1H), 5.21 – 5.02 (m, 4H), 3.49 – 3.25 (m, 6H), 3.18 (d, *J* = 4.9 Hz, 2H), 2.99 (dd, *J* = 19.0, 10.0 Hz, 2H), 1.80 – 1.69 (m, 2H), 1.34 (s, 12H), 1.15 (s, 6H); ^{13}C NMR (100 MHz, $CDCl_3$): δ 206.7, 156.7, 156.6, 143.8, 136.1, 130.9, 128.8, 128.8, 128.7, 128.6, 128.3, 128.2, 128.1, 128.0, 125.9, 83.7, 67.5, 66.6, 51.2, 46.8, 45.0, 43.6, 37.7, 27.1; 25.1, 24.7; ^{11}B NMR (128 MHz, $CDCl_3$) δ 31.85; HRMS (ESI-TOF) for $C_{38}H_{47}BN_2O_7S$ $[M+H]^+$: Calcd., 689.3432, Found, 689.3436.

***N*[1]-(2-((2,2-dimethyl-3-(2-(4,4,5,5-tetramethyl-1,3,2-dioxaborolan-yl)phenyl)propanoyl)thio)ethyl)propane-1,3-diaminium bromide (20):**

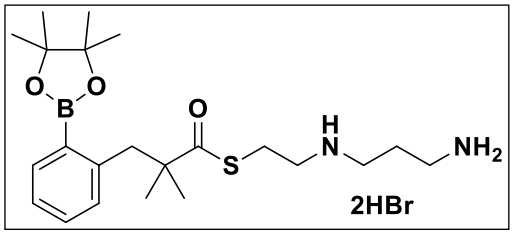

A solution of **23** (0.022 g, 0.032 mmol) in glacial acetic acid (1 ml) saturated with HBr was stirred at 0 °C under an N_2 atmosphere. After consumption of the starting material, as monitored by TLC, the solvent was evaporated under reduced pressure. The bis(hydrobromide) was precipitated from the mixture by adding ice-cold anhydrous ether (2 mL), and the ether phase was then decanted. After following the multiple washes with ether, the final compound **20** (0.006 g, 45%) as a white solid was obtained. FT-IR (ν_{max}, cm^{-1}): 3436, 2924, 1725; ^{1}H NMR (400 MHz, CD_3OD): δ 7.74 (dd, *J* = 7.4, 1.3 Hz, 1H),), 7.33 (td, *J* = 7.5, 1.6 Hz, 1H), 7.20 (td, *J* = 7.4, 1.1 Hz, 1H), 7.11 (d, *J* = 7.7 Hz, 1H), 3.32 – 3.02 (m, 10H), 1.80 – 1.69 (m, 2H), 1.37 (s, 12H), 1.20 (s, 6H); ^{13}C NMR (101 MHz, CD_3OD): δ 207.1, 145.2, 144.7, 137.0, 131.8, 131.5, 126.9, 85.0, 52.3, 49.8, 45.9, 44.7, 37.9, 25.2; ^{11}B NMR (128 MHz, CD_3OD) δ 32.18; HRMS (ESI-TOF) for $C_{22}H_{37}BN_2O_3S$ $[M+H]^+$: Calcd., 421.2696, Found, 421.2701.

4.2.4.3. WR1065 trapping experiment using mBBr

Stock solutions of **20** (10 mM), monobromobimane (**mBBr**, 10 mM) in DMSO, and H_2O_2 (100 mM) in deionized water were prepared. The reaction mixture was prepared by adding 100 μM of **20** (10 μL, 10 mM), 100 μM of **mBBr** (10 μL, 10 mM), with H_2O_2 (100 μL, 100 mM stock), and the volume was adjusted to 1000 μL using PBS (10 mM, pH 7.4) containing 100 μM DTPA in a 1.5 mL Eppendorf tube. The reaction was incubated for 60 min at 37 ˚C, and the reaction mixture was evaporated under nitrogen and subjected to MALDI analysis.

4.2.5. NMR spectra of compounds

^{1}H NMR spectra of **20**

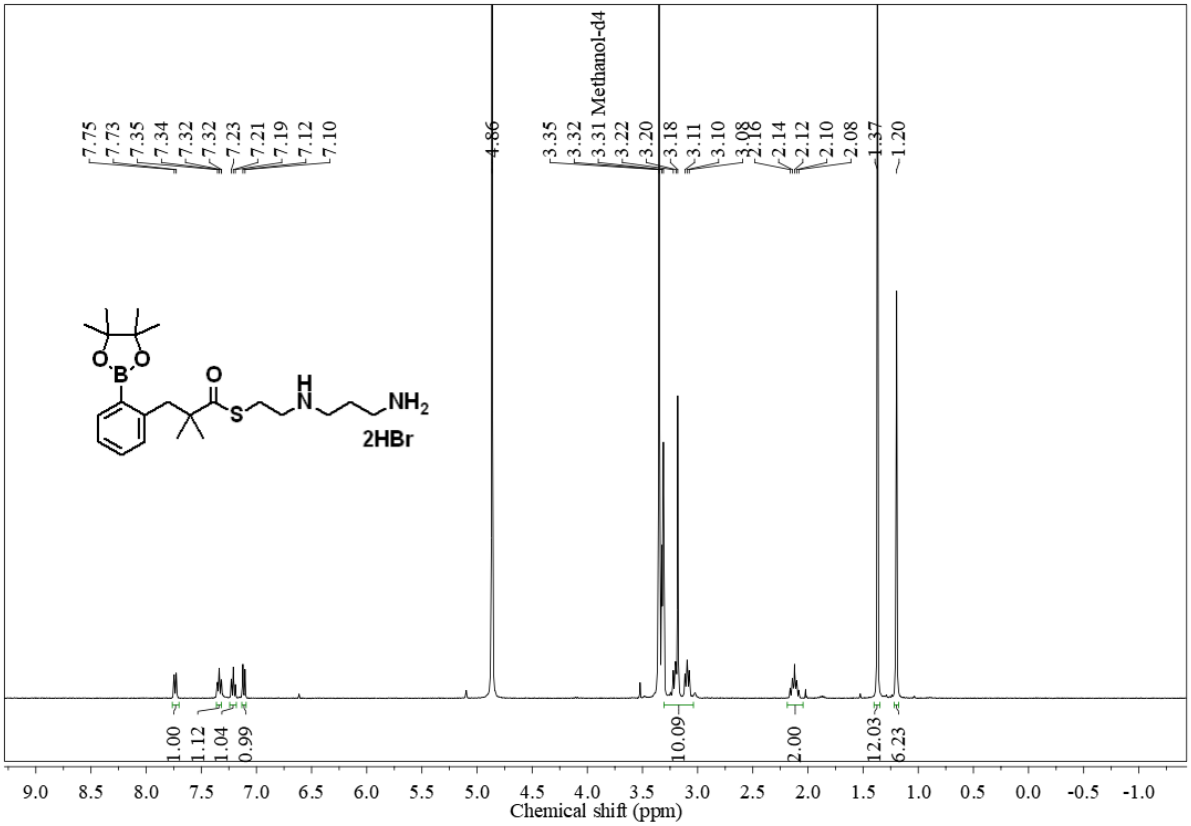

^{13}C NMR spectra of **20**

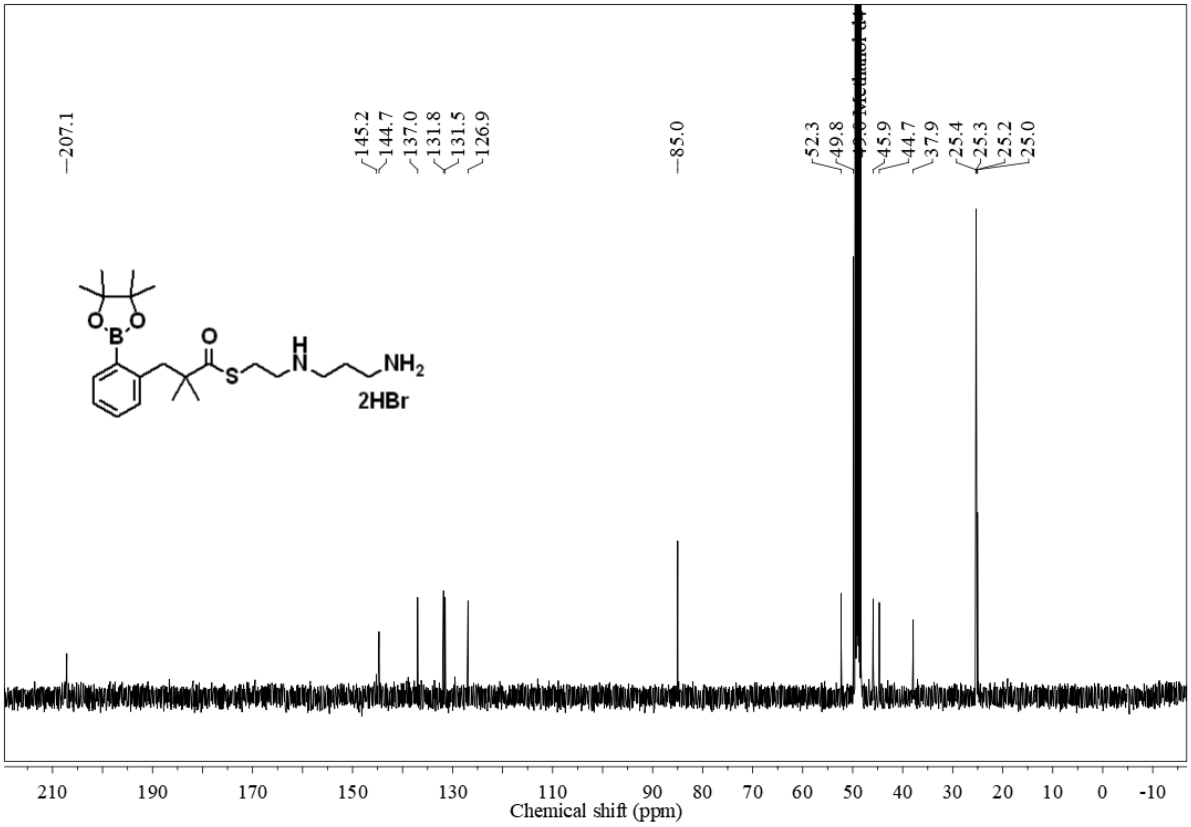

^{11}B NMR spectra of **20**

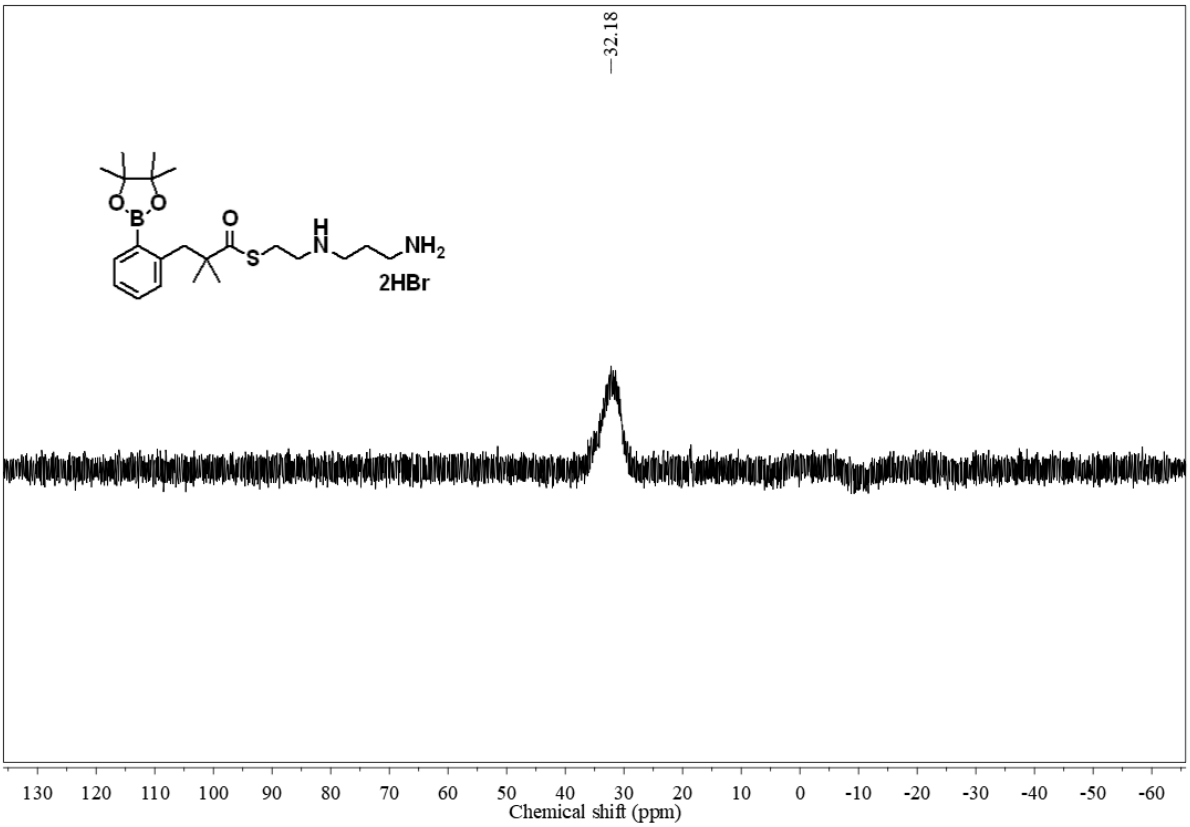

^{1}H NMR spectra of **22**

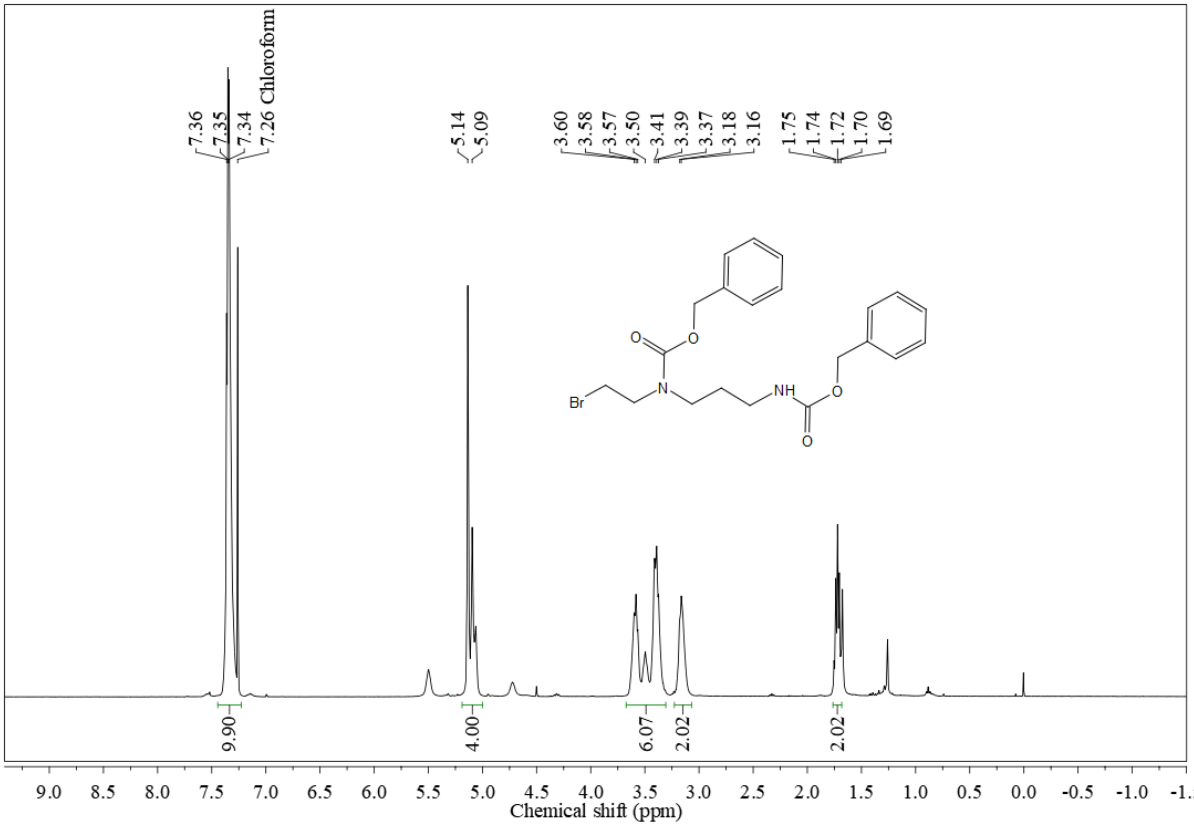

^{13}C NMR spectra of **22**

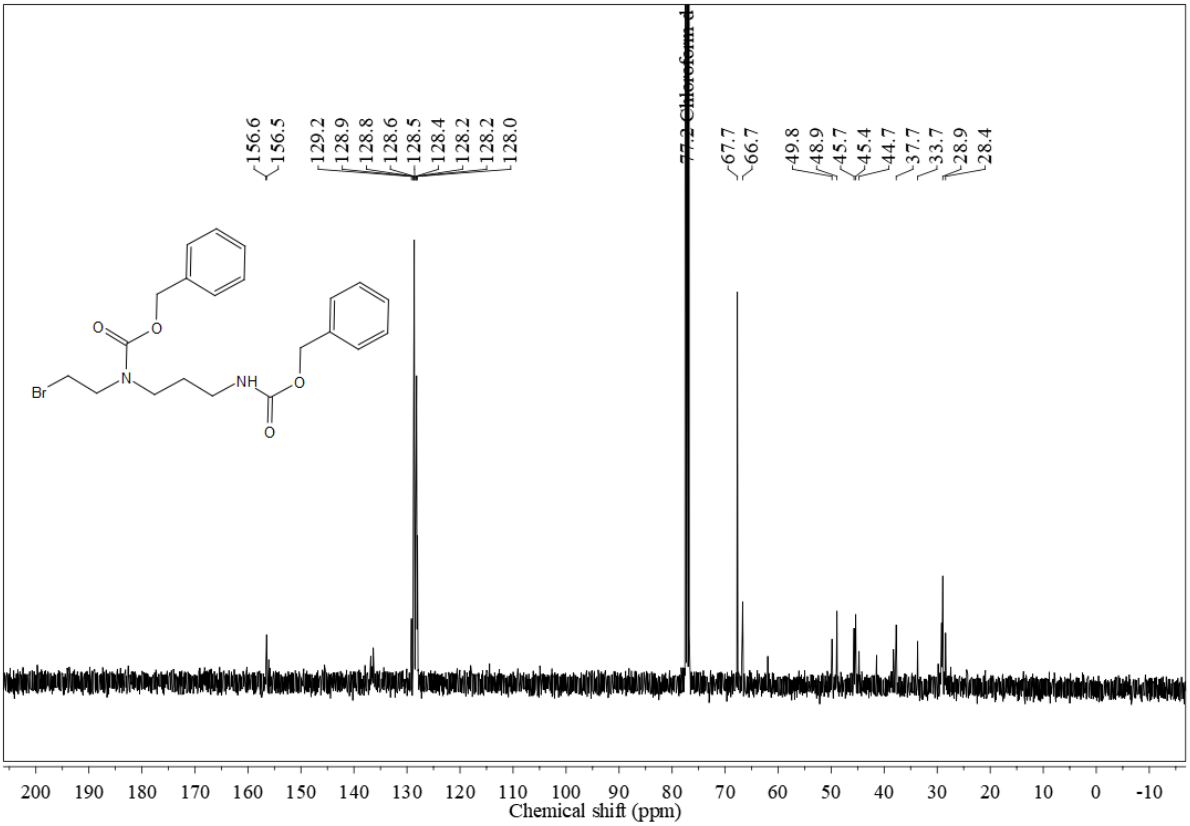

^{1}H NMR spectra of **23**

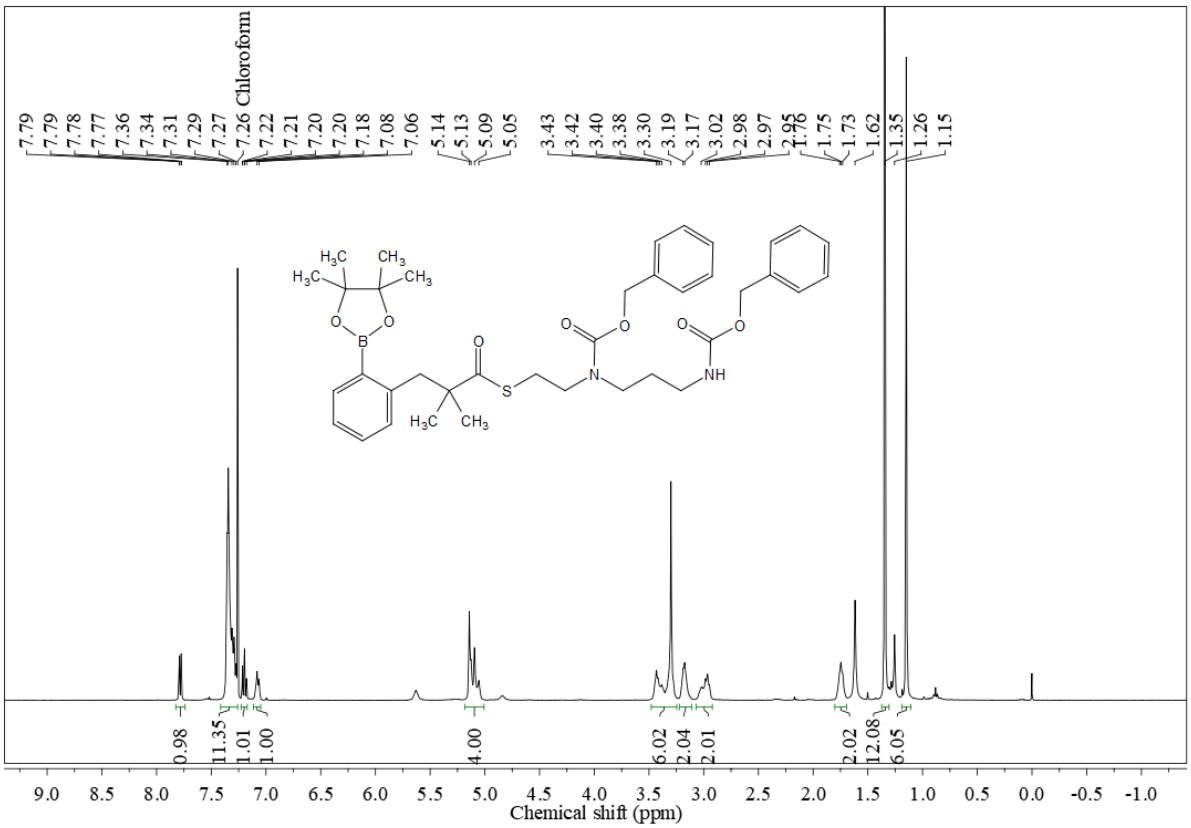

^{13}C NMR spectra of **23**

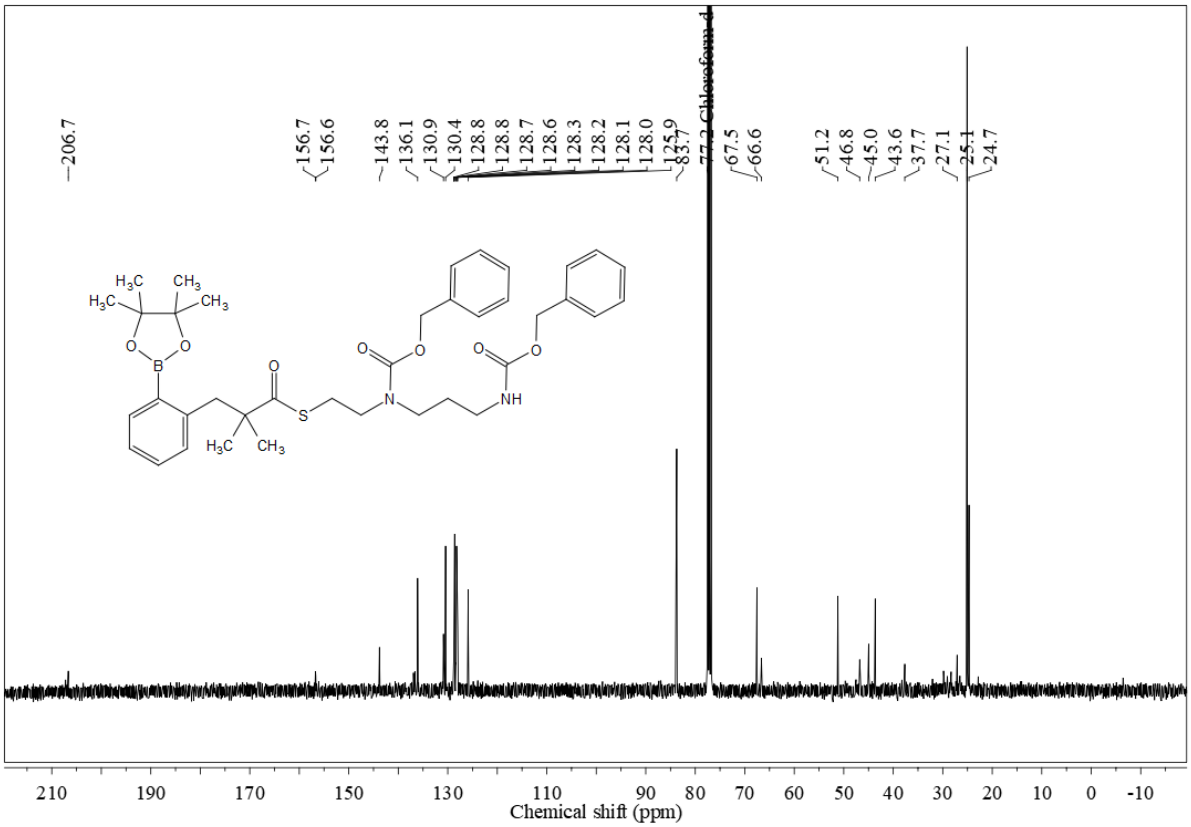

^{11}B NMR spectra of **23**

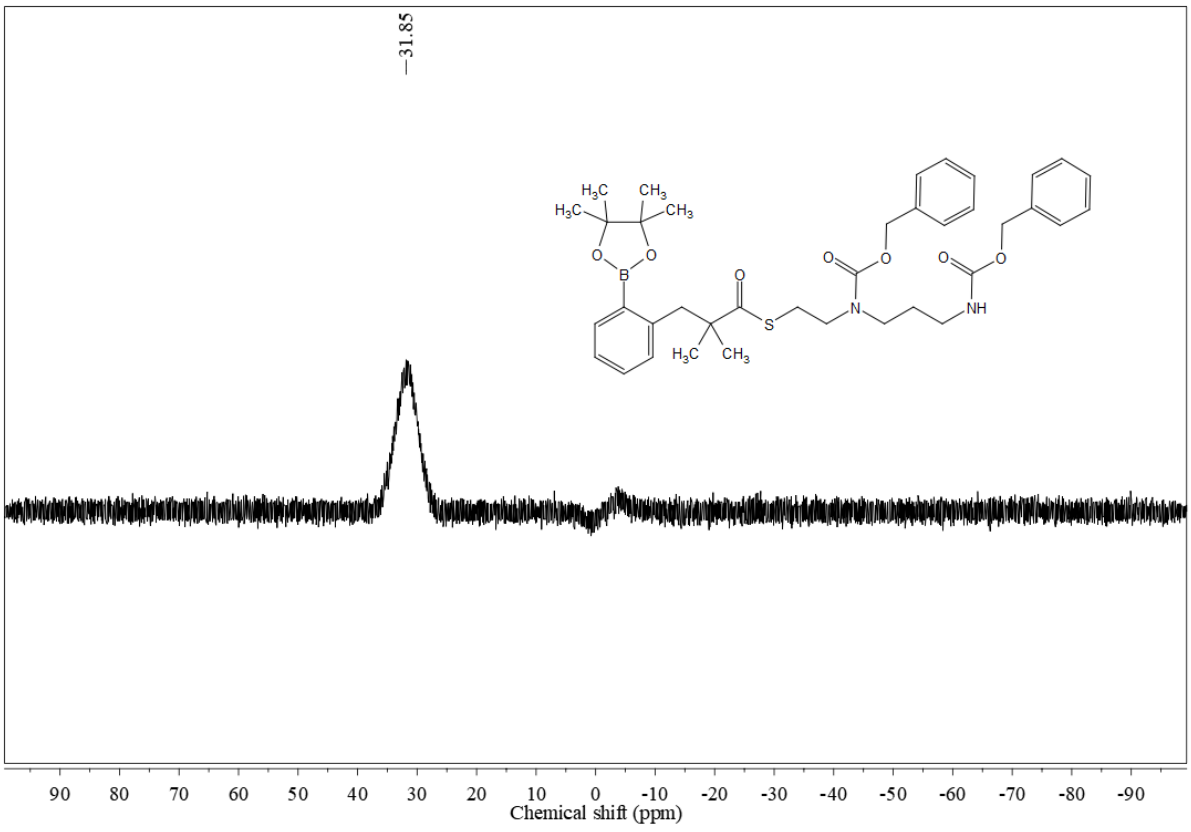

4.2.6. References

(1) Santini, V.; Giles, F. J. The Potential of Amifostine: From Cytoprotectant to Therapeutic Agent. *Haematologica* **1999**, *84* (11), 1035–1042.

(2) Koukourakis, M. I. Review Paper Amifostine in Clinical Oncology : Current Use and Future Applications. **2002**, *13*, 181–209.

(3) Dziegielewski, J.; Baulch, J. E.; Goetz, W.; Coleman, M. C.; Spitz, D. R.; Murley, J. S.; Grdina, D. J.; Morgan, W. F. WR-1065, the Active Metabolite of Amifostine, Mitigates Radiation-Induced Delayed Genomic Instability. *Free Radic. Biol. Med.* **2008**, *45* (12), 1674–1681.

(4) Singh, V. K.; Seed, T. M. The Efficacy and Safety of Amifostine for the Acute Radiation Syndrome. *Expert Opin. Drug Saf.* **2019**, *18* (11), 1077–1090.

(5) Koukourakis, M. I. Radiation Damage and Radioprotectants: New Concepts in the Era of Molecular Medicine. *Br. J. Radiol.* **2012**, *85* (1012), 313–330.

(6) Koukourakis, M. Amifostine in Clinical Oncology: Current Use and Future Applications. *Anticancer. Drugs* **2002**, *13* (3), 181–209.

(7) Oiry, J.; Pue, J. Y.; Laval, J. D.; Fatome, M.; Imbach, J. L. Synthesis and Radioprotective Activity of WR-1065 Derivatives: N-(2-Acetylthioethyl)-1,3-Propanediamine and N,N′-Bis(2-Acetylthioethyl)-1,3-Propanediamine. *Eur. J. Med. Chem.* **1995**, *30* (1), 47–52.

(8) Boddy, A. J.; Affron, D. P.; Cordier, C. J.; Rivers, E. L.; Spivey, A. C.; Bull, J. A. Rapid Assembly of Saturated Nitrogen Heterocycles in One-Pot: Diazo-Heterocycle "Stitching" by N–H Insertion and Cyclization. *Angew. Chemie Int. Ed.* **2019**, *58* (5), 1458–1462.

(9) Hankins, R. A.; Suarez, S. I.; Kalk, M. A.; Green, N. M.; Harty, M. N.; Lukesh, J. C. An Innovative Hydrogen Peroxide-Sensing Scaffold and Insight Towards Its Potential as a ROS-Activated Persulfide Donor. *Angew. Chemie - Int. Ed.* **2020**, *59* (49), 22238–22245.

Synopsis

Stimuli-Responsive Lactonization-Based Persulfide Generators

Chapter 1. Introduction

Over the past two decades, hydrogen sulfide (H_2S) has emerged as a gaseous signaling molecule involved in various biological processes such as antibiotic resistance, vasorelaxation, angiogenesis, apoptosis, aging, and metabolism.[1–4] Additionally, H_2S functions as an antioxidant, playing a vital role in maintaining redox homeostasis.[5] Alongside H_2S, persulfides (RSSH) have emerged as key players in sulfur biochemistry.[6,7] These are highly reactive and short-lived species, are formed within cells, participate in various biological processes, and are linked to cardiovascular and neurological diseases.[7,8] Furthermore, protein persulfidation - an oxidative post-translational modification involving the addition of an SH/S^- group to cysteine residues, has gained significant attention in recent years.[9] Persulfidation plays a vital role in oxidative stress protection,[10–12] DNA repair,[13] and KEAP1-Nrf2 antioxidant signaling.[5,14] Persulfides are found to have relevance in NF-κB-mediated inflammation machinery[15–17] and various neurodegenerative disorders.[18–20] Hence, regulating the persulfide concentration in cells becomes important.

Persulfides are produced in cells *via* enzymatic biosynthetic pathways. For example, cysteine persulfide (Cys-SSH), a well-known persulfide, is synthesized from cystine with the involvement of the enzymes cystathionine-β-synthase (CBS) and cystathionine γ-lyase (CSE).[21,22] Additionally, recent studies have shown that cysteinyl-tRNA synthetases (CARS) can generate Cys-SSH from L-cysteine (Figure 1).[23]

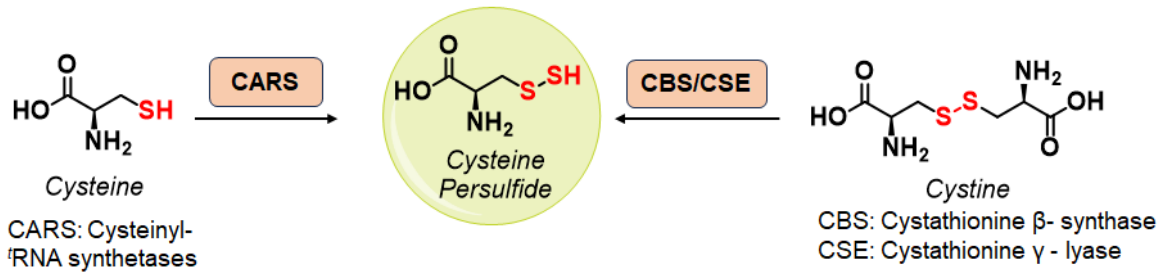

Figure 1. Cysteine persulfide formation from CBS, CSE, and CARS.

Another broad class of enzymes, known as sulfurtransferases, is present across various organisms and is responsible for the persulfide biosynthesis and sulfur trafficking in cells.[24–26] The catalytic cycle of this enzyme follows a two-step mechanism. First, the active site cysteine forms a transient persulfide intermediate (S-SH) by accepting sulfur from a donor compound. Subsequently, the sulfur is transferred to a thiophilic acceptor, regenerating the

enzyme's native state. Thiophilic acceptors can include proteins like thioredoxin or small molecule thiols such as cysteine or glutathione, which can mediate protein transpersulfidation (Figure 2).[24,25,27,28]

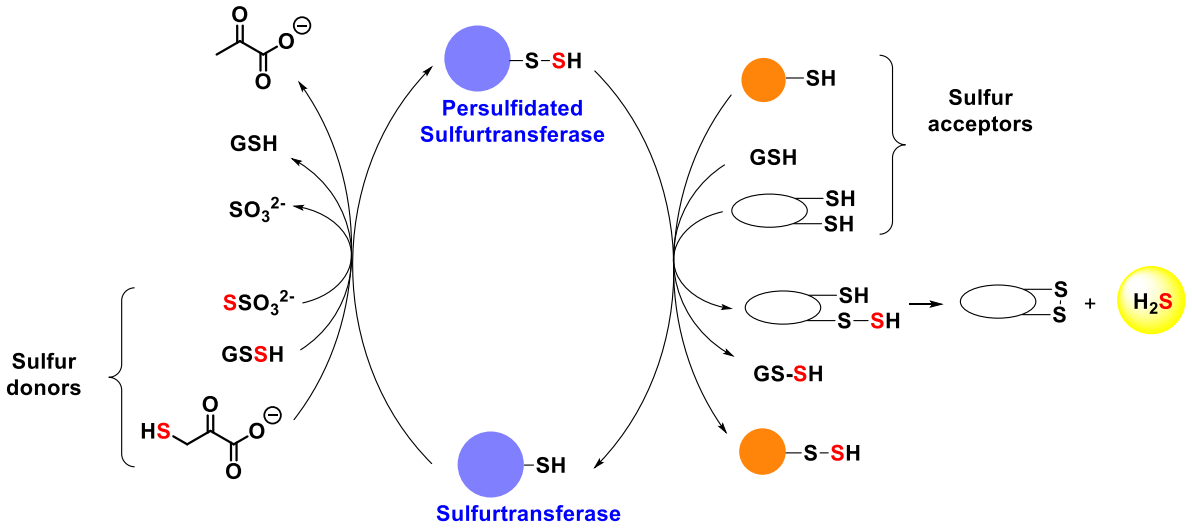

Figure 2. Substrate scope of sulfurtransferases and products.

3-Mercaptopyruvate sulfurtransferase (3-MST) plays a crucial role in sulfur metabolism by generating H_2S, persulfides, and polysulfides, *via* catalytic turnover of its natural substrate, 3-mercaptopyruvate (3-MP), contributing to sulfur trafficking and cellular signaling.[27,29–32] The activity of 3-MST is correlated with changes in its expression levels and is associated with certain pathophysiological processes.[33]

Protein persulfidation is an important signaling mechanism mediated by persulfides, supporting various physiological functions. However, persulfides are inherently unstable and rapidly undergo disproportionation in aqueous environments, making controlled *in situ* generation challenging.[34] Attempts to isolate persulfides have been largely unsuccessful, except for a few sterically hindered variants in organic media.[7] To better understand the intricate biochemistry of persulfides and their role in sulfur signaling, it is essential to develop persulfide generators or prodrugs. These generators should ideally be shelf-stable, cell-permeable, and capable of releasing active sulfur species in response to specific stimuli (Figure 3).

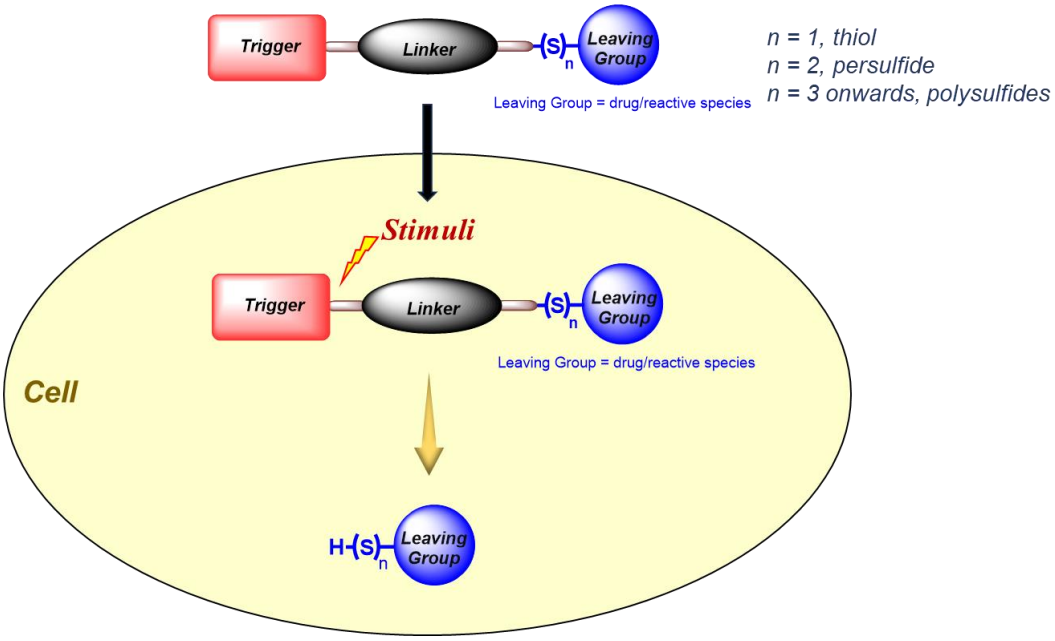

Figure 3. Prodrug strategy for intracellular generation of reactive sulfur species.

Using the aforementioned prodrug strategy, several persulfide generators have been developed using enzymes, light, ROS, pH, fluoride, and peroxynitrite as triggers.[7,35–37] However, persulfide generators reported so far have various limitations, including lack of trigger specificity, formation of potentially electrophilic byproducts,[38,39] and need of secondary assays for the detection of persulfide.[7,35,36]

Furthermore, the detection of persulfides has been a major challenge due to their inherent instability. However, several chemical tools or techniques, such as direct measurement, electrophilic trapping agents, labeling methods, and fluorescent probes, have been developed for the detection and quantification of persulfides.[6–8,35,36,40–42] These detection techniques are associated with certain limitations, such as poor selectivity between persulfides, thiols, and polysulfides, probe instability in cellular conditions, and quantification challenges due to collateral consumption of the persulfide during its detection.[7,35,36,41]

Therefore, the development of versatile persulfide generators along with byproducts that are non-electrophilic and/or fluorescent reporter is in urgent need**.**

To address these gaps, the goal was to design, synthesize, and evaluate persulfide generators that are cell-permeable, selectively triggerable, produce non-electrophilic byproducts, and include a fluorescence reporter for real-time monitoring, eliminating the need for secondary assays for detection of persulfide.

We considered the formation of a lactone as a key step in the generation of persulfide, and this strategy will generate persulfide along with a non-electrophilic lactone as a by-product upon activation by particular stimuli (Figure 4). Lactonization in such systems is reported to be quite rapid,[43,44] hence, persulfide generation will likely occur during lactonization, leading to a release of the persulfide as well as the by-product in a single molecular step.

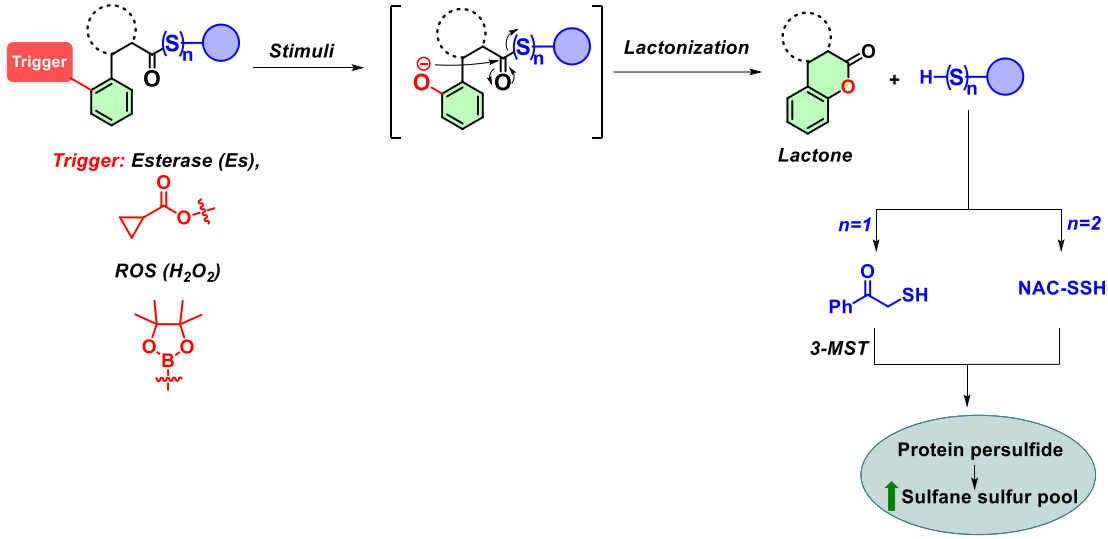

Figure 4. Design of persulfide generator using lactonization reaction with non-electrophilic lactone byproduct formation.

Based on the above design, in **Chapter 2,** using a biphenyl-based scaffold, an esterase-sensitive persulfide donor, along with a fluorescence reporter, was developed. Upon activation by esterase, it generates persulfide and a fluorescent lactone as a byproduct enabling the real-time monitoring of persulfide generation. The persulfide generator was able to protect the cells from the oxidative stress. Although this persulfide generator eliminates the need for secondary assays for persulfide detection, it suffered certain drawbacks, such as challenging synthesis and the disulfide bond being prone to nucleophilic attack. In **Chapter 3,** using similar biphenyl scaffold, we next prepared a compound that generates persulfide upon entry into cells. We utilized the persulfide biosynthetic machinery to develop an esterase-sensitive artificial substrate for the enzyme 3-mercaptopyruvate sulfurtransferase (3-MST). This compound effectively generated H_2S/persulfides in cells, enhancing antioxidant response in chondrocytes. To enhance the selectivity from a therapeutic benefit standpoint, in **Chapter 4.1**, a reactive oxygen species (ROS)-activated persulfide generator was developed by exploiting the 3-MST persulfide biogenesis. Similar biochemical assays were conducted to validate the H_2S/persulfide generation from the compound in the presence of H_2O_2. The

compound exhibited good *in vivo* anti-inflammatory response in animal model. In **Chapter 4.2,** we extended the same ROS system to another pharmacological thiol, and a WR-1065 prodrug, a known thiol-based radioprotectant, was developed. This prodrug was found to be activated by H_2O_2 to generate the lactone and the pharmacologically active thiol WR-1065.

Collectively, we have developed two distinct approaches for the generation of persulfide, along with non-electrophilic lactone byproducts, and some have an in-built fluorescence reporter. The approaches developed herein will help address important questions regarding the generation and detection of persulfides and understand their therapeutic utility.

Chapter 2. Real-Time Monitoring of Persulfide Generation

Persulfides are reactive, acidic, and have lower reduction potentials than thiols.[6,7] They are known to mitigate oxidative stress by preventing protein overoxidation and upregulating antioxidant genes via the KEAP1-Nrf2 axis,[14,45,46] with potential therapeutic applications for Parkinson's, Alzheimer's, and osteoarthritis.[7,9,47] However, their instability makes controlled generation in biological systems difficult. To address this, persulfide prodrugs activated by enzymes, light, ROS, pH, fluoride, and peroxynitrite have been developed,[7,35–37] some of them produce electrophilic byproducts that lead to electrophilic stress.[38,39] Detection of persulfides is also challenging due to their instability; there is a need for secondary detection assays.[7,35,36]

To overcome the need for secondary assays for the detection of the persulfides, the latent fluorophore strategy can be employed, which enables the real-time monitoring of the persulfide, i.e., a chemical tool that generates persulfide along with a fluorescence reporter (Figure 5.A).

Recently, a light-activated persulfide donor with a fluorescence reporter was developed, but its use is limited by electrophilic byproducts and challenges associated with light-based cellular experiments (Figure 5.B).[48] The lactonization strategy was considered to generate both a persulfide and a fluorophore in a single molecular step. A biphenyl-based system was designed, where esterase-mediated ester cleavage triggers rapid lactonization, simultaneously releasing the persulfide and producing a fluorescent lactone as a byproduct (Figure 5.C).[49,50]

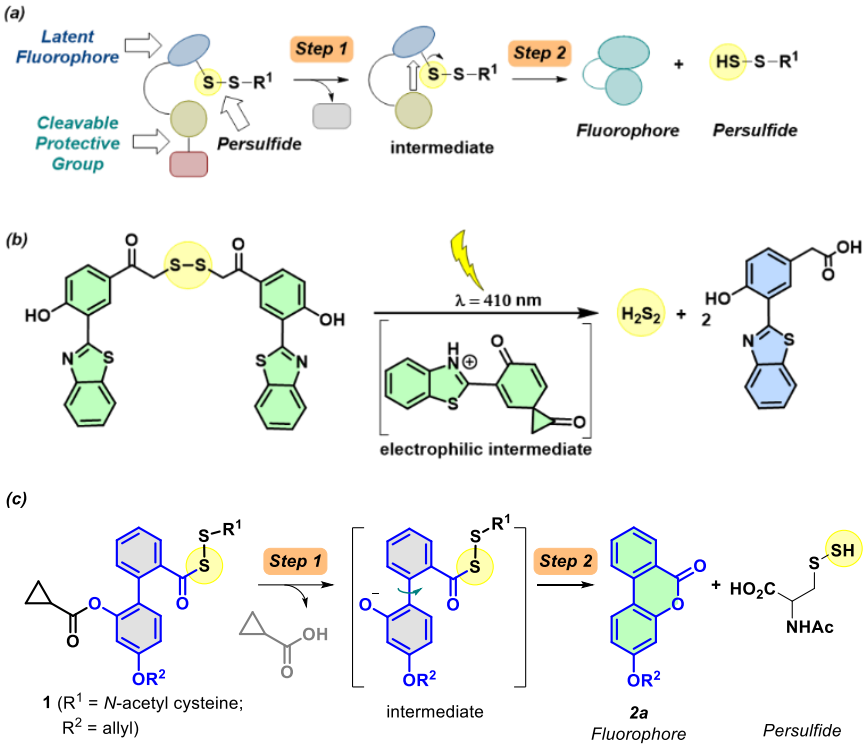

Figure 5. (A) General design for a cleavable persulfide donor with a fluorescence reporter. The first step is the cleavage of the protective group, which produces an intermediate that is then converted to a fluorophore and produces persulfide as a byproduct (B) Light-activated H_2S_2donor with a fluorescence reporter (C) Design of a biphenyl-based esterase-activated NAC persulfide generator.

Compound **1** was synthesized as the biphenyl-based esterase-activated persulfide donor in 18% yield. Firstly, the formation of lactone **2a** from **1** was monitored using fluorescence-based experiments. The compound was itself weakly fluorescent, but the addition of Es (1 U/mL) led to a significant increase in fluorescence intensity (48-fold) attributable to the formation of **2a** (λ_{ex} = 320 nm; λ_{em} = 432 nm) after incubation for 1 h in PBS (pH 7.4) (Figure 6.A). The dose-dependent studies demonstrated that the fluorescence corresponding to **2a** formation gradually increased over time and plateaued after 1 h (Figure 6.B). Further, the curve fitting for the **2a** formation to a first-order exponential equation yielded rate constants ranging from 0.047 to 0.073 min^{-1}(Table 1).

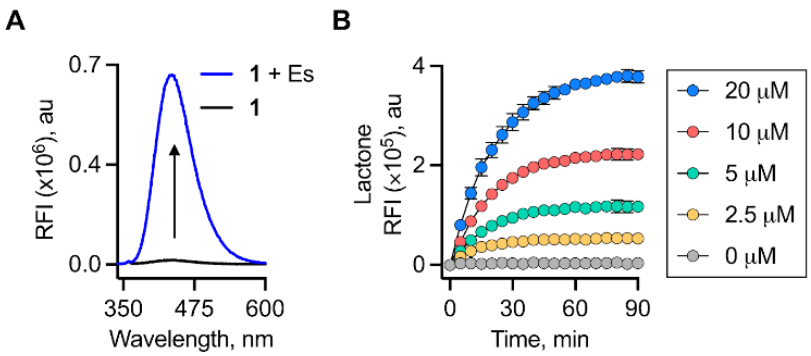

Figure 6. Monitoring the formation of lactone from **1** by fluorescence (λ_{ex} = 330; λ_{em} = 432) (A) at 20 μM without or with Es (1 U/mL) and (B) in a concentration-dependent manner (0-20 μM) with Es (1 U/mL) in pH 7.4 buffer at 37 °C.

Table 1. Rate constants and rates of **2a** formation and persulfide generation from **1**.

1 Conc. (μM)	**2a** formation ($\times 10^{-1}$ min^{-1})	Persulfide generation ($\times 10^{-1}$ min^{-1})		Rate of **2a** formation (μM min^{-1})	Rate of persulfide generation (μM min^{-1})	
		SSP2	mBBr		SSP2	mBBr
2.5	0.73	0.17	0.18	0.18	0.04	0.05
5	0.56	0.24	0.22	0.28	0.12	0.11
10	0.51	0.23	0.25	0.51	0.24	0.25
20	0.47	0.27	0.35	0.94	0.55	0.70

Once it was established that compound **1** can be cleaved by esterase and release lactone **2a** under physiological conditions, we next attempted to detect the release of the persulfide. from **1** using an electrophilic trapping agent (monobromobimane: **mBBr**)[51] and persulfide-specific fluorescent probes (**SSP2**).[52] Upon co-incubation of compound **1** with Es and **mBBr** (100 mM), a distinct time-dependent increase in fluorescence signal ((λ$_{ex}$ = 380 nm; λ$_{em}$ = 455 nm) corresponding to the **NAC-SS-bimane** was observed over 60 min (Figure 7.A). When the varying concentrations of compound **1** was co-incubated with Es and **SSP2**, a significant dose-dependent enhancement in the fluorescence intensity (λ$_{ex}$ = 482 nm; λ$_{em}$ = 518 nm), corresponding to the generation of sulfane sulfur was observed over a period of 90 min (Figure 7.B).

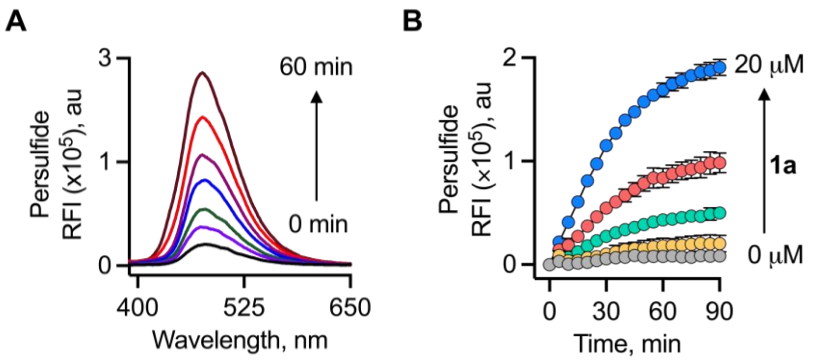

Figure 7. Detection of persulfide released from (A) **1** (100 μM) over 60 min with Es (1 U/mL) and **mBBr** (100 μM) after 60 min and (B) varying concentrations of **1** (0-20 μM) upon co-treatment of Es (1 U/mL) and **SSP2** (10 μM) over 90 min.

To establish a correlation between the lactone (**2a**) and persulfide formation (**SSP2**) from **1**, the maximum fluorescence change at 90 min was considered as the plateau was reached. These fluorescence values were normalized and then plotted. An excellent correlation between the two parameters was observed, suggesting that the release of fluorophore **2a** and NAC persulfide occur nearly concurrently following esterase-mediated cleavage of **1** and subsequent lactonization (Figure 8.A).

Similarly, the rates of persulfide generation as determined by **SSP2** and rates of **2a** formation (Table 1) from the varying concentrations of **1** were compared. A good linear correlation between the rates of persulfide and **2a** formation was observed (R^2 = 0.99) at concentrations ranging from 2.5 to 20 μM (Figure 8.B). Taken together, these data show that the fluorescence signal produced can be used as a proxy for persulfide production.

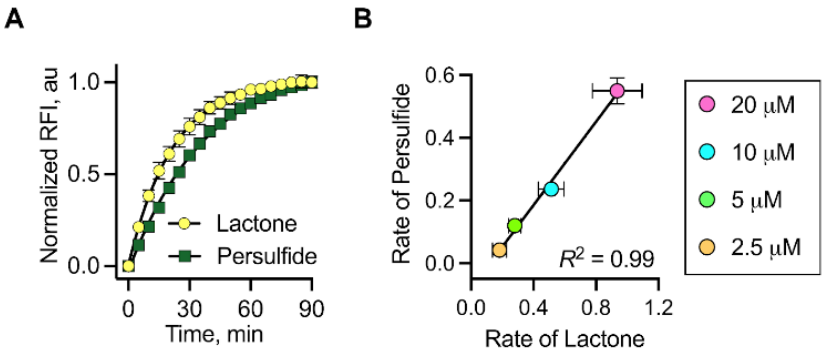

Figure 8. (A) Correlation between change in fluorescence corresponding to the formation of lactone and persulfide formed upon incubation of **1** (20 μM) with Es (1 U/mL) and **SSP2** (10 μM). (B) Correlation between the rates of lactone and persulfide formation upon treatment of **1** (2.5, 5, 10, and 20 μM) with Es (1 U/mL) in the presence of **SSP2** (10 μM)**.**

As compound **1** generates both a persulfide and fluorogenic lactone **2a**, it was evaluated for intracellular activation using confocal microscopy. Since **2a** is compatible with two-photon imaging,[53] offering advantages like deep tissue penetration and reduced photobleaching, MEF cells were treated with 50 μM of **1** for 4 h, followed by two-photon confocal imaging. The fluorescence signal attributable to **2a** formation from **1** was observed (λ_{ex} = 700 nm; λ_{em} = 432 nm) (Figure 9). Together, these results support that compound **1** is able to generate **2a** in the presence of cellular esterase.

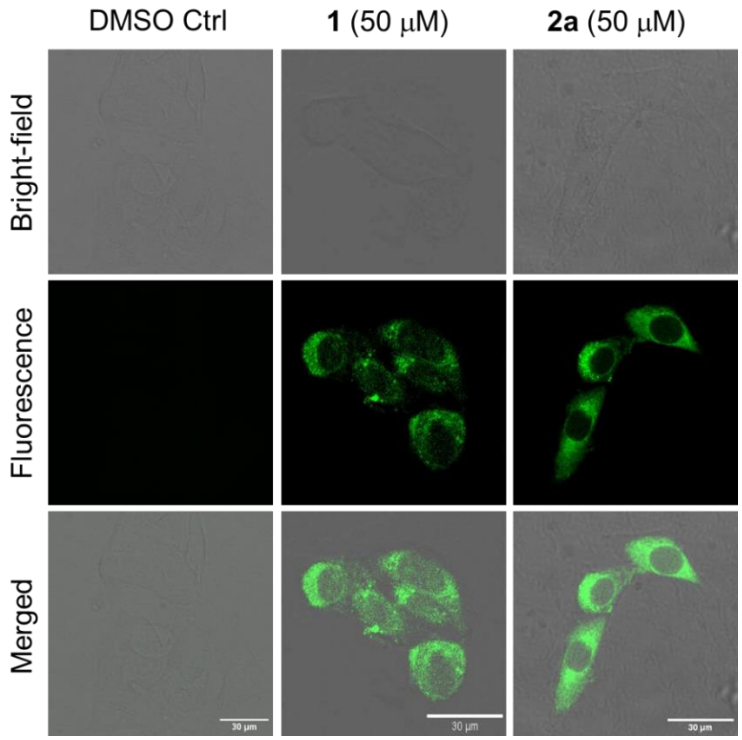

Figure 9. Two-photon confocal microscopy images of MEF cells treated with **1** and **2a** (50 μM). The excitation and emission channels were 700 nm and 432 nm, respectively. Scale bar is 30 μm.

The cytoprotective effect of persulfide donor **1** against oxidative stress was evaluated in MEF cells. Oxidative stress was induced using the ROS generator **MGR-1**,[54] and the ROS levels were measured using the **H_2-DCF-DA** assay. Cells pre-treated with 25 or 50 μM of **1** showed a dose-dependent reduction in fluorescence intensity, indicating decreased ROS levels and supporting the cytoprotective role of compound **1** (Figure 10).

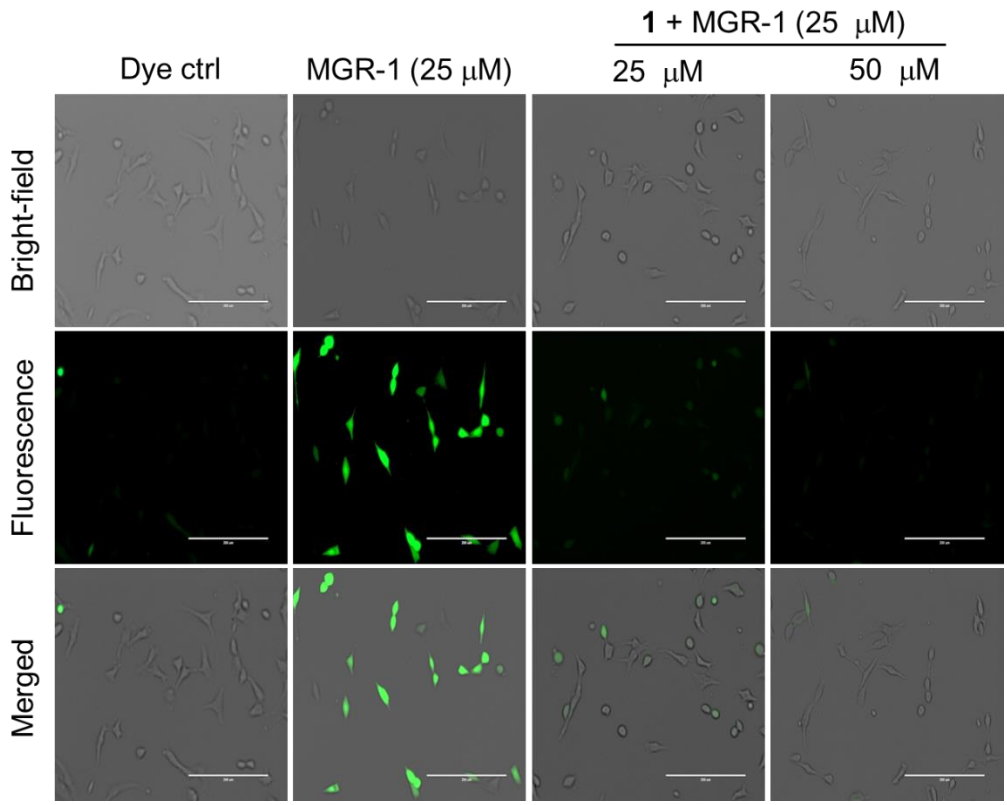

Figure 10. MEF cells were treated with varying concentrations of **1** (25 μM and 50 μM) for 4 h, followed by treatment with **MGR-1** (25 μM) for 1 h. Intracellular ROS levels were detected using DCF dye (10 μM). The cells were imaged in the 20× GFP filter. Scale bar is 200 μm.

Overall, a new probe, **1**, was developed to release persulfide and non-electrophilic fluorophore **2a** upon esterase activation in a single step, enabling real-time monitoring of the persulfide generation.

Chapter 3. Development of Esterase-Triggered Persulfide Generator *via* 3-MST Pathway

In **Chapter 2**, the development of **1**, a small molecule for real-time monitoring of persulfide generation, was described. However, **1** had limitations, including challenging synthesis and non-specific reactions due to disulfide bond susceptibility to thiols. To address these limitations, an enzymatic approach for persulfide generation was explored.

One of the important enzymes involved in persulfide biogenesis is the H_2S-producing enzyme, 3-mercaptopyruvate sulfurtransferase (3-MST), a member of the sulfurtransferase family. It catalyzes the transfer of sulfur from 3-mercaptopyruvate (3-MP) to form a transient persulfide intermediate on its active site cysteine, producing an enolate of pyruvate as a byproduct.[25,27]

The persulfide sulfur can then be transferred to small molecular thiols or target proteins or reduced by thioredoxin (Trx) to generate H_2S (Figure 11.A).[55]

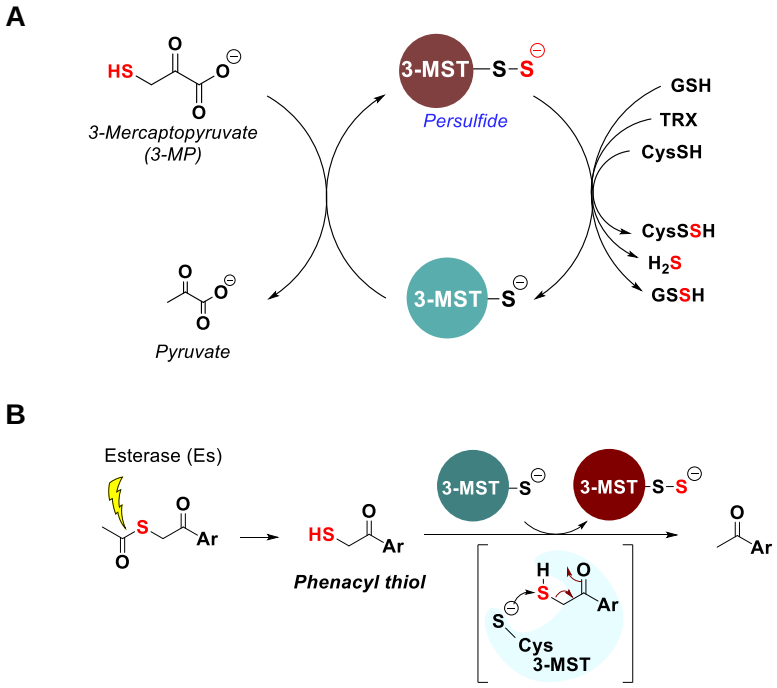

Figure 11. (A) Reaction mechanism for turnover of 3-mercaptopyruvate (3-MP) by 3-mercaptopyruvate sulfurtransferase (3-MST) to form a transient 3-MST persulfide intermediate and pyruvate as the byproduct. The 3-MST persulfide can undergo reduction to generate H_2S or transfer the sulfur to other acceptor proteins or small molecule thiol. (B) 3-MST artificial substrate developed in our lab.

The natural 3-MST substrate, 3-MP, generates H_2S non-enzymatically, which can be a potential limitation for its use.[55] To address this, a phenacyl thiol-based artificial substrate was developed, mimicking 3-MP while facilitating 3-MST persulfide formation and contributing to cellular persulfidation and H_2S generation (Figure 11.B).[56] To improve stability, thiols were protected as thioacetates, which can be deprotected by esterase. A library of artificial substrates was created, evaluated for H_2S and persulfide generation, and tested for antioxidant and anti-inflammatory properties in cellular and animal models.[56]

Leveraging the biphenyl-based NAC persulfide donor **1**, an esterase-sensitive 3-MST artificial substrate donor **11** was developed, which generates the lactone **2a** and the artificial substrate **13** in the presence of Es (Scheme 1). Then, **13** gets turned over by 3-MST to generate 3-MST persulfide.

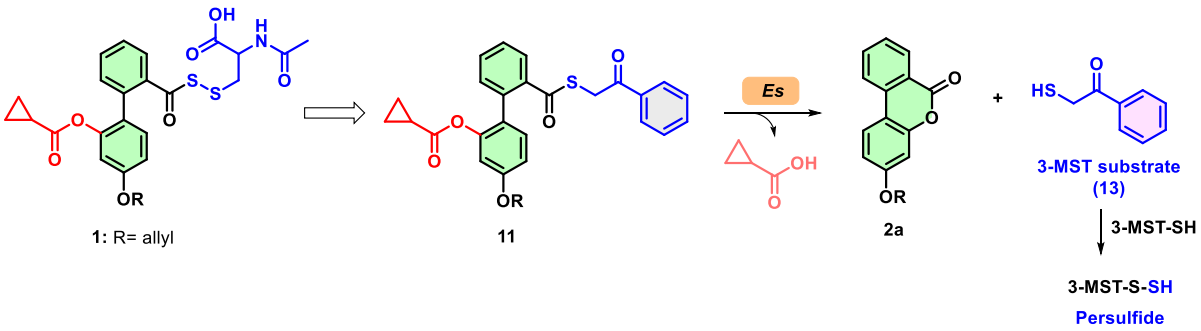

Scheme 1. Design of biphenyl-based esterase-triggered 3-MST artificial substrate.

Compound **11** was synthesized as the biphenyl-based esterase-triggered 3-MST artificial substrate in 20% yield. Compound **11**, in the presence of esterase, led to an enhancement in the fluorescence signal (λ_{ex} = 320 nm; λ_{em} = 432 nm), corresponding to the formation of **2a** (Figure 12).

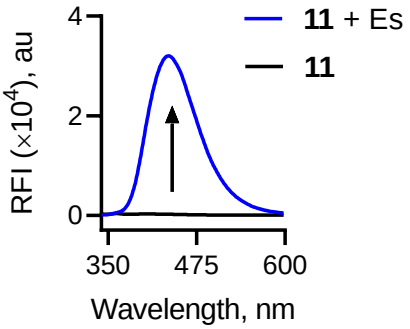

Figure 12. Monitoring the formation of lactone (**2a**) from **11** (10 μM) by fluorescence (λ_{ex} = 330 nm; λ_{em} = 432 nm) with or without Es (1 U/mL) in pH 7.4 PBS at 37 °C.

The decomposition of compound **11** in the presence of Es was studied using HPLC. The complete disappearance of **11** was observed within 60 minutes, with the formation of fluorophore **2a** and 3-MST artificial substrate **13**. From HPLC analysis, quantitative formation of **2a** and **13** was observed (Figure 13).

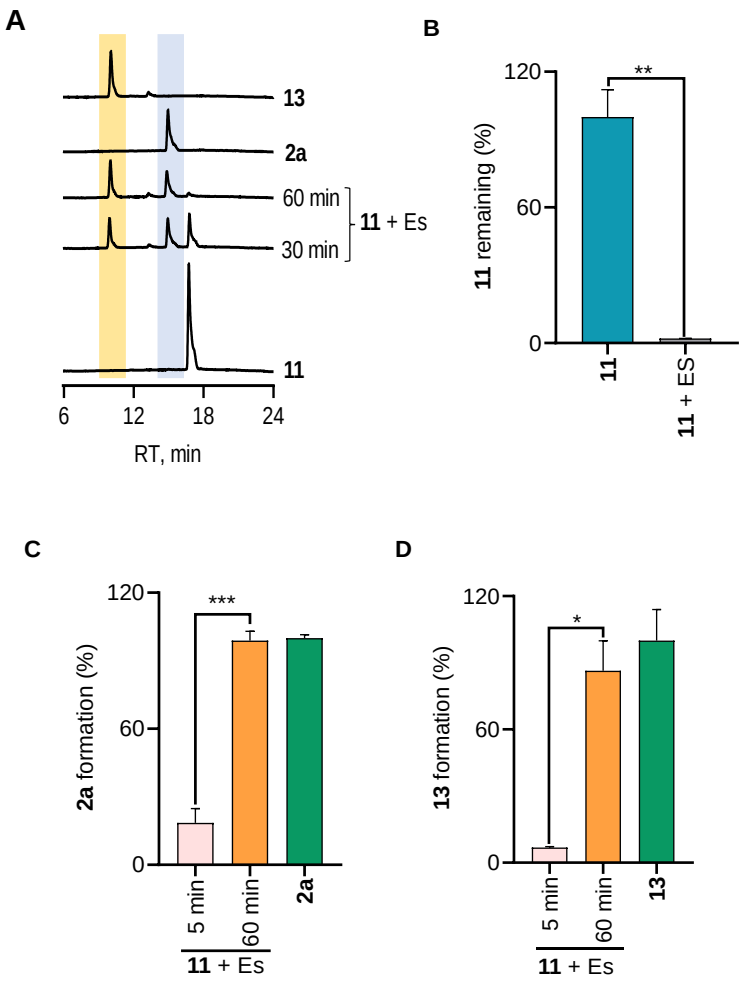

Figure 13. (A) HPLC traces for decomposition of **11** (25 μM) **a**nd formation of **2a** and **13** in the presence of Es (1 U/mL) (Abs = 250 nm) over 60 min. Area under the curve (AUC) for the peak corresponding to the (B) **11** remaining, (C) formation of **2a**, and (D) formation of **13** from **11** as monitored by HPLC. (Abs = 250 nm). Statistical significance was carried out using One-way ANOVA(*$p < 0.033$, **$p < 0.002$, *** $p \leq 0.001$).

Next, the formation of 3-MST persulfide and sulfane sulfur from **11** in the presence of Es and 3-MST was validated using the reported turn-on fluorescence probe **SSP2** (Figure 14.A).[52] The H_2S releasing efficiency of compound **11** in the presence of Es, 3-MST, and **DTT** was screened by performing lead acetate and methylene blue experiments (Figure 14.B and 14. C).[56] When H_2S releasing data of compounds **11** and **2a** were compared with **12**, **11** was able to produce a significant amount of H_2S, whereas, as expected, no signal from negative control **2a** was observed.

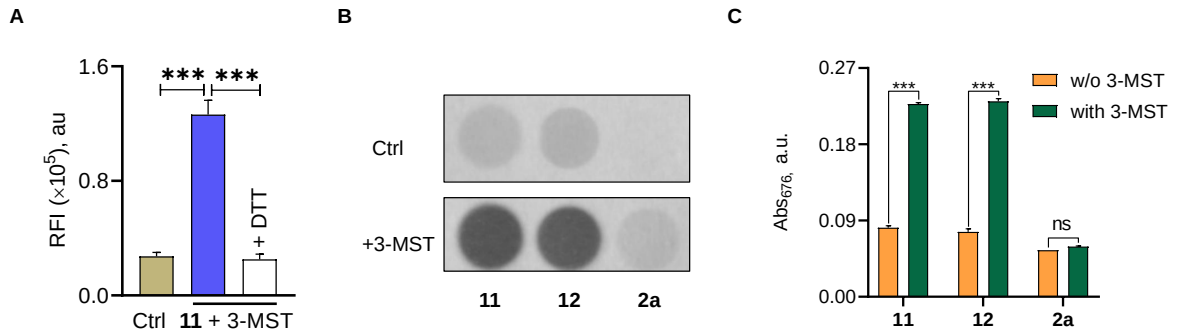

Figure 14. (A) Sulfane sulfur detection with **11** (10 μM) in the presence of *b*3-MST (1 μM), Es (1 U/mL) using **SSP2** (5 μM) based fluorescent assay. Ctrl: **11** only. +DTT: addition of DTT. λ_{ex}=482 nm and λ_{em}=518 nm. H_2S detection from compounds (**11**, **12**, and **2a** at 100 μM) in the presence of *b*3-MST (1 μM), Es (1 U/mL), and **DTT** (10 mM) for 2 h using (B) lead acetate assay. Ctrl represents only compounds. +3-MST refers to the incubation with 3-MST. **12** was used as a positive control, **2a** as a negative control, and (C) using methylene blue assay. Results are expressed as mean ± SD (n =3/group). Statistical significance was carried out using One-way ANOVA (*** $p \leq 0.001$).

Next, sulfane sulfur transfer from the 3-MST persulfide generated from **11** in the presence of Es and 3-MST to **GSH**, as the corresponding HPE-IAM adducts (**GSS-HPE-AM** and **Bis-S-HPE-AM**) were detected *via* LC/MS analysis, confirming the GS-SH persulfide and H_2S formation (Scheme 2).[57]

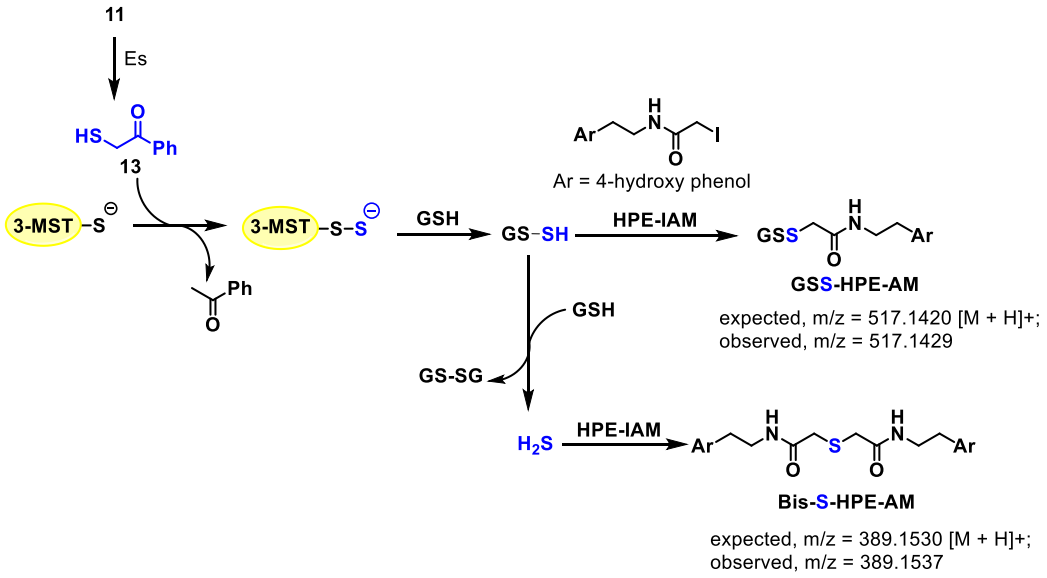

Scheme 2. LC/MS study. Reaction scheme showing the formation of **GSS-HPE-AM** and **Bis-S-HPE-AM** adducts from **11** in the presence of Es, 3-MST, and sulfur acceptor thiol GSH.

The cytoprotective effect of persulfide donor **11** against oxidative stress was evaluated in chondrocytes, a model cell line used to study osteoarthritis (OA).[58]. Pre-treatment of cells with **11** demonstrated significant protective effects from **MGR-1**-induced oxidative stress in a concentration-dependent manner (Figure 15) (Chondrocytes data was provided by Dr. Rachit Agarwal's Lab, Department of Bioengineering, IISc Bangalore).

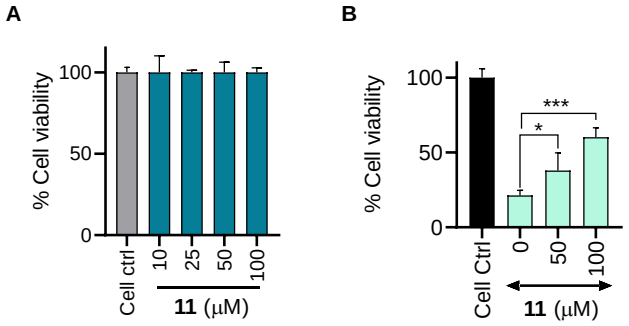

Figure 15. Cell viability assay conducted on C28/I2 cells. (A) Cells treated with varying concentrations of compound **11** for 24 h. (B) Cells treated with varying concentrations of **11** followed by treatment with **MGR-1** (15 μM). All data are presented as mean ± SD (n = 4/group). Statistical significance was established relative to **MGR-1** using One-way ANOVA (* $p < 0.033$, *** $p \leq 0.001$).

Overall, an esterase-sensitive persulfide generator **11** *via* the 3-MST pathway was developed. Compound **11** was able to enhance H_2S and sulfane sulfur in the presence of Es and 3-MST and demonstrated antioxidant property in chondrocytes.

Chapters 2 and **3** detailed the development of esterase-activated persulfide generators, but the ubiquitous nature of esterase limits the selectivity. To address this, a ROS-activated (H_2O_2) persulfide generator was designed, utilizing elevated ROS levels as a trigger for specific activation and controlled release of the active species. A boronate ester group was used as a trigger to develop ROS-activated persulfide generators. However, the attempts to develop biphenyl-based ROS-activated persulfide generators were unsuccessful due to the synthesis difficulty and complexity. An alternate strategy for persulfide generators with non-electrophilic byproduct formation was considered.

Lukesh and co-workers have developed an H_2O_2-responsive persulfide generator (**RAH393**), which undergoes intramolecular cyclization upon activation to release persulfide and a benign lactone byproduct (Figure 16.A).[59] The **RAH393** scaffold was explored for developing persulfide generators (**Chapter 4.1**) and masked drugs (**Chapter 4.2**) to expand its potential applications (Figure 16.B).

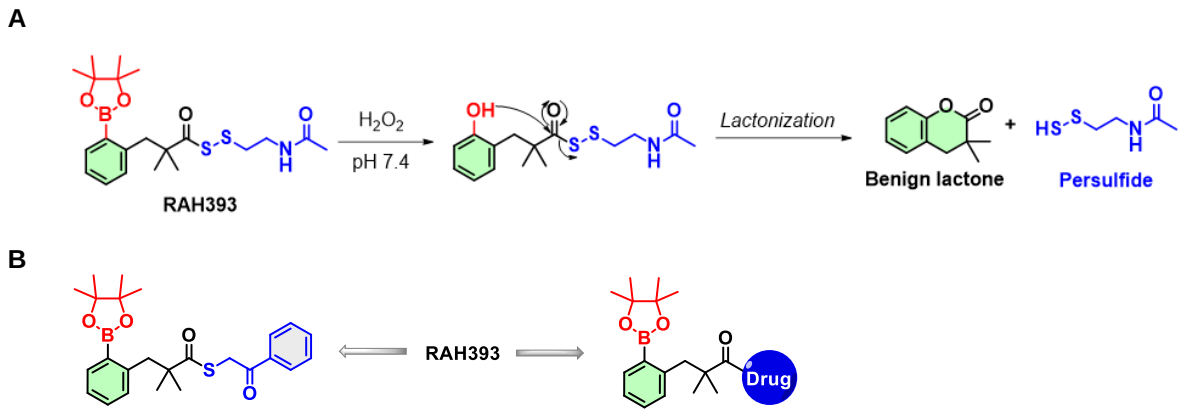

Figure 16. Development of ROS-activated persulfide donor and drug release sensitive to H_2O_2 based on **RAH393**.

Chapter 4.1. Development of ROS-activated Persulfide Generator Through 3-MST Pathway

Using the **RAH393** scaffold, a ROS-activated 3-MST artificial substrate **14** was developed. Upon activation by H_2O_2, compound **14** generates the 3-MST artificial substrate **13** and benign lactone **15** as a byproduct (Scheme 3).

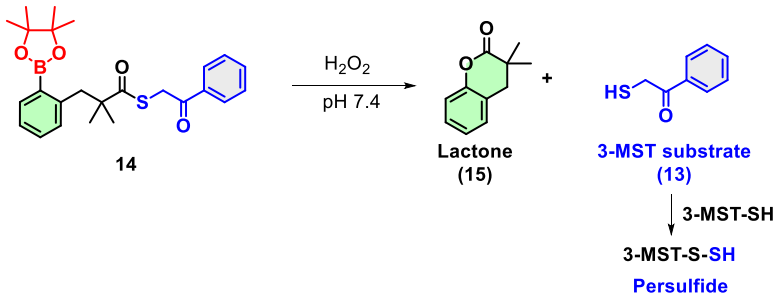

Scheme 3. Design of ROS-activated 3-MST artificial substrate donor.

Compound **14** was synthesized as the ROS-activated 3-MST artificial substrate in 21% yield. LC/MS analysis of compound **14** treated with H_2O_2 showed the formation of phenacyl thiol **13** (expected m/z = 153.0369 $[M + H]^+$; observed m/z = 153.0365, RT = 13.6 min) and lactone **15** (expected m/z = 177.0910 $[M + H]^+$; observed m/z = 177.0904, RT = 12.6 min) (Figure 17 and 18). Additionally, a broad peak with the same mass as lactone **15** mass was observed around 8.0 min, which increased over the period (Figure 18.A). This suggests further decomposition of lactone **15** due to excess H_2O_2, forming intermediates as proposed in Scheme 4. Protonation of Intermediate **II** by formic acid present in the water, an eluant in the LC/MS, leads to intermediate **V**, an open-form of lactone. A control reaction with H_2O_2-

treated lactone **15** produced a similar broad peak, confirming cleaved lactone formation (Figure 18.A).

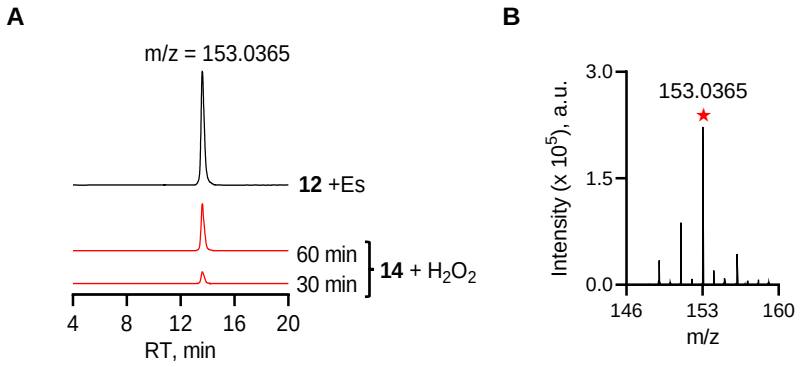

Figure 17. LC/MS study. (A) Extracted ion chromatograms for the formation of phenacyl thiol **13** and (B) Mass spectra for **13** (expected m/z = 153.0369 $[M + H]^+$; observed m/z = 153.0365) from **14** in the presence of H_2O_2.

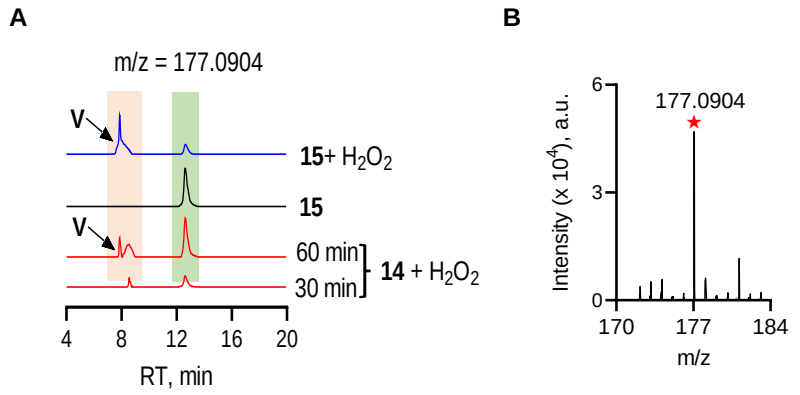

Figure 18. LC/MS study. (A) Extracted ion chromatograms for the formation of lactone **15** and (B) Mass spectra for **15** (expected m/z = 177.0910 $[M + H]^+$; observed m/z = 177.0904), from **14** in the presence of H_2O_2.

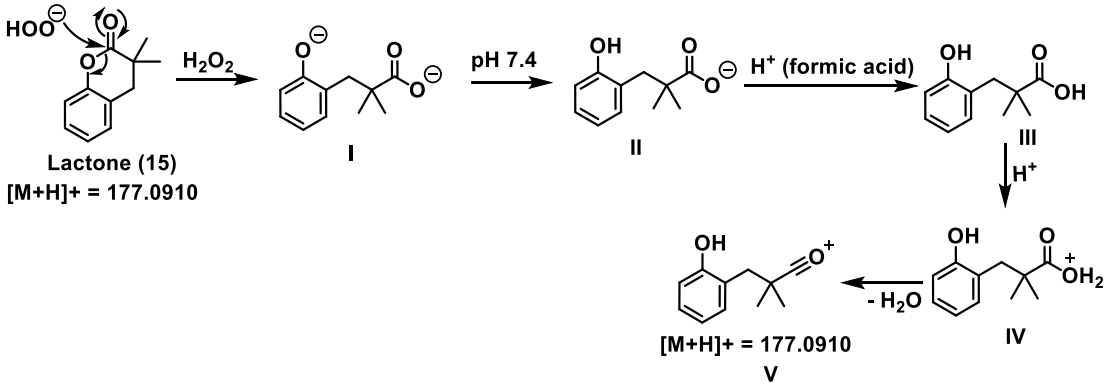

Scheme 4. Lactone **15** in the presence of excess H_2O_2.

Next, the formation of 3-MST persulfide and sulfane sulfur from **14** in the presence of H_2O_2 and 3-MST was validated using the reported turn-on fluorescence probe **SSP2** (Figure 19.A).[52] The generation of H_2S from compound **14** in the presence of H_2O_2, 3-MST, and DTT was monitored by using lead acetate and methylene blue experiments (Figures 19.B and 19.C).[56]

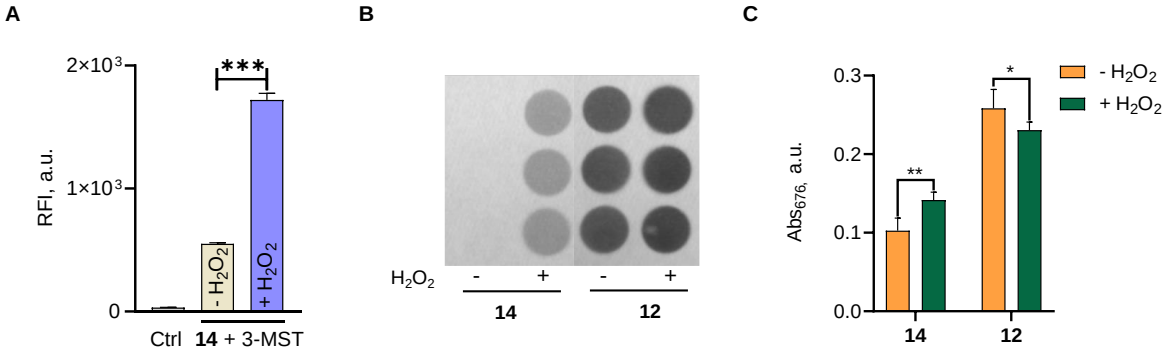

Figure 19. (A) Sulfane sulfur detection with **14** (100 μM) in the presence of *b*3-MST (10 μM), H_2O_2 (10 mM) using **SSP2** (50 μM) based fluorescent assay (λ_{ex}=482 nm and λ_{em}=518 nm). Ctrl: **14** only; + H_2O_2 or -H_2O_2: presence or absence of H_2O_2. H_2S detection from compounds (**14** and **12** at 100 μM) in the presence of *b*3-MST (1 μM), H_2O_2 (10 mM), and **DTT** (10 mM) for 2 h using (B) Lead acetate assay. **12** was used as a positive control, and (C) using methylene blue assay. Results are expressed as mean ± SD (n =3/group). Statistical significance was carried out using One-way ANOVA (*$p < 0.033$, **$p < 0.002$,*** $p \leq 0.001$).

Next, sulfane sulfur transfer from the 3-MST persulfide generated from **14** in the presence of H_2O_2 and 3-MST to **GSH**, as the corresponding HPE-IAM adducts (**GSS-HPE-AM** and **Bis-S-HPE-AM**) were detected *via* LC/MS analysis, confirming the GS-SH persulfide and H_2S formation (Scheme 5).[57]

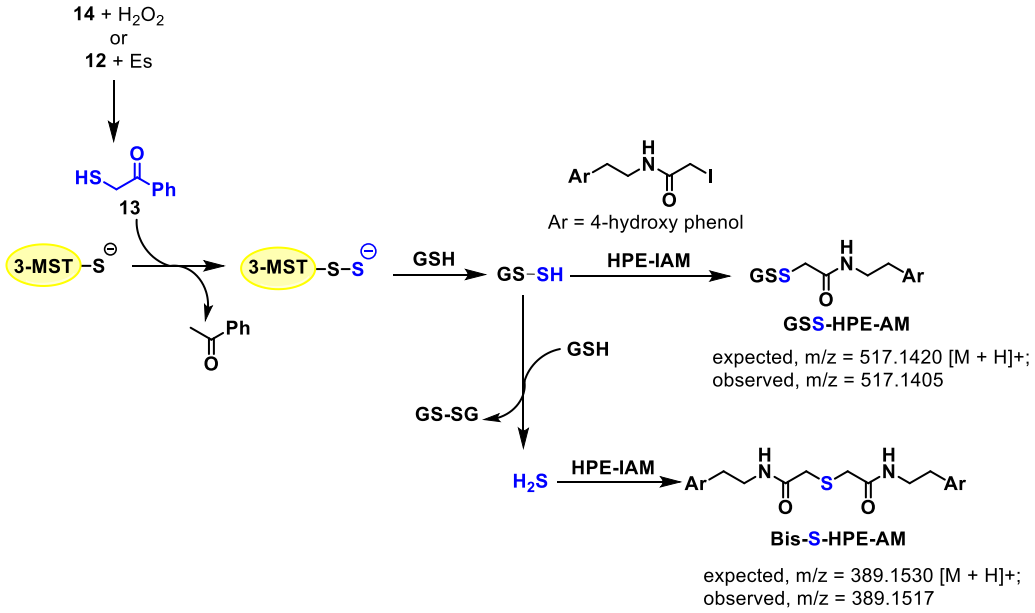

Scheme 5. LC/MS study. The reaction scheme showing the formation of **GSS-HPE-AM** and **Bis-S-HPE-AM** adducts from **14** in the presence of H_2O_2, 3-MST, and sulfur acceptor thiol GSH. **12** was used as a positive control in the presence of Es, 3-MST, and GSH.

Persulfides and polysulfides are known for their anti-inflammatory properties.[16,17] To investigate this, a mouse endotoxin shock model was used, where **LPS** induced pro-inflammatory cytokines (TNF-α, IL-6) *via* toll-like receptors.[17,56] Mice treated with compound **14** (20 mg/kg) before and after **LPS** administration (5 mg/kg) showed a significant reduction in cytokine levels compared to the **LPS**-only group (Figure 20). Overall, these results indicate that compound **14** exhibited good *in vivo* anti-inflammatory property.

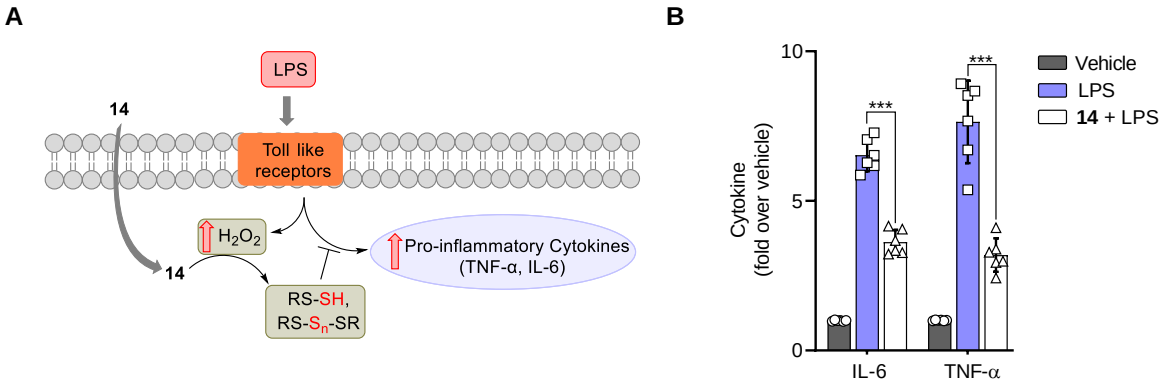

Figure 20. (A) LPS-induced pro-inflammatory cytokines and anti-inflammatory properties of persulfide and polysulfides. (B) Pro-inflammatory cytokines, TNF-α, and IL-6 measurement using a standard ELISA assay. All data are presented as mean ± SD (n = 6 per group). Statistical significance was carried out using One-way ANOVA (***p < 0.001 *vs.* LPS). The

LPS experiment was performed with the help of Simran Gupta (Prof. Harinath Chakrapani Lab, IISER Pune).

Overall, ROS-activated persulfide generator **14** through the 3-MST pathway was developed. Compound **14** was able to enhance H_2S and sulfane sulfur upon activation by H_2O_2 and 3-MST and demonstrated good *in vivo* anti-inflammatory property.

Chapter 4.2. Design and Development of ROS-triggered WR1065 Donor

In previous **Chapter 4.1,** the development of the ROS-activated persulfide generator was discussed. Next, this strategy was extended for the development of the ROS-triggered prodrug (Figure 4.2.1), which produces lactone **15** and the active drug upon activation by H_2O_2. In order to achieve this goal, the known thiol-based radioprotectant **WR-1065**, the active form of the drug amifostine, was considered.

Amifostine (**WR-2721**) is a clinically approved chemoprotective and radioprotective drug. It is an organic thiophosphate that, upon hydrolysis by alkaline liver phosphatase (ALP), generates the active thiol **WR-1065** (Figure 21),[60,61] which provides cytoprotection by detoxifying cytotoxic drugs, scavenging free radicals, and aiding in DNA repair.[62,63] Its selectivity arises from normal tissues metabolizing the drug more effectively than tumor tissues.

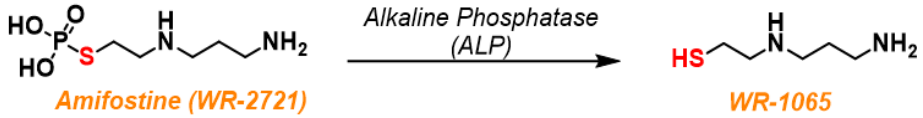

Figure 21. Activation of amifostine by ALP to produce active **WR-1065**.

By leveraging the ROS scaffold, a ROS-triggered WR-1065 donor **20** was developed. Upon activation by H_2O_2, compound **20** generates the active thiol **WR-1065** and benign lactone **15** as a byproduct (Scheme 6).

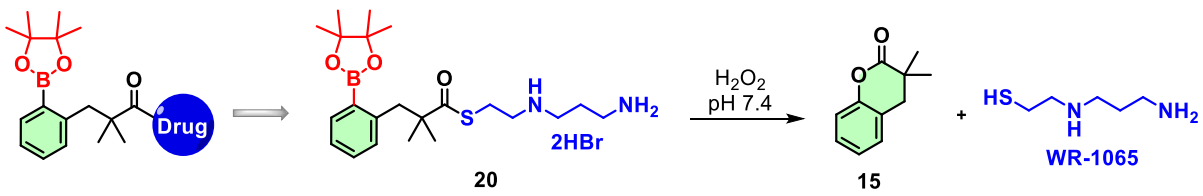

Scheme 6. Design of the ROS-triggered **WR-1065** donor.

The desired molecule **20** was synthesized in three steps. The previously synthesized carboxylic acid derivative in **Chapter 4.1** was converted into the thiocarboxylic acid **19** using Lawesson's reagent[59] and then reacted with the bromide compound **22** in the presence of the Et_3N to yield the Cbz-protected **WR-1065** compound **23** in 19% yield. Finally, using a reported protocol with some modifications,[64] the Cbz group was deprotected using HBr/AcOH to produce the ROS-activated **WR-1065** donor **20** as a hydrobromide salt in 45% yield (Scheme 7).

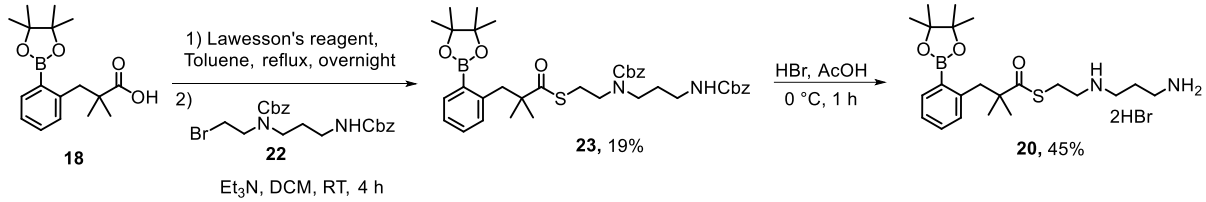

Scheme 7. Synthesis of ROS-triggered **WR-1065** donor **20**.

Next, an electrophilic trapping experiment using **mBBr** was conducted to trap the thiol **WR-1065**, upon activation of **20** in the presence of H_2O_2, as discussed in the previous **Chapter 4.1** (Scheme 8).

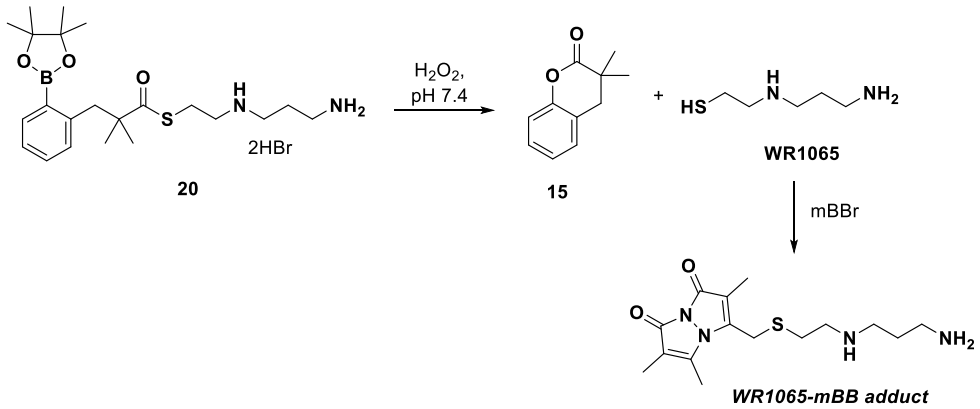

Scheme 8. Formation of the **WR1065-mBB** adduct when **20 (**100 μM) co-incubated with 100 equiv. of H_2O_2 and **mBBr** (100 μM).

In this assay, the compound **20** (100 μM) was co-incubated with 100 equiv. of H_2O_2 and 100 μM **mBBr** in pH 7.4 PBS containing 100 μM diethylenetriaminepentaacetic acid (DTPA). The mass corresponding to the formation of **WR1065-mBB** adduct (expected, m/z = 325.1693 $[M + H]^+$; observed, m/z = 325.3272) was observed by MALDI analysis (Figure 22). Overall, MALDI analysis suggests, compound **20** was able to generate the lactone **15** and the thiol **WR-1065** in the presence of H_2O_2

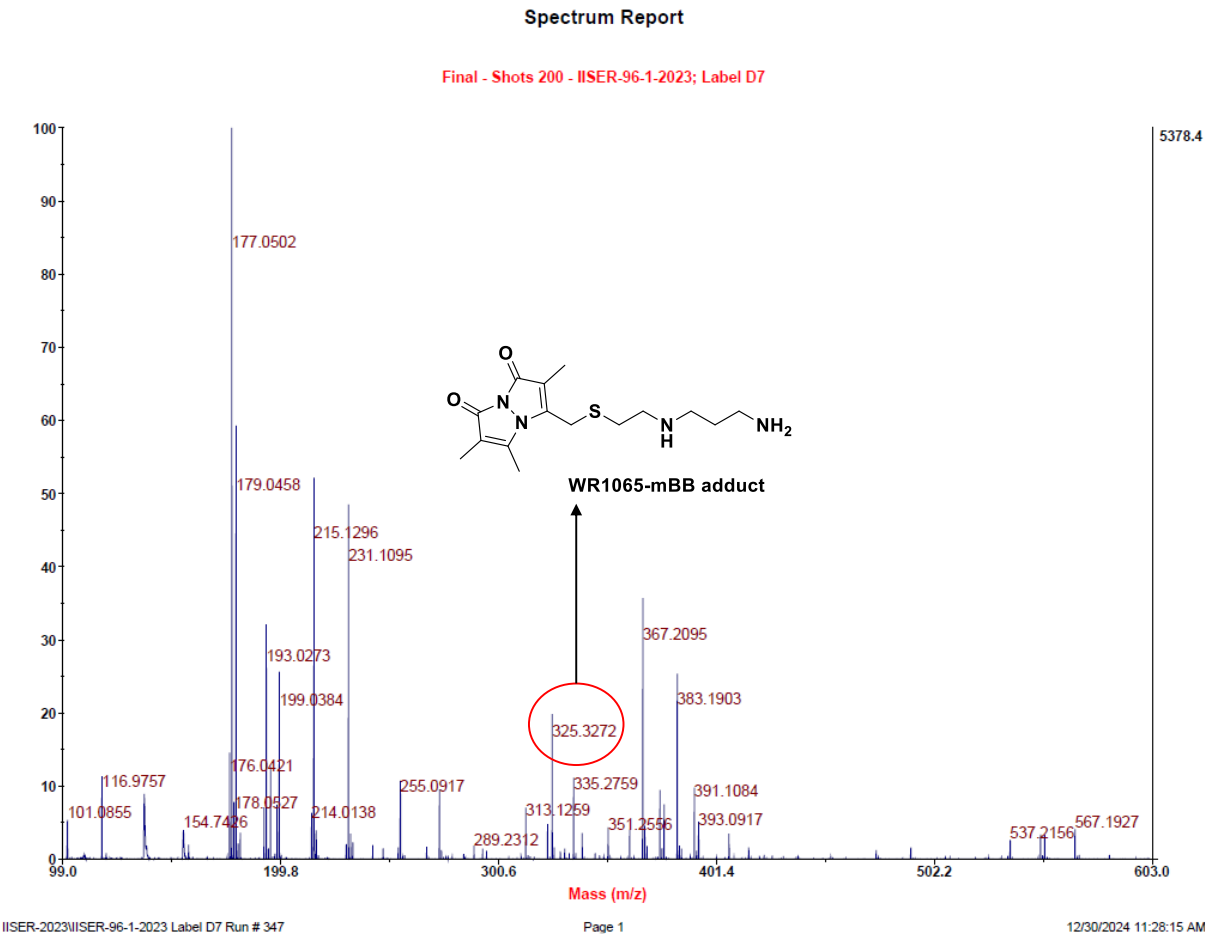

Figure 22. MALDI analysis for the formation of **WR1065-mBB** from **20** in the presence of H_2O_2 and **mBBr**. For **WR1065-mBB** (expected, m/z = 325.1693 $[M + H]^+$; observed, m/z = 325.3272).

Overall, ROS-triggered WR-1065 donor **20** was developed Upon activation by H_2O_2, **20** produces active drug **WR-1065** and a benign lactone **15**. Further experiments to evaluate and validate the activation of **20** in the presence of H_2O_2 are in progress.

Altogether, the studies described in this thesis address several awaited problems associated with the existing persulfide generators, such as triggerable, site-specific delivery of persulfide, benign byproducts, and real-time monitoring of persulfide in cells. The approaches developed herein will help address important questions regarding the generation and detection of persulfides and understand their therapeutic utility.

References:

(1) Gallyas, F. Involvement of Redox-signalling in Endogenous Hydrogen Sulfide Production. *Br. J. Pharmacol.* **2012**, *166* (8), 2228–2230.

(2) Stein, A.; Bailey, S. M. Redox Biology of Hydrogen Sulfide: Implications for Physiology, Pathophysiology, and Pharmacology. *Redox Biol.* **2013**, *1* (1), 32–39.

(3) KIMURA, H. Hydrogen Sulfide and Polysulfides as Signaling Molecules. *Proc. Japan Acad. Ser. B* **2015**, *91* (4), 131–159.

(4) Singh, S.; Lin, H. Hydrogen Sulfide in Physiology and Diseases of the Digestive Tract. *Microorganisms* **2015**, *3* (4), 866–889.

(5) Xie, Z.-Z.; Liu, Y.; Bian, J.-S. Hydrogen Sulfide and Cellular Redox Homeostasis. *Oxid. Med. Cell. Longev.* **2016**, *2016* (1).

(6) Park, C. M.; Weerasinghe, L.; Day, J. J.; Fukuto, J. M.; Xian, M. Persulfides: Current Knowledge and Challenges in Chemistry and Chemical Biology. *Mol. Biosyst.* **2015**, *11* (7), 1775–1785.

(7) Filipovic, M. R.; Zivanovic, J.; Alvarez, B.; Banerjee, R. Chemical Biology of H 2 S Signaling through Persulfidation. *Chem. Rev.* **2018**, *118* (3), 1253–1337.

(8) Yang, C.; Devarie-Baez, N. O.; Hamsath, A.; Fu, X.; Xian, M. S-Persulfidation: Chemistry, Chemical Biology, and Significance in Health and Disease. *Antioxid. Redox Signal.* **2020**, *33* (15), 1092–1114.

(9) Mustafa, A. K.; Gadalla, M. M.; Sen, N.; Kim, S.; Mu, W.; Gazi, S. K.; Barrow, R. K.; Yang, G.; Wang, R.; Snyder, S. H. HS Signals through Protein S-Sulfhydration. *Sci. Signal.* **2009**, *2* (96).

(10) Paulsen, C. E.; Carroll, K. S. Cysteine-Mediated Redox Signaling: Chemistry, Biology, and Tools for Discovery. *Chem. Rev.* **2013**, *113* (7), 4633–4679.

(11) Filipovic, M. R. *Persulfidation (S-Sulfhydration) and H 2 S*; 2015.

(12) Dóka, É.; Ida, T.; Dagnell, M.; Abiko, Y.; Luong, N. C.; Balog, N.; Takata, T.; Espinosa, B.; Nishimura, A.; Cheng, Q.; Funato, Y.; Miki, H.; Fukuto, J. M.; Prigge, J. R.; Schmidt, E. E.; Arnér, E. S. J.; Kumagai, Y.; Akaike, T.; Nagy, P. Control of Protein Function through Oxidation and Reduction of Persulfidated States. *Sci. Adv.* **2020**, *6*

(1).

(13) Zhao, K.; Ju, Y.; Li, S.; Altaany, Z.; Wang, R.; Yang, G. S-sulfhydration of <scp>MEK</Scp> 1 Leads to <scp>PARP</Scp> -1 Activation and <scp>DNA</Scp> Damage Repair. *EMBO Rep.* **2014**, *15* (7), 792–800.

(14) Yang, G.; Zhao, K.; Ju, Y.; Mani, S.; Cao, Q.; Puukila, S.; Khaper, N.; Wu, L.; Wang, R. Hydrogen Sulfide Protects Against Cellular Senescence via S -Sulfhydration of Keap1 and Activation of Nrf2. *Antioxid. Redox Signal.* **2013**, *18* (15), 1906–1919.

(15) Aggarwal, B. B.; Gupta, S. C.; Kim, J. H. Historical Perspectives on Tumor Necrosis Factor and Its Superfamily: 25 Years Later, a Golden Journey. *Blood* **2012**, *119* (3), 651–665.

(16) Du, J.; Huang, Y.; Yan, H.; Zhang, Q.; Zhao, M.; Zhu, M.; Liu, J.; Chen, S. X.; Bu, D.; Tang, C.; Jin, H. Hydrogen Sulfide Suppresses Oxidized Low-Density Lipoprotein (Ox-LDL)-Stimulated Monocyte Chemoattractant Protein 1 Generation from Macrophages via the Nuclear Factor KB (NF-KB) Pathway. *J. Biol. Chem.* **2014**, *289* (14), 9741–9753.

(17) Zhang, T.; Ono, K.; Tsutsuki, H.; Ihara, H.; Islam, W.; Akaike, T.; Sawa, T. Enhanced Cellular Polysulfides Negatively Regulate TLR4 Signaling and Mitigate Lethal Endotoxin Shock. *Cell Chem. Biol.* **2019**, *26* (5), 686-698.e4.

(18) Giovinazzo, D.; Bursac, B.; Sbodio, J. I.; Nalluru, S.; Vignane, T.; Snowman, A. M.; Albacarys, L. M.; Sedlak, T. W.; Torregrossa, R.; Whiteman, M.; Filipovic, M. R.; Snyder, S. H.; Paul, B. D. Hydrogen Sulfide Is Neuroprotective in Alzheimer's Disease by Sulfhydrating GSK3β and Inhibiting Tau Hyperphosphorylation. *Proc. Natl. Acad. Sci.* **2021**, *118* (4).

(19) Hannula, M. J.; Myöhänen, T. T.; Tenorio-Laranga, J.; Männistö, P. T.; Garcia-Horsman, J. A. Prolyl Oligopeptidase Colocalizes with α-Synuclein, β-Amyloid, Tau Protein and Astroglia in the Post-Mortem Brain Samples with Parkinson's and Alzheimer's Diseases. *Neuroscience* **2013**, *242*, 140–150.

(20) Vandiver, M. S.; Paul, B. D.; Xu, R.; Karuppagounder, S.; Rao, F.; Snowman, A. M.; Seok Ko, H.; Il Lee, Y.; Dawson, V. L.; Dawson, T. M.; Sen, N.; Snyder, S. H. Sulfhydration Mediates Neuroprotective Actions of Parkin. *Nat. Commun.* **2013**, *4* (1),

1626.

(21) Ida, T.; Sawa, T.; Ihara, H.; Tsuchiya, Y.; Watanabe, Y.; Kumagai, Y.; Suematsu, M.; Motohashi, H.; Fujii, S.; Matsunaga, T.; Yamamoto, M.; Ono, K.; Devarie-Baez, N. O.; Xian, M.; Fukuto, J. M.; Akaike, T. Reactive Cysteine Persulfides and S-Polythiolation Regulate Oxidative Stress and Redox Signaling. *Proc. Natl. Acad. Sci.* **2014**, *111* (21), 7606–7611.

(22) YAMANISHI, T.; TUBOI, S. The Mechanism of the L-Cystine Cleavage Reaction Catalyzed by Rat Liver γ-Cystathionase1. *J. Biochem.* **1981**, *89* (6), 1913–1921.

(23) Akaike, T.; Ida, T.; Wei, F.-Y.; Nishida, M.; Kumagai, Y.; Alam, M. M.; Ihara, H.; Sawa, T.; Matsunaga, T.; Kasamatsu, S.; Nishimura, A.; Morita, M.; Tomizawa, K.; Nishimura, A.; Watanabe, S.; Inaba, K.; Shima, H.; Tanuma, N.; Jung, M.; Fujii, S.; Watanabe, Y.; Ohmuraya, M.; Nagy, P.; Feelisch, M.; Fukuto, J. M.; Motohashi, H. Cysteinyl-TRNA Synthetase Governs Cysteine Polysulfidation and Mitochondrial Bioenergetics. *Nat. Commun.* **2017**, *8* (1), 1177.

(24) Melideo, S. L.; Jackson, M. R.; Jorns, M. S. Biosynthesis of a Central Intermediate in Hydrogen Sulfide Metabolism by a Novel Human Sulfurtransferase and Its Yeast Ortholog. *Biochemistry* **2014**, *53* (28), 4739–4753.

(25) Nagahara, N.; Yoshii, T.; Abe, Y.; Matsumura, T. Thioredoxin-Dependent Enzymatic Activation of Mercaptopyruvate Sulfurtransferase. *J. Biol. Chem.* **2007**, *282* (3), 1561–1569.

(26) Bordo, D.; Bork, P. The Rhodanese/Cdc25 Phosphatase Superfamily. *EMBO Rep.* **2002**, *3* (8), 741–746.

(27) Yadav, P. K.; Yamada, K.; Chiku, T.; Koutmos, M.; Banerjee, R. Structure and Kinetic Analysis of H2S Production by Human Mercaptopyruvate Sulfurtransferase. *J. Biol. Chem.* **2013**, *288* (27), 20002–20013.

(28) Libiad, M.; Yadav, P. K.; Vitvitsky, V.; Martinov, M.; Banerjee, R. Organization of the Human Mitochondrial Hydrogen Sulfide Oxidation Pathway. *J. Biol. Chem.* **2014**, *289* (45), 30901–30910.

(29) Huang, G.-T.; Yu, J.-S. K. Enzyme Catalysis That Paves the Way for S-Sulfhydration via Sulfur Atom Transfer. *J. Phys. Chem. B* **2016**, *120* (20), 4608–4615.

(30) Nagahara, N.; Katayama, A. Post-Translational Regulation of Mercaptopyruvate Sulfurtransferase via a Low Redox Potential Cysteine-Sulfenate in the Maintenance of Redox Homeostasis. *J. Biol. Chem.* **2005**, *280* (41), 34569–34576.

(31) Nagahara, N.; Nishino, T. Role of Amino Acid Residues in the Active Site of Rat Liver Mercaptopyruvate Sulfurtransferase. *J. Biol. Chem.* **1996**, *271* (44), 27395–27401.

(32) Shibuya, N.; Tanaka, M.; Yoshida, M.; Ogasawara, Y.; Togawa, T.; Ishii, K.; Kimura, H. 3-Mercaptopyruvate Sulfurtransferase Produces Hydrogen Sulfide and Bound Sulfane Sulfur in the Brain. *Antioxid. Redox Signal.* **2009**, *11* (4), 703–714.

(33) Rao, S. P.; Dobariya, P.; Bellamkonda, H.; More, S. S. Role of 3-Mercaptopyruvate Sulfurtransferase (3-MST) in Physiology and Disease. *Antioxidants* **2023**, *12* (3), 603.

(34) Kawamura, S.; Kitao, T.; Nakabayashi, T.; Horii, T.; Tsurugi, J. Aralkyl Hydrodisulfides. VIII. Alkaline Decomposition and Its Competition with Nucleophiles. *J. Org. Chem.* **1968**, *33* (3), 1179–1181.

(35) Dillon, K. M.; Matson, J. B. A Review of Chemical Tools for Studying Small Molecule Persulfides: Detection and Delivery. *ACS Chem. Biol.* **2021**, *16* (7), 1128–1141.

(36) Khodade, V. S.; Aggarwal, S. C.; Eremiev, A.; Bao, E.; Porche, S.; Toscano, J. P. Development of Hydropersulfide Donors to Study Their Chemical Biology. *Antioxid. Redox Signal.* **2022**, *36* (4–6), 309–326.

(37) Bora, P.; Chauhan, P.; Pardeshi, K. A.; Chakrapani, H. Small Molecule Generators of Biologically Reactive Sulfur Species. *RSC Adv.* **2018**, *8* (48), 27359–27374.

(38) Thompson, D. C.; Thompson, J. A.; Sugumaran, M.; Moldéus, P. Biological and Toxicological Consequences of Quinone Methide Formation. *Chem. Biol. Interact.* **1993**, *86* (2), 129–162.

(39) Ali, K.; Mishra, P.; Kumar, A.; Reddy, D. N.; Chowdhury, S.; Panda, G. Reactivity vs. Selectivity of Quinone Methides: Synthesis of Pharmaceutically Important Molecules, Toxicity and Biological Applications. *Chem. Commun.* **2022**, *58* (42), 6160–6175.

(40) Lau, N.; Pluth, M. D. Reactive Sulfur Species (RSS): Persulfides, Polysulfides, Potential, and Problems. *Curr. Opin. Chem. Biol.* **2019**, *49*, 1–8.

(41) Shieh, M.; Xu, S.; Lederberg, O. L.; Xian, M. Detection of Sulfane Sulfur Species in

Biological Systems. *Redox Biol.* **2022**, *57*, 102502.

(42) Vignane, T.; Filipovic, M. R. Emerging Chemical Biology of Protein Persulfidation. *Antioxid. Redox Signal.* **2023**, *39* (1–3), 19–39.

(43) Caswell, M.; Schmir, G. L. Formation and Hydrolysis of Lactones of Phenolic Acids. *J. Am. Chem. Soc.* **1980**, *102* (14), 4815–4821.

(44) Levine, M. N.; Raines, R. T. Trimethyl Lock: A Trigger for Molecular Release in Chemistry, Biology, and Pharmacology. *Chem. Sci.* **2012**, *3* (8), 2412.

(45) Kaspar, J. W.; Niture, S. K.; Jaiswal, A. K. Nrf2:INrf2 (Keap1) Signaling in Oxidative Stress. *Free Radic. Biol. Med.* **2009**, *47* (9), 1304–1309.

(46) Koike, S.; Ogasawara, Y.; Shibuya, N.; Kimura, H.; Ishii, K. Polysulfide Exerts a Protective Effect against Cytotoxicity Caused by t -Buthylhydroperoxide through Nrf2 Signaling in Neuroblastoma Cells. *FEBS Lett.* **2013**, *587* (21), 3548–3555.

(47) Nasi, S.; Ehirchiou, D.; Chatzianastasiou, A.; Nagahara, N.; Papapetropoulos, A.; Bertrand, J.; Cirino, G.; So, A.; Busso, N. The Protective Role of the 3-Mercaptopyruvate Sulfurtransferase (3-MST)-Hydrogen Sulfide (H2S) Pathway against Experimental Osteoarthritis. *Arthritis Res. Ther.* **2020**, *22* (1), 49.

(48) Chaudhuri, A.; Venkatesh, Y.; Jena, B. C.; Behara, K. K.; Mandal, M.; Singh, N. D. P. Real-Time Monitoring of a Photoactivated Hydrogen Persulfide Donor for Biological Entities. *Org. Biomol. Chem.* **2019**, *17* (39), 8800–8805.

(49) Fallah, A.; Noshadi, B.; Gazi, M.; Gülcan, H. O. Urolithin A and B Derivatives as ON-OFF Selective Fluorescent Sensors for Iron(III). *J. Fluoresc.* **2020**, *30* (1), 113–120.

(50) Peng, X.; Gao, J.; Yuan, Y.; Liu, H.; Lei, W.; Li, S.; Zhang, J.; Wang, S. Hypoxia-Activated and Indomethacin-Mediated Theranostic Prodrug Releasing Drug On-Demand for Tumor Imaging and Therapy. *Bioconjug. Chem.* **2019**, *30* (11), 2828–2843.

(51) Chaudhuri, A.; Venkatesh, Y.; Das, J.; Gangopadhyay, M.; Maiti, T. K.; Singh, N. D. P. One- and Two-Photon-Activated Cysteine Persulfide Donors for Biological Targeting. *J. Org. Chem.* **2019**, *84* (18), 11441–11449.

(52) Chen, W.; Liu, C.; Peng, B.; Zhao, Y.; Pacheco, A.; Xian, M. New Fluorescent Probes

for Sulfane Sulfurs and the Application in Bioimaging. *Chem. Sci.* **2013**, *4* (7), 2892–2896.

(53) McFadden, P. D.; Frederick, K.; Argüello, L. A.; Zhang, Y.; Vandiver, P.; Odegaard, N.; Loy, D. A. UV Fluorescent Epoxy Adhesives from Noncovalent and Covalent Incorporation of Coumarin Dyes. *ACS Appl. Mater. Interfaces* **2017**, *9* (11), 10061–10068.

(54) Kelkar, D. S.; Ravikumar, G.; Mehendale, N.; Singh, S.; Joshi, A.; Sharma, A. K.; Mhetre, A.; Rajendran, A.; Chakrapani, H.; Kamat, S. S. A Chemical–Genetic Screen Identifies ABHD12 as an Oxidized-Phosphatidylserine Lipase. *Nat. Chem. Biol.* **2019**, *15* (2), 169–178.

(55) Kimura, Y.; Koike, S.; Shibuya, N.; Lefer, D.; Ogasawara, Y.; Kimura, H. 3-Mercaptopyruvate Sulfurtransferase Produces Potential Redox Regulators Cysteine- and Glutathione-Persulfide (Cys-SSH and GSSH) Together with Signaling Molecules H2S2, H2S3 and H2S. *Sci. Rep.* **2017**, *7* (1), 10459.

(56) Bora, P.; Manna, S.; Nair, M. A.; Sathe, R. R. M.; Singh, S.; Sreyas Adury, V. S.; Gupta, K.; Mukherjee, A.; Saini, D. K.; Kamat, S. S.; Hazra, A. B.; Chakrapani, H. Leveraging an Enzyme/Artificial Substrate System to Enhance Cellular Persulfides and Mitigate Neuroinflammation. *Chem. Sci.* **2021**, *12* (39), 12939–12949.

(57) Hamid, H. A.; Tanaka, A.; Ida, T.; Nishimura, A.; Matsunaga, T.; Fujii, S.; Morita, M.; Sawa, T.; Fukuto, J. M.; Nagy, P.; Tsutsumi, R.; Motohashi, H.; Ihara, H.; Akaike, T. Polysulfide Stabilization by Tyrosine and Hydroxyphenyl-Containing Derivatives That Is Important for a Reactive Sulfur Metabolomics Analysis. *Redox Biol.* **2019**, *21*, 101096.

(58) Martel-Pelletier, J. Pathophysiology of Osteoarthritis. *Osteoarthr. Cartil.* **1998**, *6* (6), 374–376.

(59) Hankins, R. A.; Suarez, S. I.; Kalk, M. A.; Green, N. M.; Harty, M. N.; Lukesh, J. C. An Innovative Hydrogen Peroxide-Sensing Scaffold and Insight Towards Its Potential as an ROS-Activated Persulfide Donor. *Angew. Chemie - Int. Ed.* **2020**, *59* (49), 22238–22245.

(60) Santini, V.; Giles, F. J. The Potential of Amifostine: From Cytoprotectant to Therapeutic Agent. *Haematologica* **1999**, *84* (11), 1035–1042.

(61) Koukourakis, M. I. Review Paper Amifostine in Clinical Oncology : Current Use and Future Applications. **2002**, *13*, 181–209.

(62) Dziegielewski, J.; Baulch, J. E.; Goetz, W.; Coleman, M. C.; Spitz, D. R.; Murley, J. S.; Grdina, D. J.; Morgan, W. F. WR-1065, the Active Metabolite of Amifostine, Mitigates Radiation-Induced Delayed Genomic Instability. *Free Radic. Biol. Med.* **2008**, *45* (12), 1674–1681.

(63) Singh, V. K.; Seed, T. M. The Efficacy and Safety of Amifostine for the Acute Radiation Syndrome. *Expert Opin. Drug Saf.* **2019**, *18* (11), 1077–1090.

(64) Oiry, J.; Pue, J. Y.; Laval, J. D.; Fatome, M.; Imbach, J. L. Synthesis and Radioprotective Activity of WR-1065 Derivatives: N-(2-Acetylthioethyl)-1,3-Propanediamine and N,N′-Bis(2-Acetylthioethyl)-1,3-Propanediamine. *Eur. J. Med. Chem.* **1995**, *30* (1), 47–52.

List of Figures

List of Schemes

List of Tables

List of publications

1. **Choudhary, B. S.**; Kumar, T. A.; Vashishtha, A.; Tejasri, S.; Kumar, A. S.; Agarwal, R.; Chakrapani, H. An Esterase-Cleavable Persulfide Donor with No Electrophilic Byproducts and a Fluorescence Reporter. *Chem. Commun.* **2024**, *60*, 1727–1730.

ChemComm

COMMUNICATION

View Article Online
View Journal | View Issue

Cite this: *Chem. Commun.*, 2024, **60**, 1727

Received 9th October 2023,
Accepted 10th January 2024

DOI: 10.1039/d3cc04948e

rsc.li/chemcomm

An esterase-cleavable persulfide donor with no electrophilic byproducts and a fluorescence reporter†

Bharat S. Choudhary, ‡[a] T. Anand Kumar, ‡[a] Akshi Vashishtha, [b] Sushma Tejasri, [a] Amal S. Kumar, [a] Rachit Agarwal [b] and Harinath Chakrapani *[a]

Hydrogen sulfide (H_2S) and associated sulfur species known as persulfide or sulfane sulfur are considered among the first responders to oxidative stress. However, tools that reliably generate these species without any potentially toxic byproducts are limited, and even fewer report the generation of a persulfide. Here, using a latent fluorophore embedded with *N*-acetylcysteine persulfide, we report a new tool that is cleaved by esterase to produce a persulfide as well as a fluorescence reporter without any electrophilic byproducts. The rate of formation of the fluorescence reporter is nearly identical to the rate of formation of the persulfide suggesting that the use of this probe eliminates the need for secondary assays that report persulfide formation. Symptomatic with persulfide generation, the newly developed donor was able to protect chondrocyte cells from oxidative stress.

The gasotransmitter hydrogen sulfide (H_2S) has emerged as an important mediator of numerous cellular processes and a possible therapeutic agent in a number of diseases including progressive degenerative diseases associated with inflammation such as Parkinson's, Alzheimer's and osteoarthritis.[1–4] Recently, an oxidative post-translation modification induced by H_2S, known as protein persulfidation[4–6] where a cysteine (RSH) is modified to a persulfide (RS-SH), has been shown to have protective effects in cells under oxidative stress.[7] For example, KEAP1 an oxidative stress sensor protein forms a complex with Nrf2 under normal conditions, where Nrf2 is ubiquitinated by the Culin3-KEAP1 E3 ubiquitin ligase complex leading to proteasomal degradation. Under oxidative stress conditions, persulfidation of KEAP1 leads to the dissociation of the KEAP1-Nrf2 complex. The liberated Nrf2 then translocates to the nucleus and promotes the activation of antioxidant responsive elements (AREs).[8–10] While many tools have been developed to reliably generate persulfides, including those activated by enzymes,[11–15] light,[16,17] reactive oxygen species (ROS),[18–21] pH,[22,23] fluoride[22] and peroxynitrite.[24] One possible limitation with some of these approaches is the generation of electrophilic byproducts such as a quinone methide[13,14,18,21,24] or an aldehyde;[11,16,17,20] such byproducts may contribute to electrophilic stress.[25,26] Also, there is a need for secondary assays to report persulfide produced by these donors. To overcome the need for secondary assays to report persulfide generation, a latent fluorophore strategy can be employed. Upon activation by particular stimuli, the protective group gets cleaved (Step 1) leading to the formation of an intermediate, which subsequently dissociates (Step 2) to release persulfide along with a fluorescence reporter (Fig. 1a).

Recently, a donor that generates persulfide (H_2S_2) as well as a fluorescence reporter upon activation by light were reported (Fig. 1b).[17] However, the applicability of this tool may be limited by the generation of electrophilic byproducts as well as the limited use of light-based tools in the cellular experiments. Here, we developed a tool that generates persulfide along with a fluorophore that reports the generation of persulfide.

To achieve this goal, we considered lactonization as the key step in persulfide generation (Fig. 1c). Hence, a biphenyl-based system was chosen here, cleavage of the ester by esterase (Es) should lead to lactonization, which generates a lactone that belongs to a class of known fluorophores.[27,28] Lactonization in such systems is reported to be quite rapid;[29] hence, the persulfide generation will likely occur during lactonization leading to nearly concomitant release of the persulfide and the production of a fluorescence signal.

Compound **2a** (Scheme 1) was synthesized following a reported protocol.[30] Reduction of lactone by LAH, silyl protection of the resulting alcohol, and esterification with cyclopropyl carboxylic acid (CPCA) followed by silyl group deprotection afforded compound **6**.

[a] *Department of Chemistry, Indian Institute of Science Education and Research Pune, Pune 411 008, Maharashtra, India. E-mail: harinath@iiserpune.ac.in*
[b] *Department of Bioengineering, Indian Institute of Science, Bengaluru 560 012, Karnataka, India*

† Electronic supplementary information (ESI) available. See DOI: https://doi.org/10.1039/d3cc04948e

‡ These authors contributed equally.

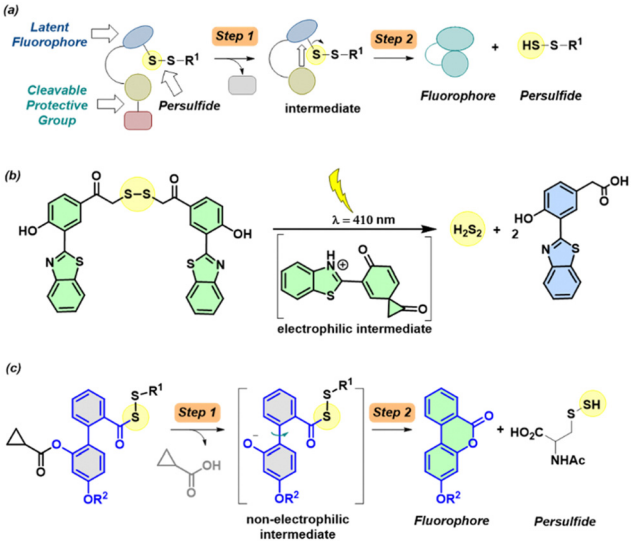

Fig. 1 (a) General design for a cleavable persulfide donor with a fluorescence reporter. The first step is the cleavage of the protective group, which produces an intermediate that is then converted to a fluorophore and produces persulfide as a byproduct. (b) Light activated H_2S_2 donor with a fluorescence reporter. (c) Proposed biphenyl-system that is cleaved by esterase to produce a phenolate intermediate that cyclizes to produce a lactone that is fluorescent and persulfide.

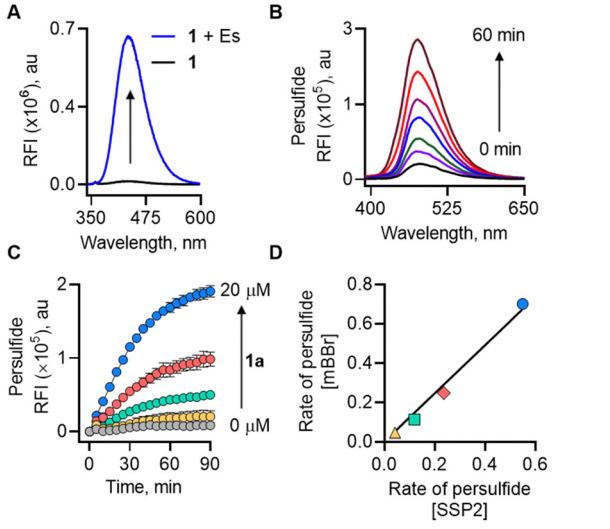

Fig. 2 (A) Monitoring the formation of lactone (**2a**) from **1** by fluorescence at 20 μM without or with Es (1 U mL^{-1}) in pH 7.4 buffer at 37 °C. (B) Detection of persulfide released from **1** (100 μM) upon treatment with Es (1 U mL^{-1}) and mBBr (100 μM) over 60 min. (C) Monitoring the release of persulfide generated upon co-treatment of Es (1 U mL^{-1}) and SSP2 (10 μM) with varied concentrations of **1** (0–20 μM) over 90 min. (D) Correlation between the rate of persulfide formation from **1** (△ 2.5 μM; □ 5 μM; ◇ 10 μM and ○ 20 μM) in mBBr and SSP2 assays.

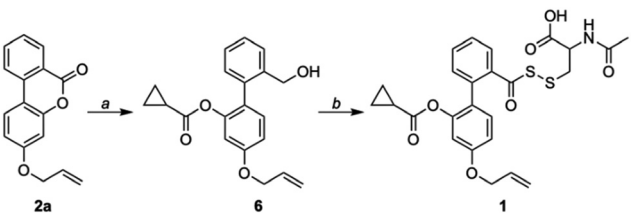

Scheme 1 Synthesis of **1**: (a) (i) LAH, THF, 0 °C; (ii) TBDMSCl, Imh, RT; (iii) CPCA, DCC, DMAP, RT; (iv) AcOH, THF:H_2O, RT; (b) (i) PCC, DCM, RT; (ii) KH_2PO_4, H_2O_2, $NaClO_2$, DCM, RT; (iii) Lawesson's reagent, toluene, 120 °C; (iv) **9** (NAC-SS-Py), $CHCl_3$, RT.

Oxidation of a primary alcohol in two steps gave carboxylic acid **8**, which was then converted to its corresponding thiocarboxylic acid using Lawesson's reagent and finally coupled with NAC-pyridyl disulfide (NAC-SS-Py) **9** to provide the persulfide donor **1** (Scheme S1, ESI†). This compound with an allyl group was used for initial experiments, since the lactone (**2b**) without the allyl group had diminished fluorescence signal when compared with **2a** (see ESI,† Fig. S1). We hence proceeded to use **1** which has an allyl group for our analysis.

We first examined the formation of lactone (**2a**) from **1** (20 μM) by monitoring the change in fluorescence in the presence of Es (1 U mL^{-1}). The compound was itself non-fluorescent, but addition of Es (1 U mL^{-1}) led to a significant increase in fluorescence intensity (48-fold) attributable to the formation of **2a** (λ_{ex} = 320 nm; λ_{em} = 432 nm;) after incubation for 1 h in pH 7.4 buffer (Fig. 2a). The formation of **2a** was independently confirmed by mass spectrometry analysis (m/z 253.0864; see ESI,† Fig. S2). Furthermore, dose-dependent studies demonstrated that the fluorescence gradually increased over time and plateaued after 1 h (see ESI,† Fig. S3). Curve fitting for lactone formation to a first-order exponential equation yielded rate constants ranging from 0.046 to 0.073 min^{-1} (see ESI,† Table S1). These results supported that **1** underwent lactonization to produce **2a** following esterase-mediated hydrolysis. We tested the ability of **1** to be cleaved under cell culture conditions and found that **1** was cleaved in cell lysates to produce a fluorescence signal (see ESI,† Fig. S4). Compound **1** was well tolerated by MEF cells up to 100 μM (see ESI,† Fig. S5). To ascertain if **1** permeates cells to generate **2a**, MEF cells were treated with **1** followed by confocal imaging after 4 h, since this class of fluorophores is known to be compatible with two-photon imaging[31] (λ_{ex} = 700 nm; see ESI,† Fig. S6). Together, these results support the suitability of **1** in cellular assays.

Next, a series of experiments were conducted to directly trap the persulfide release from **1** using electrophilic trapping agents and persulfide-specific fluorescent probes. First, a monobromobimane (mBBr)-based fluorescence enhancement assay was used.[17] Here, when **1** was co-incubated with Es and mBBr, we found a distinct time-dependent increase in fluorescence (λ_{ex} = 380 nm; λ_{em} = 455 nm) (Fig. 2b). This fluorescence was attributed to the formation of **NAC-SS-bimane** adduct ($M + Na^+$; m/z 408.0663) (Scheme S2, ESI†), which was further confirmed by MS analysis (see ESI,† Fig. S7). A dose-dependent study of **1** with mBBr showed a good linear relationship (see ESI,† Fig. S8).

Independently, we also measured the rate of persulfide generation from **1** using a well-established fluorogenic probe,

sulfane sulfur probe (SSP2).[32] Again, we observed a significant increase in fluorescence intensity (λ_{ex} = 482 nm; λ_{em} = 518 nm), corresponding to the generation of sulfane sulfur (Fig. 2c). Under these experimental conditions, the rate of persulfide formation in both mBBr and SSP2 assays showed an excellent correlation (R^2 = 0.99) (Fig. 2d).

The time course for the formation of **2a** as well as NAC persulfide at various concentrations of **1** was independently monitored by the change in fluorescence signal. When followed over 90 min, the time courses of these events were similar. The rate for lactone formation was found to be marginally higher in magnitude (2–3 fold) than the rate of persulfide generation (see ESI,† Table S1). This is expected since the lactonization occurs at a faster rate compared to the rate of formation of NAC persulfide covalent adducts that occurs through a two-step process rather than a single step. To establish a correlation between the lactone (**2a**) and persulfide formation (SSP2) from **1**, the maximum fluorescence change at 90 min was considered as the plateau was reached. These values were normalized and then plotted. An excellent correlation between the two parameters was observed, suggesting that the release of fluorophore and NAC persulfide occurs nearly concurrently following esterase-mediated cleavage and subsequent lactonization (Fig. 3a). Similarly, the rates of persulfide generation as determined by SSP2 and rates of lactone **2a** formation showed a good linear relationship at concentrations ranging from 2.5 to 20 μM (Fig. 3b). Taken together, these data show that the fluorescence signal produced can be used as a proxy for persulfide production.

Lastly, two additional assays were carried out to demonstrate persulfide and hydrogen sulfide formation. A standard LC/MS assay was conducted using an established **HPE-IAM** electrophile as a persulfide trapping agent (Scheme S3, ESI†).[33] Upon co-incubation of **1** in the presence of Es (1 U mL^{-1}) and **HPE-IAM**, a new peak attributable to a persulfide adduct, **NAC-SS-HPE-AM** (*m*/*z* 373.0891), was observed, indicating the release of NAC persulfide (see ESI,† Fig. S9 and S10). Under these conditions, we also observe **Bis-*S*-HPE-AM** (*m*/*z* 389.1537), presumably due to the reaction of HPE-IAM with H_2S formed by the decomposition of NAC persulfide through disproportionation (see ESI,† Fig. S9 and S11). Lastly, we measured H_2S formation from **1** using the standard methylene blue (MB) colorimetric assay.[34] This assay revealed the formation of H_2S from **1** in the presence of Es and excess amounts of DTT (see ESI,† Fig. S12). To independently verify H_2S release, we employed a lead acetate assay. Addition of an aliquot of the reaction mixture containing **1** and Es to lead acetate paper resulted in a dark coloration, indicating the formation of lead sulfide (see ESI,† Fig. S13).

Osteoarthritis (OA) is the most common joint disease and is characterized by a gradual loss of articular cartilage and joint hypertrophy.[35] Chronic inflammation and oxidative stress contribute to the onset and progression of OA.[36,37] We considered the antioxidant property of persulfide as a possible therapeutic strategy to alleviate oxidative stress and inflammation in chondrocytes. Persulfides are known to exhibit potent antioxidant properties, superior to thiols and H_2S against oxidative stress.[7] We first measured the cytotoxicity of **1** in the human chondrocyte C28/I2 cells and found that the compound was well tolerated up to 50 μM and the LD50 was found to be ~500 μM (Fig. 4a and see ESI,† Fig. S14). This result is consistent with no electrophilic byproducts being formed during the persulfide generation step. Next, we determined the cytoprotective effects of **1** in C28/I2 cells against oxidative stress induced by a cell-permeable ROS generator MGR-1 (Scheme S4, ESI†).[38] Cells were preincubated with **1** for 3 h and then were exposed to MGR-1 (15 μM), after which cell viability was assessed. As expected, exposure of cells to MGR-1 resulted in a drastic reduction in cell viability. Pre-treatment of cells with **1** demonstrated significant protective effects from MGR-1 induced oxidative stress in a concentration-dependent manner (Fig. 4b). A similar result was recorded when **1** was co-treated with MGR-1 or added after exposure to MGR-1 (see ESI,† Fig. S15). To understand if **1** acted through diminishing ROS levels, a standard H_2-DCFDA assay was performed in MEF cells (see ESI,† Fig. S16). These results indicate that **1** was capable of protecting as well as rescuing cells from oxidative stress.

The central characteristic of osteoarthritis (OA) is the degradation of the extracellular matrix (ECM). When chondrocytes are densely seeded (micromass) and exposed to specific growth factors, they release extracellular matrix (ECM) components,

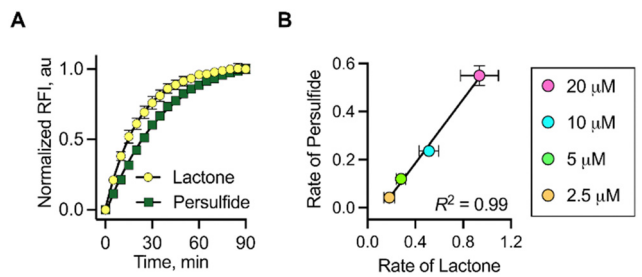

Fig. 3 (A) Correlation between change in fluorescence corresponding to the formation of lactone and persulfide formed upon incubation of **1** (20 μM) with Es (1 U mL^{-1}) and SSP2 (10 μM). (B) Correlation between the rates of lactone and persulfide formation upon treatment of **1** (2.5, 5, 10 and 20 μM) with Es (1 U mL^{-1}) in the presence of SSP2 (10 μM).

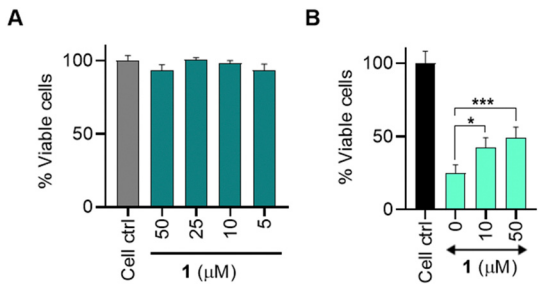

Fig. 4 A cell viability assay conducted on C28/I2 cells. (A) Cells treated with varying concentrations of compound **1** for 24 h. (B) Cells treated with varying concentration of **1** followed by treatment with MGR-1 (15 μM). All data are presented as mean ± SD (*n* = 4/group). Statistical significance was established relative to MGR-1 using one-way ANOVA (*$p < 0.033$, ***$p \leq 0.001$).

such as sulphated glycosaminoglycans (sGAG).[39] Next, we employed micromass cultures derived from the C28/I2 cell line,[40,41] which can be considered as an *in vitro* mimic of the cartilage[39,41] to assess the ability of **1** in sustaining sGAG production in the presence of oxidative stress induced by MGR-1. sGAG production was measured using Alcian blue staining as described.[39–41] When exposed to MGR-1 alone, there was a significant decrease in absorbance compared to the untreated group. However, micromasses co-treated with MGR-1 and **1** displayed an increased absorbance, similar to the untreated samples, indicating that the cells were capable of sustaining sGAG production even under oxidative stress when co-treated with **1** (see ESI,† Fig. S17). These results support the ability of persulfides generated by **1** to counter oxidative stress in a model relevant to OA. Further *in vitro* and *in vivo* experiments towards exploiting the therapeutic potential of persulfide generating systems for the treatment of OA are indicated.

In summary, we report a new probe that is cleaved by esterase to produce persulfide as well as a fluorescence signal. No electrophilic byproducts were formed during this reaction (see ESI,† Fig. S18), and the rate of persulfide generation closely correlated with the rate of generation of a fluorescence signal. Hence, the use of this new tool eliminates the need for independent assays to detect persulfides.

Financial support was provided by the Science and Engineering Research Board (CRG/2019/002900), Department of Biotechnology (HC, BH/HRD/NBM-NWB/39/2020-21) and IISER Pune, and the DST Fund for Improvement of S&T Infrastructure (SR/FST/LSII-043/2016) to the IISER Pune Biology Department for setting up the Biological Mass Spectrometry Facility. The manuscript was written with inputs from all authors. BSC, TAK, AV, ST and ASK carried out all experiments under the supervision of RA and HC.

Conflicts of interest

There are no conflicts to declare.

Notes and references

1 T. V. Mishanina, M. Libiad and R. Banerjee, *Nat. Chem. Biol.*, 2015, **11**, 457–464.
2 M. R. Filipovic, J. Zivanovic, B. Alvarez and R. Banerjee, *Chem. Rev.*, 2018, **118**, 1253–1337.
3 S. Nasi, D. Ehirchiou, A. Chatzianastasiou, N. Nagahara, A. Papapetropoulos, J. Bertrand, G. Cirino, A. So and N. Busso, *Arthritis Res. Ther.*, 2020, **22**, 49.
4 A. K. Mustafa, M. M. Gadalla, N. Sen, S. Kim, W. Mu, S. K. Gazi, R. K. Barrow, G. Yang, R. Wang and S. H. Snyder, *Sci. Signaling*, 2009, **2**, ra72.
5 C. Yang, N. O. Devarie-Baez, A. Hamsath, X. Fu and M. Xian, *Antioxid. Redox Signaling*, 2020, **33**, 1092–1114.
6 H. Kimura, *Br. J. Pharmacol.*, 2020, **177**, 720–733.
7 T. Ida, T. Sawa, H. Ihara, Y. Tsuchiya, Y. Watanabe, Y. Kumagai, M. Suematsu, H. Motohashi, S. Fujii, T. Matsunaga, M. Yamamoto, K. Ono, N. O. Devarie-Baez, M. Xian, J. M. Fukuto and T. Akaike, *Proc. Natl. Acad. Sci. U. S. A.*, 2014, **111**, 7606–7611.
8 J. W. Kaspar, S. K. Niture and A. K. Jaiswal, *Free Radical Biol. Med.*, 2009, **47**, 1304–1309.
9 S. Koike, Y. Ogasawara, N. Shibuya, H. Kimura and K. Ishii, *FEBS Lett.*, 2013, **587**, 3548–3555.
10 G. Yang, K. Zhao, Y. Ju, S. Mani, Q. Cao, S. Puukila, N. Khaper, L. Wu and R. Wang, *Antioxid. Redox Signaling*, 2013, **18**, 1906–1919.
11 Y. Zheng, B. Yu, Z. Li, Z. Yuan, C. L. Organ, R. K. Trivedi, S. Wang, D. J. Lefer and B. Wang, *Angew. Chem., Int. Ed.*, 2017, **56**, 11749–11753.
12 Z. Yuan, Y. Zheng, B. Yu, S. Wang, X. Yang and B. Wang, *Org. Lett.*, 2018, **20**, 6364–6367.
13 K. M. Dillon, R. J. Carrazzone, Y. Wang, C. R. Powell and J. B. Matson, *ACS Macro Lett.*, 2020, **9**, 606–612.
14 K. M. Dillon, H. A. Morrison, C. R. Powell, R. J. Carrazzone, V. M. Ringel-Scaia, E. W. Winckler, R. M. Council-Troche, I. C. Allen and J. B. Matson, *Angew. Chem., Int. Ed.*, 2021, **60**, 6061–6067.
15 P. Bora, M. B. Sathian and H. Chakrapani, *Chem. Commun.*, 2022, **58**, 2987–2990.
16 A. Chaudhuri, Y. Venkatesh, J. Das, M. Gangopadhyay, T. K. Maiti and N. D. P. Singh, *J. Org. Chem.*, 2019, **84**, 11441–11449.
17 A. Chaudhuri, Y. Venkatesh, B. C. Jena, K. K. Behara, M. Mandal and N. D. P. Singh, *Org. Biomol. Chem.*, 2019, **17**, 8800–8805.
18 C. R. Powell, K. M. Dillon, Y. Wang, R. J. Carrazzone and J. B. Matson, *Angew. Chem., Int. Ed.*, 2018, **57**, 6324–6328.
19 R. A. Hankins, S. I. Suarez, M. A. Kalk, N. M. Green, M. N. Harty and J. C. Lukesh, *Angew. Chem., Int. Ed.*, 2020, **59**, 22238–22245.
20 P. Bora, P. Chauhan, S. Manna and H. Chakrapani, *Org. Lett.*, 2018, **20**, 7916–7920.
21 Y. Wang, K. M. Dillon, Z. Li, E. W. Winckler and J. B. Matson, *Angew. Chem., Int. Ed.*, 2020, **59**, 16698–16704.
22 J. Kang, S. Xu, M. N. Radford, W. Zhang, S. S. Kelly, J. J. Day and M. Xian, *Angew. Chem., Int. Ed.*, 2018, **57**, 5893–5897.
23 V. S. Khodade, B. M. Pharoah, N. Paolocci and J. P. Toscano, *J. Am. Chem. Soc.*, 2020, **142**, 4309–4316.
24 Y. Xu, B. Xu, J. Wang, H. Jin, S. Xu, G. Wang and L. Zhen, *Chem. – Eur. J.*, 2022, **28**, e202200540.
25 D. C. Thompson, J. A. Thompson, M. Sugumaran and P. Moldéus, *Chem. – Biol. Interact.*, 1993, **86**, 129–162.
26 K. Ali, P. Mishra, A. Kumar, D. N. Reddy, S. Chowdhury and G. Panda, *Chem. Commun.*, 2022, **58**, 6160–6175.
27 A. Fallah, B. Noshadi, M. Gazi and H. O. Gülcan, *J. Fluoresc.*, 2020, **30**, 113–120.
28 X. Peng, J. Gao, Y. Yuan, H. Liu, W. Lei, S. Li, J. Zhang and S. Wang, *Bioconjugate Chem.*, 2019, **30**, 2828–2843.
29 M. Caswell and G. L. Schmir, *J. Am. Chem. Soc.*, 1980, **102**, 4815–4821.
30 A. T. Franks and K. J. Franz, *Chem. Commun.*, 2014, **50**, 11317–11320.
31 P. D. McFadden, K. Frederick, L. A. Argüello, Y. Zhang, P. Vandiver, N. Odegaard and D. A. Loy, *ACS Appl. Mater. Interfaces*, 2017, **9**, 10061–10068.
32 W. Chen, C. Liu, B. Peng, Y. Zhao, A. Pacheco and M. Xian, *Chem. Sci.*, 2013, **4**, 2892–2896.
33 H. A. Hamid, A. Tanaka, T. Ida, A. Nishimura, T. Matsunaga, S. Fujii, M. Morita, T. Sawa, J. M. Fukuto, P. Nagy, R. Tsutsumi, H. Motohashi, H. Ihara and T. Akaike, *Redox Biol.*, 2019, **21**, 101096.
34 A. K. Sharma, M. Nair, P. Chauhan, K. Gupta, D. K. Saini and H. Chakrapani, *Org. Lett.*, 2017, **19**, 4822–4825.
35 J. Martel-Pelletier, *Osteoarthr. Cartil.*, 1998, **6**, 374–376.
36 M. Y. Ansari, N. Ahmad and T. M. Haqqi, *Biomed. Pharmacother.*, 2020, **129**, 110452.
37 L. Liu, P. Luo, M. Yang, J. Wang, W. Hou and P. Xu, *Front. Mol. Biosci.*, 2022, **9**, 1001212.
38 D. S. Kelkar, G. Ravikumar, N. Mehendale, S. Singh, A. Joshi, A. K. Sharma, A. Mhetre, A. Rajendran, H. Chakrapani and S. S. Kamat, *Nat. Chem. Biol.*, 2019, **15**, 169–178.
39 K. V. Greco, A. J. Iqbal, L. Rattazzi, G. Nalesso, N. Moradi-Bidhendi, A. R. Moore, M. B. Goldring, F. Dell'Accio and M. Perretti, *Biochem. Pharmacol.*, 2011, **82**, 1919–1929.
40 K. M. Dhanabalan, A. A. Dravid, S. Agarwal, R. K. Sharath, A. K. Padmanabhan and R. Agarwal, *Bioeng. Transl. Med.*, 2023, **8**, e10298.
41 C. De Bari, F. Dell'Accio and F. P. Luyten, *Arthritis Rheum.*, 2001, **44**, 85–95.

